
**Systematic mutagenesis
of the mouse prion
protein to identify critical
regions for the efficient
propagation of prions**

By Savroop Kaur Bhamra

A thesis submitted to UCL for the degree of Ph.D.

Author's declaration

I, Savroop Bhamra, confirm that the work presented in this thesis is my own.
Where information has been derived from other sources, I confirm that this
has been indicated in the thesis.

A c k n o w l e d g e m e n t s

I wish to express my gratitude to my supervisor, Prof. Parmjit Jat, for his tremendous support and motivation during the entire course of my Ph.D., and for his patience during its infancy. To the former members of my lab., thank you for teaching me along the way; to the members present, thank you Sarah and Nunu for all the laughs we shared; to future members, may you find your experience here as fruitful and fulfilling as I have.

To my beautiful family, for their love and encouragement during my Ph.D. Mum, Nilu, Anand – thank you for being my audience in numerous lab. talk rehearsals, and listening to the science babble; Dindi aunty and Manjit uncle, thank you so much for always being there for me. To my dearest Papa, thank you for believing in me, picturing our world to be bigger than little Kisumu and to Chachaji for making it happen and for your ever-present counsel and guidance.

To my boyfriend Dan, thank you for more than I can condense into one page, but here goes: proof-reading this entire document and the long hours it took; correcting embarrassing typos (filbril?); love, hugs, coffees and chocolates; saving me from the horrors of low-resolution pixelated images; help with analysing data on GraFit and Prism; helping me overcome the evil sorcery of Word documents; being increasingly patient with me with the thesis deadline nearing; for introducing me to 'vo' and 'fo'; -OH groups on 'fernet and brancamenta'; and for which I cherish most, thank you for putting a smile on my face every single day.

The aim of this study was to systematically investigate the contributions of various amino acids within the prion protein, on prion propagation. To test this in a cellular system, we used a sub-cloned population of N2a cells (PK1) that are highly susceptible to RML mouse prions. A library of stable PK1 cells was generated, which expressed the full length mouse prion protein (moPrP) bearing either point, double, or triple alanine replacements. The effects these changes in the prion protein sequence had on the ability of PK1 cells to propagate RML was tested using a previously established cell based assay.

We found that: (i) in the unstructured region of the protein, alanine replacements in CC2 region 90-111 of the prion protein severely diminish, but do not abrogate the ability of cells to propagate prions whilst substitutions K23A.K24A.R25A and Q41A exerted a moderate inhibitory effect on propagation; (ii) alanine replacements in CC2 displayed a dominant negative effect by imposing their propagation inhibition phenotype in the presence of the wild-type protein; (iii) the diminished propagation abilities of cells expressing CC2 alanine mutants were a result of these cells being less susceptible to infection than their wild-type counterparts (iv) all alanine replacements tested in the structured region of the protein appeared to hamper prion propagation, regardless of their positioning within this globular domain.

Taken together, these results suggest that integrity of the structured region is vital for successful prion propagation, and that although the flexible region

of the prion protein alone (residues 23-111), does not exclusively confer infectivity and/or propagative capacity, charge interactions in this region govern the efficacy with which propagation ensues.

List of Figures

Figure I1	The cellular prion protein	37
Figure I2	Topologies of the prion protein	38
Figure I3	Structural features and domains of the prion protein	41
Figure I4	Schematic of fibril formation	44
Figure I5	β -sheet structure of amyloids	48
Figure I6	Charge Cluster 1	53
Figure I7	Octapeptide Repeats	58
Figure I8	Charge Cluster 2	61
Figure I9	Putative Transmembrane Domain	69
Figure I10	Structured region	73
Figure I11	Tagged PrP constructs used in prion research	88
Figure R1	PDB entry 2LEJ, human prion protein	117
Figure R2	Linear map of the plasmid vector pBluescriptSK+	120
Figure R3	Mutagenesis of moPrP in pBluescriptSK+ and subsequent cloning into pLNCX2	124
Figure R4	Sequencing data confirming the presence of alanine mutations at indicated sites	125
Figure R5	Linear sequence map for plasmid vector pLNCX2	127
Figure R6	Dose-response curve of KD cells to G418 antibiotic	128
Figure R7	moPrP expression in PK1 and KD cells	132
Figure R8	Immunofluorescence of KD cells reconstituted with moPrP constructs	134
Figure R9	Cell line schematic	135
Figure R10	Scrapie cell assay and ELISPOT plan	139

Figure R11	Scrapie Cell Assay output	140
Figure R12	Guide for RML prion propagation readout	142
Figure R13	Regions of interest within moPrP sequence 23-90	145
Figure R14	SCA of KDmoPrP ^{Ala} cells; moPrP mutations in region 23-33	147
Figure R15	SCA of KDmoPrP ^{Ala} cells; moPrP mutations in region 23-25	149
Figure R16	SCA of KDmoPrP ^{Ala} cells; moPrP mutations in region 41-88	152
Figure R17	SCA of KDmoPrP ^{Ala} cells; moPrP mutations in region 23-25 or residue 41	154
Figure R18	SCA of KDmoPrP ^{Ala} cells; moPrP mutations in region 23-25 and residue 41	158
Figure R19	Western blot of KDmoPrP ^{Ala} cells with mutations in CC1 and residue 41	160
Figure R20	Immunofluorescent analysis of KDmoPrP ^{Ala} cells with mutations in CC1 and residue 41	161
Figure R21	Summary of findings; region 23-88 of moPrP	163
Figure R22	Octapeptide repeats in the prion protein	170
Figure R23	PDB entry 2LEJ human PrP highlights the flexibility of N-terminal regions	176
Figure R24	SCA of KDmoPrP ^{Ala} cells; moPrP mutations in region 90-111	178
Figure R25	SCA of KDmoPrP ^{Ala} cells; moPrP mutations in region 90-111, increased RML	180
Figure R26	KDmoPrP ^{Ala} cells; mutations in region 90-111, phase contrast images	183
Figure R27	Western blot of KDmoPrP ^{Ala} cells with mutations in CC2	186
Figure R28	Immunofluorescence images of KDmoPrP ^{Ala} cells with mutations in CC2	187

Figure R29	Human and mouse prion protein sequence; region CC2	192
Figure R30	Targeted mutagenesis of the structured region of moPrP	206
Figure R31	moPrP structured region; residues 123-151	208
Figure R32	Targeted sites for mutations in region 123-151 of moPrP	210
Figure R33	SCA of KDmoPrP ^{Ala} cells; moPrP mutations in region 123-151	212
Figure R34	Immunofluorescent analysis of KDmoPrP ^{Ala} cells with mutations in structured region 123-151	213
Figure R35	Targeted sites for mutations in region 148-230 of moPrP	215
Figure R36	SCA of KDmoPrP ^{Ala} cells; moPrP mutations in region 148-230	216
Figure R37	Immunofluorescent analysis of KDmoPrP ^{Ala} cells with mutations in structured region 148-230	219
Figure R38	Targeted sites for mutations in core hydrophobic residues of moPrP	221
Figure R39	SCA of KDmoPrP cells; mutations in core hydrophobic regions of moPrP	223
Figure R40	SCA analysis of RML-infected versus non-infected KDmoPrP cells with mutations made in the core hydrophobic residues of the protein	226
Figure R41	Immunofluorescence images of KDmoPrP cells with mutations in core hydrophobic regions of the protein	228
Figure R42	SCA analysis of KDmoPrP ^{Ala} cells with mutations in the structured region testing two doses of RML inocula	229
Figure R43	CC1, Q41 and CC2 are identified as modulators of prion propagation	242
Figure R44	Single cell cloning	243

Figure R45	Immunofluorescence images of single cell clones	244
Figure R46	SCA analysis of single cell clones in region 23-111	247
Figure R47	SCA analysis of single cell clones in CC1 and Q41 at three doses of infectious inocula	249
Figure R48	Expression of moPrP ^{Ala} in KD, PK1 and iPK1 cells	252
Figure R49	PK1 cells infected with lysate from prion-infected KDmoPrP ^{Ala} cells	254
Figure R50	SCA of PK1moPrP ^{Ala} cells	258
Figure R51	Expression of moPrP ^{Ala} does not rescue iPK1 cells from prion infection	261
Figure R52	Proposed mechanism of inhibition of prion propagation by moPrP ^{Ala} mutations in CC1, Q41 and CC2 regions of the protein	268
Figure R53	Prediction of the middle region of moPrP as a membrane-traversing segment	277
Figure R54	Fibril-forming segments in the prion protein	278
Figure R55	SCA analysis of KDmoPrP ^{Ala} cells with mutations in region 111-119	283
Figure R56	SCA analysis of KDmoPrP ^{Ala} cells with mutations in region 121-127	286
Figure R57	SCA analysis of KDmoPrP ^{Ala} cells with mutations in region 127-135	289
Figure R58	Molecular modelling of the PTM region 110-136 in the human prion protein	293
Figure R59	Summary of sites within the PTM domain predicted to disrupt dimer formation, matched to SCA data	294
Figure R60	Glycine residues within the PTM domain	296
Figure R61	Transmembrane forms of the prion protein at the ER	300

Figure R62	Phase contrast images of KD cells reconstituted with moPrP mutations in the PTM region of the protein	304
Figure C1	Overall summary of cumulative SCA data on KDmoPrP ^{Ala} cells	312
Figure C2	Future directions	315

List of Tables

Table I1	Prion protein strains and their propagation in cell culture	52
Table I2	Tags and epitopes used to aid and complement detection of prions	90
Table R1	Summary table of moPrP mutagenic constructs generated in plasmid vector pBluescriptSK+	119
Table R2	Standard PCR conditions for site-directed mutagenesis	121
Table R3	List of moPrP alanine mutations in region 23-88 of the protein.	174
Table R4	Antibodies available against PrP region CC2	195
Table R5	List of mutations made within CC2	203
Table R6	List of mutations made within the structured region of moPrP	230
Table R7	List of mutations made within the unstructured region of the mouse prion protein.	273
Table R8	Helical propensity of various amino acids	279
Table R9	Mutations made within region 111-119 of moPrP	281
Table R10	Mutations made within region 121-127 of moPrP	285
Table R11	Mutations made within region 127-135 of moPrP	288

Abbreviations

14-3-3	A class of regulatory proteins ubiquitously expressed in eukaryotic cells
β -PrP	Beta-sheet-rich form of the prion protein
A_{600}	Sample absorbance at 600 nm
AmpR	Ampicillin resistance gene
A β	Amyloid beta, a 40-42 amino acid-long peptide generated via sequential cleavage of the amyloid precursor protein by β - and γ -secretases
ANOVA	Analysis of variance
AP	Alkaline phosphatase
APP	Amyloid precursor protein
Bax	Bcl-2-associated X protein
BSE	Bovine Spongiform Encephalopathy
C1	Fragment corresponding to residues 110-230 of prion protein (mouse numbering)
CaCl ₂	Calcium chloride
CC1	Charge cluster 1
CC2	Charge cluster 2
CJD	Creutzfeldt-Jakob disease
CMV	Cytomegalovirus
CNS	Central nervous system
CO ₂	Carbon dioxide
C tm PrP	PrP peptide with C-terminal half of the protein in the ER lumen
DAPI	4',6-diamidino-2-phenylindole
DMEM	Dulbecco's Modified Eagle's Medium
DNA	Deoxyribonucleic acid
dNTPs	Deoxyribonucleotide triphosphates
<i>DpnI</i>	Restriction endonuclease GATC recognition site
ECL	Enhanced chemiluminescence

EDTA	Ethylenediaminetetraacetic acid
EGFP	Enhanced GFP
ELISA	Enzyme-linked immunosorbent assay
ER	Endoplasmic reticulum
EtOH	Ethanol
FCS	Foetal calf serum
G418	Geneticin
GAG	Glycosaminoglycan
GFP	Green fluorescent protein
GPI	Glycosylphosphatidylinositol
GSCN	Guanidinium thiocyanate
GSS	Gerstmann-Sträussler-Scheinker
HC	Hydrophobic core
HCl	Hydrochloric acid
HDX	Hydrogen-deuterium exchange
<i>Hind</i> III	Restriction endonuclease AAGCTT recognition site
HRP	Horseradish peroxidase
huPrP	Human prion protein (cellular form)
ICSM35b	Biotinylated form of ICSM35
ID	Intrinsic disorder
IDP	Intrinsically disordered protein
IgG	Immunoglobulin G isotype
IMAC	Immobilised metal-affinity chromatography
Indel	Insertion/deletion mutation
iPK1	Chronically infected PK1 cells
iPK1moPrP ^{Ala}	Chronically infected PK1 cells expressing alanine-mutant forms of murine PrP
KanR	Kanamycin resistance gene
KD	Knockdown

KDmoPrP ^{Ala}	Knockdown PK1 cells expressing the full-length, form of the murine prion protein (cellular form) with single, double or triple alanine mutations
KDmoPrP ^{WT}	Knockdown PK1 cells expressing the full-length, wild-type form of the murine prion protein (cellular form)
LB	Luria Broth
LRP1	Low-density lipoprotein receptor-related protein 1
LTR	Long terminal repeat
MCS	Multiple cloning sites
MgCl ₂	Magnesium chloride
mGluR5	Metabotropic glutamate receptor 5
MMLV	Moloney Murine Leukemia Virus
moPrP	Mouse prion protein (cellular form)
moPrP ^{Ala}	Alanine-mutant forms of the prion protein (cellular form)
moPrP ^{WT}	Full-length, wild-type form of the murine prion protein (cellular form)
moPrP ^{WT(Sc)}	Full-length, wild-type form of the murine prion protein (disease-associated form)
N-SS	N-terminal signal sequence
N1	Fragment corresponding to residues 23-109 of prion protein (mouse numbering)
N2a	Neuro-2a, a murine neural crest-derived cell line
NaCl	Sodium chloride
NaN ₃	Sodium azide
NaOH	Sodium hydroxide
NeoR	Neomycin resistance gene
NI	Non-infected
NMDAR	N-methyl-D-aspartate receptor
NMR	Nuclear magnetic resonance
NR2B	N-methyl D-aspartate receptor sub-type 2B
N tm PrP	PrP peptide with N-terminal half of the protein in the ER lumen

o/n	Overnight
OFCS	Opti-MEM containing 10% FCS and 1% penicillin/streptomycin
OPR	Octapeptide repeat
OPRI	Octapeptide repeat insertions
ORF	Open reading frame
PAGE	Polyacrylamide gel electrophoresis
PBS	Phosphate buffered saline
PBST	PBS containing 0.1% Tween-20
PCR	Polymerase chain reaction
PFA	Paraformaldehyde
PK	ProteinaseK
PK1	A highly RML prion-susceptible sub-clone of N2a cells
PK1moPrP ^{Ala}	PK1 cells expressing alanine-mutant forms of moPrP
PMSF	Phenylmethylsulfonyl fluoride
POPG	1-palmitoyl-2-oleoylphosphatidylglycerol
SecPrP	PrP peptide fully secreted into the ER lumen
<i>Prnp</i>	Gene encoding murine prion protein
PrP ^C	Cellular form of the prion protein
PrP ^{Sc}	Scrapie form of the prion protein (disease-associated)
PTM	Putative transmembrane domain
PVDF	Polyvinylidene fluoride
recA	Protein involved in DNA repair and maintenance
RML	Rocky Mountain Laboratory prion strain (mouse-derived)
RNA	Ribonucleic acid
rPrP	Recombinant prion protein
RT	Room temperature
<i>SalI</i>	Restriction endonuclease GTCGAC recognition site
ScN2a	Constitutively infected N2a cells
SCA	Scrapie cell assay

SCEPA	Scrapie cell end-point assay
SDS	Sodium dodecyl sulfate
SH2	Src Homology 2
ShaPrP	Syrian hamster prion protein
shRNA	Short hairpin RNA
siRNA	Small interfering RNA
<i>Sma</i> I	Restriction endonuclease CCCGGG recognition site
SOD	Superoxide dismutase
SS-C	C-terminal signal sequence
SSC	Single-cell clone
ssNMR	Solid-state NMR
Stat3	Signal transducer and activator of transcription 3
TBST	Tris-buffered saline containing 0.1% Tween-20
TC	Tetracysteine
TCIU	Tissue culture infectious units
TSE	Transmissible spongiform encephalopathy
Tris	Tris(hydroxymethyl)aminomethane
U	Units
UTR	Untranslated region
WB	Western blot
WT	Wild-type
<i>Xho</i> I	Restriction endonuclease CTCGAG recognition site

Contents

Author's declaration	2
Acknowledgements	3
Abstract.....	4
List of Figures.....	6
List of Tables	11
Abbreviations	12
1. INTRODUCTION.....	23
1.1 Introduction to Amyloids	24
1.1.1 Protein misfolding and the amyloid cascade hypothesis	24
1.1.2 Folded, unfolded and misfolded protein states	25
1.1.3 Intrinsic disorder in proteins.....	27
1.1.4 Amyloids: toxic or protective?.....	29
1.1.5 Shared features of amyloids.....	31
1.2 The prion protein.....	34
1.2.1 Sequence conservation of the prion protein.....	42
1.2.2 Toxicity of the prion protein: oligomers, protofibrils and fibrils	44
1.2.3 Prion disease: clinical manifestation	49
1.2.4 Cell models of prion disease and prion strains	50
1.3. Roles of individual domains within the prion protein.....	53
1.3.1 Charge cluster 1 (CC1) residues 23-27	53
1.3.2 Clathrin-dependent endocytosis.....	54
1.3.3 CC1 as a modulator of PrP ^{Sc} propagation	55
1.3.4 Accessory binding site to CC2	56
1.3.5 Heparin binding site.....	57
1.3.6 Octapeptide repeat (OPR) region residues 51-90	58
1.3.7 Charge cluster 2 (CC2) residues 90-111	61

1.3.8 CC2 and A β	62
1.3.9 PrP-induced neurotoxicity.....	64
1.3.10 Copper binding capacity linked to neuroprotective function.....	65
1.3.11 Regulation of prion conversion	66
1.3.12 Putative transmembrane domain (PTM) residues 111-126	69
1.3.13 Structured region C-terminal domain (126-230).....	73
1.4 Disease-associated mutations in the prion protein	77
1.4.1 Mutations in the flexible domain (residues 23-126).....	77
1.4.2 Mutations in the globular structured domain (residues 126-231).....	79
1.5 Study of epitope-tagged or labelled prion proteins	84
1.5.1 Need for unique epitopes and tagged PrP constructs	84
1.5.2 Positional insertion of tags within the PrP sequence	86
1.5.3 Biochemical nature of tags and their influence on prion propagation.....	87
1.6 Current opinions in the prion field about regions that confer prion propagation	93
1.7 Project rationale	98
2. MATERIALS AND METHODS	99
2.1 Alanine mutants of the mouse prion protein	100
2.1.1 Preparation of plasmid DNA.....	100
2.1.2 Primer design and site-directed mutagenesis	101
2.1.3 DNA sequencing.....	102
2.1.4 Plasmid DNA digest gel extraction and ligation	103
2.1.5 Preparation of transformation-competent JS4 cells	104
2.1.6 Transformation of competent cells	104
2.1.7 PCR screen for moPrP insert in pLNCX2 vector.....	105
2.2 Expressing the mouse prion protein in PK1 cells.....	106
2.2.1 Transfection of Phoenix Eco-tropic cells	106

2.2.2 PK1 cell culture.....	106
2.2.3 Dose-response curves.....	107
2.2.4 Transduction of PK1 and KD cells with retroviral supernatent.....	107
2.2.5 Single cell cloning.....	107
2.2.6 Scrapie Cell Assay (SCA).....	108
2.2.7 Harvesting cells; total protein extraction by freeze-thaw method.....	111
2.2.8 Western Blotting	112
2.2.9 Immunofluorescence analysis of moPrP expression in PK1 cells.....	113
2.2.10 Cell viability assay	113
2.2.11 Dot blot of cellular PrP expression	114
3. RESULTS	115
3.1 Generation of an alanine-mutant mouse prion protein library	116
3.1.1 Experimental strategy.....	116
3.1.2 Site-directed mutagenesis of the mouse prion protein.....	120
3.1.2 Expressing moPrP ^{Ala} in mammalian cells	126
3.1.3 Generating a PK1 cell line knocked-down for expression of moPrP.....	130
3.1.4 Reconstitution of KD cells with alanine mutants of moPrP	133
3.2 KD cells reconstituted with moPrP propagate RML prions in the Scrapie Cell Assay	136
3.2.1 Experimental strategy.....	136
3.2.2 Scrapie Cell Assay for reconstituted KD cells	137
3.2.3 moPrP deletion mutant Δ 23-88 does not support prion propagation.....	143
3.3 Polybasic region CC1 and residue 41 mediate the efficiency of prion propagation	144
3.3.1 Experimental strategy.....	144
3.3.2 Effects of charge cluster I (CC1) mutations on prion propagation.....	144

3.3.3 CC1 amino acids K23.K24.R25 are important for efficient prion propagation.....	150
3.3.4 Q41 is identified as a novel modulator of prion propagation within region 36-88 of the mouse prion protein	150
3.3.5 Propagation efficiency of moPrP mutations K23A.K24A.R25A and Q41A can be improved with increased infectious dose	153
3.3.6 Combination moPrP mutation K23A.K24A.R25A+Q41A does not have a cumulative effect on limiting prion propagation capacity	156
3.3.7 Lack of propagation in moPrP mutations K23A.K24A.R25A and Q41A is not due to lack of protein expression.....	159
3.3.8 With the exception of K23A.K24A.R25A and Q41A where prion propagation is limited, all moPrP alanine replacements in the flexible region 23-88 of the protein propagate RML fully	162
3.3.9 Role of CC1 residues K23.K24.R25 in prion propagation.....	164
3.3.11 Q41 is a novel regulator of prion propagation	171
3.3.12 Q41 has a stronger control over prion propagation than K23.K24.R25	173
3.4 Charge cluster 2 replacements reduce prion propagation	175
3.4.1 Experimental strategy.....	175
3.4.2 Charge cluster 2 mutations significantly influence prion propagation.....	177
3.4.3 Do CC2 mutations support prion propagation?.....	181
3.4.4 Cells expressing CC2 mutations in moPrP are viable	182
3.4.5 Lack of propagation in moPrP mutations within the CC2 region is not due to lack of protein expression or cell-surface localisation	184
3.4.6 Minimal mutations in prion protein CC2 significantly reduce prion propagation.....	189
3.4.7 CC2 is a solvent-exposed region of the prion protein with multiple interactors.....	193
3.4.8 Minimal segment required for efficient prion propagation extends beyond a five-amino acid sequence (100-NKPSK-104).....	199
3.4.10 Summary of mutations at moPrP region 90-111 (CC2)	204
3.5 Targeted mutations in the structured region negatively impact prion propagation	205

3.5.1 Experimental strategy	205
3.5.2 Substitution of native residues for alanine between the first β -sheet strand and the first α -helix of moPrP compromise prion propagation	207
3.5.3 Alanine mutations made between the first and third α -helices of moPrP display strong inhibition of prion propagation	214
3.5.4 Mutations made within the core hydrophobic region of moPrP to destabilise the protein lower its capacity for propagating prions.....	220
3.5.5 Integrity of the structured region 123-230 of the prion protein is necessary for efficient prion propagation	231
3.5.6 Effects of alanine mutations in α -helix 1 on prion propagation	234
3.5.7 Loop regions determine prion propagation propensity.....	235
3.5.8 Protein stability as a determinant of prion propagation	236
3.5.9 The miniprion and its implication in PrP domains required for efficient prion propagation	239
3.5.10 Summary	240
3.6 Dominant-negative inhibition of prion propagation by mutations in CC2	241
3.6.1 Experimental strategy	241
3.6.2 Single-cells clones versus bulk cultures	242
3.6.3 Clonal cell populations for alanine replacements in CC1, Q41 and CC2 of the mouse prion protein	245
3.6.4 Experimental strategy II	250
3.6.5 Lysates of RML-infected KD cells reconstituted with moPrP bearing alanine mutations in CC1, Q41 and CC2 retain infectivity and lead to prion propagation in PK1 cells.....	253
3.6.6 Expression of moPrP constructs bearing alanine mutations in PK1 cells	256
3.6.7 Expression of moPrP constructs bearing alanine mutations in chronically RML-infected PK1 (iPK1) cells	260
3.6.8 N-terminal mutations in moPrP at charge cluster regions protect cells from prion infection.....	262
3.6.9 Dominant-negative inhibition of prion propagation by residues within CC2	264

3.6.10 Alanine replacements in CC2 inhibit <i>de novo</i> formation of prions, but cannot reverse the fate of existing prions.....	267
3.6.11 Features of charge cluster regions within PrP that may contribute to regulation of prion propagation.....	269
3.6.12 Mutational analysis of the flexible N-terminal tail of moPrP reveals three distinct regions that exert varying control over prion propagation.....	274
3.7 Middle conserved region 112-135 of the prion protein may traverse the lipid bilayer	276
3.7.1 Experimental strategy.....	276
3.7.2 Scrapie cell assay analysis of mutations in residues 111-119 of moPrP	282
3.7.3 Does helix stability of the PTM region in moPrP correlate well with propagation efficiency?	290
3.7.4 Probing the PrP homodimer hypothesis.....	291
3.7.5 PTM as a determinant of PrP-membrane association	299
4. RESULTS SUMMARY, CONCLUSIONS AND FUTURE DIRECTIONS	306
4.1 Structural integrity is required for prion propagation and three sites in the N-terminal region mediate the efficacy of propagation	307
4.2 Conclusions and final remarks.....	311
4.3 Future directions.....	313
5. REFERENCES.....	316
6. APPENDIX.....	338
6.1 Mouse prion protein open reading frame as cloned in pBluescriptSK+ plasmid vector.....	339
6.2 Primers designed for the site-directed mutagenesis of moPrP.....	340
6.3 Mouse prion protein open reading frame in pBluescriptSK+ and pLNCX2	352
6.4 Mouse prion protein open reading frame (protein sequence)	353
6.5 ELISPOT revelation: plate reader visualisation	354

Chapter 1

Introduction

1.1 Introduction to Amyloids

1.1.1 Protein misfolding and the amyloid cascade hypothesis

In an optimal cellular system, all newly synthesised proteins would be made error-free, follow correct localisation patterns and never misfold. In reality, cellular systems work hard to maintain proteostasis with the help of chaperones and the proteasome network¹. There is still an underlying low error-rate in protein biosynthesis, but these are usually silent mutations with minimal effects on the finished protein product². However, as the cell ages, its protein synthesis and degradation pathways become increasingly error-prone¹. In some cases, deviation from the native protein sequence further compounds the issue, often resulting in higher propensities for protein misfolding³, exerting extra stress upon the proteasomal degradation pathway⁴.

Continued stress on the proteasomal systems lead to accumulation of misfolded, aggregated proteins: a characteristic of neurodegenerative diseases, such as Alzheimer's, Parkinson's and prion diseases. Most protein misfolding diseases appear to share mechanisms where the native protein is altered from a fully-functional soluble form, to a conformer with increased beta-sheet content and lower solubility^{5, 6}. This study is focused on the prion protein which shows a remarkable and unique ability of nucleotide-free, self-propagation in the misfolded, disease-associated state⁶.

1.1.2 Folded, unfolded and misfolded protein states

In order to grasp the flux of conformational states occupied by the prion protein from its synthesis to production of the disease-associated state, general principles of protein folding are revised. Upon protein transcription and translation, the nascent polypeptide assembles into its native folded state that allows it to exercise its encoded function. The fold adopted is determined wholly, by the amino acid sequence encoded by the protein⁷; polypeptide chains usually follow the rule of hydrophobic collapse, where core hydrophobic residues are clustered in the centre of the protein fold, leaving the charged/ hydrophilic residues to interact with the cytosolic surroundings⁷. Exceptions arise in the case of membrane-spanning proteins that have outer residues forming contacts with the hydrophobic lipid bilayer⁸. For large and complex proteins, or those with a highly hydrophobic sequence, molecular chaperones assist in assembling the protein correctly⁹. Most living cells maintain networks of chaperone proteins, which work synergistically to maintain protein homeostasis. They carry out their function by 'sensing' short segments of hydrophobicity in nascent protein chains and guide their correct folding. Protein folding can happen co-translationally, but only reaches completion upon peptide release from the ribosome¹⁰. Chaperones protect the newly released proteins from non-native interactions, both intra-protein and with existing entities of the crowded cytosolic environment⁹. Broadly speaking, there are two classes of chaperone proteins: chaperones linked in protein synthesis and chaperones triggered by stress response which work in different ways to establish the native fold of their target protein¹¹. All proteins pass certain quality-control

before delivery to their respective cellular destinations. Such checks include presence of exposed hydrophobic residues, unpaired (reduced) cysteine groups and immature glycans⁹. Proteins that escape this stringent quality-control are targeted for degradation via the proteasomal network¹¹. Build-up of misfolded proteins however, drains the proteasomal system of its maximal efficiency, slowing down the cellular machinery, eventually exacerbating the existing problem¹. If the rate of misfolding and aggregation exceeds that of proteasomal clearance, intracellular aggregates accumulate, overwhelming the pressured cellular machinery and ultimately cause cell death. This somewhat summarises the amyloid cascade hypothesis¹².

The amyloid cascade hypothesis was first proposed by John Hardy and Gerald Higgins in 1992, when describing the molecular events leading up to Alzheimer's disease¹². They suggested that following translation, improper processing of the precursor protein renders it amenable to misfolding and initiates a cascade of events that culminate in the accumulation of protein aggregates followed inevitably by neurodegeneration¹². Initial hypotheses in the field of protein misfolding centred around the belief that it is mostly proteins involved in misfolding diseases that show a propensity for aberrant folding and aggregation. Current opinions highlight the fact that all proteins have the capacity to misfold, albeit to varying degrees and various triggers can alter the probability of the protein entering such misfolding pathways¹³.

1.1.3 Intrinsic disorder in proteins

In 1935, Astbury, Dickinson and Bailey, accurately described what we now call folded and misfolded states when describing the conformation of globular proteins as native and misfolded¹⁴. A widely accepted theory then, was that proteins associated with misfolding disorders actually underwent misfolding, while other 'non-suspect' proteins were exempt from such inclinations¹⁴. Later work by Glenner, led to the discovery that biological amyloids can arise from proteins not usually associated with amyloid diseases, and a case in favour of the present-day hypothesis was born¹⁵. We now acknowledge that most proteins are soluble in nature and although they possess the potential to misfold, homeostasis is maintained unless under exceptional cellular stresses. This concept has held true for many soluble proteins that have no links to protein misfolding diseases; in fact, the process of ageing itself makes some amyloid accumulation inexorable¹⁶. Viewed through the energy landscape for protein folding, there are a multitude of conformations that a protein can adopt at the primary sequence level, allowing for correct folding through hydrophobic collapse¹⁷. As it gets post-translationally modified, it is restricted to certain folds depending on rotation of the backbone carbons in the polypeptide, steric hindrance due to glycans and bulky side chains, disulphide bridge constraints and so on. As we move down the hypothetical folding funnel, the protein has access to a much diminished scope of conformations, searching for the lowest energy state, which represents the ground state¹⁷. Free energy values around this state often correspond folded states marginally different to the ground state

which allow greater freedom for parts of the protein that execute its function¹⁸.

How do native proteins then, overcome this energy barrier to exit the ground state and enter misfolding pathways? This can occur as protein intermediates form in the folding funnel, and through non-native interactions, fall down the aggregation pathway through a random process¹⁸; the probability of this happening increases for some proteins bearing disease-associated mutations¹⁹. Equally, a small fraction may unfold to expose 'amyloidogenic' segments that form a stable nucleus which other intermediates may simulate, thus templating formation of new intermediates and attaching to one another, forming protofibrils²⁰. Repetition of this process leads to an assembly of highly ordered structures, called amyloid fibrils²⁰. One well-known example of a disease-associated protein in which fibrils are formed is the huntingtin protein. In Huntington's disease, the huntingtin protein is rich in poly-Glu repeats whose length correlates with age of disease onset²¹. Based on parameters such as protein hydrophobic content and backbone flexibility, a number of aggregation prediction algorithms have been written. These include, but are not limited to: ZipperDB²⁰, Paircoil2²², Waltz²³, TANGO²⁴, PASTA²⁵, Zyggregator²⁶, PAPA (a prion-specific algorithm)²⁷ and AMYLPRED2²⁸ for use with proteins implicated in amyloidoses. Most of them propose partial protein unfolding which exposes otherwise 'hidden' residues to solvent and form non-native interactions tallying with the notion of native fold destabilisation. The availability of bioinformatics tools in this sense is incredibly useful for scanning thousands of variations in sequence, which may not be

experimentally possible in a reasonable time-frame in a wet-lab environment, and almost unrealistic in terms of animal studies.

1.1.4 Amyloids: toxic or protective?

Interestingly, not all amyloids are detrimental. Certain cellular systems express functional amyloids and in some cases researchers believe amyloids form, so as to lower the amounts of neurotoxic pre-fibrillar forms of misfolded protein by accumulating these species into one cluster¹³. Studies on functional amyloids follow from data-mining of all intrinsically disordered proteins (IDP) available in the literature²⁹. Regions of intrinsic disorder (ID) are involved in pathways associated with regulation, signalling and control in particular^{29, 30}. Some examples of ID regions include the N-terminal domain of the prion protein³¹, N-terminal activation domain of heat-shock transcription factors³², and the C-terminal domains of α - and β -tubulin³³ binding domains. The significance of natively disordered proteins has been well studied and thought to be a prerequisite to the diversity of functions employed by the same protein; most IDPs transition from a state of disorder-to-order upon activation of function (this may be upon association to binding partners or sensing changes in the microenvironment)^{34, 35}. There are a number of advantages to possessing some degree of disorder: (i) high specificity yet low affinity reactions; (ii) one-to-many signalling; (iii) countermand steric restrictions; (iv) regulation of binding thermodynamics; (v) increased rate of specific macromolecular association; (vi) rapid protein turnover³⁵. Dunker et al. proposed The Protein Trinity Paradigm, a model for protein structure-function relations which entails the existence of three

thermodynamic protein states: ordered, molten globule, and random coil³⁶. Function of the protein is then predetermined by the presence of these states, each of which can be referred to as a 'native' state from which a multiplicity of functions can be executed, the predominant function arising from the ratio of the native states available³⁶. In the instance of the prion protein, the largely disordered N-terminus undergoes a disorder-to-order transition upon copper binding, which is achieved through coordination of the metal ions through histidine side chains³⁷; this can in turn facilitate PrP^C endocytosis in a clathrin-dependent manner³⁸.

1.1.5 Shared features of amyloids

The reigning hypothesis in the protein misfolding field is that almost all proteins can misfold and precipitate out of solution under certain conditions; this usually ends in amyloid formation²⁰. In all forms of amyloidosis recorded, this catastrophic cascade of molecular events occurs many years and often decades before disease onset³⁹. For all known amyloids, regardless of sequence, fibril formation in the offending protein is preceded by a myriad of soluble oligomers, pre-fibrillar aggregate and protofibril states⁴⁰. Varied as they may be in primary sequence, all amyloids display high β -sheet content, form stacking interactions of hydrophobic groups and hydrogen bonds at the protein backbone level, making them incredibly stable and indeed resistant to most conventional forms of protein degradation⁴⁰. Furthermore, amyloids demonstrate Thioflavin T birefringence and are positive for Congo Red staining⁵. They also exhibit templating and conversion abilities⁵.

The characteristic cross- β X-ray diffraction pattern of amyloids is seen perpendicular to the fibre axis. β -strands are normal to the long axis while the amyloidogenic segments form interdigitating side chains, forming the steric zipper of the growing fibrils⁴⁰. The fibril spine is almost always a dual β -sheet steric zipper, with the non-spine forming regions of the protein remaining natively structured. The spine is calculated to be 4.7Å along the fibrillar axis and 10Å along the equatorial axis (between the β -sheets). It is widely accepted that a short sterically complementary sequence is necessary, but not sufficient for fibril formation^{20, 40}. Additional parameters

for successful fibrillation include conformational freedom (usually achieved with the presence of glycine residues) on the protein surface. The presence of one such segment in a protein can drive fibrillation of the whole protein, provided it is properly positioned²⁰.

Another amyloid signature is the ability of protofibrils to bore holes in cell membranes^{41, 42}. This is akin to modes of bacterial pathogenesis such as crystal toxins from *Clostridium bifermentans* (α -helical conformation) or more likely, cytolysin (β -conformation) from *Vibrio cholera*, which are soluble proteins that can assemble into pore forming complexes at the cell membrane⁴³. How toxicity is elicited by protofibrils is unclear, but is thought to take effect through an assortment of factors such as glutamate dysregulation leading to excitotoxicity, ER stress and disruption of intracellular calcium levels, protease inhibition, upregulation of toxic extracellular proteins, production of reactive oxygen species, altered axonal transport, synaptic vesicle defects and loss of tight junction proteins⁴³.

Seminal work by David Eisenberg's group provided evidence of multiple tertiary forms of aggregated proteins; as the amyloids are characteristically high in β -sheet content, they may be formed by β -sheets in parallel or antiparallel register; face-to-face or face-to-back; up-up or up-down with respect to each other⁴⁰. Using their methods of categorising steric zippers, the human prion protein segment SNQNNF which falls in the loop region N-terminal to α 2, is the only known example of a class 2 zipper: face-to-face, up-up⁴⁰. This multiplicity of available conformations may provide answers to elusive traits such as the varying degrees of neurotoxicity elicited in amyloid

diseases and strain specificity in prion diseases. It is important to bear in mind however, that such experiments subject the protein sample to non-native conditions which may not always arise in a cellular context.

1.2 The prion protein

The prion protein, and specifically its propagation, has long been a topic of heated debate, as it represents the first instance of nucleic acid-free protein replication⁴⁴. The idea of protein replication in the absence of nucleic acid is not in agreement with the central dogma, which states the genetic information must be passed from DNA, to RNA, to protein⁴⁵ and not ever protein-to-protein, as is suggested in prion diseases. The most concrete evidence for this was the ability to generate infectious, conversion-supporting, peptides nucleotide-free *in vitro*⁴⁶, that demonstrated pathogenesis and transmissibility *in vivo*⁴⁷. It is well established that the native cellular protein, PrP^C, must be present for the disease-associated form, PrP^{Sc}, to form⁴⁸. Just like the amyloid precursor protein, the prion protein undergoes N-terminal cleavage^{49, 50}; mutations in the protein that reside at or around the cleavage site correspond to disease states in which amyloid deposition is observed^{50, 51}.

In prion diseases, formation of PrP^{Sc} is thought to impinge on the surrounding population of native PrP^C proteins, encouraging formation of the disease-associated conformer and essentially shifting the equilibrium in favour of PrP^{Sc}⁵². The initial conversion step is considered to be one of the earliest and most fundamental events in disease progression. The current study aims to assess the contributions of various amino acids along the length of the native moPrP sequence that promote/discourage this equilibrium shift in favour of PrP^{Sc}. Getting a better understanding of this process at the cellular and molecular level may provide insights into the

mechanism of protein-to-protein replication, thereby pin-pointing key areas that could be targeted to hinder PrP^{Sc} replication, and aid in the development of therapeutics to delay or even prevent disease onset and progression. To identify minimal residues that are crucial for this protein-to-protein replication phenomenon to occur efficiently, we generated a library of alanine mutants that essentially work as a method of removing individual side chain contributions⁵³. This was then applied in a cellular setting and target spots for prion propagation identified.

To date, the exact biological function of the prion protein remains unknown. Ablation of the prion protein gene (*Prnp*) in mice produces no stand-out phenotype, from which gene function may be inferred; the mice display 'normal' appearance and behaviour profiles⁴⁸. There is however, compelling evidence in the literature to suggest that whereas removal of the entire protein does not suppress normal cellular function, mutations or deletions within the central hydrophobic regions of the protein give rise to an inexorably neurotoxic phenotype⁴⁸. This supports a toxic gain-of-function hypothesis. Most inherited forms of the disease are found in individuals expressing a mutated version of the protein, which argues that deviation from the native sequence is not well tolerated and increases chances of misfolding in this protein⁵⁴.

Prion research in recent years has linked the native role of PrP to neural signalling networks; knockdown studies of the prion protein homolog in zebra fish resulted in increased mortality rates post-fertilisation and impaired brain development, suggesting a role of PrP^C in neurogenesis and

embryogenesis⁵⁵. The cellular function(s) for PrP may not be clear-cut, but of the many propositions put forward, oxidative stress responses^{56, 57}, metal ion transport^{37, 58, 59}, central nervous system (CNS) development and neuroprotection/neurotoxicity^{60, 61} top the list.

Although maximal localisation of the prion protein lies in neurons of the CNS⁶, it is expressed ubiquitously in the nervous system; expression pattern varies with brain region, cell type and cell biochemistry⁶. Mature PrP is found predominantly as a cell-surface protein, tethered to the outer leaflet of the lipid bilayer by a glycosylphosphatidylinositol (GPI)-anchor at its C-terminus⁶² (Figure I1); other topologies of intracellular forms of the protein (pertaining to nascent chains) have been reported to be associated with known disease-related mutations⁶³ (Figure I2). The pro-protein contains an N-terminal signal sequence, which codes for localisation at the cell membrane, while the C-terminal signal sequence encodes a motif that allows for attachment of a GPI membrane anchor. The mature prion protein is produced following cleavage of the N-terminal (residues 1-22) and C-terminal (residues 231-254) signal sequences of the pro-protein^{6, 62}. It may then be glycosylated at either/both residues Asn180 and Asn196, or left unglycosylated.

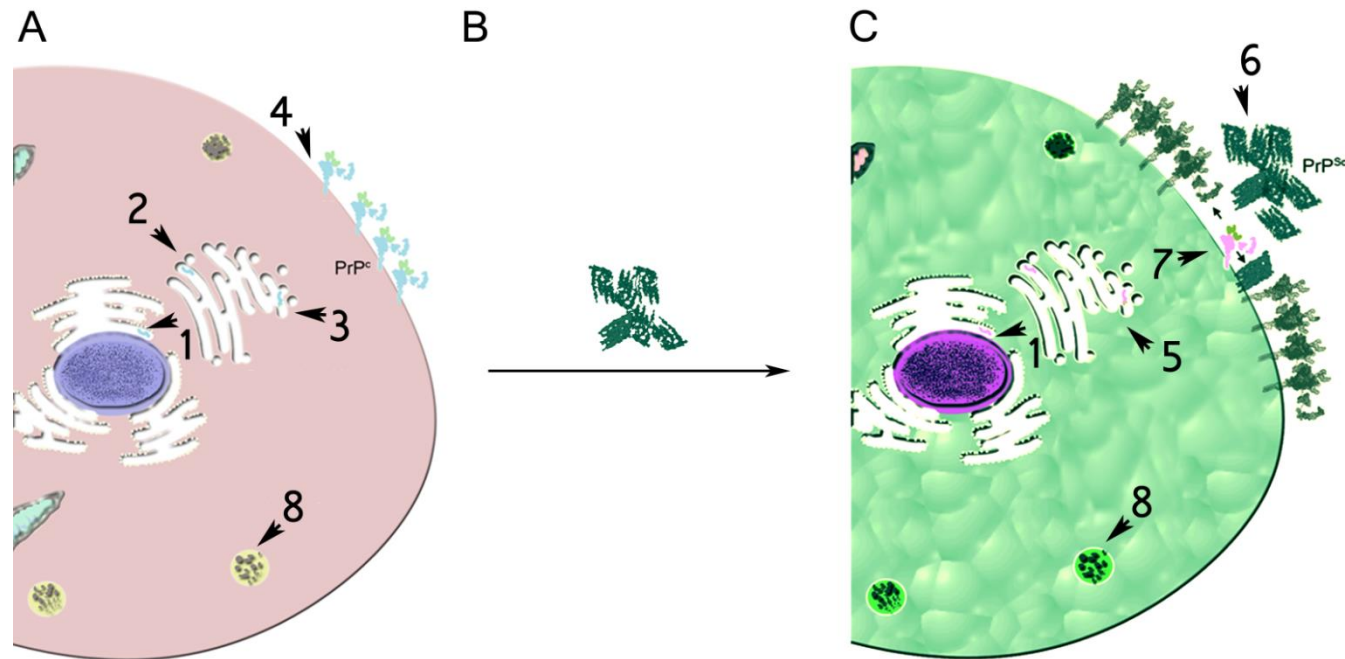


FIGURE I1: THE CELLULAR PRION PROTEIN

PrP^C is expressed on cells of the nervous system. (A) The nascent polypeptide chain is synthesised and processed, with the N-terminal signal sequence guiding protein localisation at the cell surface; the C-terminal signal sequence allows for attachment of the folded protein to the outer leaflet of the lipid bilayer using a GPI anchor. (B) When cells expressing PrP^C are subjected to infection with PrP^{Sc} (depicted in green), it is postulated that conversion of the cellular form of the protein to the misfolded (PrP^{Sc}) state occurs at the cell surface in a matter of minutes. (C) As more PrP^{Sc} molecules accumulate, propagation inevitably affects surrounding cells and prion infection is established. (1) nascent peptide trafficked from ER to Golgi for post-translational modifications; (2) N- and C-terminal signal sequences processed for cell surface localisation and GPI-anchor attachment respectively; (3) Glycosylation events; (4) Cell surface localisation; (5) Alternative topologies at the ER membrane, associated with aberrant protein forms; (6) PrP^{Sc}-PrP^C interaction at the cell membrane; (7) propagation; (8) lysosome.

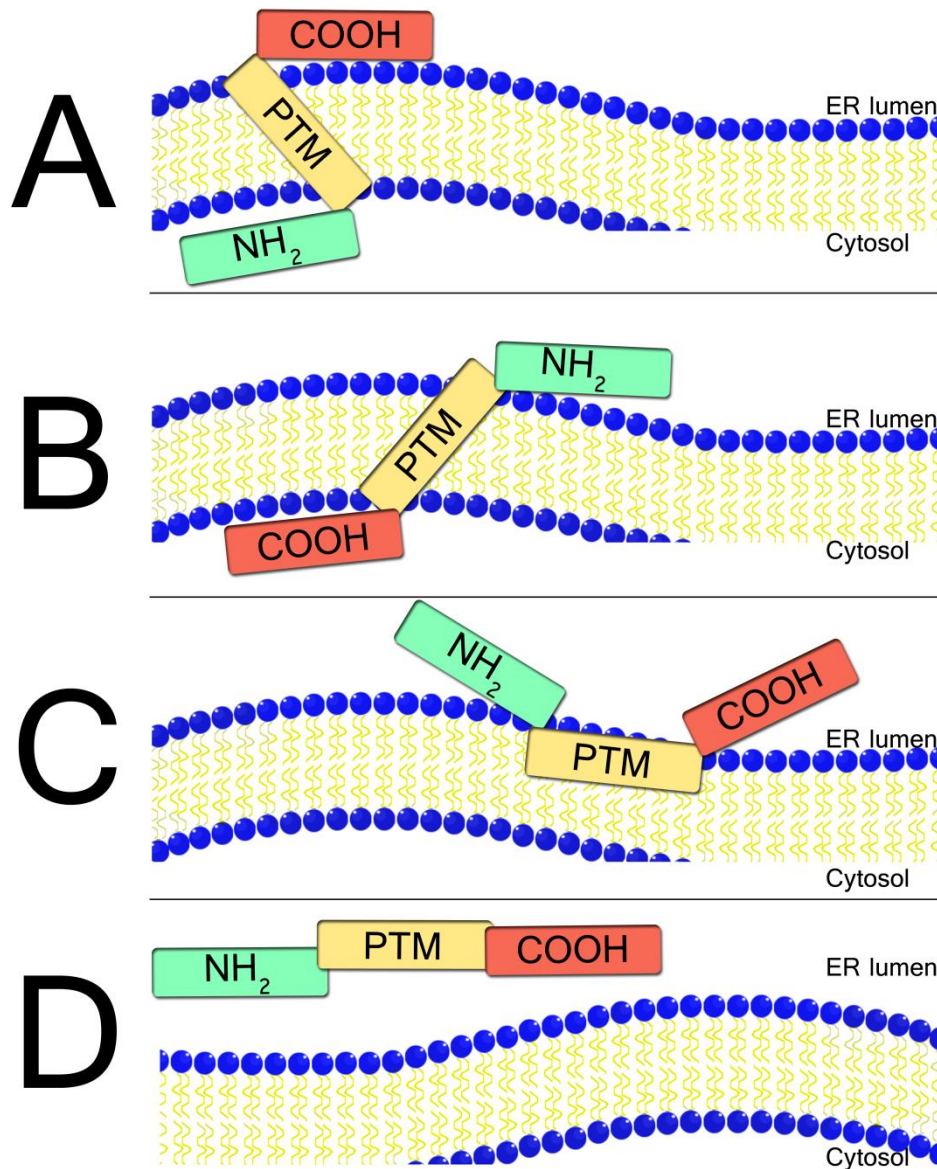


FIGURE 12: TOPOLOGIES OF THE PRION PROTEIN

A number of transmembrane forms have been reported for PrP where the protein is able to span the membrane through its putative transmembrane domain, region 111-135. Shown in A-C are various forms of PrP-transmembrane topologies, namely: (A) CtmPrP; (B) NtmPrP; (C) this alternative topology is reported by Wang F *et al.*⁶⁴, as a possible other transmembrane form; (D) the cellular, native form of the prion protein is fully translocated in the ER lumen as it is processed; this is termed SecPrP fully secreted form of the protein, ^{Sec}PrP. Other topologies of the protein are linked to prion disease states.

Variation in glycosylation gives PrP a distinct three-band pattern when analysed by Western blot, with protein bands corresponding to di-glycosylated, mono-glycosylated, and un-glycosylated PrP species.

From a structural perspective, only the cellular form of the protein has ever been acquired as a high-resolution structure, and this is limited to the C-terminal globular half of the protein⁶⁵. This structure is well defined using X-ray crystallography (residues 117-230)⁶⁶ and giving a slightly wider picture, NMR techniques (residues 90-230)^{19, 67}. The amino-proximal half (residues 23-120) of the protein is enriched with glycines, which greatly contribute to its flexibility by allowing maximal rotation of the protein backbone at these points. Additionally, resolving NMR data of the wild-type protein is complicated by the large number of possible conformations sampled in the flexible regions for accurate structure determination¹⁹.

As for the structure of the disease-associated form of the protein, the caveats remain common to all proteins involved in protein misfolding diseases: obtaining enough of the sample that is of useable quality, sample uniformity and most importantly, solubility. Nevertheless, attempts have been made to attain the ultrastructure of the misfolded prion protein conformer using methods such as electron microscopy, which do not allow detailed distinction at the atomic level, but provide an overall 3D image, outlining the electron density⁶⁸. When discussing the sequence and structure of the prion protein, it may be divided into three distinct domains: (i) the flexible, glycine rich, N-terminal domain (23-120) which encompasses two regions of charge clusters CC1 and CC2 and five octapeptide repeats

(OPRs); (ii) a highly hydrophobic region that has sequence characteristics of a membrane-traversing helix and is referred to here as the putative transmembrane domain (PTM, 110-134); (iii) and a globular structured domain (121-230) thought to be the principal proliferating component in prion disease. The following chapters bear the aforementioned subdivisions of the protein in mind (Figure I3).

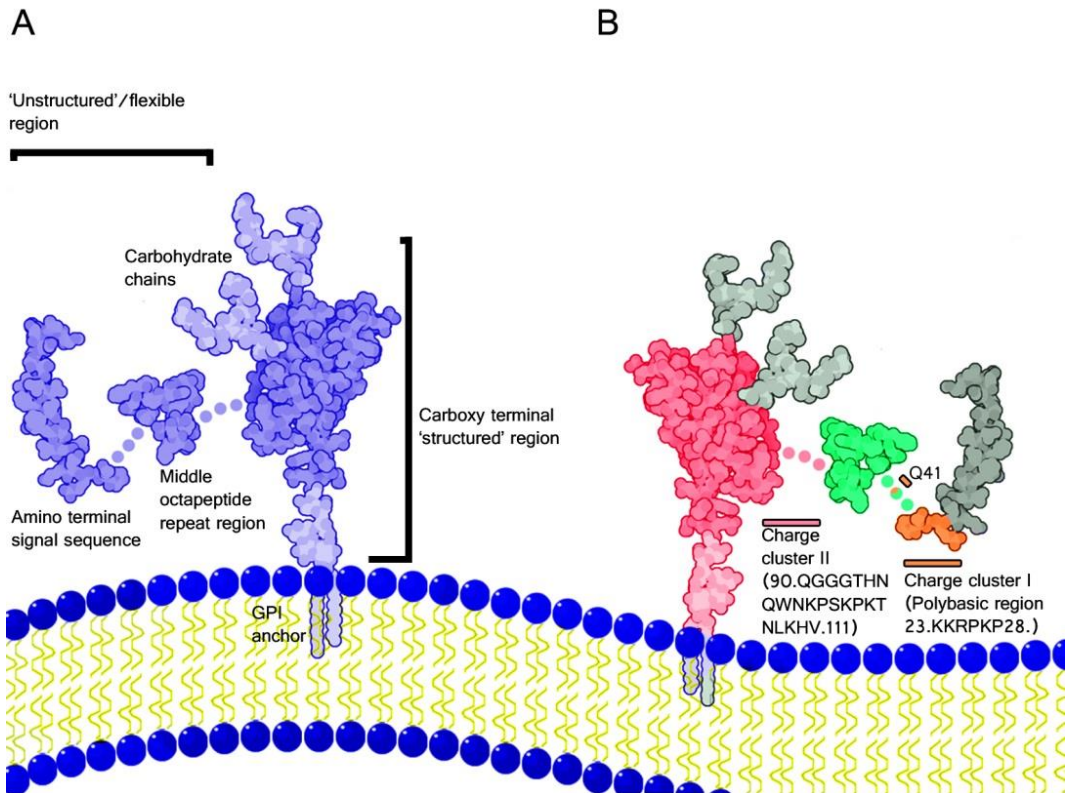


FIGURE 13: STRUCTURAL FEATURES AND DOMAINS OF THE PRION PROTEIN

(A) The folded state of PrP^C shows a doubly-glycosylated molecule (carbohydrate chains at residues Asn180 and Asn196); PrP^C can be categorised into (i) a largely flexible amino terminal domain which encompasses two charge clusters, (ii) an octapeptide region which has been linked to disease stated when there is an increase in the number of octapeptide repeats expressed, (iii) A globular structured domain that is preceded by a stretch of hydrophobic residues that bear semblance to a membrane traversing segment. (B) The carboxy terminal regions (pink) are thought to be the principle proliferating agent in prion diseases. However, there is also evidence to suggest that N-terminal segments influence the efficiency of prion infection. N-terminal regions pertinent to this study are indicated.

1.2.1 Sequence conservation of the prion protein

The prion protein is remarkably conserved across mammalian species. In an excellent paper by van Rheede et al., it was shown that protein glycosylation sites, residues across the hydrophobic core region and the cysteines that form a disulphide link between $\alpha 2$ and 3 are perfectly conserved across twenty-six mammalian prion proteins⁵⁴. Such widespread and complete conservation would suggest that these amino acids in particular play an essential role in the function of the normal cellular prion protein. Alternatively, we could reason that the strong conservation may be due to any mutations in the regions specified, being deleterious. It is interesting to consider that the species barrier phenomenon exists when there is so much sequence homology between prion protein sequences of species that are highly susceptible to prion infection such as the bank vole, and conversely, those that are comparatively more resistant, like rabbits⁶⁹. When comparing the mouse prion protein sequence used in this study to the rabbit homolog, there are a total of 22 differences in the 254 residue protein chain⁵⁴. Certainly conversion rate is achievable at high efficiencies when there is maximal sequence homology between the infectious prions and the cellular forms, but even at low homologies, it happens nonetheless albeit at a much diminished rate⁷⁰.

In vivo and *in vitro* studies have shown that the flexible region 23-88 of the prion protein can be removed altogether, without impeding PrP^{Sc} formation⁷¹. The authors of that study suggested that this effect, as it lies within the unstructured flexible part of the molecule, may be involved in

intra- or inter- molecular interactions that influence the efficiency of prion propagation⁷¹. It is emphasised nonetheless, that the overall tertiary structure is the main determining factor for PrP^{Sc} susceptibility, rather than individual amino acids⁷¹.

In the context of cell death, overexpression of apoptotic stimuli such as Bax induces cell death in neuroblastoma cells and co-expression of the full length PrP but not that lacking the OPR region reversed this Bax-mediated apoptotic event⁷². The N-terminal tail of the protein is probably a multi-functional domain of PrP^C as it is unlikely to only be randomly coiled *in vivo*³¹. Experimental evidence shows that transgenic mice with deletion of this flexible region display a phenotype of cerebellar lesions and ataxia⁴⁸. Naslavsky and others propose that the lipid environment acts as a framework supporting some defined structure for this otherwise highly flexible region^{73, 74}.

1.2.2 Toxicity of the prion protein: oligomers, protofibrils and fibrils

The cellular prion protein can misfold and assume β -sheet-rich structures which in turn contribute to fibril formation⁴⁰. Studies done as early as 1993 had identified fibril-forming regions 106-147⁷⁵ and alluded to the now widely accepted concept of the miniprion as the minimal segment of the protein required for infection: with the miniprion defined as bearing two deletions, one in the flexible N-terminal tail of the prion protein Δ 23-88 and another that entirely removes the first α -helix and second β -sheet in the structured domain of the protein, Δ 141-176⁷⁶.

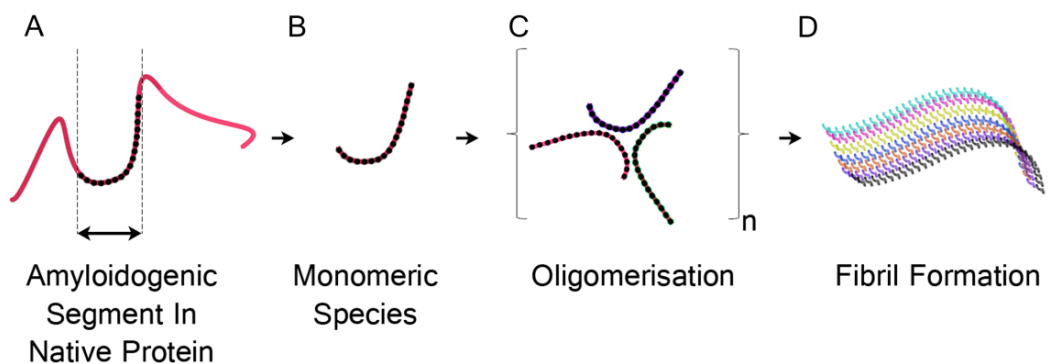


FIGURE I4: SCHEMATIC OF FIBRIL FORMATION

(A) A small segment within a protein, thought to be amyloidogenic, has a high propensity to alter its conformation to drive local conformations to a more β -sheet state. (B) When individual amyloidogenic segments are free from self-association they are referred to as monomeric species, and (C) Oligomers when they form self-associations. (D) Propagation of such self-assemblies, leads to fibril formation.

The same laboratory showed that synthetic peptides of human PrP (huPrP) sequence 106-126 which encompasses the PTM domain formed straight fibrils similar to those found in the brains of Gerstmann-Sträussler-Scheinker syndrome (GSS) patients, whereas peptides corresponding to β 1- α 1 (sequence 127-147) formed twisted fibrils resembling scrapie-associated fibrils isolated from patients with Prion diseases⁷⁵. Peptides corresponding to the PTM domain or β 1- α 1, but not OPR (residues 57-64) or CC2 (89-106), were only sparingly soluble in water and readily formed fibrils⁷⁵. The amyloid core was further delineated to residues 127-143 in an amyloid seeding assay by Chatterjee *et al.*, who showed using recombinant mouse prion protein (moPrP) that fibrils formed from region 127-143, but not 107-126 were able to seed amyloid fibril formation in the full length peptide, moPrP 23-230⁷⁷.

PrP can form long straight 8 – 10nm-wide amyloid fibrils at under neutral pH, salt and denaturant conditions; smaller fibrils are formed under more acidic conditions (2nm) and are associated with a higher toxicity potential in amyloid diseases⁷⁸⁻⁸¹. β -rich oligomers formed from recombinant moPrP are composed of monomers, as well as small and large oligomers⁷⁸⁻⁸¹. All three species of aggregates described irrespective of their morphological and mass differences, were shown to be capable of eliciting toxicity by disrupting cell membrane integrity⁸², a common feature of amyloids⁸³. It is not known whether the cellular toxicity elicited in prion diseases is a matter of PrP^C dysregulation leading to atypical and detrimental signalling interactions, or a result of PrP^{Sc} formation and propagation. It is clear

however, that once fibrils are formed, for propagation to ensue, pre-formed fibrils must dissociate in order for further fibril formation to proceed^{84, 85}.

Hydrogen-deuterium exchange (HDX) experiments on the aggregated proteins illustrated that residues between $\beta 2$ and $\alpha 2$ are at the start of the amyloid core⁸⁶. Additionally, worm-like fibrils display a higher degree of HDX protection suggesting that these forms of aggregates are more ordered and compact than the oligomeric forms. The moPrP sequence spanning $\alpha 2$ - $\alpha 3$ forms the core of both small and large oligomers, with formation of worm-like fibrils linked to the expansion of this core region⁷⁸. The primary difference between the straight fibrils and the worm-like ones is the presence of, or lack of a continuous stretch of core sequence respectively⁷⁸. PrP domains PTM, $\alpha 1$ - $\beta 2$ and to a lesser extent region 32-55 (between CC1 and OPR1), are also shown to be structured in the aggregated forms, but with much lower stability than the C-terminal domain⁷⁷. Most structural studies of PrP use N-terminally truncated proteins, so the finding that region 32-55 possesses structure and can adopt multiple conformations in the worm-like fibrils could implicate the flexible region of the protein in important functions of PrP^C stability and PrP^{Sc} assembly⁷⁷. Indeed, a study by Qi *et al.* highlighted the role for the flexible region N-terminal to CC2 as being important for propagation of prions, as they observed fibril dissociation in full length recombinant protein, but not in a $\Delta 23$ -90 mutant⁸⁷. They hypothesised that the flexible N-terminal tail of the protein (missing in the $\Delta 23$ -90 mutant) could contribute to charge repulsion between CC2 and pre- $\alpha 1$ regions, following protonation (acid-induced) of the histidine side chains at OPR and CC2, and promote fibril dissociation⁸⁷. Norstrom and Mastrianni

studied a PrP construct with a deletion in the palindromic sequence 112-AGAAAAGA-119 and found it to be aggregation-compatible⁸⁸. Altering the polarity within this sequence was found to reduce the stability of the hydrophobic core and consequently its ability to fibrilise when alanine residues were replaced by serine groups⁸⁸. Additionally, Walsh, Simonetti and Sharpe undertook rigorous tests to show by ssNMR that segment 102-126 forms in-register parallel β -sheets, stacked in an anti-parallel fashion⁸⁹. The PTM region is purported to form a tight inter-digitating interface between the β -sheets⁸⁹.

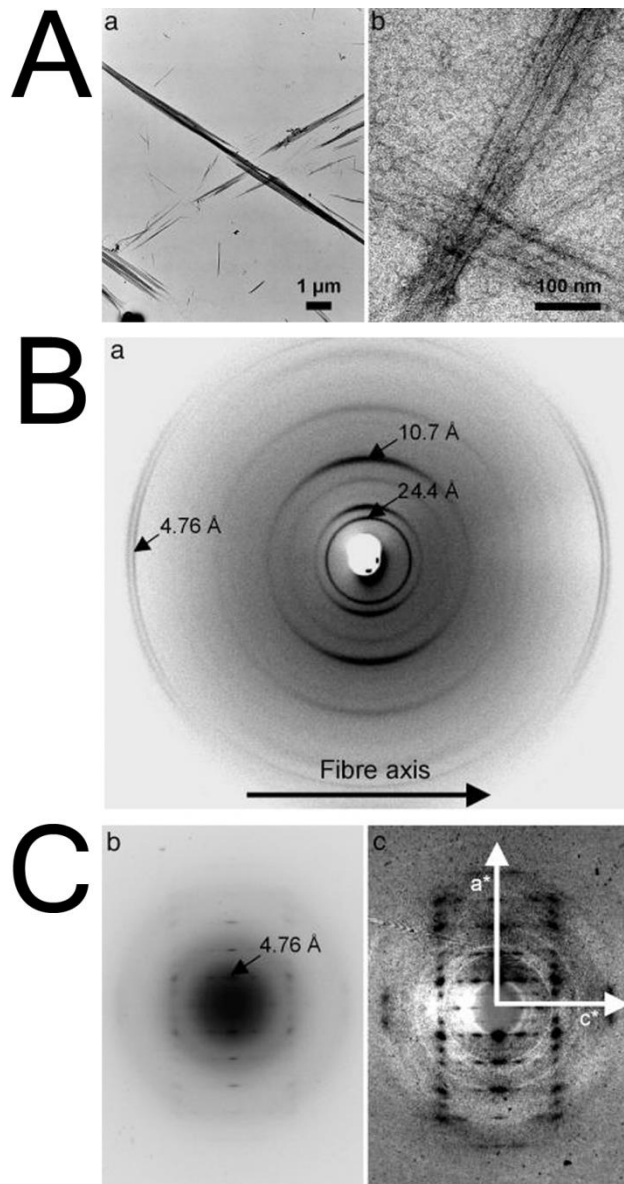


FIGURE 15: B-SHEET STRUCTURE OF AMYLOIDS

Electron micrographs of fibrous crystals of peptide AAK incubated in PBS. (A) Negative-stain transmission electron microscopy shows fibrous crystals in a field view at low magnification (left) and at higher resolution showing striations running parallel to the fibre axis(right). (B) X-ray diffraction pattern obtained by synchrotron radiation from partially aligned, bundled fibres. (C) Electron diffraction patterns obtained with incident beam parallel to the [0 1 0] zone axis showing high resolution crystalline order pre- (left) and post- (right) contrast enhancement. Adapted from Makin *et al.*⁹⁰

1.2.3 Prion disease: clinical manifestation

Prion diseases are not immediately apparent in patients suffering from them, as they have remarkably long periods before any noticeable signs appear. This is referred to as a long incubation time⁶. Patients often present with early symptoms of depression, anxiety, memory impairment, insomnia, compromised motor coordination, erratic behaviour, fatigue and visual disturbances⁴⁴. These symptoms can vary between patients and disease can be remarkably difficult to diagnose as it is often misdiagnosed for other neurodegenerative diseases such as Alzheimer's and Huntington's disease^{44, 91}. Once successfully diagnosed however, better scales for monitoring prion disease severity have been established⁹². As the disease progresses patients show signs of muscle paralysis, slurred speech, difficulty with swallowing, dementia and even coma. There is marked clinical heterogeneity in prion disease and though not fully understood, they correlate to some extent with the type of prion disease that is active: variant, iatrogenic, Kuru, inherent or sporadic⁹². The 'spongiform encephalopathy' nomenclature in TSEs comes from the sponge-like appearance in the brains of deceased prion disease patients⁵¹. These 'holes' are caused by cell death amassed over time, most frequently in the cerebellar regions of the brain with focal Purkinje cell loss, moderate loss of granular layer cells and gliosis of the astrocytes and Bergmann glia⁹³. Visualised by immunohistochemistry, dense amyloid plaques and inclusions can be identified in patients with prion disease; however, the nature varied with prion disease type⁹³.

1.2.4 Cell models of prion disease and prion strains

PrP^{Sc} arises from a conformational change in PrP^C that favours a higher β -sheet structure⁵. In turn, the type of PrP^{Sc} that forms and the ease with which this occurs depends on the sequence similarity between the infectious protein and the cellular protein⁹⁴. Moreover, PrP^{Sc} forms can differ in (i) their infectious capacities depending on cell line (tropism); (ii) glycoform ratios expressed; (iii) incubation times; (iv) resistance to ProteinaseK. These biochemical features define prion strains⁴⁶. Typically, the PrP^{Sc} formed in cells *de novo* is identical to the form used to initially infect the population of PrP^C expressing cells. This is known as faithful propagation: the strain type is preserved⁹⁴.

When PrP^{Sc} proliferates in mammals, the term prion diseases define the malady in humans, Bovine Spongiform Encephalopathy (BSE) in cattle, Scrapie in sheep and Chronic Wasting Disease (CWD) in deer and elk. For research purposes, these prion strains are often serially mouse-passaged so as to make them infectious to murine cell lines and study their properties through both cell culture and transgenic mouse models^{48, 95}. RML is a mouse-adapted prion strain derived from sheep infected with Scrapie by W. Hadlow at the Rocky Mountain Laboratories in Hamilton, Montana⁹⁶. This strain is used extensively in prion research along with 22L and Me7 strains, when studying mouse prions as it has the ability to infect a multiplicity of cell lines compared to other available strains (Table 1) and propagate faithfully^{95, 97}. Since cells of the nervous system are predominantly the target of PrP^{Sc}, neuronal cell types such as N2a, SHSY-5Y, GT1, PC12 and SN59

are widely used as cell culture models in prion research, with a number of non-neuronal cell types such as LD9 and CAD5 to study peripheral infection^{98, 99}. N2a cells are particularly susceptible to prion infection when the inoculum is from mouse-adapted strains as they were originally derived from a spontaneous mutation in A/J mice, a *Prnp*^{a/a} (allele of the mouse prion gene associated with short incubation times: Leu108, Thr189) mouse strain^{96, 97}.

GT1 cells originate from hypothalamic neurons immortalised by genetically targeted tumourigenesis in transgenic mice. It appears as though GT1 cells are more readily infected than standard N2a cells and retain infectivity for a longer passage than N2a cells. They are also the only CNS-derived population of cells susceptible to prion infection⁹⁹. Nonetheless, N2a cells can be cultured to be 80-90% infectious maintaining susceptibility and producing high infectious titres^{95, 97}; N2a cells have been tremendously useful in researching prion biology and available within the MRC Prion Unit as: (i) subclones that are highly susceptible to RML prions (PK1); (ii) silenced PK1 cells for suppression of endogenous PrP^C expression (KD) and (iii) chronically infected PK1 cells (iPK1)⁹⁷. PK1 cells report sensitivity to RML prions at a thousand fold higher than non-cloned cells⁹⁷. KD lines suppress the expression of endogenous PrP^C via maintenance of shRNA that binds the 3' Untranslated Region (UTR) of *Prnp*. iPK1 represent Scrapie-infected PK1 cells that persistently propagate PrP^{Sc100}.

Cell line derivation	Neuroblastoma (neural crest)	Neuroblastoma (hypothalamus)	Neuroblastoma (N2a subclone)	Fibroblast (connective tissue)	CNS (catecholaminergic neural tumour)
Prion Strain	N2a	GT1	PK1	LD9	CAD5
RML	Light red	Light red	Dark red	Light red	Light red
Me7	White	White	White	Dark red	Light red
22L	Light red	Light red	Light red	Light red	Dark red
139A	Light red	Light red	Light red	Light red	Light red
Chandler	Light red	Light red	White	White	White
FU	Light red	Light red	White	White	White
SY	White	Light red	White	White	White
C506	Light red	White	White	White	White
22F	White	White	Light red	Light red	Dark red

TABLE I1: PRION PROTEIN STRAINS AND THEIR PROPAGATION IN CELL CULTURE

A wide range of prion strains and cell lines are used in prion research; only a subset of these have been shown for clarity. White spaces are indicative of an 'incompatible' combination where the cell line is resistant to infection from the prion strain and accents of red represent the strength of the strain-cell line compatibility.

1.3. Roles of individual domains within the prion protein

1.3.1 Charge cluster 1 (CC1) residues 23-27

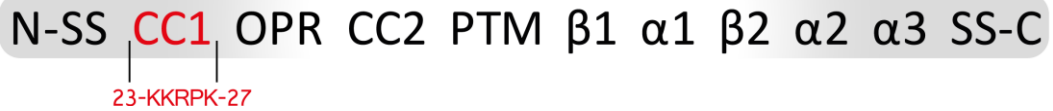


FIGURE I6: CC1

Schematic of the prion protein with its various domains; N-SS: N-terminal signal sequence; CC1: charge cluster 1; OPR: octapeptide repeat region; CC2: charge cluster 2; PTM: putative transmembrane region; α1: helix 1; β1: strand 1; α2: helix 2; α3: helix 3; SS-C: C-terminal signal sequence. Highlighted in red are residues of CC1.

When compared to the rest of the protein, the flexible unstructured region of the prion protein is responsible for the highest number of interactions or association to various cellular factors³¹. This may be because of the inherent flexibility within the 23-111 domain, allowing this region greater access to these components; it may also be due to charge interactions arising from CC1 and CC2³¹. The majority of molecules that bind this region are reported to affect the cellular form of the prion protein in a number of ways, including: conformational preference¹⁰¹, endocytosis^{37, 102}, reactive oxygen species (ROS) response⁵⁰, metal binding³⁷, GAG binding¹⁰³, tubulin binding^{33, 104}, Aβ interactions¹⁰⁵⁻¹⁰⁷ and lipid binding^{73, 108} to name but a few.

1.3.2 Clathrin-dependent endocytosis

One of the earliest indications of prion protein recycling between the plasma membrane and the endocytic compartments came from the Harris laboratory in 1994¹⁰⁹. They showed, using immunogold labelling of chicken PrP, up to five-fold higher expression within clathrin-coated vesicles in neuroblastoma cells¹⁰⁹. This experiment was later repeated by the same group using the mouse prion protein and the N-terminal region of the protein was deemed essential for endocytosis via clathrin-mediated pathways¹¹⁰.

CC1 consists of basic residues that are fundamental to endocytosis via coated pits^{38, 110}. It is usual for GPI-anchored proteins that are devoid of any cytoplasmic segments, to engage in endocytosis through extracellular binding of transmembrane receptors, which possess the required endocytosis motifs¹¹¹; CC1 may therefore regulate some aspects of PrP^C recycling via this mechanism, with an as yet unidentified transmembrane receptor¹¹².

Transgenic mice expressing PrP with a large N-terminal deletion, Δ 23-88, were able to propagate PrP^{Sc} and though this evidence might appear to nullify the role of CC1 in prion protein recycling, it is not the case if CC1 is only partially responsible for recycling, with compensatory mechanisms at hand to handle proper trafficking in the CC1 deletion mutant^{48, 102}. For example, low-density lipoprotein receptor-related protein 1 (LRP1) has been shown to regulate PrP^C endocytosis via CC1 interactions. Additionally, heparin sulphate proteoglycans have also been shown to co-internalise with

PrP^C in N2a cells, following addition of copper ions to stimulate PrP endocytosis¹¹³.

1.3.3 CC1 as a modulator of PrP^{Sc} propagation

The concentration of positive charge in this cluster is thought to act in synergy with CC2 in a number of instances where PrP^C interacts with itself and other cellular factors^{114, 115}, including A β (Section 1.4.2)¹⁰⁷. With respect to prion propagation following infection, deletion mutants in CC1 are found to exhibit higher protein expression compared to wild-type controls, presumably due to lower rates of internalisation¹¹⁵. When analysed by immunoblotting, CC1 deletion mutants of PrP^C gave rise to markedly lower levels of ProteinaseK-resistant forms of the protein than wild-type controls, when scrapie-infected cells were transiently transfected with plasmids encoding these constructs¹¹⁶. Furthermore, transgenic mice expressing CC1 deletions had longer survival times and expressed less ProteinaseK-resistant material than those expressing the wild-type sequence following RML scrapie infections^{48, 116}. Still, once PrP^{Sc} was formed from a CC1 deletion mutant, this was able to infect susceptible cells with the same efficiency as wild-type PrP^{Sc}¹¹⁶. The authors highlight the importance of this region in the initial PrP^C-PrP^{Sc} interaction and state that the reduced PrP^{Sc} in the CC1 deletion state is not a result of differential trafficking or localisation of the mutant protein¹¹⁶. Another way to view this phenomenon is in light of evidence implicating CC1 as an essential factor governing the overall prion protein fold¹¹⁷. In CC1 deletion mutants of PrP, the protein was reported to have reduced conformational stability. Moreover, in the

presence of salt PrP lacking CC1 showed a greater loss of stability than its full length counterpart, indicating that the small charged region CC1 can make an impression on the overall fold of the globular protein; though physically distant in sequence they may come into close spatial proximity in cellular settings¹¹⁷.

1.3.4 Accessory binding site to CC2

The concentration of positive charge in the CC1 cluster is thought to act in synergy with CC2 in a number of instances where PrP^C interacts both with itself and other cellular factors. These include proteins involved in neural growth and neurogenesis, neural cell adhesion, neurosignalling, apoptosis and protein folding^{55, 107, 116-120}. In the case of A β binding, the A β peptide is thought to bind PrP^C primarily at CC2, with binding also influenced by CC1¹⁰⁶. The KKRP stretch of sequence was shown to influence β -secretase activity on the amyloid precursor protein (APP): only the full length form of the protein, not CC1-deleted PrP^C, was shown to inhibit APP cleavage at the cell surface^{121, 122}. Earlier work reporting interactions between these proteins was carried out on recombinant proteins using biophysical approaches. Recent publications on cellular interactions between A β and PrP have accelerated the interest in this field⁶¹. Whether region 23-31 is important in mediating A β toxicity is yet to be established, but mouse models deleted for this region of PrP have been generated and could be tested to this end¹¹⁶.

1.3.5 Heparin binding site

CC1 displays strong binding to highly sulphated glycosaminoglycans (GAGs), namely heparin^{103, 113, 123}. GAGs are highly charged polysaccharides found on the surface of most extracellular matrix proteins. Several GAG binding domains have been identified in the N-terminal tail of PrP^C, including CC1 with interactions at Lys 23, Lys24 and Lys27¹¹³. The other heparin binding domains on PrP^C were found to lie in the OPR and CC2 region¹¹³. Pan et al. showed that the PrP-heparin interaction is lost in a PrP Δ 23-25 deletion mutant¹⁰³ whereas others suggest that this interaction is required for the successful incorporation of PrP^{Sc} into cells¹²⁴.

1.3.6 Octapeptide repeat (OPR) region residues 51-90

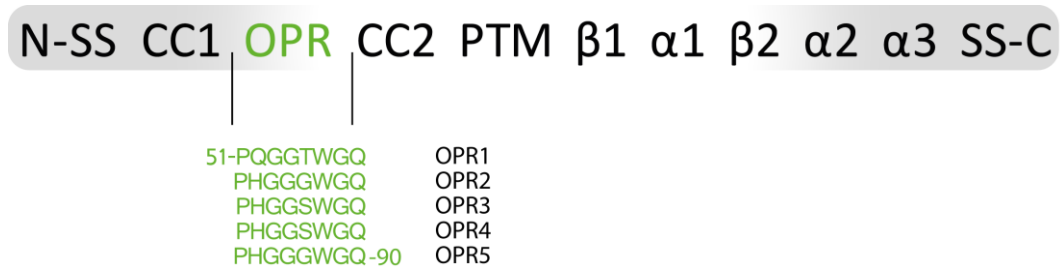


FIGURE I7: OPR

Schematic of the prion protein with its various domains; N-SS: N-terminal signal sequence; CC1: charge cluster 1; OPR: octapeptide repeat region; CC2: charge cluster 2; PTM: putative transmembrane region; α1: helix 1; β1: strand 1; α2: helix 2; α3: helix 3; SS-C: C-terminal signal sequence. Residues within each of the five OPRs are indicated by single letter amino acid.

Often associated with an expansion of repeats, the octapeptide repeat (OPR) region is one of most heavily studied sections of the prion protein. Five repeats of a glycine-rich, eight-amino acid sequence is found within residues 51-91 (human numbering) in healthy individuals. Anywhere between one and nine additional octapeptide repeat insertions (OPRI) have been found in patients with Creutzfeldt-Jakob disease (CJD) and this insertion is thought to increase the risk of developing the disease with most cases showing earlier signs of disease onset compared to cases of sporadic or inherited prion disease. The average age of onset for people bearing one to four OPRI is 64, while this decreases dramatically to 38 for those with five or more OPRI⁵¹.

Indeed PrP^C with additional OPRs has been shown to have a strong propensity to aggregate and form amyloids¹²⁵; increased OPR insertions directly impact the hydrophobic content of the sequence and this is thought

to promote disorder at the N-terminus¹²⁶. Using circular dichroism spectroscopy Leliveld et al. were able to demonstrate that OPR expansion impacted the PrP folding landscape by upregulating certain misfolding pathways, rather than hampering production of the natively folded form of the prion protein¹²⁷. Deletion mutagenesis studies in this region of the protein have been plentiful and most conclude that the OPR region can be disregarded in terms of generating PrP^{Sc} from PrP^C¹²⁸. Its significance in OPRI therefore remains abstruse; we may speculate that the extended conformation of the flexible N-terminal tail region alters physiological inter/intra-protein interactions that afford it a higher misfolding propensity, or that it alters the native function of neighbouring domains in the protein.

The most remarkable feature of the OPRs is their copper binding and copper transport abilities^{37, 129}; this is attributed to histidine side chains between the repeat regions that coordinate copper ions¹²⁹. Copper binding to PrP^C which occurs in a concentration-dependent manner is thought to both increase rate of protein endocytosis and provide neuroprotection against oxidative stress¹²⁹. PrP^C endocytosis upon copper binding has been shown in cells expressing wild-type PrP, as well as recombinant PrP (rPrP) with up to seven OPRI, but this is constrained in PrP with eight or more OPRI¹³⁰. Interestingly, once the OPRI approach eight, copper binding affinity is ten-fold tighter. The prion protein is reported to have at least five copper binding sites, four of which lie in the OPR region and the fifth in histidine residues of the CC2 domain. Copper-binding activity of PrP^C is reported to increase its aggregation tendency at lower than physiological temperatures, in a reversible manner¹³⁰. Copper-bound PrP^C adopts a

slightly different morphology to its unbound equivalents, as it brings CC2 in close proximity to $\alpha 1$ and the loop region preceding this helix. Additionally, $\alpha 2$ was purported to interact with the fifth repeat in the OPR region¹³¹. If both of these reported long-range interactions occur as reported by the authors are observed upon copper binding in the protein, it would exhibit a much more compacted state than the metal-free form of the protein and may bear some significance on the susceptibility of infection by PrP^{Sc}¹³¹. Suffice to say, the OPR region imparts no crucial feature for PrP^{Sc} propagation that could be demonstrated experimentally, but facilitates the process upon initiation of conversion¹³¹.

1.3.7 Charge cluster 2 (CC2) residues 90-111

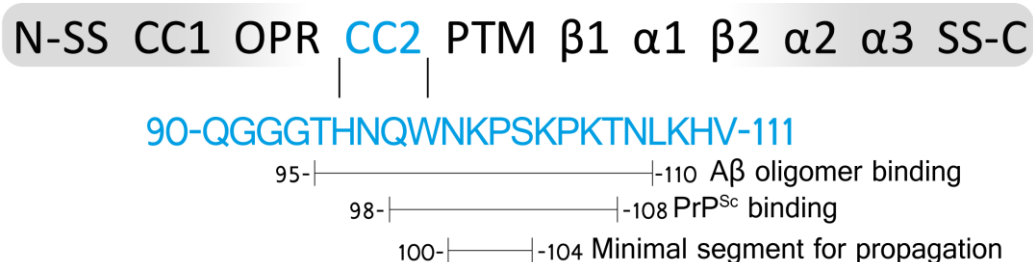


FIGURE I8: CC2

Bar schematic of domains within moPrP. N-SS: N-terminal signal sequence; CC1: charge cluster 1; OPR: octapeptide repeat region; CC2: charge cluster 2; HC: conserved hydrophobic region; α1: helix 1; β1: strand 1; α2: helix 2; α3: helix 3; SS-C: C-terminal signal sequence. Charge cluster 2 (CC2) is defined as region 90-111. Amino acids 95-110 within CC2 are reported to bind Aβ oligomers^{105, 132}. Residues 98-108 on PrP^C are believed to interact with PrP^{Sc133}. Residues 100-104 when were found to be the minimal sequence that mediates conversion of the prion protein from PrP^C to PrP^{Sc134}.

This region is one of the most immunogenic parts of the protein, with many anti-prion antibodies raised against CC2: PrP-AA (105-109)¹³⁵; 3F4 (109-112); 6D11 (93-109)¹³⁶ and ICSM35 (91-111)¹³⁷. The high charge content of this region makes it amenable to a multitude of protein interactions, further aided by the flexibility of the N-terminal tail^{35, 138}. CC2 is reported as the interaction site for Aβ oligomers^{107, 132, 139}, is suggested to be involved in heparin binding interactions^{103, 113} and believed to mediate the rate of conversion to PrP^{Sc}, amongst other functions¹¹⁶.

1.3.8 CC2 and A β

Both PrP^C and A β are concentrated at synaptic boutons and bind with nanomolar affinity^{61, 139}; a strong case for their interaction is the finding that PrP-knockout mice show full immunity to Alzheimer's disease¹⁰⁵. Moreover, several studies have shown that treatment with antibodies raised against the CC2 region of PrP^C protect against several A β -induced deleterious effects, including synapse loss as well as memory and learning impairment⁶¹. High-affinity interactions between the two proteins have been published by many groups and been established reproducibly in biophysical settings^{132, 139}; it is widely accepted that PrP^C binds the oligomeric and not the monomeric form of A β . Fewer instances of this interaction have been reported in a cellular framework: in COS-7⁶¹ and SH-SY5Y cells¹⁰⁸, and in cultured hippocampal neurons¹⁰⁷. A β binds PrP^C primarily at CC2, with accessory sites reported at CC1 and Helix1^{106, 132}. Laurén et al., have mapped region 95-110 of PrP^C as the prerequisite for A β binding, showing that anti-prion antibody 6D11 directly competes with A β for PrP¹⁰⁵. Fluharty and colleagues have also shown that the flexible amino terminal region is both necessary and sufficient for binding early oligomeric intermediates during A β maturation into amyloid fibrils¹⁰⁷.

Many lines of evidence show that PrP interacts with A β primarily through its CC2 domain although this is not the only binding site^{105-108, 139}. More recently, Kang et al. reproduced this finding, reporting PrP^C region 93-119 as the main A β binding domain using an ELISA-based method¹⁴⁰; binding activity was also assigned to CC1 (residues 23-39)¹⁴⁰. These two sites

interacted with PrP^C independently in this study, but have been previously shown to act synergistically¹³². Reversal of the ELISA set-up as tested by Kang et al. involved anti-A β antibody binding to PrP^C but the interaction site could not be delineated¹⁴⁰. Interestingly, five out of forty-four 17-mer peptides corresponding to PrP sequence could not be generated due to their aggregation propensity; three of these correlate to the CC2 region, one at a loop region N-terminal to helix 1 and lastly a loop region between helices 2 and 3¹⁴⁰. These regions may therefore interact with the rest of the PrP^C molecule or other cellular factors to avoid spontaneous aggregation in healthy cells. CC1's role as a secondary site may be ascribed to the polybasic residues KKRPK. Aside from the charge dependence of A β binding CC1 and CC2, it is also reliant on the length of sequence between these two regions¹⁰⁶.

1.3.9 PrP-induced neurotoxicity

Interactions between PrP^C and A β go hand-in-hand with cell toxicity. They have been found to co-internalise, accumulate in endosomes and traffic to lysosomes in an LRP1-dependent pathway¹⁰⁸. There is gathering evidence to suggest that A β -induced cytotoxicity is mediated by PrP^C in Alzheimer's disease^{107, 139}. More debated however, is how exactly this toxicity is regulated: directly, indirectly, and through which molecular intermediates. PrP^C is able to inhibit the enzyme β -secretase, which is responsible for APP cleavage N-terminal to the A β domain and thereby leads to amyloidogenic processing of APP¹⁴¹. It has been shown that PrP-A β binding triggers activation of Fyn kinase, which has in turn been shown to phosphorylate the NR2B subunits of NMDARs, resulting in calcium influx and subsequent cytotoxicity^{61, 108}. Larson et al. also showed that active Fyn can phosphorylate tau; phosphorylated tau and A β being the two main toxic species in Alzheimer's disease, points to PrP as the link between these disease-linked entities¹⁴². PrP^C is purported to trap misfolded A β in an oligomeric form at CC2¹³⁹ – it is tempting to hypothesise a native cellular function for the high affinity interaction between these two proteins, as it cannot be completely attributed to charge interactions, especially as there is so much potential for misfolding and toxicity¹³. When examining A β oligomer-induced toxicity, the N1 fragment of PrP^C (encompassing CC1 and CC2) is able to block this toxicity by binding to the assumed toxic fragment (residues 106-126)¹²¹. PrP^C overexpression in N2a cells was shown to down-regulate tau protein via the Fyn pathway; an effect which can be regulated by A β oligomers¹⁴³. Resenberger et al. also demonstrated binding

of PrP to various β -sheet conformations, including A β oligomers, and found that toxic signalling elicited by this initial binding was mediated by N-terminal residues⁶⁰.

1.3.10 Copper binding capacity linked to neuroprotective function

PrP-copper interactions are well-established and occur at multiple sites on the protein^{37, 129}. This binding is pH-dependent and at CC2 is regulated by imidazole rings at His95 and His110 and deprotonated amide groups forming five-, six, or seven-membered rings³⁷. As mentioned, CC2 is a heparin binding site¹¹³ and interestingly, copper coordination enhances heparin binding to PrP^C instead of competing for the same binding site^{123, 124}. Brown et al. depicted the native role of PrP^C as a superoxide dismutase (SOD) that converts superoxide radicals to peroxide and oxygen; however this proposal is not without controversy^{37, 130}. They argue that the amount of copper associated with PrP^C depends on the concentration of the ions in the protein's microenvironment; binding capacity tested in cell culture is reached at four copper ions per molecule of PrP^C¹³⁰. No SOD-like activity of the protein was observed when PrP^C was singly occupied by copper, but this activity was present upon coordination of more copper – a phenomenon which can be inhibited by the presence of the neurotoxic PrP peptide fragment 106-126¹³⁰.

However, this was not seen by either the Aguzzi or Jackson groups who reported an absence of SOD-like activity of PrP^C^{144, 145}. What is universally agreed upon by prion researchers is that PrP^C displays specific copper-

binding activity; more debated is whether this binding regulates signal transduction, copper sensing and homeostasis, apoptosis, neurogenesis or a combination of these³⁷. Some have even argued that copper coordination may influence prion conversion, owing to the copper binding site at His95 proximal to the proteolytic cleavage site¹²⁹. Although depleting cells of PrP^C appears to have no discernible effects, it may be seen to lower the threshold of stress levels cells are able to tolerate¹³¹. Supporting this theory is the evidence that PrP^{Sc} added to cells inhibits copper binding to endogenous PrP^{C146}, while cross-linking PrP^C with monoclonal antibodies triggers rapid neuronal apoptosis¹³³.

1.3.11 Regulation of prion conversion

PrP^C expression is compulsory for PrP^{Sc} formation⁴⁸. Rate of conversion is determined by primary sequence identity⁶⁹, rate of PrP^C turnover⁹⁴ and lipid environment¹⁴⁷ amongst other considerations; one such mediator is the availability of CC2 on PrP^C for PrP^{Sc116}. The significance of lipids in PrP^{Sc} formation has been well-documented. There are well-known co-factors reported to aid formation the infectious agent^{64, 74, 120}. Many approaches to study PrP use recombinant proteins in denaturing and refolding experiments; infectivity attributed to rPrP amyloid fibres is much reduced compared to PrP^{Sc} and this may be explained by the misfolded protein adopting slightly different conformations⁷⁸. PrP interacts with liposomes via electrostatic binding interactions at positively charged residues on PrP and anionic lipid head groups with this association strengthened through hydrophobic side chains and lipid acyl chains: such interactions promote

higher β -sheet conformations of PrP and protect the globular C-terminal domain from proteolytic cleavage¹⁴⁸. PrP binds lipids in both a GPI-dependent and independent manner^{62, 149}. To test where in the native PrP^C sequence lipids are bound, Wang et al. carried out an iodixanol density gradient analysis of rPrP mutants with 1-palmitoyl-2-oleoylphosphatidylglycerol (POPG) and found that not only does this entity enrich the population of infectious PrP^{Sc} formed, it does so by binding the CC2 and PTM regions of the protein⁶⁴. CC2 deletions or point mutations at this region reduced electrostatic interactions but did not disrupt association of rPrP at the PTM region with anionic lipids; they did however, markedly reduce rPrP protease resistance suggesting a role of CC2 in positioning rPrP and supporting formation of protease-resistant conformers⁶⁴. Mounting evidence highlight the CC2 region along with the PTM domain as critical regions at which conformational changes are observed during the PrP^C-to-PrP^{Sc} transition⁶⁴.

Following a minimal mutagenesis approach such as that undertaken in this study, Hara et al. were able to pinpoint a five-residue sequence that regulates conversion of moPrP: 100- KPSKP-104¹³⁴. They adopted two methods to reach this conclusion; the first being exchange of moPrP residues in CC2 for equivalent residues in the chicken homolog to create chimeric proteins and determine their propensity for PrP^{Sc} formation/their cell curing potential; secondly, generating alanine-point mutations to study the effect they would have on the conversion process, as assessed by a peptide inhibition assay¹³⁴. Both methods incorporated use of a 3F4 epitope within the CC2 region itself (108-111)¹³⁴. They reported a marked reduction

in the intensity of PrP^{Sc} accumulation in chronically infected cells expressing alanine replacement mutations K100A, S102A, K103A, P104A, which they termed 'nonconvertible dead-end mutants' and showed this to not be true for more N-terminal mutations¹³⁴. They predict that this five-stretch segment forms an outward extended loop structure that arises from the core β -helical architecture¹³⁴. They acknowledge that the primary binding interface between PrP^C and PrP^{Sc} resides in the C-terminal portion of the protein, but that this segment may provide an auxiliary interaction site that accelerates the conversion¹³⁴.

1.3.12 Putative transmembrane domain (PTM) residues 111-126

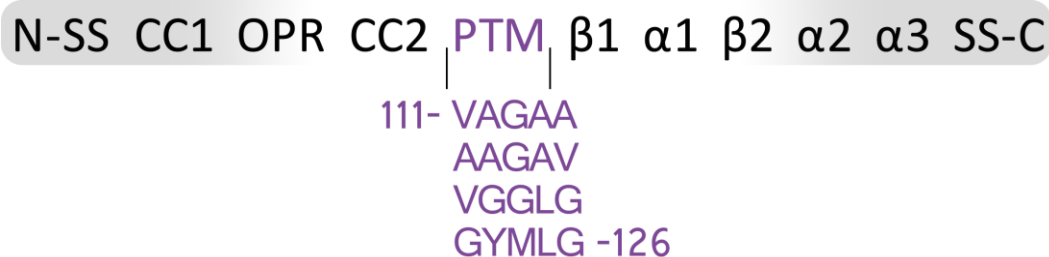


FIGURE I9: PTM

Bar schematic of domains within moPrP. N-SS: N-terminal signal sequence; CC1: charge cluster 1; OPR: octapeptide repeat region; CC2: charge cluster 2; HC: conserved hydrophobic region; α1: helix 1; β1: strand 1; α2: helix 2; α3: helix 3; SS-C: C-terminal signal sequence. Residues 111-126 of moPrP are indicated in single letter amino acid sequence.

The middle section of the protein has a stretch of residues that many sequence prediction programmes predict to be a helical transmembrane segment. In fact, one such study which predicted this, used four algorithms to predict a transmembrane site, each of which use a unique way to analyse the presented sequence: (i) positive-inside rule (ii) greater conservation a stretch of amino acids relative to the rest of the protein (iii) artificial neural network that is taught on a transmembrane-protein database (iv) hidden Markov model to find the most-likely topology¹⁵⁰. Work by Hegde et al., showed that this section can indeed be found associated with the membrane, in various topologies (Figure I2)⁶³. PrP^C is known to bind lipids independently of its GPI-anchor. Specific residues responsible for this interaction are yet to be identified, but overall binding has been attributed to hydrophobic interactions arising from the PTM domain of the protein, with CC1 and CC2 providing electrostatic interactions for charged phospholipid head groups⁶⁴.

The prion-lipid interaction was shown to be abolished by removal of residues 111-131 leading to a reduction in the amount of lipid-induced ProteinaseK-resistant PrP^{Sc} formed⁶⁴. When smaller deletions were made in this region (and stretching N-terminally into CC2), transgenic mice expressing these constructs displayed severe pathologies: ataxia, cerebellar loss and white matter disease. This phenotype is quite different from that seen in typically Scrapie-sick mice and can be overcome by expression of the full-length native protein¹¹⁹.

It is interesting to note that transgenic mice expressing CC2 deletions in concert with PTM deletions are resistant to prion infection, highlighting the possible role of these regions in prion conversion from PrP^C to PrP^{Sc76}. Norstrom and Mastrianni reported the PTM region as not fundamental for PrP aggregation, but claimed its absolute requirement for de novo generation of the specific PrP^{Sc} conformation and association of PrP^{Sc} with PrP^{C88}. This was tested in N2a cells and in a heterologous yeast expression system, with its association characteristics ascribed to the AGAAAAGA palindrome at residues 112-119⁸⁸. Additionally, due to the flexibility afforded to this region, it is not restricted in its position; it can exist at least transiently, in a series of conformational forms ranging from structured α -helical, variable and partially denatured³¹. Partial denaturing or unfolding of the N-terminal tail in PrP^C facilitates conversion of the protein to alternative fold states including PrP^{Sc19}. Collating experimental evidence from PrP^{Sc} inhibition experiments using region-specific peptides, epitope blocking assays using antibodies and PrP^C PTM deletion mutants, points to PrP^{Sc} binding PrP^C at a site proximal to, but not exactly at the hydrophobic

centre^{77, 116, 119, 151}. Nonetheless, PrP^{Sc} is unable to form (at a detectable level) when PrP^C is devoid of some PTM residues, with these deletion mutants demonstrating dominant negative inhibition when expressed in constitutively infected N2a (ScN2a) cells¹¹⁹.

The PTM deletion mutants in turn show lower aggregation propensities and are trafficked to the cell surface more efficiently than their full-length counterparts¹¹⁹. Moreover, pathogenic mutations within the PTM interfere with both the attachment of the C-terminal GPI-anchor and the folding dynamics of PrP^C which in turn lead to increased formation of misfolded forms of the protein⁶². Chatterjee et al., report amyloid core formation resulting from the moPrP loop region between β 1 and α 1 with no input from the PTM region⁷⁷. This conclusion was based on experiments involving short moPrP peptides that act as seeds for full-length recombinant moPrP⁷⁷. However, it should be noted that in this study, PTM-spanning peptides were less thermodynamically soluble compared to the loop peptides and required high monomer concentrations for initiation of fibril formation, which may widen the margin of experimental error⁷⁷.

Unconventional topologies of PrP^C at the ER lumen include ^{Ctm}PrP and ^{Ntm}PrP (Figure I2) and these have been studied extensively by the Hegde group^{63, 152, 153}. The majority of PrP^C once synthesised is fully secreted into the ER lumen, and termed ^{Sec}PrP⁶³. Intriguingly, mutations in PrP^C that upregulate ^{Ctm}PrP formation can lead to neurodegenerative disease in mice and in some heritable prion diseases¹⁵². Generation of this topological variant however is unlinked to PrP^{Sc} generation and thereby non-transmissible^{63, 152}. It still contributes to overall neurodegeneration by

influencing cell susceptibility upon PrP^{Sc} infection – this was tested by the Hegde laboratory using two PrP mutants with opposing roles: overproduction and down regulation of the transmembrane forms ^{Ctm}PrP and ^{Ntm}PrP¹⁵². They found that each of the topological forms formed from the nascent polypeptide chain prior to PTM synthesis; furthermore, disruption of the extreme N-terminal signal sequence (residues 1-22) abolished generation of all topological forms¹⁵². Because of the irregular charge distribution pattern either side of PTM, the orientation predicted to be preferred by PTM (N-term cytoplasmic; C-terminus exoplasmic) negates that commanded by the signal sequence (translocation of the N-terminus)¹⁵².

In fact, improving the signal efficiency in transgenic mice reduced the level of ^{Ctm}PrP and levels of cytosolic aggregates¹⁵². Essentially, it is the overall message delivered to the cell over these opposing pressures that determines the outcome of the PrP topology delivered¹⁵². So although the strength of the nascent signal sequence for initiating translocation suppresses ^{Ctm}PrP formation, features of the PTM can modulate the degree of suppression¹⁵². Wang et al., have shown that ^{Ctm}PrP elicits toxicity and it is speculated that this may be the trigger for neurodegeneration in some cases of prion disease¹⁵⁴. How exactly toxic pathways are activated is not known, but a proposed mechanism is through ^{Ctm}PrP accumulation, possibly within the proteasome, and subsequent cellular stress; this stress further accentuated by PrP^{Sc} accumulation.

1.3.13 Structured region C-terminal domain (126-230)



FIGURE I10: STRUCTURED REGION

Bar schematic of domains within moPrP. N-SS: N-terminal signal sequence; CC1: charge cluster 1; OPR: octapeptide repeat region; CC2: charge cluster 2; HC: conserved hydrophobic region; α1: helix 1; β1: strand 1; α2: helix 2; α3: helix 3; SS-C: C-terminal signal sequence. β-strands, loop regions and α-helices are shown in pink, grey and green respectively.

The structured region of PrP^C, also referred to as the globular domain, comprises three alpha helices and two beta sheets with a GPI-attachment at the extreme C-terminus (Figure I3). Residues Cys178 and Cys213 form a disulphide bond, connecting helices 2 and 3, contributing in some part to the overall stability of this region¹⁵⁵. Some of the earliest experiments in prion biology employed a deletion mutagenesis approach to decipher critical regions in PrP^C that led to PrP^{Sc} formation; from this it was concluded that the structured region of the molecule held the vital residues/ components for prion conversion to proceed^{93, 128}. Present-day experiments support this

hypothesis, but also indicate that N-terminal regions of the protein and other cellular factors modulate the overall conversion efficiency³¹. The most striking change in PrP^C upon conversion is the shift from a mainly α -helical content to β -sheet-rich conformation⁴⁰. A fresh wave of research on prion protein stabilisation and its influence on conversion to PrP^{Sc} indicates that it is governed to a large extent by helices 2 and 3¹⁵⁶⁻¹⁶⁰. The β 2- α 2 loop region is thought to be important for prion propagation with α 1- α 2 associations facilitating this effect¹⁶¹. Using seed-induced amyloid formation experiments with rPrP to identify residues in the makeup of PrP^{Sc}, Chatterjee et al. detected residues 127-143 but not 107-126 in an amyloid seeding assay, thus stating the more N-terminal peptide was not crucial for amyloid formation⁷⁷. Backing this theory, a chimeric mouse-hamster PrP expressed in transgenic mice was able to support PrP^{Sc} formation in the absence of residues 23-88 and 141-176¹⁶².

Yamaguchi et al. prepared peptides corresponding to various domains of moPrP and scored their amyloidogenic properties; α 2 and α 3 were found to be the major hydrophobic regions; α 2 had a high intrinsic β -sheet propensity and readily formed amyloid-like fibrils¹⁶³. Conversely, α 3 peptides exhibited a preference for α -helix conformations – this was also true for the hydrophilic α 1 peptides¹⁶³. When these peptides were tested in the presence of full-length moPrP, α 2 peptides induced formation of fibrils more readily than any other peptide fragment¹⁶³. The authors reason that although the native fold of PrP^C under physiological conditions prevents the molecule slipping into an amyloid state, the C-terminal region especially α 2, has an inherent amyloidogenic capacity¹⁶³.

Support for $\alpha 2$ as an amyloid-state facilitator comes from experiments where introducing a more rigid loop structure (as observed in cervids) into the moPrP sequence between $\beta 2$ and $\alpha 2$ resulted in greater misfolding propensity compared to the native moPrP sequence¹⁶⁴. Further mutagenesis experiments centred around $\alpha 1$ and $\alpha 2$ of moPrP implicate this region and the sequence C-terminal to it as being vital to PrP-PrP interaction¹⁶⁵. The more rigid loop structure showed similar thermodynamic stability in both wild-type and mutant forms of moPrP; the authors deduced that increased prion protein conversion as observed in cervids arises not from loop rigidity, but from a boost in amyloidogenic potential due to changes in the native sequence at the $\beta 2$ - $\alpha 2$ expanse¹⁶⁴.

When comparing sequence identity between rabbit and hamster loop regions between $\beta 2$ and $\alpha 2$ of PrP^C Sweeting et al. showed that this segment comprises a helix cap motif that could influence β -state-misfolding propensities of the protein; this may be a determining factor for degree of prion susceptibility and relates to hydrogen-bonding interactions within the motif¹⁵⁸.

There are also a large number of point mutations in the vicinity of $\alpha 2$ and $\alpha 3$ that are associated with inherited forms of prion disease⁵¹. Cappings are usually present in regions of the polypeptide chain immediately preceding or succeeding an α -helix and play an important role in stabilising helices by compensating for the absence of intrahelical hydrogen bonds between the first and last turns of the helix¹⁶⁶. Looking more closely at helix capping in the $\alpha 2$ and $\alpha 3$ regions of moPrP, Iovino et al., used a molecular dynamics

simulation approach to selectively mutate $\alpha 2$ and $\alpha 3$ regions of moPrP. They found the wild-type sequence displayed stability throughout its trace whereas mutants showed varying degrees of stabilisation¹⁶⁷.

Apostol et al. described a novel motif for oligomer formation using a fragment from huPrP comprising regions $\alpha 2$ and $\alpha 3$ linked via the disulphide bond¹⁶⁸. They report a hexameric assembly, as opposed to the characteristic steric zipper profile observed for amyloids with residues HDCVNI at $\alpha 2$ and EQMCIT at $\alpha 3$ forming this assembly^{40, 168}. The overall structural configuration of one subunit was described as a hexamer made up of 'three four-stranded antiparallel β -sheets arranged like the faces of a triangular prism'¹⁶⁸. This assembly is presumably driven by hydrogen bonding between the β -sheets and burial of hydrophobic side chains¹⁶⁸.

1.4 Disease-associated mutations in the prion protein

Human prion diseases can be divided into three main categories, distinguished by aetiology: sporadic, inherited and acquired⁵¹. This section will focus on mutations within the prion protein which either pose a risk or provide a protective function to the gene carrier. Population analysis studies have revealed a number of naturally occurring prion protein mutations which vary depending on the demographic sampled, and range from insertions/deletions (indels) to missense and nonsense mutations⁹¹. Indels usually arise around the OPR region due to the genetic instability of this site (residues 51-91, human numbering)⁵¹.

Typically, the prion protein consists of five OPRs with an increase or decrease in number (in particular, a drop to three OPRs) associated with the inherited form of prion disease⁶. Nonsense mutations recorded for the prion protein comprise Y145X, Q160X, Y163X, and more recently, Y226X and Q227X⁶. It is stressed that this section is not an exhaustive compilation of all prion protein mutations identified to date, but paints an overall picture of the most common ones and the region of the protein in which they lie.

1.4.1 Mutations in the flexible domain (residues 23-126)

Mutations in this region are coupled to GSS-related amino acid replacements: P102L, P105L/S/T, G114V and A117V (human numbering)⁵¹. Mutations in various regions of the structured domain of PrP also give rise to the GSS phenotype and include G131V (C-terminal to β 1),

V180I (within $\alpha 2$), F198S (N-terminal to $\alpha 3$) and D202N, Q212P and Q217R (all within $\alpha 3$)^{6, 51}. The archetypal purified GSS amyloids formed by huPrP bearing the A117V mutation consists of 7kDa PrP peptides, whereas those containing F198S mutations tend to form 8kDa fragments¹⁶⁹. Both configurations implicate a role for the N-terminus in formation of PrP^{Sc}, as the purified amyloid peptides from GSS patients corresponded to OPRs three and four in the case of F198S, and to OPR five and CC2 for the A117V mutation, as determined by sequence analysis of the ProteinaseK-cleaved peptides¹⁶⁹. The most prominent GSS-linked mutations are those at position 102 and 105 (human numbering)¹⁷⁰. When Tremblay *et al.* synthesised a 55-residue peptide spanning the P102L mutation site (P101L in mice) they found that it refolded preferentially to a β -sheet structure¹⁷¹.

Additionally, circular dichroism studies on wild-type moPrP versus P101L moPrP demonstrated attenuation of helical content in the mutant form¹⁷¹. The most compelling evidence for the importance of the N-terminal domain in prion diseases comes from the finding that the neurotoxicity elicited by PrP arises from peptides corresponding to amino acids 106-126 (CC2 boundary and PTM region)^{172, 173}. Forloni *et al.*, showed that peptides 89-106 are neurotoxic when the P102L mutation is present but not when P105L is expressed¹⁷⁴. Furthermore, A117V mutations appear to reduce the capacity for helix formation in the 'neurotoxic' peptide^{174, 175}. Schiff *et al.*, show that in a setting where either P105L or A117V PrP is co-expressed with the wild-type form, the cellular localisation of the wild-type protein is affected, often resulting in an increased amount of PrP with alternative membrane topology (Figure I2)¹⁷⁶. Almost all known mutations that fall

within the PTM region of the protein correlate well with production of CtmPrP¹⁷⁵. There is currently a lack of comprehensive analyses tracking the effect of minimal changes in the PTM on the overall protein and its propensity to propagate prions; this issue is addressed in the present study.

1.4.2 Mutations in the globular structured domain (residues 126-231)

Residues in the C-terminal structured domain of the prion protein form part of the amyloid core and are central to disease progression^{77, 89}. This has been shown by numerous groups using a plethora of techniques: structure prediction and bioinformatics applications¹⁷⁷, yeast-two-hybrid screening and studying yeast prions^{81, 178}, recombinant and chimeric protein expression^{78, 87}, structure determination^{65, 66, 179}, various cell models of prion disease⁹⁸, transgenic studies⁴⁸, and reports from clinical studies detailing the molecular profiles of huPrP in patients bearing mutations at these sites⁶. R148H lies in α 1 and is so far the only disease-associated mutation found to reside at this helix¹⁸⁰. Krebs *et al.*, demonstrated differential gel mobility of protease-resistant, wild-type PrP versus one with an R148 mutation¹⁸¹. This residue replacement is suspected to weaken one of the salt bridges formed during production of native PrP^C and alters PrP^{Sc} in the R148 protein in a manner that makes it indistinguishable from that seen in the sporadic CJD phenotype¹⁸¹.

Intra-helix salt bridges are formed between two aspartic acid- arginine ion pairs at positions 144 and 148, and at residues 147 and 151¹⁷⁹. When mutations were engineered at these sites to replace the native residues with

alanine in Syrian hamster PrP (ShaPrP), thermal and chemical denaturation experiments revealed that the mutants are not substantially destabilised, but appear to engage in a different unfolding pattern¹⁷⁹. Cell-free conversion data however, showed a higher efficiency of protein conversion if the mutations were in place, thereby arguing a case the native intra-helix salt bridges stabilising α 1 and preventing conversion to a misfolded moiety¹⁷⁵.

179.

Nonsense mutations such as Y145X, Q160X, Y163X, and more recently, Y226X and Q227X put a premature stop to PrP translation and are often characterised by intense amyloid deposition of this anchorless protein¹⁸². Such events inevitably results in protein malfunction, or in this case increased propensity for misfolding due to lack of complete structure¹⁸².

Using ssNMR and a CS-Rosetta averaging paradigm, Skora and Zweckstetter have modelled a left-handed β -helix for PrP expressing the Y145X mutation, comprised of three β -strands with contributions from 111-HMAGA-115 (CC2-PTM region), 120-AVVG-123 (PTM region) and 128-YMLGSAMSR-136 (spanning β 1 of the structured domain)¹⁸³. They suggest a mechanism whereby the third strand at P137 twists so as to extend the existing β -helix at 138-IIHF-141. The palindromic sequence 113-AGAAAAGA-120 acts as a loop region connecting the two β -strands¹⁸³.

Prion protein with mutations D178N and E196K are thought to be more prone to aggregation in crowded cellular environments compared to their wild-type counterparts¹⁸⁴. Expression of D178N results in a lack of stabilising contacts for α 1 with the remaining structured part of the molecule

and along with mutations V180I, T183A, F198S and E200K, is reported to show variable glycosylation patterns¹⁸⁵.

The V180I mutation is capable of conversion *in vitro* but does not display any evidence of such activity in patient brains. Transgenic mice expressing PrP lacking the first glycosylation site appeared to be resistant to prion infection while those lacking the second site were fully susceptible¹⁸⁵. It is possible that the region between the loop and the first glycosylation site may be more prone to dominant negative inhibition due to steric hindrance.

A H187R mutation results in the introduction of a positive charge group in an otherwise hydrophobic pocket and consequently a strong repulsive electrostatic interaction with R156, causing considerable local changes in PrP^C folding¹⁸⁶. The folded structure of PrP^C, if mutated to H187R, causes the hydrophobic core to be solvent-accessible, exposing the previously buried F198 residue^{186, 187}. Some authors have alluded to this as a mechanism for increased misfolding propensity as the water-filled void lowers the activation energy for fibril formation by promoting protein stabilisation¹⁸⁷. Hosszu *et al.* used NMR chemical shift and structural data to show that the principal effect of H187R on PrP structure is at α 1 and α 2 with little change to the remainder of the protein¹⁸⁶. In particular, acidification (arginine replacement) shortens α 1 C-terminally and creates disorder in α 2 with rearrangement of the salt-bridge reported as the prominent factor¹⁸⁶. Many other known pathogenic mutations around this region of the protein also introduce a positive charge (E196K, F198S, T188R/K, E200K, D202N) while others introduce a bulkier side chain (V203I, R208H, V210I) or

constrict backbone rotation of the alpha carbon (Q212P)^{6, 19}. The β 2- α 2 linking residues were shown through prediction programmes to form a potential steric zipper (Class 2), as described by Eisenberg *et al*⁴⁰. β 1 and β 2 have been purported to initiate seed formation towards a β -sheet-rich conformer, via strand elongation, driving α 1 unfolding⁷⁷.

E211Q is located in the third α -helix of PrP⁶⁵. Substitutions at this codon were found to affect protein stability as analysed by molecular dynamics and differential calorimetric experiments with rPrP¹⁸⁸. The mutation affects the proteins cellular folding pathway and promotes aggregation by altering the native state of the protein¹⁸⁹. Interestingly however, a more conservative mutation E211D, showed a higher propensity to form high molecular weight oligomers¹⁸⁹. This mutation also promotes formation of a salt bridge between R208 of α 3 and E146 of α 1, which is not the case for the wild-type protein or even for E211Q¹⁸⁹. Through this interaction, the E211D mutation is able to destabilise α 1 by favouring its detachment from the α 2- α 3 subdomain¹⁸⁹.

Q217R mutations are linked to GSS-type pathology and thought to undergo misfolding in a mechanism dissimilar to E211Q proteins¹⁹⁰. Using molecular dynamics simulations, De Simone *et al.* have studied the role of surface and partially buried water molecules in PrP. They report that the Q217R substitution has the effect of immediately expelling water from an internal 'pocket' as insertion of the bulkier side chain leaves no room for internal waters¹⁹¹. They also report the mutation's effect on spatially neighbouring residue R220, as with the two arginine side chains repelling each other's

positive charges and argue that Q217R mutations aberrantly affect the structured domain of PrP by displacing conserved waters. These waters play an important role in holding critical residues in their respective orientations, as Hydrogen-bond atoms interacting with adjacent water can lower the activation energy required to unfold¹⁹¹.

P238R/S/T mutations are observed in familial cases of CJD and lie in the C-terminal signal peptide portion of the protein. It was found that neither of these mutations affected addition of the GPI-anchor, but are still able to elicit cytotoxicity^{62, 149, 192}. Suggested hypotheses included alteration of PrP processing preceding ER translocation which would alter PrP topology in the ER (Figure I2), or impairment of signal cleavage, resulting in abnormal ER retention or secretion of anchorless PrP¹⁴⁹. Gu *et al.* demonstrated the role of this signal peptide as an efficient ER-targeting and GPI attachment signal for PrP, and that P232R and P232T mutations are associated with PrP occupying a Ctm topology at the ER membrane, which is thought to be neurotoxic¹⁹³.

1.5 Study of epitope-tagged or labelled prion proteins

Since there is still uncertainty about the exact physiological function of PrP^C and how it is processed *in vivo*, a vast range of tagged PrP constructs have been generated over time to provide a better understanding of the cryptic benefit of ubiquitous prion protein expression¹⁹⁴⁻¹⁹⁷. The types of tags used to study PrP, the suitability of certain tags for particular experimental set-ups, the position at which tags are inserted and the benefits and limitations of doing so, must all be taken into consideration as this may have a major impact on the aspect of protein processing under investigation¹⁹⁸.

1.5.1 Need for unique epitopes and tagged PrP constructs

When studying the role of PrP, and its propensity to aggregate and form infectious particles, it is very difficult to distinguish *de novo* production of PrP^{Sc} from the original inocula used to infect the native protein. These complexities arise since: (i) PrP^{Sc} and PrP^C share the same protein sequence and PrP^{Sc} must be added to cells expressing PrP^C to study prion propagation; (ii) unless the infectious inoculum or the expressed PrP^C has been labelled, applied PrP^{Sc} and newly formed PrP^{Sc} are indistinguishable. Some groups have reported that due to differences in the folded conformations of PrP^C (more α -helical) and PrP^{Sc} (higher β -sheet content), different epitopes may be exposed in the two forms, that allows some degree of distinction^{82, 199}; however, the caveat is that differential binding is only seen in a sub-population of fibrils formed⁸².

In order to differentiate between these biochemically different forms, limited proteolysis experiments have often been the norm in characterising the different species, as PrP^C unlike PrP^{Sc} is not resistant to ProteinaseK digestion. Nonetheless, this technique is not always feasible as it cleaves a significant portion of N-terminal residues^{200, 201} and alternative approaches must be employed to simultaneously track the activity of the two conformers. Further compounding the issue of distinguishing PrP^C from PrP^{Sc} is the finding that the disease-associated conformer is not always present in the protease-resistant fraction and in some instances, shows higher infectivity in the soluble fractions²⁰². Thus, an obvious approach to distinguish one form from the other would be to generate fusion constructs, fluorescent or affinity tags, so as to efficiently separate the two moieties.

When analysed in protein overexpression cell systems, newly formed labelled PrP^{Sc} is readily separated from the un-tagged infectious inocula^{195, 196}. Total PrP^{Sc} can be calculated using standard measures and the amount of *de novo* protein determined based on expression of the reporter protein or presence of a unique epitope. Furthermore, detection of the tagged protein is substantially more sensitive than conventional methods using anti-prion antibodies and allows for detailed intracellular trafficking experiments^{100, 198}. Lastly, tagged constructs have been used in attempts to isolate and identify PrP-binding factors and PrP-interactors that may play a role in disease pathogenesis¹⁹⁵. Given the tendency for prions to misfold³⁵, considerable care is given to the type of tag chosen for insertion and indeed as to where in the sequence the tag or epitope be attached, so as to avoid generating a prion protein with: (i) increased misfolding propensity³⁴; (ii) loss

of propagative capacity (iii) deficiencies in infectivity (iv) disruption of the native fold, and if the construct is expressed in cells susceptible to prions, (v) loss of the susceptibility phenotype, as either of these scenarios would hamper experimental analysis of cellular prion propagation.

1.5.2 Positional insertion of tags within the PrP sequence

The majority of the reported modifications to the prion protein sequence lie either at the extreme N- or C-terminus of the mature protein, or at various positions within the CC2 region^{140, 195, 203}. In each case, special attention was given to conserve signal sequences as interfering with these regions leads to atypical protein sorting¹⁵². Large tags such as GFP are never used in the middle protein region such as at the PTM region of the prion protein or the $\alpha 2$ - $\alpha 3$ structured region. In the instance of the PTM region, this is because the domain (as the name implies), carries a high hydrophobic content and the inserted tag/epitope would likely be inaccessible for detection purposes as it might be hidden within the protein core, or may generate misfolded forms²⁰⁴. Alternations within $\alpha 2$ - $\alpha 3$ are predicted to significantly alter the native fold and thus tag insertions here may hamper native protein function or alter its cellular targeting²⁰⁵. Additionally, this helical region is left largely unchanged as it is considered to hold the infectious and propagative capacities of the protein²⁰⁶. The N-terminus appears to be the chief site for modification by tag or epitope insertion^{116, 140, 203}. This may be due to the flexibility afforded to this region which can accommodate change with little effect on the structured domain. Moreover, as N-terminal modifications tend to lie in proximity to charge regions that

have a greater likelihood of being solvent accessible, they are more likely to be detected²⁰³. A number of studies have been carried out assessing the ability of the protein to propagate and transmit a PrP^{Sc} phenotype to susceptible cell when the native sequence has been tagged^{195, 207}.

1.5.3 Biochemical nature of tags and their influence on prion propagation

Charge interactions can play an influential part in the process of prion protein interactions and undeniably, in mediating stability of the native form over propagation of the misfolded conformer^{88, 114, 116, 117}. For clear detection and purification of protein samples, it is sometimes necessary to use a multi-tag system whereby tagged constructs of the protein are generated and the protein of interest extracted from a milieu of other cellular factors in a two-step method. In this way, EGFP and FLAG tags have been useful in understanding the trafficking of the native protein pre- and post-infection with PrP^{Sc}.

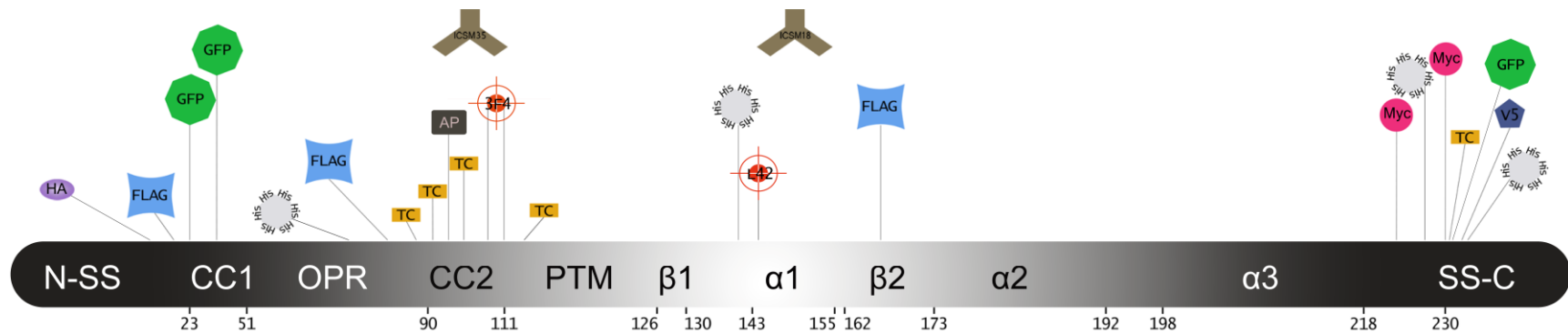


FIGURE I11: TAGGED PRP CONSTRUCTS USED IN PRION RESEARCH

Schematic of the prion protein showing segments of the protein as ascribed by structure or biochemical property. Shown above the sequence structure are a series of tagged constructs which have all been used individually or in tandem to dissect various roles of PrP. The tags are shown to be preferentially clustered at the N- or C-terminal ends of the sequence, followed by CC2 and the region around $\alpha 1$. N-SS: N-terminal signal sequence; CC1: charge cluster 1; OPR: octapeptide repeat region; CC2: charge cluster 2; PTM: Putative transmembrane region; $\alpha 1$: helix 1; $\beta 1$: strand 1; $\alpha 2$: helix 2; $\alpha 3$: helix 3; SS-C: C-terminal signal sequence. Types of fusion proteins tested by various groups involved the use of: FLAG^{203, 208}, GFP²⁰⁷⁻²¹⁴, His^{204, 215-218}, TC (tetracysteine)^{196, 197, 219, 220}, AP (alkaline phosphatase)²²¹, 3F4^{222, 223}, L42²²⁴, Myc^{100, 195, 225} and V5²²⁶ epitopes. Shown above the tags are the positions on the protein at which antibodies ICSM35 (CC2) and ICSM18 (α -helix 1), used in this study, bind moPrP.

Harris *et al.* used this method to identify intracellular sites of protein conversion²²⁷ and Lee *et al.* identified a modulatory role for copper ions on PrP internalisation using a GFP-tagged construct²⁰⁹. When expressed in transgenic mice, the fusion protein was shown to localise correctly and exhibit wild-type protein capacities, in its ability to rescue mice from toxicity elicited by PrP deletion mutant Δ 32-134²⁰⁷. The fusion protein model was reported to be supportive of prion replication, but at a reduced efficiency²⁰⁸.

More recently, Myc-tagged PrP was used to demonstrate rapid cell surface conversion of the protein following infection¹⁰⁰. Tags such as polyhistidine are used mainly with recombinant PrP, their advantage being the specificity and ease of detection when processing the sample²¹⁸. Poly-His-tagged PrP can be detected and captured using immobilised metal-affinity chromatography (IMAC) to isolate metal-binding peptides, based on the interaction between the negatively charged His residues and transition metal fixed on the matrix²²⁸. Purification can be carried out under denaturing conditions and the protein then renatured²²⁸. Unfortunately, the use of imidazoles can result in protein aggregates, especially in the instance of PrP and can encumber its physiological activity²²⁹. Supattapone *et al.* have characterised various poly-His affinity-tagged miniprions, reporting spontaneous formation of protease-resistant conformers that bore some resemblance to PrP^{Sc204}.

Tag	Sequence Inserted	Molecular Weight (Da)
Myc	EQKLISEEDL	1202
Tetracysteine	CCPGCC	585
FLAG	DYKDDDDK	1012
His ₍₆₎	HHHHHH	1000
GFP	MSKGEELFTGVVPILVELDGDVNGHKFSVSGEG EGDATYGKLTCLKFICTTGKLPVPWPTLVTTFSYG VQCFSRYPDHMKQHDFFKSAMPEGYVQERTIFF KDDGNYKTRAEVKFEGDTLVNRIELKGIDFKE DGNILGHKLEYNYNSHNVYIMADKQKNGIKV NFKIRHNIEDGSVQLADHYQQNTPIGDGPVLLP DNHYLSTQSALS KDPNEKRDHMLLEFVTAAGI THGMDELYK	27000
Epitope	Sequence Recognised	
3F4	KTNMK	620
L42	GNDYEDRYRENMYRPNQ	2550

TABLE 12: TAGS AND EPITOPES USED TO AID AND COMPLEMENT DETECTION OF PRIONS

A number of modifications to the native prion protein sequence make it easily distinguishable using anti-tag and epitope-specific antibodies. Listed in the table are a few common ones that have been used to track expression of PrP.

Tetracysteine (TC) tags, considerably smaller in size than most typical varieties, have been used in moPrP studies with native-like protein folding^{196, 220}. TC motifs bind fluorescent biarsenical dyes (FIAsH) and allow specific detection of labelled PrP¹⁹⁷. When inserted at the extreme N- or C-terminus of the protein, TC-tagged PrP supported fibril formation whereas tags within the α 2- α 3 region inhibited conversion¹⁹⁶. This method is amenable for live cell imaging and has been used by Taguchi *et al.* to internally label PrP at the unstructured region and identify sites of protein interaction¹⁹⁷. It is possible that the presence of inherent cysteines and histidine-rich regions in PrP may result in non-specific binding interactions and in the case of PrP, the presence of the histidine tag could alter the copper binding activity of the protein and may alter the ratio of preferred conformers in solution^{129, 230}. A more conservative change is the widely used 3F4 epitope on moPrP; moPrP does not have a 3F4 epitope, unlike its human and hamster counterparts. This difference is exploited and a 3F4 epitope is inserted within the CC2 domain of moPrP¹⁹⁴.

By far the most conservative approach for investigating intermolecular interactions, and a popular technique, is alanine scanning mutagenesis⁵³. Here, native amino acids are singly, doubly or triply replaced with alanine, to create a series of constructs for each region of interest in the mouse prion protein. This introduces minimal deviation from the native sequence compared to conventional tagging methods. It differs from deletion mutagenesis which may give stronger phenotypes, but also increased uncertainty as to the overall effect of the deletion on the folded native state of the protein. These alanine constructs can be considered to be the closest

representation of the native protein and abundantly useful in instances where protein function is probed, as small interferences such as single amino acid replacements can give rise to strong phenotypes if a critical area of the molecule is altered.

1.6 Current opinions in the prion field about regions that confer prion propagation

Whether or not the flexible N-terminus of the prion protein plays a major role in infection and propagation of prions has often been a bone of contention, with some authors disregarding it altogether and others showing incriminating evidence for its role in producing the aberrant conformer. Methods used to deduce these conclusions, inclinations and hypotheses regarding the incriminating segment that partakes in PrP^{Sc} formation, vary between laboratories. However, a general consensus has emerged in the prion field about regions of the protein that are responsible for the successful propagation of prions, and unanimous acceptance for the role of the structured region of PrP^C in the conversion process.

Typically, PrP^C predominantly undergoes α -cleavage between 109 and 110 under physiological conditions, to produce N1 (23-109) and C1 (110-230) fragments, as determined by radiosequencing huPrP (position 111 human numbering). PrP^{Sc} however, preferentially undergoes β -cleavage more N-terminally, at around residue 90, generating N2 and C2 fragments. Partial digestion of PrP^{Sc} with ProteinaseK yields a protein fragment of 27-30kDa in size that is cleaved at the N-terminus, bordering residue Q90 and retains infectious properties; conversely, PrP^C is digested completely. Various segments of the protein have been linked to diverse pathways such as induction of toxicity, neuroprotection, cell signalling, apoptosis, cell development and oxidative stress responses. The focal point in this section

is on regions of the protein that allow it to self-propagate and form the misfolded state.

A double-deletion mutant of PrP ($\Delta 23-88$ and $\Delta 141-176$) devoid of $\alpha 1$ and the N-terminus except for CC2 was able to propagate PrP^{Sc}^{76, 231}. Such a construct is termed a miniprion and defined as the minimal sequence of PrP that supports prion propagation^{76, 231}. A study carried out using C-terminally His₍₆₎-tagged chimeric construct that replaces residues 108 and 111 of moPrP with ShaPrP to generate a 3F4 epitope, was the first of its kind to demonstrate the miniprion phenomenon^{204, 231}. The authors make a distinction however, regarding the ProteinaseK-resistant product formed from PrP^{Sc} versus the double-deletion mutant; the mutant misfolds relatively easily even in the absence of an infectious misfolded stimulus, whereas the full length protein requires PrP^{Sc}²⁰⁴. This conformational change may be attributed in some part, to positive charges in the affinity tag and suggests that positioning, spacing and charge of any tag in the native PrP sequence can have an impact on the molecules ability to propagate prions²⁰⁴. In another study where a synthetic peptide was generated to mimic the same double deletions in moPrP, it was shown that this sequence is able to induce nerve cell degeneration in primary cell cultures and glial cell activation *in vitro*⁷⁶. Although the miniprion is a useful model to study aggregation kinetics of the peptide, it is by no means a direct comparison to PrP^{Sc}. Using this peptide, numerous studies have been carried out to infer and elucidate mechanisms by which PrP^{Sc} carries out its neurodegenerative function. This includes hypotheses to test the involvement of the PTM

domain²³², regulation of membrane viscosity and intracellular calcium levels^{233, 234}, SOD activity and copper coordination²³⁵.

Some patients with prion disease present with mutation Y145X; peptides made to mimic this mutation give rise to a parallel in-register alignment of the β -sheet core¹⁸³. Such evidence suggest a region stretching from CC2 through to α 1 plays an important role in PrP^{Sc} formation, with residues 112-129 (PTM region) thought to be essential for generation of a productive 'PrP^C-PrP^{Sc} complex'^{80, 118}. Indeed peptides drawn from this region can form irregular coils, α -helices or β -sheets, in line with the conversion of the full-length protein from α -helical to β -sheet⁷⁵. Studies on the N-terminus of the protease-resistant core of PrP^{Sc} determined residue 90 as the start site for the infectious prion domain^{77, 183}. For the most part, as vast as the evidence that links the N-terminus to PrP^{Sc} formation is, it has never been directly linked to maintaining the native structure of the globular region of PrP^C nor is it solely responsible for conversion to PrP^{Sc}. This phenomenon is credited to the α 2- α 3 regions of the protein, without which a vast majority of prion amyloids would not exist. However, when deletions were made to the N-terminal region of the protein, so as to eliminate entire OPR region, there was a marked difference in the amount of protease-resistant PrP detected in transgenic mice expressing these constructs^{128, 236}.

A peptide corresponding to the PTM region was shown to be able to induce neuronal toxicity in a manner comparable to that of the miniprion, and through electron microscopy, shown to generate pre-fibrillar structures under physiological conditions led to destabilisation of phosphatidyl choline

membranes, as analysed by atomic force microscopy²³². Together, these data allude to a mechanism of PrP^C-independent cell death, at least when the PTM region is concerned. This region was considered highly toxic by the authors, as the peptide appeared to display an inability to cultivate protofibrils into mature fibrils, thereby giving rise to a protofibril-rich environment, which is considered conducive to neurodegeneration²³².

In terms of maintaining the stability of the native fold, the β 2- α 2-loop regions in tandem with the α 2- α 3 region, confer a high degree of structural organisation^{164, 237}. Alterations made to the protein within these regions, and mutations residing here play an influencing role in destabilising PrP^{C160}. Minimal mutations such as Q212P and V210I display similar globular architecture, but introduce novel local structural changes within the α 2- α 3 inter-helical interfaces when analysed by solution NMR²³⁸. The majority of the mutations arising in the structured domain of the protein leave it vulnerable to solvent-exposed hydrophobic surfaces, promoting misfolding events. Legname has proposed that the β 2- α 2 loop and specifically the interactions of this loop with the extreme C-terminus determine the levels of hydrophobic region solvent exposure and thereby manipulate intermolecular contacts^{67, 238}. This underscores the importance of α 1 and its tertiary contacts on preserving PrP^C stability. It is also possible to analyse data on the miniprion from the point of view of structured region expression as a stable part of the whole protein as opposed to focusing on the removal of the N-terminus. More evidence for the sure-fire involvement of the C-terminal structural domain of the prion protein in the initiation of misfolding, fibrillation, infection and propagation of the misfolded conformer, comes

from more recent and more rigorous studies that wholly support previous findings stressing the significance of this region in prion propagation^{77, 239}. Helix stability is highest for $\alpha 1$, followed by $\alpha 3$ and lastly $\alpha 2$ ²⁴⁰. Fibril formation is readily achievable for $\alpha 2$ segments of the protein under acidic conditions where the disulphide bond joining it to $\alpha 3$ is reduced and $\alpha 2$ undergoes partial unfolding²⁴⁰. The local conformational changes were dependent on the delicate balance of hydrophobic and electrostatic interactions of $\alpha 2$ which in turn are influenced by the pH of the surrounding environment²⁴⁰. The authors argue that the existence of a variety of fibril types (reversible and non-reversible) may explain some of the diversity observed in prion strains²⁴⁰. In conclusion, the structured region of the prion protein is the principle proliferating agent in prion diseases that contributes to accumulation of aggregated material, which we label as amyloid as it leaves signature plaques and inclusions. The amino-terminal part of the protein, in particular charge regions and the inherent flexibility of this domain, act to alleviate or exacerbate the effects of the C-terminal domain, depending on the orientation of the nascent polypeptide, which is likely influenced by associations of the PTM region^{152, 153}.

1.7 Project rationale

The mouse neural crest-derived Neuro-2A (N2a) cell line is widely used in the field of neurology. Here, this cell line was subcloned in-house to be highly susceptible to infection by mouse RML prions. Expression of the endogenous prion protein (moPrP) was then silenced using shRNA against the 3'UTR of the protein and silencing maintained under antibiotic selection, giving rise to a knock-down cell line (KD). KD cells were reconstituted with either the full-length native sequence of the mouse prion protein (moPrP^{WT}), or various mutants of the protein and analysed for their ability to propagate RML mouse prions *in vitro*. Comparison of mutant-expressing lines to wild-type expressors allowed us to discern regions within PrP^C that play a modulatory role in prion propagation.

Chapter 2

Materials & Methods

2.1 Alanine mutants of the mouse prion protein

2.1.1 Preparation of plasmid DNA

Template DNA used in this study was pBluescriptSK+ plasmid DNA bearing the open reading frame (ORF) of the murine prion protein, provided by Emmanuel Asante, within the department. The ORF of the mouse prion protein was PCR-amplified with the addition of a 5' *Sal*I site and a 3' *Xho*I site. This was then cloned into a pBluescriptSK+ vector by blunt-ended ligation at the *Sma*I site (CCCGGG) of the Multiple Cloning Site (MCS) of the vector (See Appendix). Plasmid DNA was prepared using the QIAGEN Plasmid Maxi (QIAGEN, Cat.No.12163) and Mini (QIAGEN, Cat.No.12125) kits. The protocols were followed as detailed by the manufacturer, using the provided reagents as instructed by the handbook for the relevant procedures. As large quantities of the template DNA pBluescriptSK+(containing the ORF of interest) and vector DNA (pLNCX2) were required, Maxi-preps of these were prepared. For all other mutants generated in this study, mini-prep DNA was sufficient to generate desired mutations in the final vector pLNCX2.

2.1.2 Primer design and site-directed mutagenesis

Primers were designed as suggested by the Stratagene QuikChange[®] site-directed mutagenesis kit (Stratagene, Cat.No.200523). Briefly, 18-45mer primers were designed to have at least 50% GC content where possible and maximal sequence homology (Eurofins MWG Operon; Unmodified DNA oligos); the intended mutations were created in the middle of each forward and reverse primer. The codon GCC was chosen to encode alanine due to codon bias in the mouse genome, as murine PrP was used in this study and future work would include mouse experiments.

PCR parameters were as follows: melting temperature: 95°C for 30 sec; annealing temperature: 55°C for 1min; extension temperature: 68°C for 3 min. These three steps were cycled 16 times for control samples and 18 times for test samples. Strand extension was completed at 72°C for 5 min and reactions cooled to 4°C. In cases where it was difficult to attain amplification, particularly in GC-rich regions of the sequence, touch-down PCR worked better than standard PCR, starting with an annealing temperature of 65°C and lowering this by 1°C per cycle down to 55°C, and then completing the reaction with a further 10 cycles at this temperature. Where primers were designed for deletion mutagenesis, touch-up PCR was used when standard conditions did not generate the amplified product of interest: starting with an annealing temperature of 55°C and increasing this by 1°C per cycle up to 65°C, and then completing the reaction with a further 10 cycles at this temperature. 10 ng of template DNA was used in each reaction, with mutagenic primers used at a concentration of 100ng/μl and

PhuUltra DNA polymerase at 2.5U/μl per reaction. Amplification of the samples was verified on 1% agarose gels. PCR products were *DpnI*-digested (1μl per 50μl PCR reaction for 1h at 37°C) prior to transformation to digest the parental (non-mutant) DNA strands. XL1-Blue super competent cells were used to transform the alanine mutants of moPrP in its parent pBluescriptSK+ vector. Note that reagents required for the mutagenesis steps including super competent cells are provided in the Stratagene QuikChange[®] site-directed mutagenesis kit (Stratagene, Cat.No.200523). All of the generated mutants were sequence-verified prior to sub-cloning into plasmid vector pLNCX2 using JS4 competent cells (made in-house).

2.1.3 DNA sequencing

Sequencing reactions were carried out in non-skirted 96-well plates. 1ul of mini-prep DNA (at a concentration of about 150ng/μl) was added to a well of a 96 well plate per sequencing reaction tested. 1x sequencing reaction contained 1μl Big Dye Mix (Applied Biosystems[®], Cat.No.4337449), 5μl Better buffer (Microzone, Cat.No 3BB-5), 5μM of primer, 5M Betaine (Sigma-Aldrich[®], Cat.No.B0300), 4.25μl PCR-grade water (Ambion[®], Cat.No.AM9935). After reactions were added to all required wells, the 96-well plate was centrifuged for 10 sec at 1650 x *g* to ensure sample was evenly distributed before PCR on a DNA Engine Tetrad[®] 2 Thermal Cycler (Bio-Rad, Cat.No. PTC-0240G) PCR conditions are outlined. Melting temperature: 95°C for 1 min; annealing temperature: 55°C for 1min; extension temperature: 68°C for 3 min. These three steps were cycled 20

times, and followed by a final melting and extension step for 5 min. Following amplification steps, 3.75µl 0.125M EDTA (Ethylenediaminetetraacetic acid; Sigma-Aldrich®, Cat.No.03609) is added to all wells, followed by 45µl 100% EtOH (Ethanol; Sigma-Aldrich®, Cat.No.459844) and a 15 min incubation at room temperature. The plate is then centrifuged for 30 minutes at 3000 x *g*, at 4°C. Plates are inverted and centrifuged briefly at 185 x *g* to remove liquid from the pellet. 60µl of 70% EtOH is added the plate centrifuged for 15 min at 4°C. The plate is inverted and centrifuged at 185 x *g* again. The plate is then left uncovered to allow final traces of EtOH to evaporate before running in the sequencer (Applied Biosystems 3730xl DNA Analyzer). Sequence data was analysed in Sequence Scanner v1.0 software.

2.1.4 Plasmid DNA digest gel extraction and ligation

The mouse prion protein ORF was excised from the pBluescriptSK+ vector using *HindIII/XhoI* (New England Biolabs (UK) Ltd, Cat.No. R0104T /Cat.No. R0146S) and gel extracted using a QIAquick Gel Extraction Kit (QIAGEN, Cat.No.28704) following the manufacturer's instructions. pLNCX2 was linearised with *HindIII/SalI* (New England Biolabs, Cat.No. R0104T /Cat.No. R0138T). Ligations between the extracted DNA were carried out using USB high concentration T4 DNA ligase enzyme (Affymetrix, Cat.No. 70042X 500 UN) with a 5:1 vector-to-insert ratio at 16°C overnight.

2.1.5 Preparation of transformation-competent JS4 cells

Following preparation of a small overnight culture of JS4 cells, LB (Luria Broth; Sigma-Aldrich®, Cat.No. L3522-250G) was inoculated with the stationary phase JS4 culture at a dilution of 1:500. Cultures were grown at 37°C until an A_{600} reading of 0.8 was achieved. The cells were then chilled on ice and harvested at 1,500 x *g* for 20 min at 4°C. Cell pellets were resuspended 1:10 in cold 0.1M CaCl₂ (Calcium chloride; Sigma-Aldrich®, Cat.No.C1016) relative to starting volume, and harvested at 1,500 x *g* for 10 min at 4°C. Cell pellets were then resuspended 1:100 in cold 0.1M CaCl₂:glycerol (85:15) and aliquoted at 50µl into eppendorf tubes before quick-freezing in liquid nitrogen. Frozen cells were stored at -80°C. Prior to transformation, competent cells were thawed at 4°C and 0.95µl cold 0.1M CaCl₂ was added to obtain a working concentration.

2.1.6 Transformation of competent cells

14ml Falcon™ polypropylene tubes (BD Biosciences, Cat.No. 352059) were chilled on ice, and competent cells also thawed on ice. When using XL-1 Blue cells, 50µl was aliquoted per reaction; for JS4 cells, 100µl was used per reaction. DNA of interest (1µl if PCR product; 10µl if ligation) was added to the chilled competent cells, gently mixed and incubated on ice for 30 min. Transformations were heat-pulsed for 45 sec at 42°C and placed on ice for 2 min. 0.5ml LB pre-heated to 42°C was added to the samples and cells grown for 1 h at 37°C in a shaking incubator (220rotations per min). Cells were plated onto LB-agar plates (10g LB, 6g Agar (to give 1.5%;

(Invitrogen™, Cat.No. 30391-023) made up to 400ml with PCR-grade water; ampicillin (Gibco®, Cat.No.11593-027) added at a final concentration of 100µg/ml) and grown overnight at 37°C. The plates were checked for presence of colonies the following day and picked into 10ml LB media cultures for mini-prep DNA, or for PCR screening of the moPrP insert in pLNCX2.

2.1.7 PCR screen for moPrP insert in pLNCX2 vector

Bacterial colonies from a transformation of a ligation reaction between mutant moPrP ORF insert DNA and linearised pLNCX2 were picked to check for the presence of the insert. Each reaction for the PCR screen contained 100µM LNCX2 forward and 100µM LNCX2 reverse primers, 10mM dNTPs, 50mM MgCl₂, 1xPCR buffer, 0.05U/µl GoTaq® DNA polymerase and the DNA of interest. Melting temperature was at 95°C; strands were annealed at 58°C, extended at 68°C and these three steps cycled 30 times for all samples. Strand extension was completed at 72°C and reactions cooled to 4°C.

2.2 Expressing the mouse prion protein in PK1 cells

2.2.1 Transfection of Phoenix Eco-tropic cells

moPrP_{pLNCX2} mutants were introduced with the aid of FuGENE[®] transfection reagent (Roche, Cat.No.11814443001) into the Phoenix-Eco helper-free retrovirus producer line (Nolan lab, Stanford University). Phoenix cells were seeded in 10cm tissue culture dishes at 10⁶ cells per 10ml of DMEM (Dulbecco's modified Eagle's medium; Gibco[®], Cat.No.11995065) supplemented with 2mM glutamine (Invitrogen[™] Cat.No.25030024) and grown overnight at 37°C, 5 CO₂. The transfection mix was prepared as 100µl serum-free media plus 12µl FuGENE, which was incubated for 5 min before adding 5-10µg moPrP_{pLNCX2} mutant DNA. Following 15min incubation with the DNA, the transfection mix was added drop-wise to 50-60% confluent Phoenix cells. Fresh media was put on the cells the next day, 24 h after which viral supernatant was collected, filtered through a 0.45µm filter and frozen at -80°C for later use in transductions.

2.2.2 PK1 cell culture

Murine PK1 neuroblastoma cells (D-Gen Ltd, UK) were cultured in Opti-MEM (Gibco[®], Cat.No.31985-070) containing 10% FCS (foetal bovine serum – gamma-irradiated; Life Technologies, Cat.No.10500, Lot.No.07Q1437K) and 1% PS (penicillin/streptomycin; Gibco[®], Cat.No.15240-062). This media is referred to as OFCS. All cells were grown at 37°C, 5% CO₂ and sub-cultured in OFCS when they reached confluency.

2.2.3 Dose-response curves

In a 6-well plate, 5 concentrations of geneticin G418 and puromycin (Sigma-Aldrich[®], Cat.No.A1720 and P8833 respectively) were tested on KD cells grown to 40% confluency. Selection media (OFCS plus G418/puromycin) was replenished and cell death assessed by eye. 100% cell death was observed after 3 days for puromycin selection at 4µg/ml and 10 days for G418 selection at 200µg/ml.

2.2.4 Transduction of PK1 and KD cells with retroviral supernatant

2ml of filtered viral supernatant was added onto KD (50-60% confluent) in 8ml OFCS. The polycation Polybrene (Sigma-Aldrich[®], Cat.No.H9268) was added at a final concentration of 8µg/ml and cells grown overnight at 37°C, 5% CO₂. The following day, viral supernatant was replaced with full OFCS and cells grown to confluence at 37°C, 5% CO₂ before addition of antibiotics (puromycin at 4µg/ml and G418 at 200µg/ml) for selection of clones. For PK1 cells without suppression of the endogenous prion protein, only G418 selection was used at 300µg/ml to select pLNCX2-containing cells.

2.2.5 Single cell cloning

KD cells were plated at limiting dilutions prior to transfection with viral supernatant. This ensured that upon selection, individual clones could be picked from the plate, which would be genetically identical as they originated from a single successfully transduced cell. Clones were picked from a 10cm dish, transferred to individual wells of a 96-well plate and

expanded in selection media (puromycin at 4µg/ml and G418 at 200µg/ml) from thereon to establish stable cell lines expressing the mouse PrP mutants of interest.

2.2.6 Scrapie Cell Assay (SCA)

This assay was developed within the Prion Unit⁹⁷ and allows for the detection of single cells that are positive for PrP^{Sc}.

Briefly, cells are plated in replicate on 96-well plates, infected with a predetermined dose of infectious RML prions (diluted in the same cell culture media they were seeded in). Maintaining the format in which cells were seeded initially and the wells containing infectious inocula, the cells undergo six passages into new 96-well plates, with samples taken for ELISPOT analysis (in 96-well plates with a PVDF membrane attached) at the last three splits, to determine the proportion of RML-infected cells.

All steps were undertaken in a class II microbiological safety cabinet in a containment level II laboratory used primarily for tissue culture involving infections with mouse RML prions.

Sample cells: Following 7-10 days of antibiotic selection cell lines were seeded at 18,000 cells per well on a 96-well plate. RML mouse prions (10% homogenate) were added to the cells the following day at a dilution of 3×10^{-5} , which corresponds to 6309 tissue culture infectious units. Cells were grown at 37°C, 5% CO₂ for the duration of the experiment (three weeks).

SCA control cells: PK1 cells were seeded at 18,000 cells per well and infected with a range of concentrations of RML mouse prions This control was used to ensure the assay generated reproducible and expected results.

A double log plot of PrP^{Sc}-positive cells against tissue culture infectious units should result in a linear relationship (Figure R11).

Splitting cells: cells were split 1:8 every 3 days and cell samples collected at splits 4, 5 and 6 for analysis of PrP^{Sc} accumulation via ELISPOT (enzyme-linked immunosorbent spot) assay.

Dilution series: The 10% RML mouse prion homogenate was serially diluted to concentrations of 3×10^{-5} , 1×10^{-5} , 3×10^{-6} , 1×10^{-6} , 3×10^{-7} and 1×10^{-7} , which corresponds to TCIU (tissue culture infectious units) of 6309, 1893, 631, 189, 63.1, and 18.9, respectively.

ELISPOT for SCA: At splits 4, 5 and 6, cells were counted and seeded at 25,000 cells per well on activated ELISPOT plates (Enzyme-linked Immunospot Multiscreen Immobilon-P 96-well filtration plates, Millipore, Cat.No. MSHAN4550). The 0.45µm PVDF membrane at the bottom of the plate was activated using 70% EtOH. Plates were washed twice with 1xPBS (Gibco®, Cat.No.70013-073) before seeding cells and filtering through a vacuum manifold. Plates were dried at 50°C for 1 h or until all wells were dry. The cells were treated with 2.0-2.5 U/mg ProteinaseK (Roche) in 1xPBS for 30 min (lysis) at 37°C, washed twice with 1xPBS and incubated with 2µM PMSF – a ProteinaseK inhibitor (Phenylmethanesulfonyl fluoride; Sigma-Aldrich®, P7626) for 10 min at RT. Treatment with GSCN (Guanidine thiocyanate; Sigma-Aldrich®, Cat.No. G9277) for 20 min at RT followed as a decontamination procedure. Supernatant was discarded into NaOH (Sodium hydroxide; Sigma-Aldrich®, Cat.No.S8045) as waste and wells washed 7 times with 1xPBS. For the immuno-reaction, SuperBlock (Thermo Scientific; Cat.No.37545) was added to the washed wells for 1 h

at RT, followed by primary antibody ICSM18 (D-Gen Ltd, UK) at 1:6000 dilution of a 3mg/ml stock in 1xTBST/1% non-fat milk powder for 1 h at RT. The supernatant was discarded into NaOH and wells washed 5 times with 1xPBS. Anti-IgG1-AP (secondary antibody) was added at a 1:6000 dilution in 1xTBST/1% non-fat milk powder for 1 h at RT. The supernatant was discarded into NaOH and wells washed 5 times with 1xPBS. Plastic under-drains were removed from the plates which were left to dry at RT under a hood. Colour development was carried out using an AP Conjugate Substrate Kit (Bio-Rad, Cat.No.170-6432) with a 30 min reaction time. Plates were washed twice with water, dried at RT under a hood and stored at -20°C in the dark (foil covered).

Determination of PrP^{Sc}-positive cells: To count stained cells, the detection settings of the WellScan (Imaging Associates, Oxfordshire, UK) software were optimised for wells with PrP^{Sc}-positive cells and wells with non-infected cells. For single cells the object size of the detection module was set to 9 and the threshold (detection sensitivity) adjusted until all visible spots of the well were detected - the threshold is indirectly proportional to the sensitivity of detection. After all visible spots were detected, the classifier was reset and positive spots added to adjust the new parameters of the classifier. After training of the classifier had been completed, the shape factor was set to 0.4 to exclusively detect spherical objects. Wells with non-infected cells were scanned and if required, settings for a low background were optimised by varying threshold amounts. Recommended values for threshold are 25 to 30.

2.2.7 Harvesting cells; total protein extraction by freeze-thaw method

Adherent PK1 cells were collected in ice-cold 1xPBS, and pelleted at 300 x *g*. The cell pellets were washed twice in ice-cold 1xPBS, resuspended in a small volume of PBS and frozen at -20°C. Lysates were prepared by resuspending the cell pellet in lysis buffer (150mM NaCl, 50mM Tris-HCl, pH 7.5, 0.5% Triton-X-100, 0.5% sodium deoxycholate, 1mM EDTA, 40U/ml benzonase). Cell debris was pelleted at 4°C, 7826 x *g* for 1 min and cell lysates collected in chilled eppendorf tubes. An aliquot of the lysate was collected for determining protein concentration via Bradford assay; lysates were then adjusted to 1mg/ml and stored at -20°C.

2.2.8 Western Blotting

Protein concentration of cell lysates was determined via the Bradford method and 25µg of protein was loaded per well (diluted in 1xPBS), unless stated otherwise. Sample buffer containing β-mercaptoethanol was added to the lysates which were spun down in a micro-centrifuge at 100 x *g* for 1 min. Samples were boiled at 100°C for 10 min, vortexed, centrifuged at 226 x *g* and loaded onto 16% Novex® Tris-Glycine mini gels (Invitrogen, Cat.No.EC6495BOX). Working concentrations of the running buffer for the gel contained 25mM Tris, 192mM glycine and 1% w/v SDS pH 8.6. Gels were run at 200V for 80 min. Transfer of the proteins from the gel was performed on PVDF membranes with 1x blotting buffer containing 20mM Tris, 150mM glycine pH 8.5, and 20% v/v methanol. In all cases, transfer was carried out at 35V for 90 min. Following transfer, the membrane was blocked in 5% non-fat dry milk in 1xPBST for 1 h and washed 4 times in 1xPBST. PrP was detected using ICSM18 at 1:10,000 . Primary antibody was applied for 1 h followed by 45 min of 1xPBST washes (2x 15 min washes; 3x 5 min washes). Secondary detection was carried out for 45 min, followed by 1 h of 1xPBST washes (buffer changed every 5 min) using goat-anti-mouse IgG-HRP (for ICSM18 primary antibody) or goat-anti-mouse IgG-streptavidin-HRP (for ICSM35b primary antibody) at 1:10,000. Immunoblot was developed using ECL.

2.2.9 Immunofluorescence analysis of moPrP expression in PK1 cells

Sterile 22mm glass coverslips were coated with 1mg/ml Poly-L-Lysine (Sigma-Aldrich®, Cat.No.P1399) for 30 min, washed with 1xPBS under the hood and dried, prior to seeding cells at 20,000 cells per coverslip. Cells were grown in 5% CO₂ at 37°C and fixed using 4% w/v PFA (paraformaldehyde, Sigma-Aldrich®, Cat.No.P6148 - pH 7.4, filtered through a 0.22µm filter) for 20 min at RT before immunofluorescence. Cells were washed 3 times with 1xPBS and subsequently incubated with primary antibody ICSM18 (D-Gen Ltd, UK) at a 1:7000 dilution for 1 h at RT, prior to 3 further washes with 1xPBS. AlexaFluor 488-conjugated goat anti-mouse (Molecular Probes®, Cat.No A-11001) was subsequently added at 1:1000 for 1 h at RT. After three washes with 1xPBS, coverslips were mounted using ProLong® Gold Antifade Reagent (Life Technologies, Cat.No.P10144) containing DAPI for nuclear staining, and left to dry. They were stored in a cool dark place prior to imaging.

2.2.10 Cell viability assay

Cell viability was assessed using the CellTiter-Glo® Luminescent Cell Viability Assay (Promega, Cat.No.G7570). PK1 cells were seeded in flat-bottomed plates at a density of 2.5 x 10⁴ cells/well and exposed to various concentrations of G418 for 10 days. Antibiotic-containing media was subsequently removed from all wells and replaced with 84 µl/well CellTiter-Glo® reagent, which was reconstituted following the manufacturer's

instructions. Cells were lysed by shaking for 2 min and plates incubated for 10 min at RT prior to recording luminescence (integration time = 100 ms).

2.2.11 Dot blot of cellular PrP expression

Cells were harvested, counted and subsequently centrifuged at 300 x *g* for 4 min. The supernatant was discarded and the pellet resuspended in lysis. Nitrocellulose membrane and three filter papers were then soaked in lysis buffer and fitted to a dot blot manifold. The volume of lysate corresponding to the desired number of intact cells was applied to the top of the manifold and serial 1:2 dilutions of cells blotted down the membrane. Membranes were blocked in Odyssey Blocking Buffer (LI-COR Biosciences; consists of a non-mammalian blocking reagent and 0.1% NaN₃ in PBS) for 1 h at RT, and PrP detected by incubating blots with 0.6 µg/ml ICSM18 for 1 h at RT. Bound ICSM18 was detected by incubating blots with 0.25 µg/ml goat anti-mouse IRDye® 800CW Infrared Dye (LI-COR Biosciences, Cat.No.926-32210) for 1 h at RT. Blots were washed twice with PBS, dried and visualised using an Odyssey infrared scanner.

Chapter 3

Results

3.1 Generation of an alanine-mutant mouse prion protein library

3.1.1 Experimental strategy

In order to test the contributions of individual residues of the cellular prion protein on the propagative potential of prions, we adopted a minimal mutagenesis approach. Various constructs of the mouse prion protein (moPrP) were generated, bearing alanine mutations: in the unstructured region (amino acids 23-111), the conserved hydrophobic region (amino acids 111-121) and the structured region (amino acids 121-230; Figure R1). In the unstructured region, alanine was substituted for one, two or three amino acids at a time within the sequence encoding the mature protein. Replacing existing residues with alanine effectively worked as a method for substituting individual native side chains with simple methyl groups. This method of alanine scanning allowed the examination of contributions from individual side chains to the function of the protein⁵³.

Alanine replacements were also made within the hydrophobic core and structured regions of the protein to test the influences of these regions on prion propagation. In the conserved hydrophobic region, we generated additional mutations to leucine, isoleucine, valine, proline and glutamate to investigate the putative role of membrane association^{63, 241} within this region on propagation.

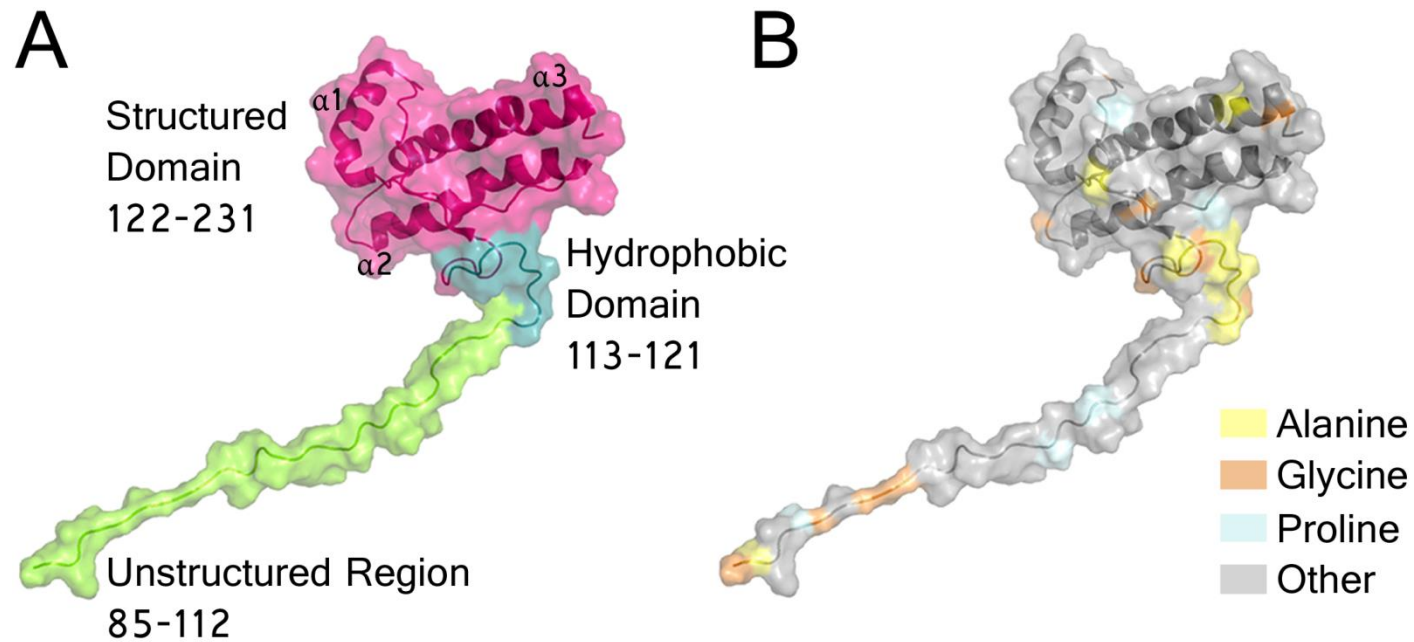


FIGURE R1: PDB ENTRY 2LEJ, HUMAN PRION PROTEIN

Mutations made in the moPrP mutant library are mapped onto prion protein PDB entry 2LEJ, modelled in PyMol (DeLano Scientific LLC). Note that human prion protein (huPrP) numbering shown here (2LEJ) differs from moPrP by +1, i.e. moPrP 84 is equivalent to huPrP 85. (A) Protein coloured by domain highlighting its main components. Note that residues 23-84 are missing from the structure. The unstructured flexible segment of the protein is highlighted in blue, the conserved hydrophobic domain in green and the globular structured domain in orange. (B) Regions coloured in yellow, orange and blue represent Ala, Gly and Pro residues, respectively, and highlight regions left largely unaltered so as to minimise structural changes; grey represents all residues other than Gly, Ala and Pro, most of which are mutated to alanine in this study.

Information on the solvent-exposed regions of the folded PrP structure is available from NMR and X-Ray Crystallography-derived structures^{67, 242}. Using this information, surface residues of the protein were primarily targeted for mutagenesis to identify which face/side of the protein is important for propagation.

Three spatially-proximal points on the protein surface were selected, and mutated to alanine. In this way, we ensured that cumulatively, most solvent-exposed regions of the protein were mutated to determine their contribution to prion propagation. This study differs from the typical targeted approaches to study PrP function, in that the whole protein, and not selected domains, were analysed for their contributions to prion propagation. Furthermore, to our knowledge it is the first extensive, cell-based mutagenic screen of the prion protein that assesses the effect of minimal mutations on prion propagation without interference from the endogenous protein. We have amassed a library consisting of over one hundred mutant constructs of the mouse prion protein that can be used to probe many questions about cellular and aberrant functions of PrP. Here, the library was used to investigate regions of the protein that regulate prion propagation (Table R1). The mutations covered more than 55% of the overall protein (Figure R1). The remaining unaltered 45% represent regions with existing alanine, glycine and proline residues and the bulk of non-surface-exposed residues within the structured region of PrP (Figure R1).

Unstructured region

PTM

Structured region

1	K23A	21 Q74A	35 V111M	55 G125A	75 Δ117-124	95 H176A
2	K24A	22 H76A	36 A112L	56 G126A	76 G123A.L124A.G125A	96 C178A
3	R25A	23 S79A.W80A	37 G113L	57 G126L	77 M128A	97 V179A
4	K23A.K24A.R25A	24 Q82A	38 A115G	58 G126V	78 L129A.S131A	98 V179A.I183A
5	P26A.K27A	25 H84A	39 A115L	59 Y127F	79 S134A.R135A	99 I183A
6	P28A	26 W88A	40 A116L	60 Y127P	80 H139A.G141A	100 V188A.T191A.T192A
7	W31A.N32A.T33A	27 Q90A	41 A117L	61 Y127R	81 H139A.G141.D146A	101 K193A.E195A
8	S36A.R37A.Y38A	28 T94A.H95A.N96A	42 A117R	62 M128L	82 N142A.N144A.E145A	102 T198A.D201A
9	Q41A	29 Q97A.W98A	43 G118A	63 M128V	83 D146A	103 K203A.E206A.R207A
10	K23A.K24A.R25A.Q41A	30 N99A.K100A	44 G118L	64 L129A	84 R147A.R150A.E151A	104 M204A
11	S43A	31 S102A.K103A	45 A119L	65 G130A	85 Y148A	105 M204Q.M205Q
12	N47A.R48A.W49A	32 K105A.T106A.N107A	46 A119P	66 G130L	86 M153A	106 V209Q.M212Q
13	Q52A	33 L108A.K109A	47 V120A	67 S131A	87 R155A	107 M204Q.M205Q.V209Q.M212Q
14	T55A.W56A	34 H110A.V111A	48 V121A	68 A132L	88 Q159A	108 E210A.Q211A
15	Q58A		49 G122A	69 S134A	89 Y162A	109 C213A
16	H60A		50 G122L	70 R135A	90 Q216A	110 K219A.E220A.Q222A
17	W64A		51 G123A	71 R135E	91 R163A.Y168A	111 Y224A
18	Q66A		52 L124A	72 H139A	92 S169A.N170A	112 Y225A
19	H68A		53 L124I	73 G141A	93 F174A	
20	S71A.W72A		54 L124V	74 Δ112-129	94 F174A.V179A	

TABLE R1: SUMMARY TABLE OF MOPRP MUTAGENIC CONSTRUCTS GENERATED IN PLASMID VECTOR PBLUESCRIPTSK+

All mutations were created in pBluescriptSK+ by site-directed mutagenesis, and sequence-verified.

3.1.2 Site-directed mutagenesis of the mouse prion protein

To generate the library of mutant constructs listed in Table 1, pBluescriptSK+ bearing the un-mutated, full-length moPrP open reading frame (ORF) was used as template DNA. This is equivalent to the endogenous protein and is therefore signified as the wild-type protein: moPrP^{WT}. The small size of pBluescriptSK+ makes it an ideal template for mutagenesis (Figure R2).

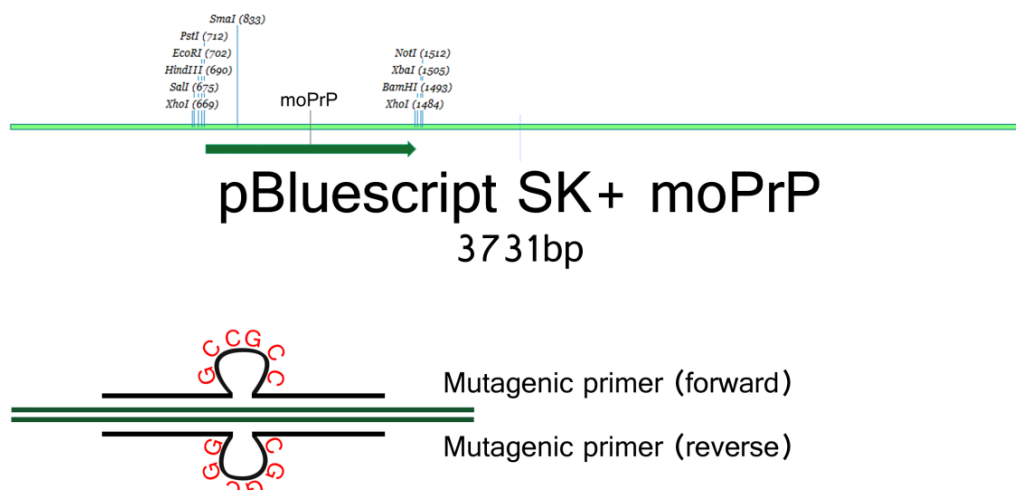


FIGURE R2: LINEAR MAP OF THE PLASMID VECTOR PBLUESCRIPTSK+

Linear map of the plasmid vector pBluescriptSK+ with moPrP ORF cloned at the *SmaI* site. Mutagenic primers were designed to anneal perfectly to the template sequence either side of the mutation site for both forward and reverse primers (panel 2). Primer pairs are indicated in black with non-annealing segments represented as loop regions bearing alanine codon GCC (sense) and CGG (anti-sense) in red. They were typically designed to be 30-mers, with longer primers (40-mers) designed for those more difficult to amplify (Appendix).

Mutations were introduced into the moPrP ORF using Stratagene®'s site-directed mutagenesis kit. Complementary pairs of primers were designed per intended mutation to bind the same region of DNA on both sense and antisense strands for site-directed mutagenesis (Figure R2). Depending on the GC content within the sequence, annealing temperatures and cycle numbers varied for optimal amplification (Table R2).

	Step	Process	Temp	Time	
Standard PCR	1	Melting parental strands	95°C	30 sec	
	2	Melting strands	95°C	30 sec	
	3	Annealing	55°C	1 min	
	4	Extending	68°C	3 min	
	5	Cycle steps (2-4) 16x for DNA template /samples and 18x for controls			
	6	Complete extension	72°C	5 min	
	7	Cool reaction	4°C	o/n	

TABLE R2: STANDARD PCR CONDITIONS FOR SITE-DIRECTED MUTAGENESIS

Site-directed mutagenesis for all mutants generated was carried out using the appropriate mutagenic primer pairs and the PCR cycling conditions shown (o/n: overnight). For reactions that did not amplify well using this method, touch-down PCR was used.

Following successful amplification, as assessed by visualisation on 1% agarose gels (Figure R3 B), the PCR product was *DpnI*-digested to selectively cleave template DNA. The *DpnI* enzyme only cleaves methylated DNA strands, leaving newly synthesised, un-methylated, mutated DNA intact. *DpnI*-digested PCR product was then transformed into XL-1 Blue supercompetent cells, and colonies were picked to grow bacterial cultures. Plasmid minipreps were prepared and sequence-verified for the presence of the intended mutation, and also to confirm there were no errors within the ORF (Figure R4). Sequencing results were analysed using Sequence Scanner (v1.0).

moPrP mutant DNAs correct for the intended mutation were digested with *HindIII/XhoI* and the excised insert ligated to pLNCX2, which was linearised with *HindIII/SalI*. The ligation reaction was transformed into competent JS4 cells, a *recA*-derivative of MC1061²⁴³, and the resulting colonies screened by PCR for the presence of insert using pLNCX2-specific primers (Figure R3 E).

Single digest of pBluescriptSK+ with either *HindIII* or *XhoI* yielded a single band indicative of linearised DNA. pBluescriptSK+ with moPrP^{WT} ORF (Figure R2) also produced a single band when digested with *HindIII*. However, when digested with *XhoI* pBluescriptSK+ with moPrP^{WT} ORF produced two bands, one migrating at approximately 3Kb and the other at about 850bp (Figure R3 A). Two fragments on the agarose gel indicated that the plasmid had been digested twice with *XhoI*, suggesting two cut sites. The additional *XhoI* site was introduced in pBluescriptSK+ when the

ORF of moPrP^{WT} was cloned into this plasmid (Appendix). The sequence of moPrP^{WT} cloned into pBluescriptSK+ is 815bp in length. When JS4 colonies were screened for the presence of moPrP insert in pLNCX2, bright bands were observed at 1Kb (Figure R3 E). This increase in size is the result of the screening primers binding the vector sequence approximately 150bp from the cloning sites, thereby incorporating the extra base pairs.

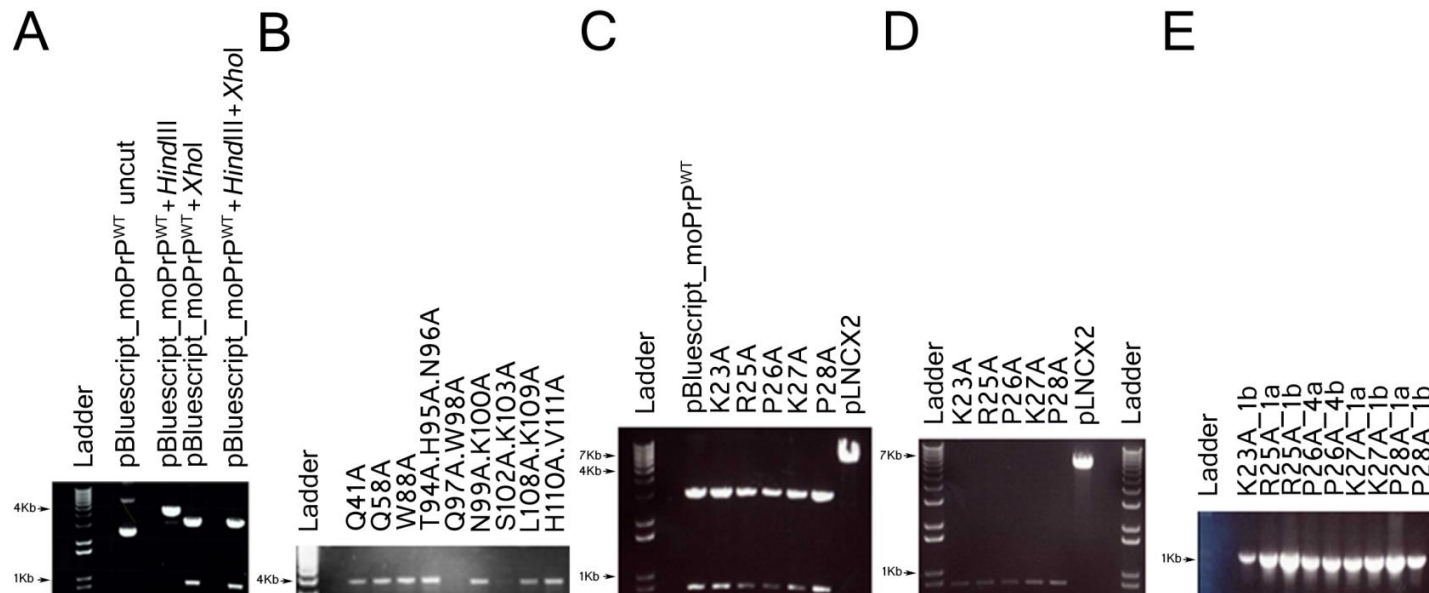


FIGURE R3: MUTAGENESIS OF MOPrP IN pBLUESCRIPTSK+ AND SUBSEQUENT CLONING INTO pLNCX2

All gels shown here are 1% agarose gels with 5 μ l of Track It 1Kb ladder in lane 1 (A) Control digests: pBluescriptSK+ DNA bearing the mouse prion protein ORF is approximately 4Kb; nicked circle and supercoil versions of the plasmid were seen in the uncut DNA. Plasmid digested with *HindIII* displayed a singly cut band; digestion with *XhoI* gave two bands of 3Kb and 1Kb, with the smaller band running slightly lower when doubly digested. (B) 10 μ l of the PCR product was loaded to check for successful amplification. (C) Double digests: pBluescriptSK+ DNA bearing either moPrP^{WT} ORF or moPrP^{Ala} ORF digested with *HindIII/XhoI*, giving bands at 3Kb and 850bp. The last lane shows the final plasmid vector, pLNCX2, linearised with *HindIII/SalI*. (D) 10 μ l of gel extract obtained from purification of DNA from (C) was run to check for level of recovery. (E) PCR colony screening of JS4 colonies. Bright bands at 1Kb are indicative of the moPrP ORF being present.

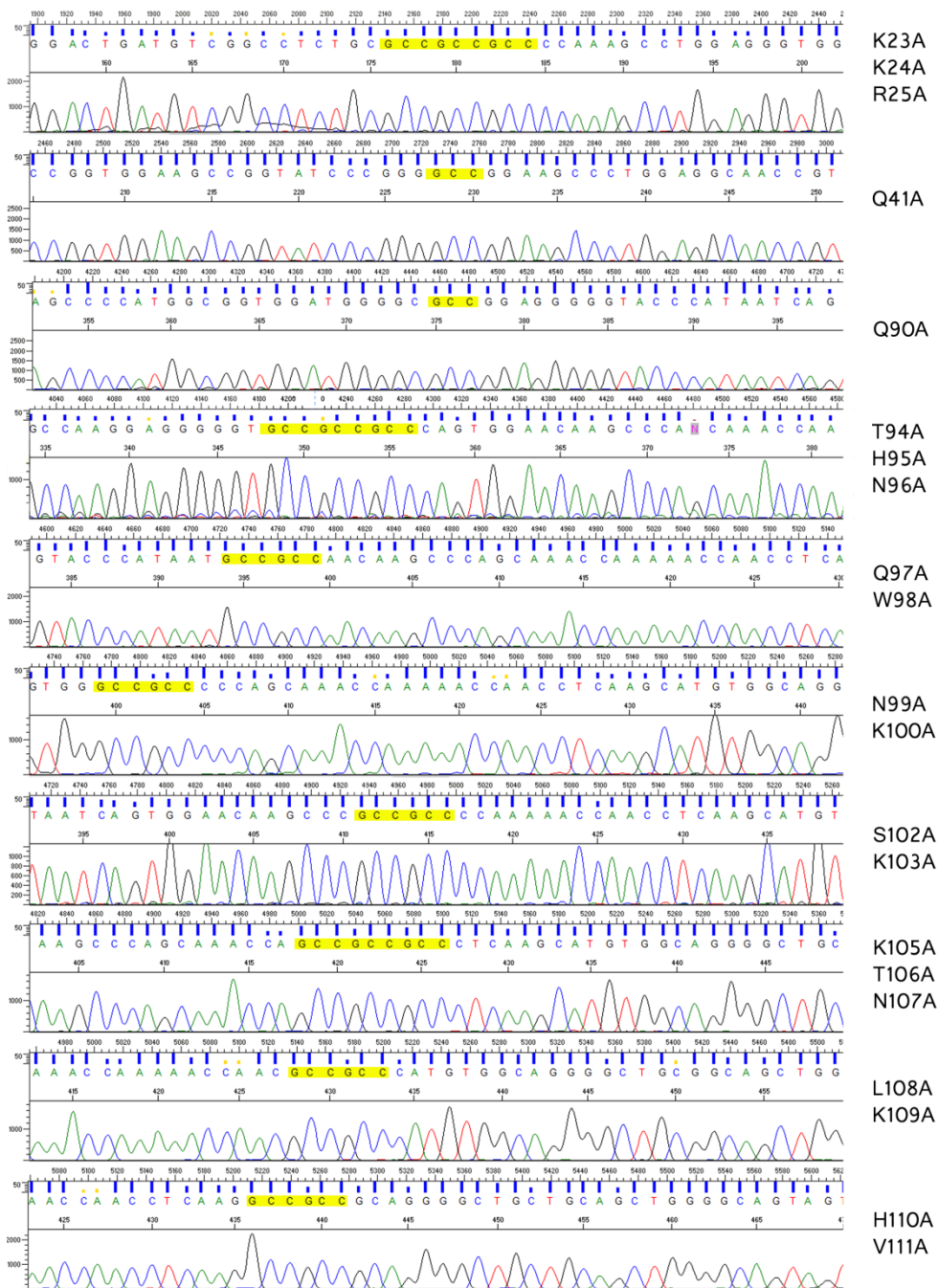


FIGURE R4: SEQUENCING DATA CONFIRMING THE PRESENCE OF ALANINE MUTATIONS AT INDICATED SITES

Small sections of sequencing are shown for the mutants of greatest interest. Segments corresponding to the mutated codons are highlighted in yellow within the sequence frame. All alanine replacements bear an XXX – to GCC change.

3.1.2 Expressing moPrP^{Ala} in mammalian cells

This study required stable expression of moPrP^{WT}, and engineered mutants of moPrP, in a cell line such as PK1 cells that can report prion propagation. PK1 cells are a derivative of mouse N2a neuroblastoma cells that are highly susceptible to RML prions. One of the most efficient ways of gene delivery in mammalian cells is through retroviruses²⁴⁴. Here we used Phoenix retroviral cells, an ecotropic packaging cell line originally created in the Nolan laboratory²⁴⁵, to package the retroviral vector plasmids containing moPrP into ecotropic viruses.

The pLNCX2 vector was selected to introduce moPrP into mammalian cells on the basis that it is a retroviral vector, which can be used to package the construct into ecotropic viruses by transient transfection. The plasmid vector is able to transiently express, or integrate and stably express, a transcript containing the viral packaging signal, a selectable marker and the gene of interest, which is cloned into the MCS under control of the CMV (Figure R5), which works very well in PK1 cells. The 5' viral LTR drives expression of the neomycin resistance gene for G418 selection in mammalian cells. Phoenix retroviral cells are adherent cells that can be easily transfected. They contain the elements required to facilitate packaging, reverse transcription and integration. The Phoenix cells have the functions gag, pol and env stably integrated in them, which are required in *trans* to package the retroviral vector.

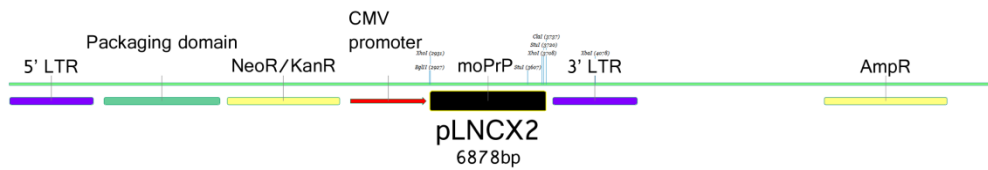


FIGURE R5: LINEAR SEQUENCE MAP FOR PLASMID VECTOR PLNCX2

Linear sequence map for plasmid vector pLNCX2 showing presence of long terminal repeats (LTRs) in purple (derived from Moloney murine leukemia virus, MMLV); packaging element in green; resistance genes neomycin/kanamycin (NeoR/KanR) and ampicillin (AmpR) in yellow, cytomegalovirus (CMV) promoter in red. The multiple cloning site (MCS) lies between the CMV promoter and the 3'UTR. Insertion of moPrP is shown as a black bar within the MCS.

When pLNCX2 is introduced into Phoenix cells it has the packaging signal in *cist* on the RNA, which allows the construct to be inserted into the empty virus particles. The viral packaging signal (ψ) directs incorporation of vector RNA into viral particles, additional signals allow the reverse transcription, repeat regions at both ends of DNA allow for transfer, and partially inverted repeats at the ends of viral LTRs allow for integration²⁴⁶. Transfected Phoenix cells rapidly produce recombinant viral particles (between twenty-four to forty-eight hours post-transfection) for the efficient infection of dividing cells. The viral particles are released into the cell media, which can be filtered and applied immediately onto target PK1 cells. Filtering through a 0.45 μ m filter allows the virus particles to pass through whilst preventing any floating cells from contaminating the viral supernatant. Once PK1 cells were transduced, the culture was maintained in the presence of G418 until all cells in the non-transduced culture died out from antibiotic selection (10-14 days; Figure R6).

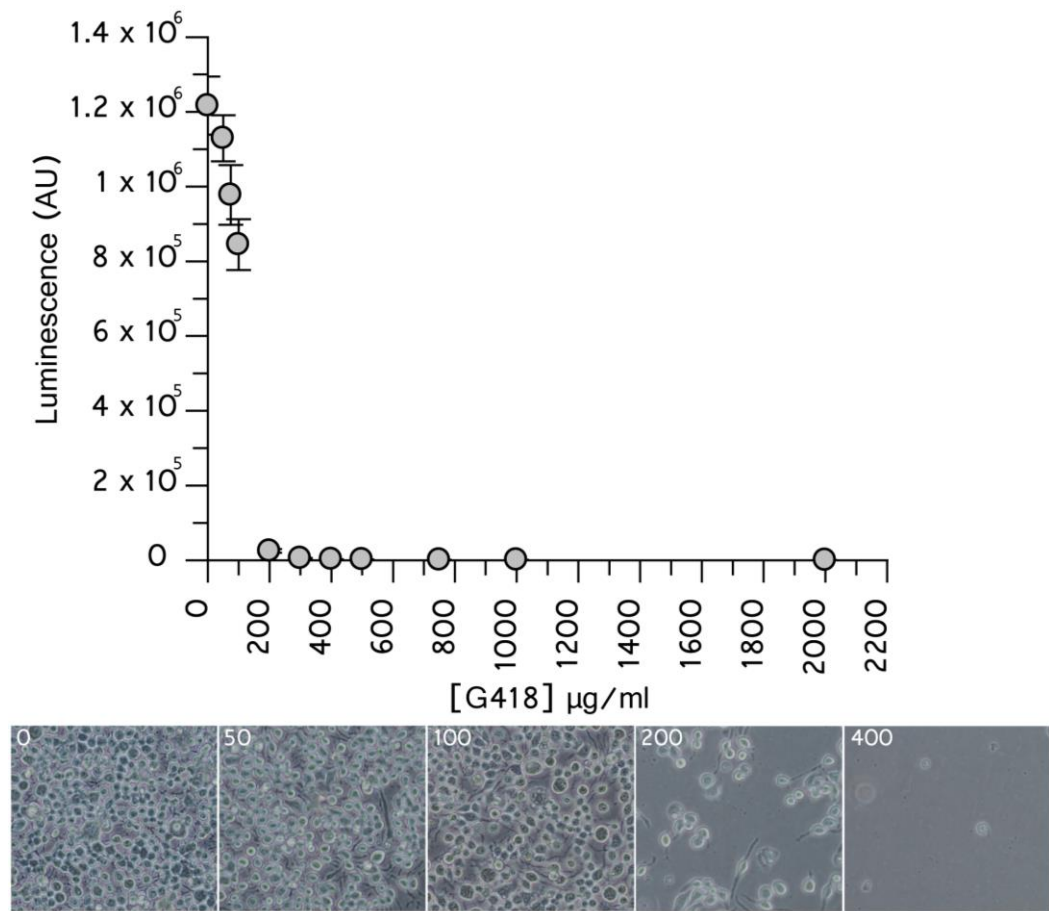


FIGURE R6: DOSE-RESPONSE CURVE OF KD CELLS TO G418 ANTIBIOTIC

KD cells were seeded on to a 96-well plate at a density of 25,000 cells/well. G418 was added to the cell media at concentrations ranging from 0 to 2mg/ml and passaged for ten days. Luminescence for each well was determined using a cell viability assay and used to establish the optimum concentration for antibiotic selection. The panel below shows phase contrast images of the KD cells under G418 selection at 0, 50, 100, 200 and 400 $\mu\text{g/ml}$. Magnification at x20.

The G418 added in the selection phase ensured that only cells that had the stably integrated provirus survived. Successfully transduced cultures were frozen down in bulk, with a new vial used per experiment. PK1 cells were frozen down at low passage numbers whenever possible since they have been observed to lose susceptibility to infectious prions if cultured long-term (unpublished data). PK1 cells are particularly susceptible to infection by a well-characterised, mouse-adapted prion strain known as Rocky Mountain Laboratory (RML)²⁴⁷.

It is important to note that the method adopted here produced bulk cultures containing pools of mixed clones: multiple independent daughter cells were established from individual transductions. Each successful transduction initially generates single cell clones (SCCs). If they are not separated at this stage, multiple SCCs proliferate, creating a mixed population (referred to as a bulk culture) where all cells expressing moPrP with alanine replacements (moPrP^{Ala}) bear the same intended mutation, but may vary in some cellular aspects such as doubling time and expression level. This is due to random but preferred retroviral integration²⁴⁸.

The bulk cultures represent an average of all successfully transduced SCCs. All mutants created in this study were tested this way initially. Cells stably expressing moPrP^{Ala} were tested via a standard Scrapie Cell Assay (SCA)⁹⁷, for their respective propagation profiles following RML infection.

3.1.3 Generating a PK1 cell line knocked-down for expression of moPrP

PK1 cells, a derivative of N2a cells, are routinely used within the department for their high susceptibility to infection by RML prions. Expression of the endogenous *Prnp* gene in PK1 cells was silenced by shRNA targeting the 3'UTR of *Prnp*. Eight shRNA were designed and cloned into pRetroSuper, and tested for their ability to reduce expression of endogenous PrP in PK1 cells.

Expression of the cellular form of the prion protein is necessary for that cell to be infected with, and propagate prions. PK1 cells in which *Prnp* had been silenced were tested for their ability, or lack thereof, to propagate RML prions. shRNA8 yielded the highest level of silencing of endogenous PrP and was taken forward.

Next, 100 SCCs of PK1 cells, into which shRNA8 had been stably transduced by puromycin selection, were isolated. These 100 SCCs were then individually reconstituted with moPrP^{WT}; through SCA, the SCCs that presented the phenotype of silenced cells and were not susceptible to infection with RML, but regained susceptibility upon reconstitution with moPrP^{WT}, were identified. Of these, SCCs that propagated RML to levels comparable with wild-type PK1 cells were expanded and SCC PK1-10/si8#9 was found to meet these criteria.

This represents a line of PK1 cells that are highly sensitive to RML prions (PK1 cells, single cell clone 10), but are silenced for expression of endogenous PrP protein (shRNA8 was most effective) and report near wild-

type susceptibility to RML prions once reconstituted (#9) with moPrP^{WT}. These moPrP knockdown cells are referred to as KD from hereon.

KD cells were the main cell line used for this study as it allowed us to test the contributions of discrete mutations within moPrP on prion propagation, without interference from the endogenous protein. KD cells were found to have approximately 88% reduction in the level of PrP expression. (Figure R7). This residual level of protein expression did not support prion propagation.

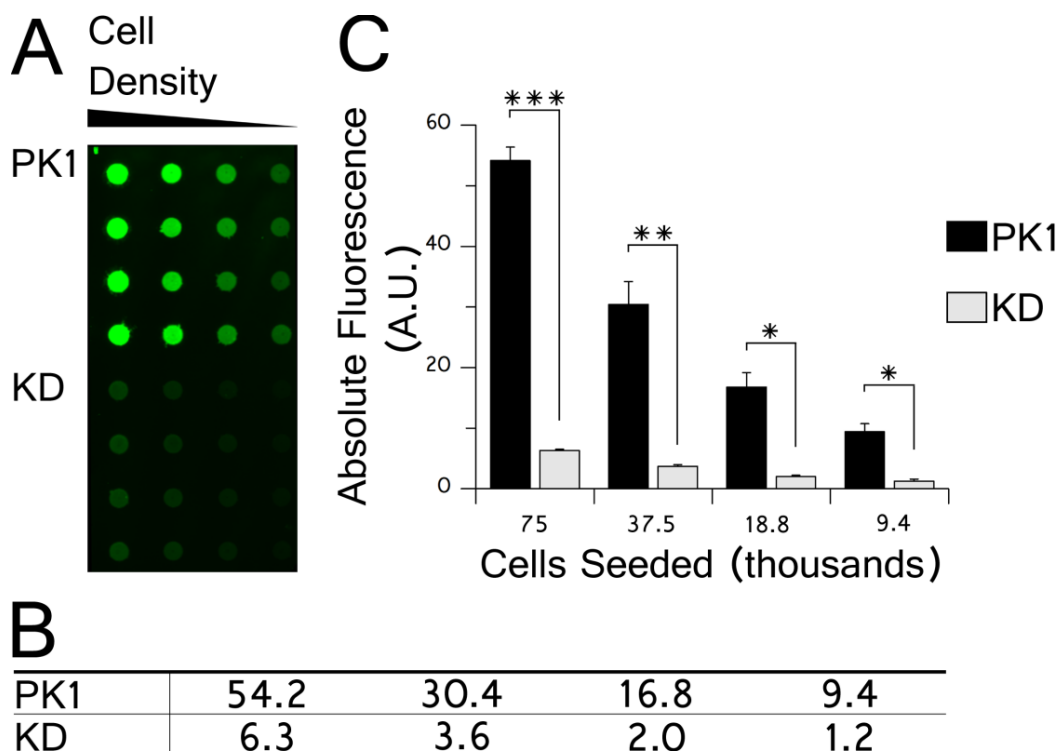


FIGURE R7: MOPrP EXPRESSION IN PK1 AND KD CELLS

PK1 and KD cells were lysed and seeded at four cell densities, ranging from 75K to 9.4K cells per well, in a 96-well plate. moPrP expression was detected using ICSM18 antibody. Following standard dot blot procedure, expression levels were quantified based on absolute fluorescence as determined by Li-Cor Odyssey® Infrared Imaging System. (A) Fluorescence image from dot blot experiment showing PK1 and KD cells with four replicates per tested cell density; (B) Raw values for absolute fluorescence; (C) Bar chart for direct comparison of moPrP expression in PK1 cells versus KD cells. *P*-values for cells were calculated using an unpaired *t*-test with *** representing *P*- values ≤ 0.0001 , ** ≤ 0.0005 and * ≤ 0.005 . Knockdown levels of moPrP were calculated to be approximately 88%.

3.1.4 Reconstitution of KD cells with alanine mutants of moPrP

The silencing of endogenous PrP by targeting the 3'UTR of *Prnp* allowed for reconstitution of KD cells with moPrP^{WT} without interference from shRNA8 and/or the endogenous PrP protein.

KD cells displayed similar growth and morphological characteristics to PK1 cells, as did KD cells reconstituted with the full-length wild-type protein: KDmoPrP^{WT} cells. This was also true for KD cells reconstituted with the moPrP deletion mutation Δ 23-88: KDmoPrP Δ 23-88 (Figure R8). These KD cells were previously made by Parineeta Arora, but are described in detail to document how they were established and why they are suitable for reconstitution with both moPrP^{WT} and alanine mutants of PrP: moPrP^{Ala}.

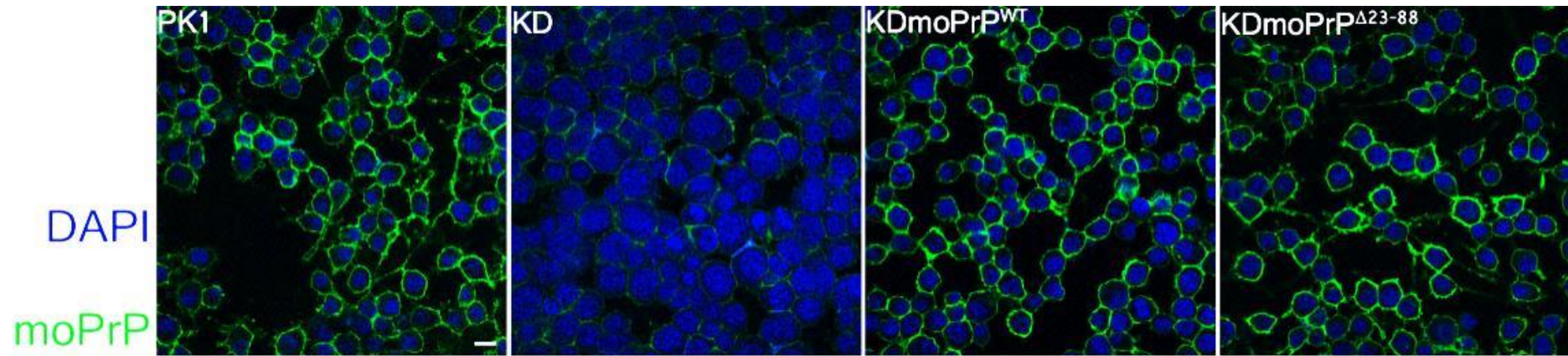


FIGURE R8: IMMUNOFLUORESCENCE OF KD CELLS RECONSTITUTED WITH moPrP CONSTRUCTS

Panel showing confocal images of cells. moPrP expression is shown in green (ICSM18 antibody) and nuclear staining in blue (DAPI). PK1 cells showed surface labelling of the endogenous protein; KD cells exhibited very low levels of moPrP expression. KD cells reconstituted with either moPrP^{WT} or an N-terminal deletion (Δ 23-88), showed similar protein expression. Scale bar represents 20 μ m. Magnification at x40.

KD cultures, both transduced and non-transduced with virally packaged pLNCX2, were cultured in 4µg/ml puromycin to prevent the multiplying cells from losing the shRNA against *Prnp* 3'UTR that silences expression of the endogenous prion protein. This concentration was determined previously by Parineeta Arora in generating the KD cell line (unpublished data). Using this approach we generated KD cells expressing the moPrP mutants indicated in Table 1 (Figure R9).

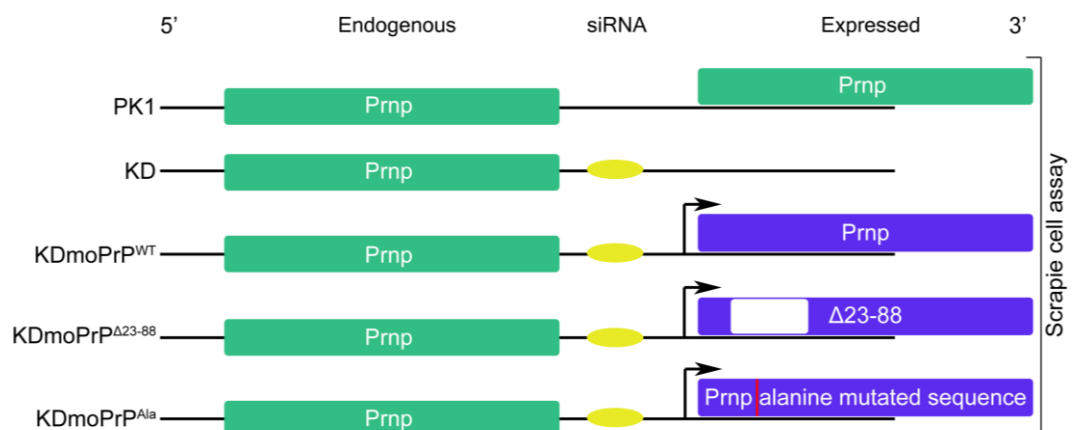


FIGURE R9: CELL LINE SCHEMATIC

PrP is represented by green bars in this schematic. KD line was established through stable integration of a pRetroSuper construct expressing shRNA against the 3'UTR of *Prnp*; when shRNA8 is processed to siRNA8, expression of the endogenous protein is silenced. This KD line was used as the template to reconstitute expression of moPrP^{WT}: KDmoPrP^{WT} (packaged DNA shown in purple inside the virus particle), or to exclusively express mutant forms of moPrP. This includes deletion mutants of the protein such as moPrP^{Δ23-88} or alanine replacements: KDmoPrP^{Ala}.

3.2KD cells reconstituted with moPrP propagate RML prions in the Scrapie Cell Assay

3.2.1 Experimental strategy

The Scrapie Cell Assay (SCA) is routinely used in the MRC Prion Unit as a quantitative method of assessing the ability of a cell line to propagate prion infection⁹⁵. The cell lines used here were PK1 cells, KD cells and KD cells reconstituted with moPrP^{WT} and its mutant forms. RML prions were applied to the cells seeded at a fixed density and their propensity to propagate prions was measured by the scrapie cell assay (SCA).

RML prions are well-defined mouse-adapted prions derived from sheep infected with Scrapie by W. Hadlow at the Rocky Mountain Laboratories in Hamilton, Montana²⁴⁷. RML is suitable for prion studies in mouse cell lines and highly infectious to PK1 cells used in this study. It is prepared as a 10% brain homogenate from mice infected with these prions, and its potency measured in a limiting dilution assay (SCEPA); SCEPA is quicker than, but as sensitive as, mouse bioassays at determining infectious titre^{95, 97}.

It involves determining the number of prion-infected cells and calculating infectivity based on the proportion of 'positive' wells to 'negative' wells, $P_{(0)}$, from the total number infected, $N_{(0)}$. This is given by the Poisson equation that is: $P_{(0)} = N_{(0)}/N = e^{-m}$ where m denotes the mean number of infected cells per well⁹⁵. Both SCA and SCEPA give an indication of a cell line's ability to propagate prions. There were a number of reasons why we adopted the SCA approach over SCEPA. Firstly, for both SCEPA and SCA

there is a user-defined threshold for what constitutes as propagation. However, in SCA these raw spot numbers can be graded so as to define the capacity of a cell line to propagate prions, as in this study, to full, reduced, severely limited and abrogated propagation. In SCEPA, there is only one threshold for a cell line being classified as positive or negative for propagation and comparisons between the propagative capacities are measured by the ratio of positive to negative wells. Since the propagation capacity of the moPrP alanine-mutant lines to propagate RML, was not pre-determined, we did not want to bias the results in either direction and thus opted for data collection in the form of raw spot numbers – SCA. Additionally, SCEPA is generally a lengthier assay, with two additional cell passages equivalent to an extra week of experiments relative to SCA; SCA therefore provides a quicker turnaround time.

3.2.2 Scrapie Cell Assay for reconstituted KD cells

Each moPrP^{Ala}-expressing cell line was seeded at 18000 cells/well in 96-well plates, typically with 8 repeats per line, and infected with RML homogenate at a 10^{-5} dilution (Figure R10). Duplicate plates were set up for non-infected cultures. All plates were split 1:8 twice a week, for six splits. At splits 4, 5, and 6, cell suspensions corresponding to 25000 cells per well are applied to pre-activated ELISPOT plates for detection of ProteinaseK-resistant PrP. A serial dilution of the homogenate was always applied to PK1 cells as a positive control for the SCA, and a double log plot of the observed spot number against tissue culture infectious units (TCIU) was prepared (Figure R10). This should be linear to indicate that the assay has

worked. Wild-type PK1 cells and KDmoPrP^{WT} cells consistently reported maximum spot numbers above 800 whereas spot numbers for non-infected samples were below 30. Note that at split 6, a plateau was reached for higher concentrations of RML, but linear for splits 4 and 5 (Figure R11). The combination of RML dilution used here (1×10^{-5}) and sampling the cell population at splits 4, 5, and 6, allowed for a window of detection that was large enough to accommodate samples which propagate well and sensitive enough to pick up low signals from those that did not propagate as profusely. Furthermore, the standard SCA can detect propagation from background from split 3 onwards, as there is sufficient dilution of the applied inocula at this time point to call true positives from residual RML. Sampling the alanine-mutant moPrP cell lines at splits 4, 5 and 6 for propagation increases confidence in the data that the spots observed are generated from the reconstituted KD cells *de novo*. It is also important to note that the 96-well layout of cells and subsequence applied infectious titres of RML prions is maintained throughout the assay.

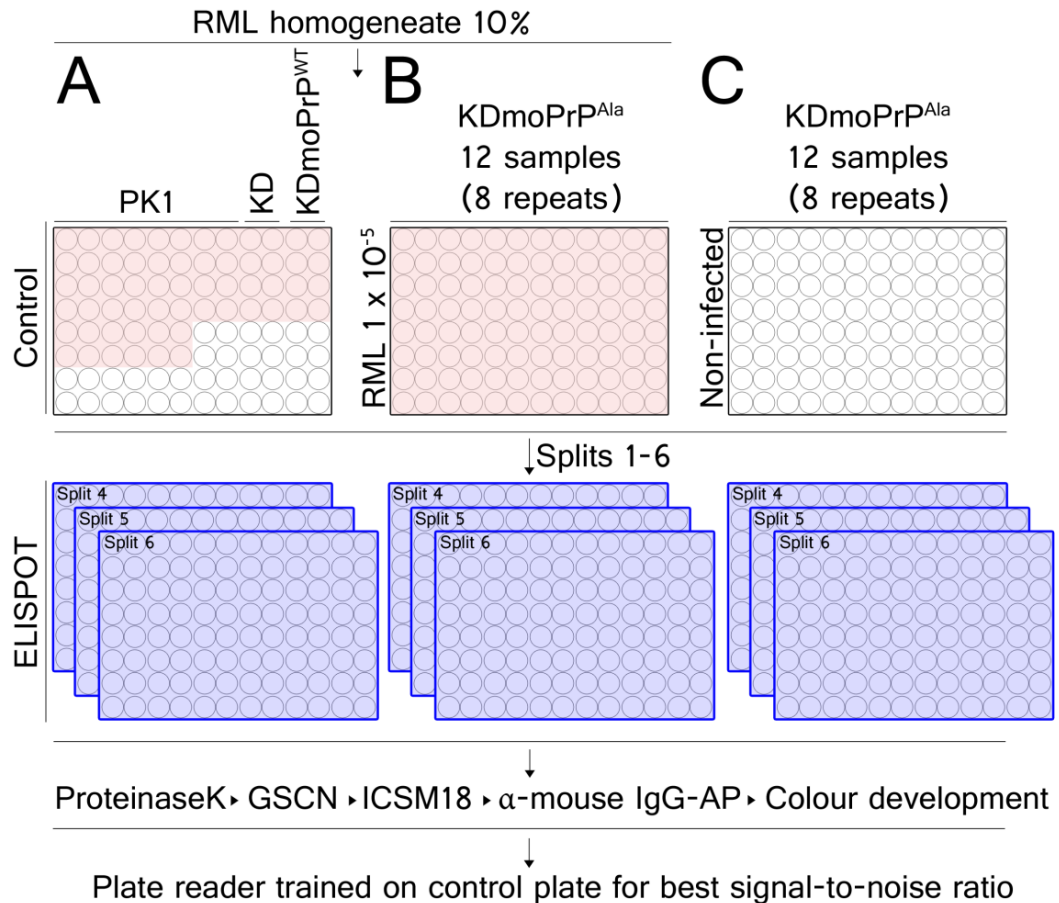


FIGURE R10: SCRAPIE CELL ASSAY AND ELISPOT PLAN

Schematic of screening alanine mutants of the mouse prion protein by SCA. All cells were seeded at 18000 cells/well. (A) Control plate in which RML was serially diluted down the plate from 3×10^{-5} to 1×10^{-7} . Pink denotes infected wells and clear wells represent non-infected wells. KD and KDmoPrP^{WT} were used as additional controls to PK1 cells. (B) An RML dilution of 1×10^{-5} was used to infect KDmoPrP^{Ala} cells; each column represents one cell line. (C) Cells were seeded following the same layout as in (B), but left non-infected. Cells were split 1:8 for six splits, but only at splits 4, 5, and 6 were sampled for ELISPOT. Revelation of ELISPOT plates following ProteinaseK treatment, GSCN denaturation, antibody incubation and colour development, was followed by reading the plates; Plate reader output was in the form of spot numbers per well.

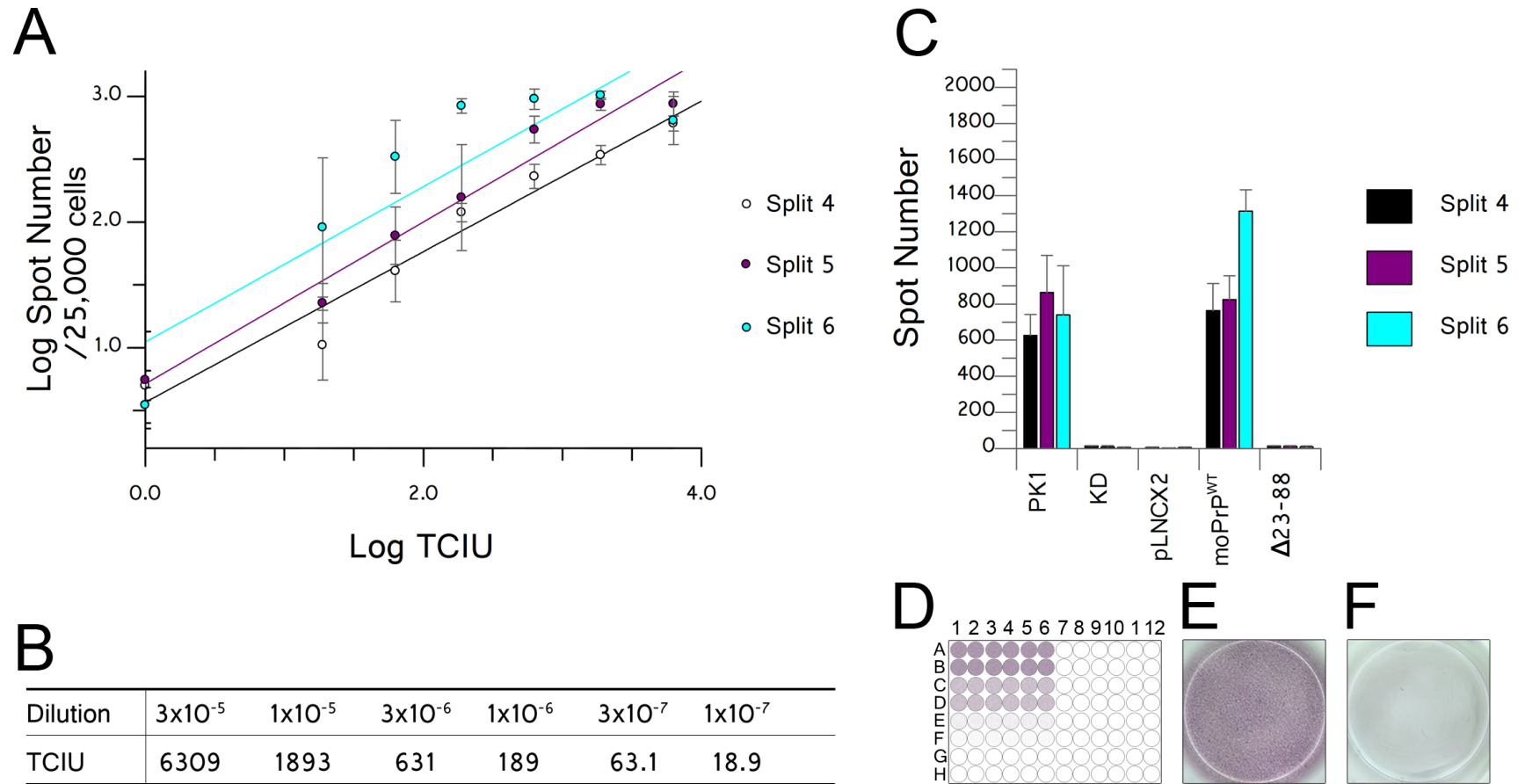


FIGURE R11: SCRAPIE CELL ASSAY OUTPUT

(A) Double log plot of spot number against tissue culture infectious units (TCIU). (B) Serial dilution of RML homogenate and calculated SCEPA data for TCIU. (C) SCA data from control cell lines PK1 (wild-type); KD (silenced for *Prnp*); pLNCX2 (vector only); moPrP^{WT} (reconstituted KD cells); Δ23-88 (N-terminal truncation of moPrP). (D) Schematic of RML serial dilution in 96-well plate format for six concentrations shown in (B); (E) ELISPOT revelation of a positive well; (F) ELISPOT revelation of a negative well.

ELISPOTs were developed through a chromogenic assay, where an alkaline phosphatase (AP)-conjugated secondary antibody was added to wells treated with ProteinaseK and pre-incubated with anti-prion antibody ICSM18 (Figure R10). Increasing amounts of ProteinaseK-resistant PrP resulted in higher spot numbers, which were taken to represent the number of cells infected by RML. Infected cells that efficiently propagate prions showed a split-to-split increment in spot number. This however, is not an absolute requirement; depending on the days between splits (two or three) there may be slight variances such that Split 5 readouts are occasionally lower than Split 4. The best indication for efficient propagation is taken to be a value of about eight hundred spots achieved at split 6 (Figure R12). Note that the following conditions for SCA were used as standard in the following chapters:

- 1) 10% RML homogenate as stock inoculum for all SCAs from which required dilutions are made in cell culture medium
- 2) For general screening of propagation profiles, cells were infected with 1893 TCIU of RML, which was applied as a 1×10^{-5} dilution of the 10% homogenate, based on SCEPA calculations. This concentration (1893 TCIU) is referred to as a 1×10^{-5} dilution of RML homogenate from hereon.
- 3) RML batches I8700 and I14051 were used in this study. TCIU are given (Figure R11) for I8700; I14051 displayed similar infectivity (data not shown).

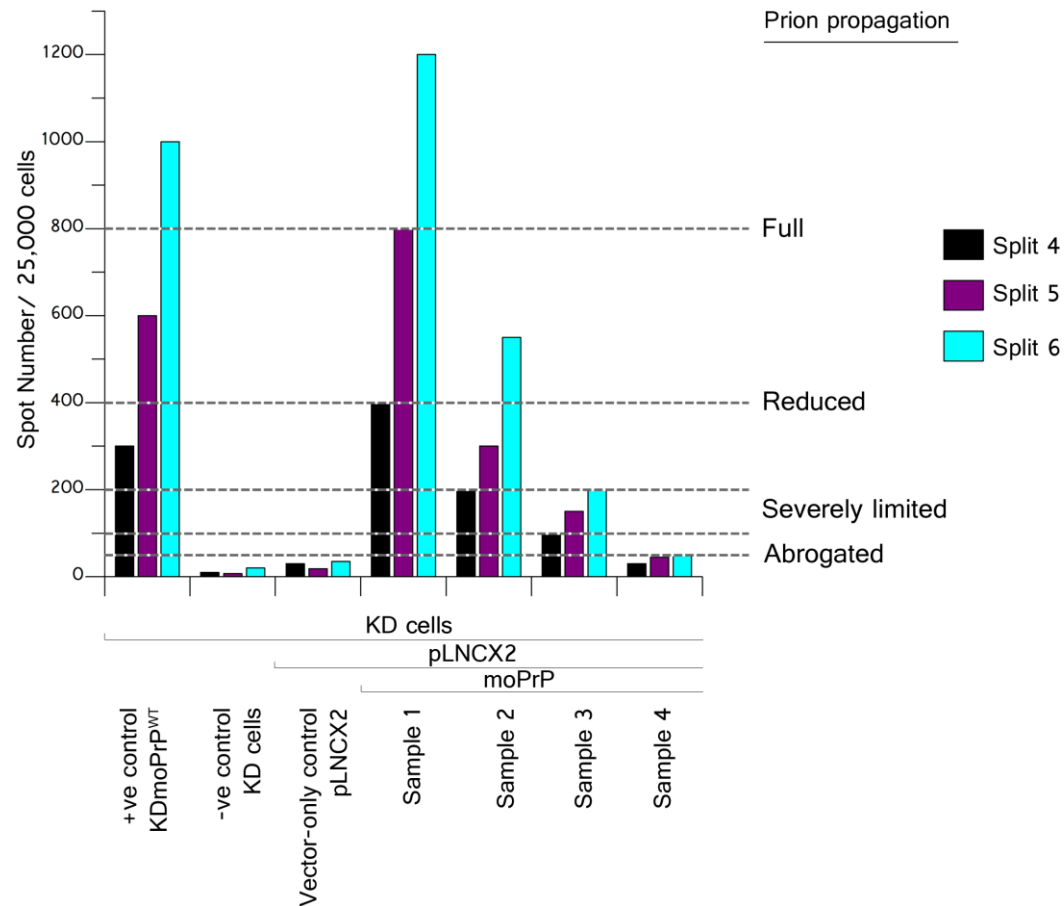


FIGURE R12: GUIDE FOR RML PRION PROPAGATION READOUT

Example of prion propagation profiles. SCA analysis of cells infected with RML: data shown for three consecutive splits (4, 5 and 6). KDmoPrP^{WT} cells are knockdown (KD) cells reconstituted with the wild-type moPrP sequence and represent a positive control that can propagate prions efficiently - above 800 spots at split 6. KD and KD cells expressing the empty vector (pLNCX2) do not propagate prions and present spot numbers below 50. Samples 1, 2, 3 and 4 are shown as cells in which propagation relative to KDmoPrP^{WT} is fully efficient, reduced, severely limited and abrogated, respectively.

3.2.3 moPrP deletion mutant Δ 23-88 does not support prion propagation

KDmoPrP^{WT} propagated RML with a similar efficiency to PK1 cells (Figure R11). KD cells showed no propagation whatsoever; this demonstrated that susceptibility of KD cells to RML was fully restored upon reconstitution. KD cells expressing pLNCX2 represent cells transduced with the empty vector; lack of prion propagation in this line demonstrated that there was no contribution from the plasmid vector in terms of prion propagation, and that it was a suitable system for testing the effects of moPrP^{Ala} in KD cells.

KD cells expressing of moPrP Δ 23-88 lacked propagative capacity as the propagation profile for this construct mimics that of the negative control lines, that is, KD and KDpLNCX2 (Figure R11). This result was observed previously in our laboratory (Parineeta Arora, *Personal communication*) and was the basis for this study. It has also been reported by others^{114, 134} and suggested that the octapeptide-inclusive N-terminal segment of PrP region 23-88 regulates propagation of the prion protein³⁷.

Our initial aim was to investigate discrete regions within this domain, and then extend this study to the remainder of the protein, to delineate which amino acids within the prion protein are required for its efficient propagation. Note that for all SCA results shown in graphically, spot number is the total number of ProteinaseK-resistant PrP detected from 25,000 cells infected with RML prions.

3.3 Polybasic region CC1 and residue 41 mediate the efficiency of prion propagation

3.3.1 Experimental strategy

Bulk cultures of KDmoPrP^{Ala} cells were established and assayed on at least three independent SCAs to investigate their propagative potential following infection with RML prions. For cell lines that reported a reduced capacity for propagation compared to wild-type PK1 cells and KD reconstituted controls (KDmoPrP^{WT}), protein expression levels were checked by Western blotting and cell surface expression of PrP^C by immunofluorescence.

3.3.2 Effects of charge cluster I (CC1) mutations on prion propagation

KD cells were reconstituted with moPrP bearing minimal mutations (KDmoPrP^{Ala}), or the wild-type protein (KDmoPrP^{WT}). It was shown that N-terminal deletion Δ 23-88 in moPrP does not support prion propagation (Figure R11). Here, alanine replacements were made along the 23-88 sequence to determine which residues within this sequence, contribute to the 'loss of propagation' phenotype observed in mutant Δ 23-88 when expressed in KD cells.

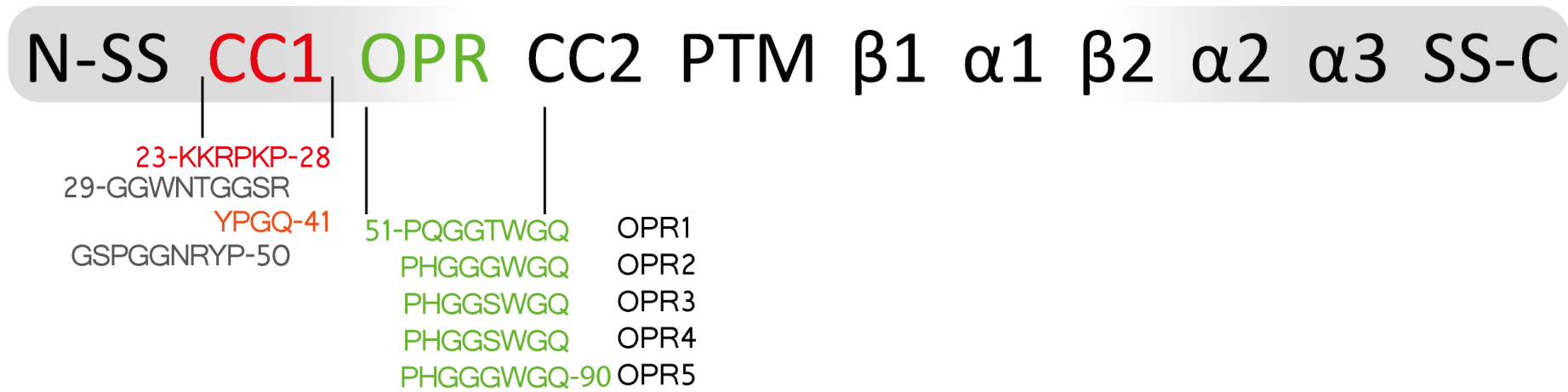


FIGURE R13: REGIONS OF INTEREST WITHIN MOPrP SEQUENCE 23-90

Bar schematic of domains within moPrP. N-SS: N-terminal signal sequence; CC1: charge cluster 1; OPR: octapeptide repeat region (repeats are labelled 1-5); CC2: charge cluster 2; PTM: putative transmembrane region; α1: helix 1; β1: strand 1; α2: helix 2; α3: helix 3; SS-C: C-terminal signal sequence. Residues 23-90 of moPrP are indicated in single letter amino acid code. Charge cluster 1 is highlighted in red; YPGQ in orange as a YXXQ motif site; OPRs are shown in green.

Residue K23 is the most N-terminal amino acid in the moPrP sequence, following cleavage of the signal sequence (residues 1-22). K23 is followed by more positively charged amino acids, denoting region 23-31 of the protein as charge cluster 1 (CC1). A series of alanine mutations were created as point, double, or triple mutations to cover region 23-88 of the protein, to identify those that participate in reducing propagation, as observed in moPrP with deletion Δ 23-88 (Figure R11).

Alanine replacements K23A.K24A.R25A, P26A.K27A, that lie within CC1 were created alongside neighbouring residues P28A, and W31A.N32A.T33A, to investigate their contributions to propagation. KD cells reconstituted with these constructs were assayed for their propensity to propagate RML (Figure R14). SCA output is in the form of spot numbers where the number of spots is taken to be a measure of propagation; thus, high spot numbers represent high levels of propagation/efficient propagation (Section 3.2). It was found that KD cells reconstituted with triple mutation K23A.K24A.R25A propagated fewer prions compared to KD cells reconstituted with the wild-type protein (Figure R14). However, KD cells expressing moPrP mutation P26A.K27A, as well as neighbouring replacements P28A and W31A.N32A.T33A showed no deficiency in propagation (Figure R14). Thus, within CC1, only changes in sequence segment 23-25 had a modulatory effect on prion propagation.

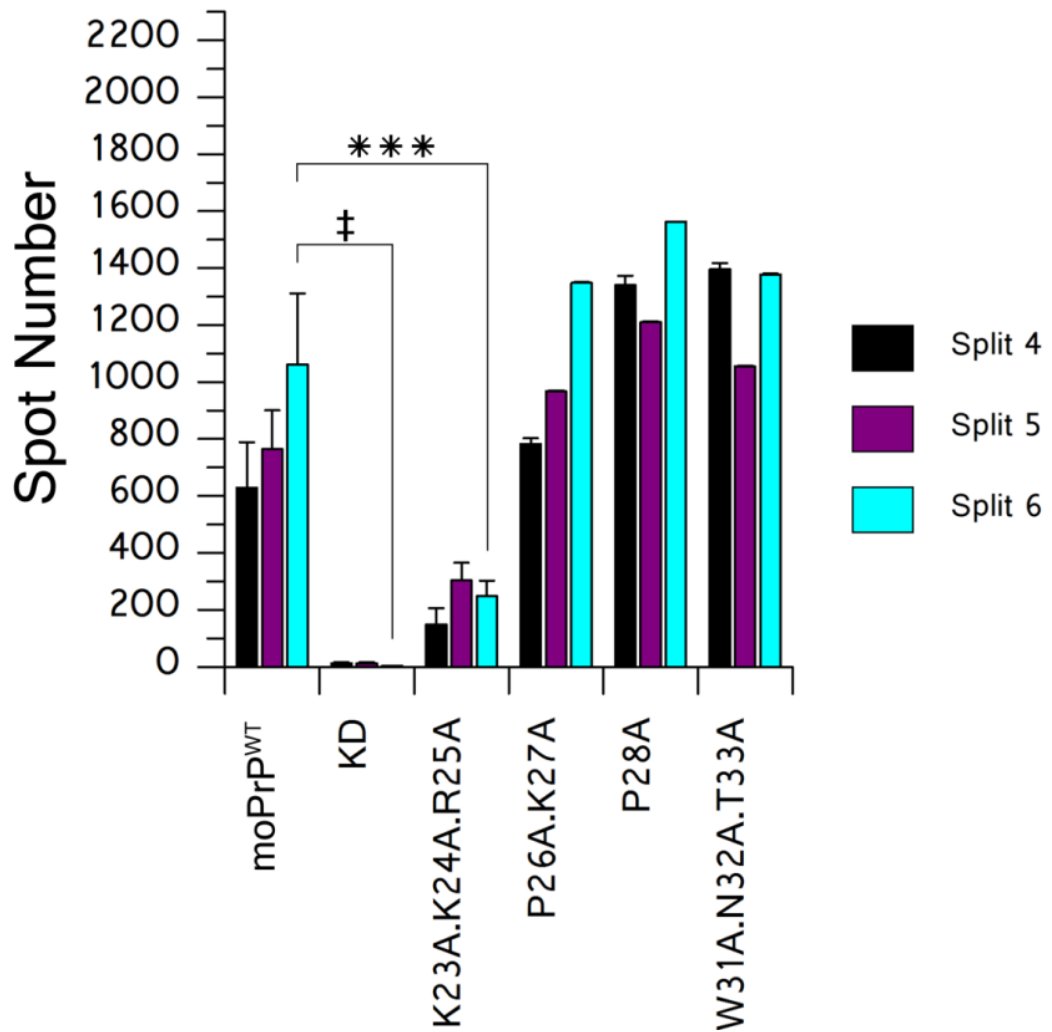


FIGURE R14: SCA OF KDMoPrP^{ALA} CELLS; MOPrP MUTATIONS IN REGION 23-33

SCA analysis of region 23-33 of moPrP revealed CC1 as a modulator of propagation. KD cells reconstituted with alanine-mutant forms of moPrP were compared to KDmoPrP^{WT} cells for their propensity to propagate prions. Spot numbers for triple mutation K23A.K24A.R25A were significantly lower than KDmoPrP^{WT} at all splits assayed in a one-way ANOVA with a Bonferroni correction for multiple comparisons. Significance is indicated by *** for $P \leq 0.0002$ and ‡ for $P \leq 0.0001$. Significance only shown for split 6 for clarity.

Additionally, the lowered propagation phenotype observed in K23A.K24A.R25A maintained spot numbers below four hundred for all time points at which the cells were sampled: splits 4, 5 and 6 (Figure R12). Based on the SCA guide (Figure R12) this is indicative of reduced propagation relative to wild-type controls.

All mutations in region 23-33 other than K23A.K24A.R25A, had no effect on reducing propagation, as spot numbers at three individual time points sampled, matched and surpassed those of KD cells expressing the wild-type protein. The triple change to alanine reduced the propagation relative to wild-type PrP approximately five-fold; K23A.K24A.R25A reported spot numbers in the two hundreds, whereas moPrP^{WT}-expressing cells that lack any mutation, gave spots approaching one-thousand (Figure R14).

The observed lower propagation capacity was further probed by generating and testing point mutations within K23A.K24A.R25A, to assess which residue in particular within the continuous three amino acid stretch was central to reduced propagation (Figure R15). None of the point mutations generated in this region, (K23A, K24A or R25A) showed a deficit in propagating RML prions as each reported spot numbers equalling and surpassing those of KD cells reconstituted with the wild-type protein (Figure R14).

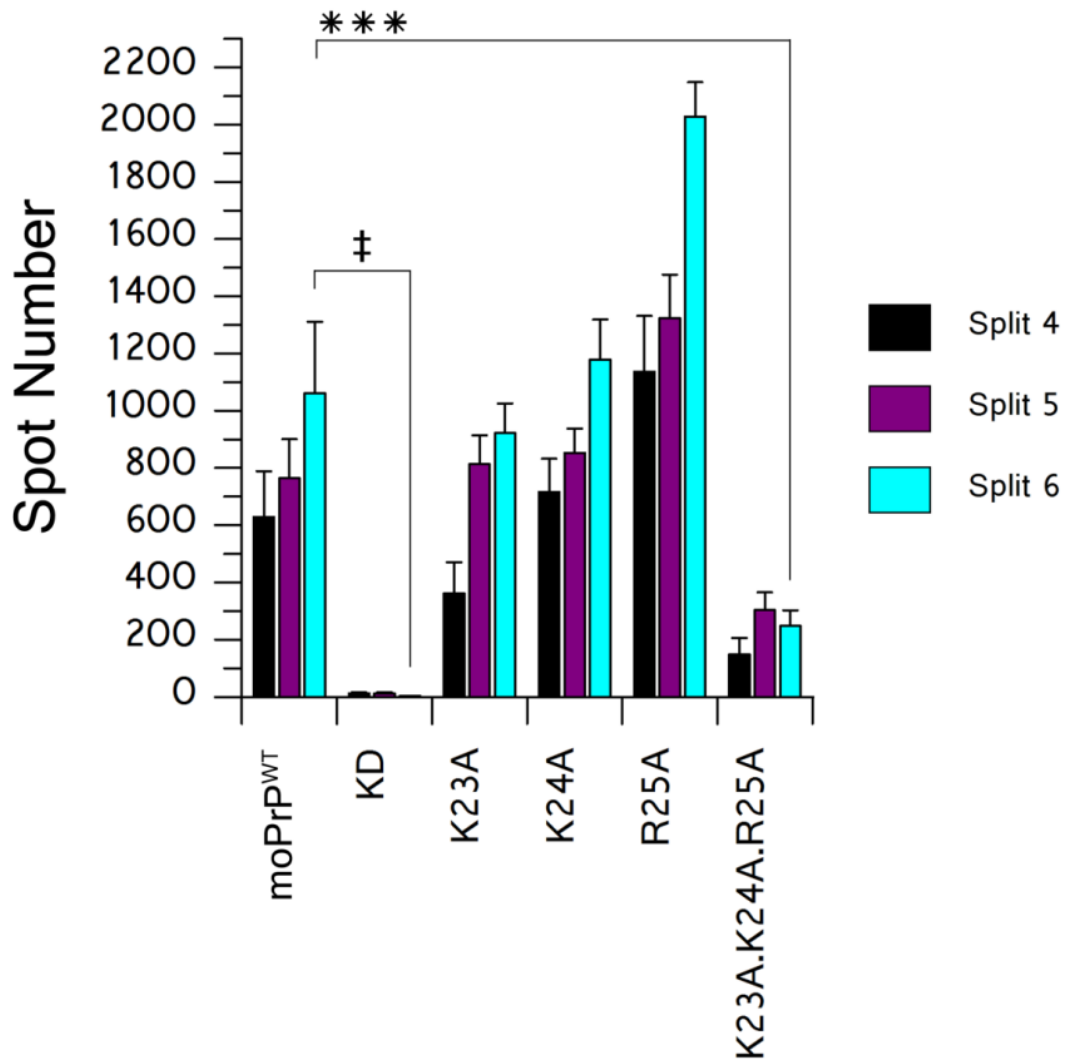


FIGURE R15: SCA OF KDMoPrP^{ALA} CELLS; MoPrP MUTATIONS IN REGION 23-25

Propagation was markedly reduced for the triple alanine moPrP construct K23A.K24A.R25A, but not for individual mutations K23A, K24A or R25A, within this segment. Significance is indicated by *** for $P \leq 0.0002$ and ‡ for $P \leq 0.0001$. Significance only shown for split 6 for clarity; calculated in a one-way ANOVA with a Bonferroni correction for multiple comparisons.

3.3.3 CC1 amino acids K23.K24.R25 are important for efficient prion propagation

Results from the triple mutation K23A.K24A.R25A in CC1 and subsequent experiments testing individual mutations K23A, K24A and K25A clearly indicated that K23.K24.R25 is a distinct cluster of positive charge within the prion protein that is important for propagation efficiency, as compromising the native sequence in this section led to sub-optimal propagation of prions.

3.3.4 Q41 is identified as a novel modulator of prion propagation within region 36-88 of the mouse prion protein

Region 36-88 of moPrP is largely composed of octapeptide repeats 1-5 that start at residue P51 and end at residue Q90 (Figure R13). A total of eighteen alanine-substituted moPrP constructs were created and expressed in KD cells to assay the contributions of residues within region 36-88 to prion propagation. Scrapie cell assay analysis of RML-infected KD cells reconstituted with alanine mutations in region 36-88 showed that surprisingly, the only substitution that had an effect on propagation was Q41A (Figure R14). All other mutations made in region 36-88, including those neighbouring Q41 at either termini, showed no loss of propagation (Figure R14). Single replacement at Q41 had a significantly lower propensity to propagate RML compared to KD cells reconstituted with moPrP^{WT} (Figure R16).

When analysed by SCA, KD cells reconstituted with moPrP bearing mutation Q41A gave spot numbers of one hundred, compared to one-thousand for moPrP^{WT}-expressing cells at the same split (Figure R16). This

is a ten-fold reduction in propagation, introduced by a single amino acid mutation in the prion protein. What is interesting and perhaps unexpected, is that no mutations made within the OPR regions reduced propagation as expansions in this region are known causes for familial prion disease⁵¹.

Furthermore, OPRs are comprised of residues known to be involved in copper coordination^{37, 129} which in turn mediates cellular functions of PrP^C such as endocytosis²⁴⁹. The five octapeptide repeat regions are defined by OPR1 (residues 52-58), OPR2 (residues 59-66), OPR3 (residues 67-74), OPR4 (residues 75-82) OPR5 (residues 83-90); their SCA profiles as tested in KDmoPrP^{Ala} cells challenged with RML prions demonstrated that these residues are not crucial for prion propagation (Figure R16).

Mutations S36A.R37A.Y38A and S43A, which are N-terminal and C-terminal to Q41 respectively, also had no inhibitory effect on prion propagation (Figure R16). The finding that all alanine replacements made and tested within region 36-88 of moPrP, except Q41A, exerted no limitations on the ability of cells expressing these mutations to propagate prions, defines Q41A as a discrete point of interest in the flexible N-terminal tail of the prion protein that can mediate propagation.

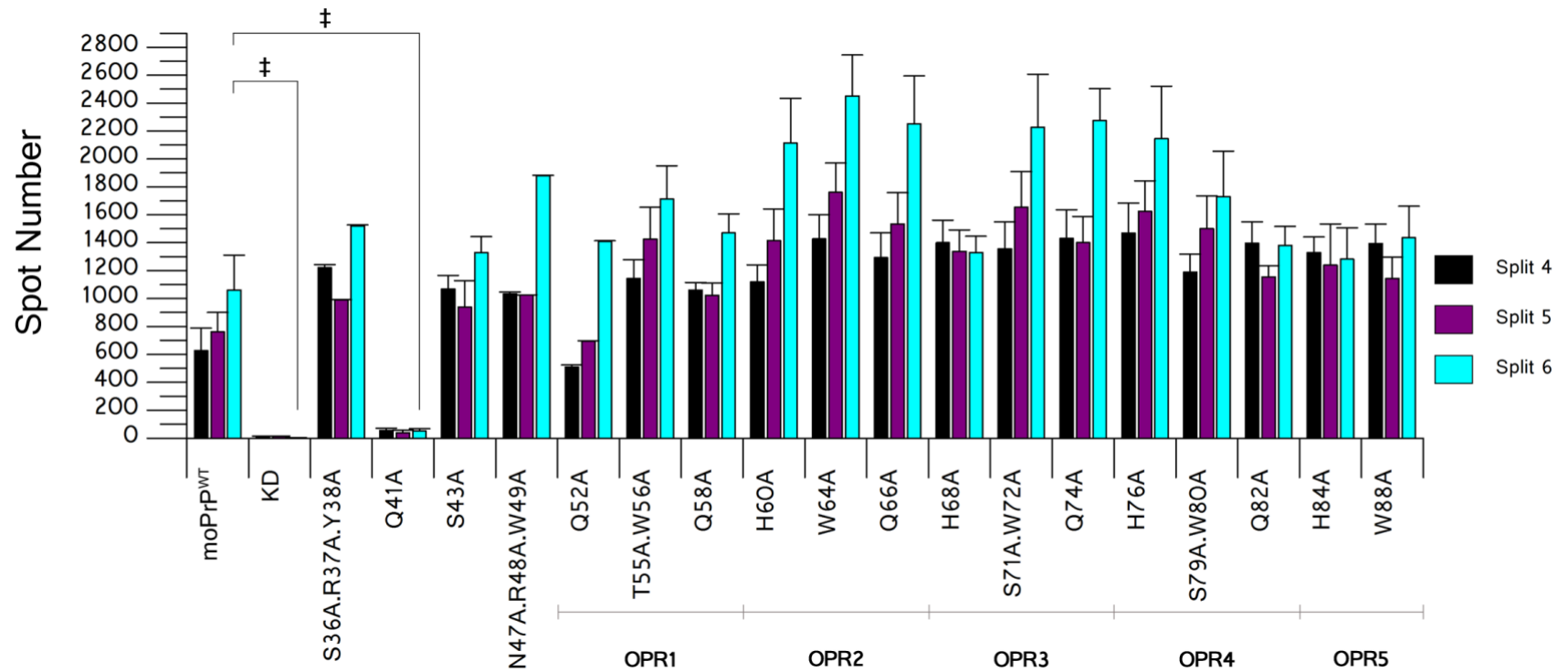


FIGURE R16: SCA OF KDMoPrP^{ALA} CELLS; MOPrP MUTATIONS IN REGION 41-88

Reconstitution of KD cells with Q41A severely reduced the cells ability to propagate prions. Mutations either side of Q41A did not inhibit propagation. All other alanine replacements that were tested in region 34-88 did not reduce propagation, including region 52-88 which is within the OPR segment of the protein. Significance is indicated by ‡ for $P \leq 0.0001$; for clarity, this is only shown for split 6. Significance calculated in a one-way ANOVA with Bonferroni correction for multiple comparisons. Mutations that fall within OPRs 1-5 are indicated below the graph.

3.3.5 Propagation efficiency of moPrP mutations K23A.K24A.R25A and Q41A can be improved with increased infectious dose

Within regions 23-88 of the mouse prion protein, only K23A.K24A.R25A and Q41A of the alanine mutants generated, showed any effect on lowering prion propagation. For the triple mutation, the highest spot numbers achieved following infection with RML prions was three hundred spots, and for Q41A, one hundred. These two constructs represent two out of twenty-six alanine-mutants of moPrP in region 23-88 that reduced propagation.

To test whether spot numbers of these N-terminal mutations had an upper limit of three hundred spots or one hundred spots for K23A.K24A.R25A and Q41, respectively, KD cells reconstituted with these mutations were infected with RML at a ten-fold higher concentration than before (Figures R14, R16): here, the infectious inoculum was applied at a dilution of 1×10^{-4} instead of the standard 1×10^{-5} used for SCA in this study (Figure R17).

KD cells reconstituted with CC1 mutation K23A.K24A.R25A and single replacement Q41A appeared to reproducibly propagate RML at a level that was significantly less than KD cells reconstituted with the wild-type protein at both concentrations of RML (Figure R17). However, Q41A propagated RML prions at a lower capacity than K23A.K24A.R25A at both concentrations tested (Figure R17).

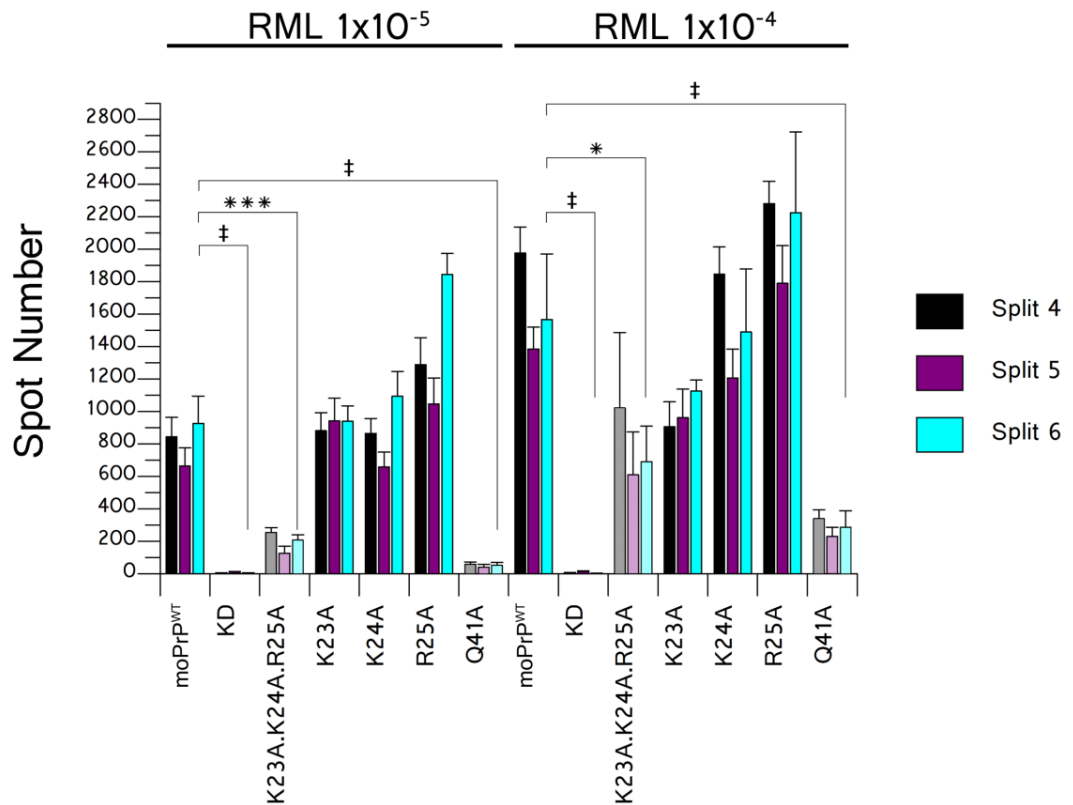


FIGURE R17: SCA OF KDMoPrP^{ALA} CELLS; MOPrP MUTATIONS IN REGION 23-25 OR RESIDUE 41

KD cells reconstituted with moPrP mutations K23A.K24A.R25A, Q41A, and point mutations within segment 23-25, were tested for their propagation propensity at two concentrations of RML inocula via SCA. K23A.K24A.R25A- and Q41A-expressing cell lines are highlighted in lighter pastels for easier comparison. All cell lines reported higher spot numbers at a ten-fold higher dose of RML. Significance is indicated by ‡ for $P \leq 0.0001$, *** for $P \leq 0.0002$, * for $P \leq 0.005$; for clarity, this is only shown for split 6. Significance calculated in a one-way ANOVA with Bonferroni correction for multiple comparisons.

At the higher dose, cells expressing Q41A propagated roughly five-fold less, and K23A.K24A.R25A approximately two-fold less, than wild-type-expressing cells. Thus, increasing the concentration of infectious inocula resulted in improved propagative capacity for K23A.K24A.R25A and Q41A, but the presence of these mutations still has a limiting effect on propagation, as they did not achieve spot numbers comparable to KD cells reconstituted with the wild-type protein, or single replacements K23A, K24A and R25A (Figure R17).

This result that moPrP mutation K23A.K24A.R25A within CC1 and point mutation Q41A lowered propagation at high doses of infectious inoculum, strengthens the notion that these two regions play an important role in prion propagation. This was further supported by the finding that none of the residues neighbouring these sites displayed deficiencies in propagation (Figures R14, R16).

3.3.6 Combination moPrP mutation K23A.K24A.R25A+Q41A does not have a cumulative effect on limiting prion propagation capacity

Two regions were identified within the 23-88 segment of the mouse prion protein that propagated sub-optimally, when the native amino acids were substituted for alanine: K23A.K24A.R25A and Q41A (Figure R17). Taken together with the finding that Δ 23-88 did not support prion propagation (Figure R11), it would seem logical to suggest that the propagation limiting effects in Δ 23-88 arise due to missing residues 23-25 and residue 41. Since neither of these mutations expressed separately in KD cells, had as much of an effect on propagation as Δ 23-88, we generated a moPrP mutant bearing both changes, such that residues 23-25 as well as residue 41 was substituted by alanine in the same construct. The resultant construct was labelled K23A.K24A.R25A.Q41A.

If expression of alanine mutations at both positions in moPrP sequence (23-25 and 41) had an additive effect, it would suggest two independent pathways or mechanisms are affected in each mutant moPrP construct. If not, we could presume that there will be no greater limit on propagation observed by expressing both sets of mutations (23-25 and 41) compared to expression of these mutations individually (23-25 or 41) since the same pathway is compromised.

To test this, pBluescriptSK+ DNA bearing the K23A.K24A.R25A mutation was used as template DNA for the site-directed mutagenesis PCR of Q41. This created a construct bearing both K23A.K24A.R25A and Q41A. Using

the techniques described in Chapter I for generating KDmoPrP^{Ala} cells, KD cells were reconstituted with this construct (K23A.K24A.R25A.Q41A).

KD cells reconstituted with moPrP bearing mutations K23A.K24A.R25A.Q41A did not show evidence of K23A.K24A.R25A acting in synergy with Q41A when assayed for their propagation capacity by SCA (Figure R18). K23A.K24A.R25A and Q41A when expressed independently of each other displayed spot numbers between one hundred to three hundred, and when expressed as K23A.K24A.R25A.Q41A, gave spot numbers of about two hundred under standard SCA conditions of 1×10^{-5} RML dilution (Figure R18). This increased to nine hundred, three hundred and seven hundred for K23A.K24A.R25A, Q41A and K23A.K24A.R25A.Q41A respectively, at a higher dose of inoculum (1×10^{-4} RML dilution; Figure R18).

Thus, expressed individually, each of these mutations showed limited propagation. Combined, they demonstrated an averaging of their respective propagation profiles (Figure R18).

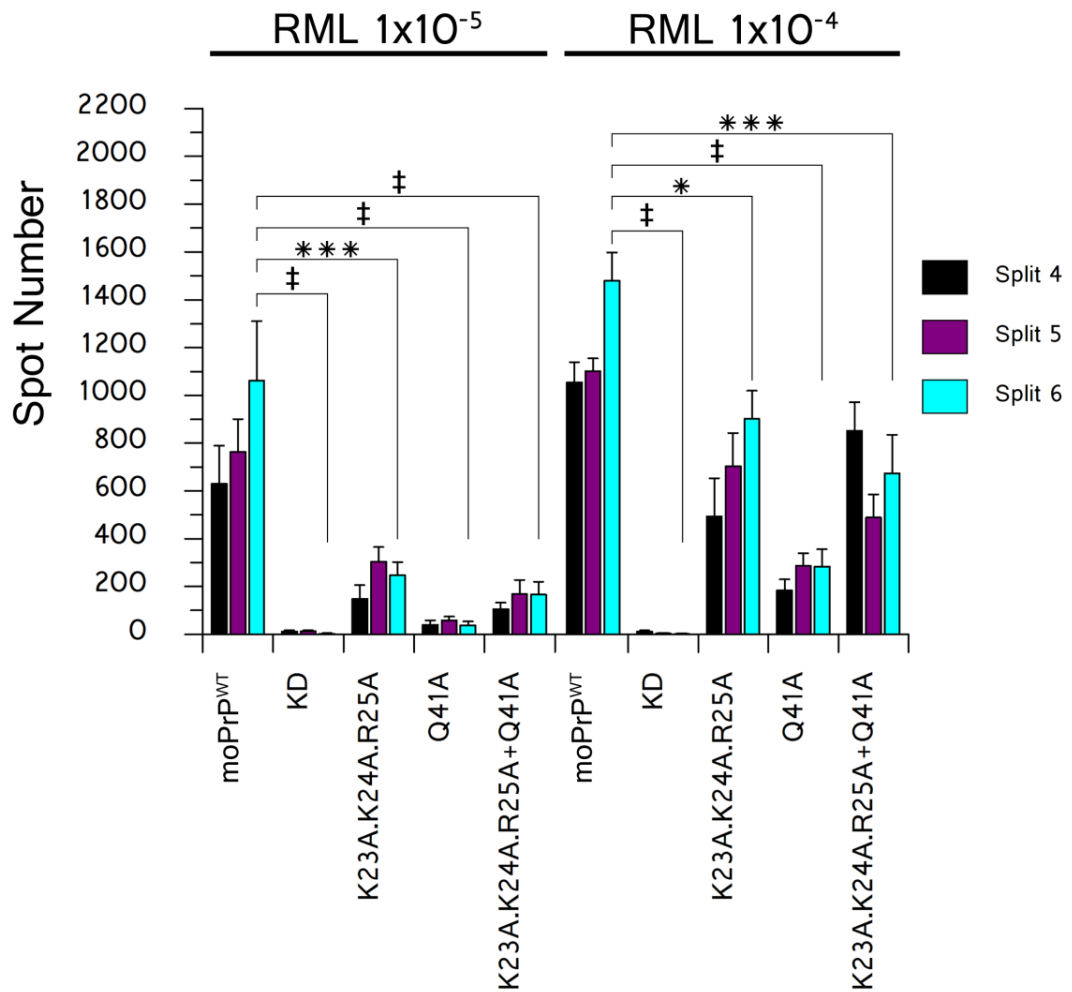


FIGURE R18: SCA OF KDMoPrP^{ALA} CELLS; MOPrP MUTATIONS IN REGION 23-25 AND RESIDUE 41

Cells bearing the triple alanine moPrP construct K23A.K24A.R25A displayed significantly reduced propagation compared to KDmoPrP^{WT} cells. KD cells and KD cells reconstituted with moPrP Δ 23-88 did not propagate RML at any time point tested. Combining mutations K23A.K24A.R25A and Q41A did not hinder propagation any more than Q41A alone. Spot numbers for K23A.K24A.R25A.41A fell between those of the individual mutations K23A.K24A.R25A and Q41A. Significance is denoted by * for $P \leq 0.005$ *** for $P \leq 0.0002$ and † for $P \leq 0.0001$. Significance only shown for split 6 for clarity; calculated using a one-way ANOVA plus Bonferroni correction for multiple comparisons.

3.3.7 Lack of propagation in moPrP mutations K23A.K24A.R25A and Q41A is not due to lack of protein expression

KD cells do not propagate prions as they do not express moPrP at a sufficient level to support propagation (Figure R11). The approach used here to test regions of PrP required for propagation, required reconstitution of KD cells in order to express the desired alanine mutation of moPrP. It could therefore be argued that the reason some reconstituted KD cells are unable to propagate RML prions fully may be down to lack of, or low-level prion protein expression.

To demonstrate that the effects of mutations K23A.K24A.R25A and Q41A on propagation were due to modification of native residues at these sites and not simply inefficient expression, cells expressing these mutations were immunoblotted for protein expression, using α -moPrP antibody ICSM18 (Figure R19). Since it has been shown that prion conversion occurs primarily at the cell surface¹⁰⁰, mutant proteins were examined for cell surface expression by immunofluorescence. Cells were grown on glass coverslips and analysed for protein expression using the anti-PrP mouse monoclonal antibody ICSM18 for detection by immunofluorescence (Figure R20).

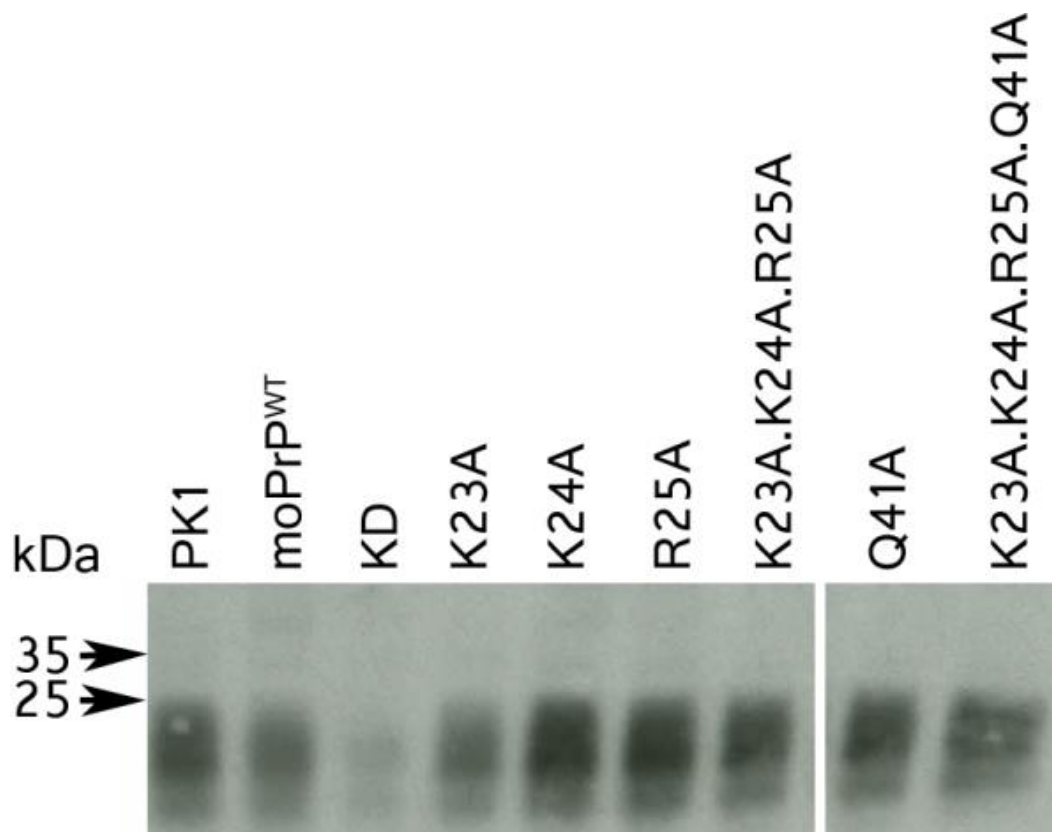


FIGURE R19: WESTERN BLOT OF KDMoPrP^{ALA} CELLS WITH MUTATIONS IN CC1 AND RESIDUE 41

Expression of moPrP mutant constructs in KD cells. PK1 cells were taken as a positive control for expression of moPrP and KD the negative control.

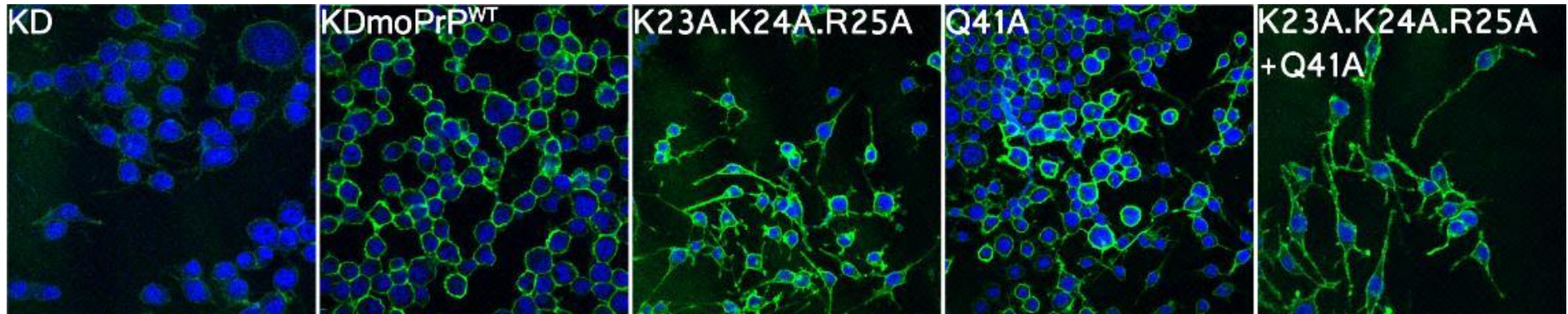


FIGURE R20: IMMUNOFLUORESCENT ANALYSIS OF KDmoPrP^{ALA} CELLS; MUTATIONS IN CC1 AND RESIDUE 41

Immunofluorescent analysis of KD cells, KDmoPrP^{WT} cells and KD cells reconstituted with moPrP alanine mutants: K23A.K24A.R25A, Q41A and combined mutation K23A.K24A.R25A.Q41A. All moPrP-expressing cells displayed similar expression and distribution of the protein, which was detected at the cell surface. Magnification x40.

3.3.8 With the exception of K23A.K24A.R25A and Q41A where prion propagation is limited, all moPrP alanine replacements in the flexible region 23-88 of the protein propagate RML fully

Deleting residues 23-88 from moPrP resulted in a protein that when expressed in cells, did not propagate RML prions as tested by SCA (Figure R11). Charge cluster 1 mutant K23A.K24A.R25A, and point mutation Q41A were found to propagate RML to a much lesser extent compared to cells expressing the full-length native protein (moPrP^{WT}) and were the only mutations found to reduce prion propagation capacity in region 23-88 of moPrP.

The reduction in propagation was not as stark as that observed for Δ 23-88, which was akin to the negative control KD cells (Figure R18). Q41A was less able to propagate RML compared to K23A.K24A.R25A, despite it being a smaller change in the protein sequence (Figure R18). This suggested that it may have a stronger modulatory role on propagation than the more N-terminal charge cluster at 23-25. Since the propagation efficiency of KD cells expressing the K23A.K24A.R25A mutant can be improved to half-maximal potential compared to KDmoPrP^{WT} cells, it may be that increasing the dose of inoculum compensates for the disruptions in propagation brought about by the triple mutation. Possible roles of these amino acids and how they may impact propagation are discussed.

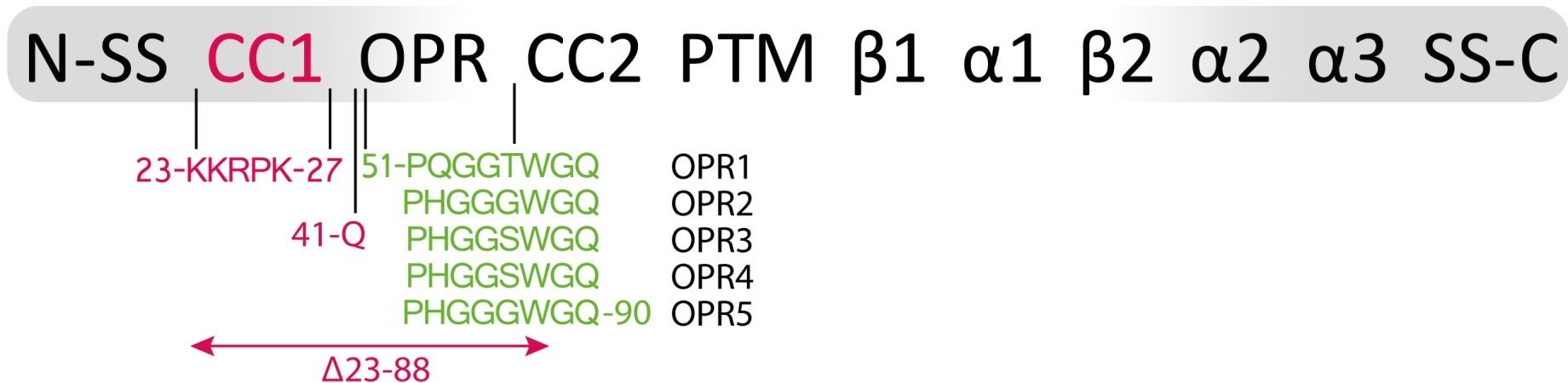


FIGURE R21: SUMMARY OF FINDINGS; REGION 23-88 OF MOPrP

Schematic of the prion protein sequence, as individual domains and structural elements within it. N-SS: N-terminal signal sequence; CC1: charge cluster 1; OPR: octapeptide repeat region; CC2: charge cluster 2; HC: conserved hydrophobic region; α 1: helix 1; β 1: strand 1; α 2: helix 2; α 3: helix 3; SS-C: C-terminal signal sequence. K23.K24.R25 in CC1 and Q41 replacements led to reduced prion propagation and are highlighted in pink (glycine and proline replacements were not tested with the exception of P26 and P28). Residues of the OPR region when replaced with alanine showed no loss of propagative capacity (green). However, deletion of residues 23-88 abrogated prion propagation (pink arrow).

3.3.9 Role of CC1 residues K23.K24.R25 in prion propagation

Although PrP is located in lipid rafts and tethered to the cell membrane by a GPI-anchor, aspects of cellular prion protein endocytosis have been ascribed to CC1 in a number of ways: (i) clathrin-mediated³⁸, (ii) interaction with heparan sulphate proteoglycans¹¹³, (iii) glycosaminoglycan (GAG) interaction¹⁰². Additionally, region 23-33 has been found to be crucial for interactions with dynein family members to allow correct intracellular trafficking²⁵⁰. These actions involve modulation of cell surface expression and recycling of the cellular protein – processes that are also critical for successful prion infection and eventual propagation^{100, 115, 251}.

Region 23-30 which is inclusive of K23.K24.R25 is believed to contribute to the efficient folding of PrP to its native cellular conformation¹¹⁷ thereby contributing to protein stability. Furthermore, lysine residues within region 23-30, specifically K23.K24.K27, are required for association of PrP with GAGs¹⁰³. With both protein instability and GAG association believed to promote PrP^{Sc} formation¹²³, it is possible that mutation K23A.K24A.R25A dampens this reported upregulation of PrP^{Sc} formation or indeed as evidence from our SCA data suggests, downregulates propagation of prions (Figure R17).

CC1 represents the first of two charge clusters in the prion protein, thought to be involved in the protein's endocytosis^{38, 58, 252}. It has also been ascribed functions of neurotoxicity modulation⁶⁰, zinc regulation²⁵³, interaction with tubulin to inhibit microtubule formation¹⁰⁴, in addition to being a secondary binding site for A β oligomers^{106, 107}. PrP^C-mediated cytotoxicity of A β

oligomers is thought to be dependent on the transmembrane protein, LRP1¹⁰⁸. LRP1 in turn, is required for the copper-mediated endocytosis of PrP²⁴⁹ and N-terminal region 23-107 of PrP binds the transmembrane protein with nanomolar affinity¹⁰².

Since CC1 plays a modulatory role in a multiplicity of processes including recycling of the protein^{38, 252}, it is possible that triple mutations in this region may disrupt native interactions which in turn inhibit this particular aspect of moPrP regulation. These mutations do not however, inhibit other forms of moPrP trafficking achieved through its GPI-anchor²⁵⁴. It is clear from SCA data that triple alanine mutations at CC1 residues K23.K24.R25 limit, but do not abolish prion propagation (Figure R17). Thus, the cellular pathway(s) involved in propagation have contributions from segments of the cellular protein other than CC1, that allow for moderate propagation.

The finding that mutations at CC1 lead to a reduction in the amount of ProteinaseK-resistant prion protein detected after infection (Figure R15) are supported by data from Turnbaugh *et al.*, who used RML inocula to test this hypothesis *in vivo*: mice expressing moPrP^{Δ23-31} displayed a much lower susceptibility to prion infection and accordingly, accumulated lower levels of PrP^{Sc114}. The same laboratory also showed that part of PrP-related toxicity is attributed to the 23-26 region of CC1 and is uncoupled from endocytosis activities¹¹⁹. Data presented here shows that propagation is not inhibited, but reduced, and that higher levels of propagation can be achieved with increased inocula (Figure R17).

Curiously, KD cells reconstituted with moPrP bearing single mutations within the same region of CC1 (K23A, K24A and R25A) propagated prions as well as full-length expressors (Figure R15). Ostapchenko *et al.*, discovered through deletion mutagenesis of the 23-30 N-terminal segment of PrP that modifications to this region can affect overall fibril morphology¹¹⁷. This may explain why point mutations in CC1 (K23A, K24A and K25A) in our study had no detectable propagation deficiency, whereas a larger replacement K23A.K24A.R25A led to a reduced propagation phenotype (Figure R14). It does not however, explain why mutation P26A.K27A which is also in region 23-30 did not exhibit reduced propagation (Figure R14). The data presented suggest that CC1 has a regulatory role with which the efficiency of PrP propagation proceeds, and that it is controlled by multiple residues (Figure R15). Considering the negligible effect of the single mutants on propagation (Figure R15), a direct interaction of moPrP residues K23.K24.R25 with a factor that modulates propagation is unlikely: if K23.K24.R25 falls within part of a recognition motif or binding site, it is reasonable to assume that at least one of the single mutations would mirror the reduced propagation phenotype of the triple mutant; this is not the case (Figure R15). More probable, is that mutations at K23.K24.R25 lead to the loss of an accessory site, or of a weak interaction (if any), that aids propagation such that the conversion process is not forgone in its absence, but merely hindered.

It is possible that the concentration of charge at residues 23-25 (KKR) contributes to propagation efficiency and that loss of charge from individual amino acids through point mutation is not sufficient to affect propagation,

but cumulatively, lowers propagation capacity. Indeed, expression of the cellular mouse prion protein lacking residues 23-31 has been shown to reduce susceptibility to prion infection and reduce the levels of PrP^{Sc} that accumulate following infection and propagation¹¹⁶. This reduced propagation was attributed to the deletion mutant on PrP^C binding PrP^{Sc} with a lower affinity, thereby implicating segment 23-31 as a polybasic region that mediates propagation¹¹⁶.

In this study, the initial experimental setup did not include mutating proline residues at positions 26 and 28 in moPrP. Thus, the possibility that these residues, encompassed within region 23-31 highlighted by Turnbaugh *et al*¹¹⁶, also lowered propagative potential when mutated to alanine could not be ruled out. Following this result, KD cells expressing P26A.K27A, and P28A moPrP mutations were made to determine how residues neighbouring region 23-25 affected propagation. Our results suggest that a collection of residues at the N-terminus of PrP mediate some aspects of prion propagation, as their substitution led to diminished propagation activity (Figure R14). Since P26A.K27A and P28A propagated prions as well as moPrP^{WT}, it can be inferred that residues P26, K27 and P28 do not play a significant role in limiting prion propagation, but K23, K24 and R25 taken collectively, do (Figures R14 and R15).

It is important to note that the possibility of K23A.K24A.R25A combined with mutation K27A (as in K23A.K24A.R25A.K27A), further limiting propagation capacity has not been tested. If such a finding is established, then lysine residues within region 23-31 are key mediators of propagation in the 23-88 region of moPrP. The data presented here supports the argument of

Turnbaugh *et al.*, and further delineates the region of interest within the polybasic segment of PrP, to a minimal segment of the protein: K23.K24.R25 that together, governs the efficacy of prion propagation.

3.3.10 PROPAGATION-SUPPORTING ALANINE MUTATIONS IN MOPRP

Just as the data from SCA analysis of K23A.K24A.R25A emphasises the importance of maintaining sequence identity in this region to uphold maximum propagation capacity, SCA data from regions of the protein that can be altered without lowering propagation is important in delineating which segments of the protein are more amenable to change. These include amino acids 26-38 and 43-88 in moPrP. The two sequence segments are separated by residue Q41, where alanine replacement Q41A significantly reduced propagation (Figure R17).

Mutations made in the more N-terminal segment 26-38 included moPrP^{Ala} constructs P26A.K27A, P28A, W31A.N32A.T33A and S36A.R37A.Y38A. Lack of propagation inhibition in these mutants demonstrates that this region of the protein is not absolutely required for successful propagation and that despite the high conservation in sequence⁵⁴, the prion protein has a high tolerance for changes in the native sequence at these positions (Figures R14 and R16).

The second segment of propagation-supporting KDmoPrP^{Ala} cells, bore changes in region 43-88 and cover the OPR region. The result that alanine replacements within this region support propagation is interesting, considering that insertion mutations within the OPRs are linked to

accumulation of aggregated protein and early onset prion disease¹³⁰. It may be reasoned that in OPRI, the increased histidine and glutamine residues have effects on the overall copper coordinated by PrP^C and its charge interactions; indeed such correlations have been reported¹³⁰. If this were the case though, we would expect that eliminating some of these influences in alanine mutants Q52A, Q58A, H60A, Q66A, H68A, Q74A, H76A, Q82A or H84, may give an indication of reduced propagation, were such factors to influence the efficacy of prion propagation (Figure R16). Our data does not support this (Figure R16): instead, the single amino acid changes made in this region (residues 51-88) may be too small to significantly affect copper coordination individually; rather, longer stretches of mutations may be required to see a significant effect on prion propagation as that observed for deletion of segment 23-88 (Figure R11). That none of the mutations in OPR1-OPR5 lowered the capacity for RML propagation, taken with the result that deletion mutation Δ 23-88 did not propagate prions, suggests that the increased length of the flexible N-terminal chain (as in OPRI) favours misfolding of PrP^C into a more PrP^{Sc}-like formation, as opposed to the chemistry of the P(H/Q)GGG(-/G)WGQ sequence in the OPR region being the key contributing factor for propagation. It is possible that the flexibility afforded by glycine residues in this region may influence prion propagation, as shown by Yu *et al.*, on yeast prion protein determinant, Ure2¹⁷⁸. Overall, however, it appears as though the chain length offered by the N-terminal portion of moPrP has a greater effect on propagation propensity than the individual residues in the 43-88 region of the protein.

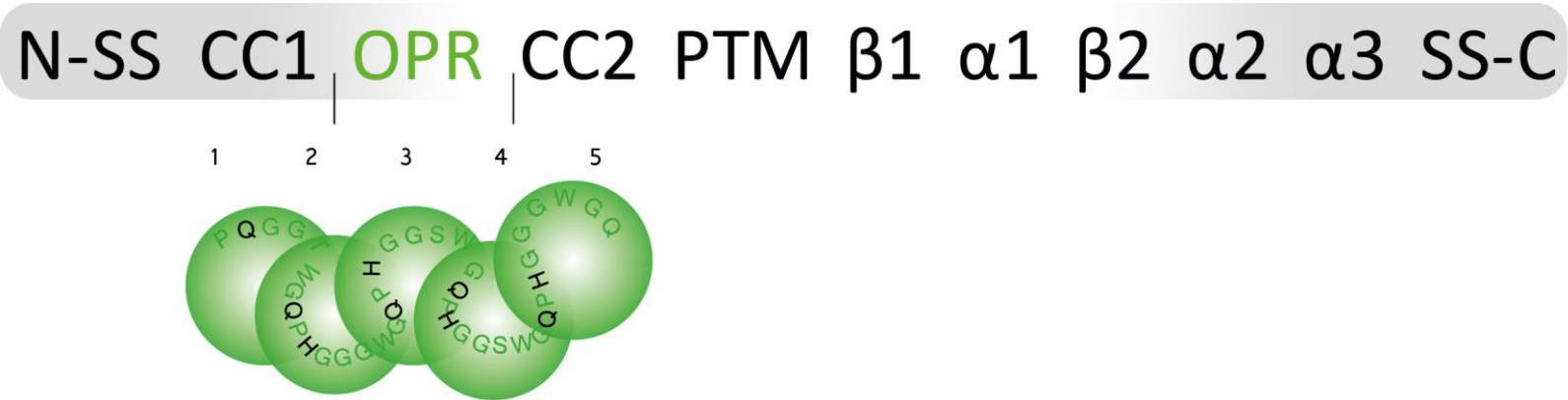


FIGURE R22: OCTAPEPTIDE REPEATS IN THE PRION PROTEIN

The prion protein usually bears five octapeptide repeats (the first being a pseudo repeat), numbered 1-5 below the OPR label. These are represented as circles of equal size. Within the OPR sequence Gln (Q) and His (H) residues are highlighted as potential sites for charge interactions where the protein may associate with cellular components within its microenvironment. Each of the highlighted residues has been investigated through alanine substitution to assess its contributions on propagation of prions (Q52A, Q58A, H60A, Q66A, H68A, Q74A, H76A, Q82A, and H84A). None of these mutations resulted in a form of moPrP that was non-convertible and each was able to propagate RML to the same efficacy as cells expressing the wild-type protein.

3.3.11 Q41 is a novel regulator of prion propagation

moPrP residue Q41 when replaced by alanine (Q41A) displayed a pronounced loss in its ability to propagate RML prions (Figure R16). This loss is greater than that seen in K23A.K24A.R25A (Figure R17), another alanine mutant in the flexible region 23-88, that displayed limited propagation. Interestingly, alanine replacements S43A and S36A.R37A.Y38A, that neighbour residue 41, displayed no deficiency in RML propagation (Figure R16). Furthermore, none of the KDmoPrP^{Ala}-expressing cells in regions between CC1 and Q41 and between S43 and W88 were hindered in their ability to propagate RML prions (Figures R14 and R16). This delineates both regions CC1 (KKR) and Q41 as specific sites of interest that regulate prion propagation, through mechanisms thought to be charge-linked, at least for CC1¹¹⁶ (Figure R15).

Codon 41, to our knowledge, has at no time been assigned any function with regards to PrP^C or PrP^{Sc} function. At most, it lies within epitope QGSPGGN (moPrP 41–47) that has recently been identified in one study as an epitope recognised in PrP^{Sc}, but not PrP^{C101}. Q41 also lies within a YPGQ sequence pattern that bears the endocytosis motif YXXQ, a consensus sequence for designating recruitment and activation of Stat3 (signal transducer and activator of transcription 3), through its SH2 (Src Homology 2) domain²⁵⁵. Stat3 belongs to a family of proteins that are analogous to transcription factors in their actions: they translocate from the cytoplasm to the nucleus upon activation by cellular factors to regulate gene function by binding DNA elements and up-regulating specific genes. *Prnp*

has been shown to regulate *Nanog* mRNA expression²⁵⁶; both *Nanog* and *Stat3* are key markers for pluripotency²⁵⁷, with *Nanog* recently shown to amplify *Stat3* activation to synergistically induce the naïve pluripotent program²⁵⁸. Although a direct interaction of PrP with *Stat3* has not been shown, this cooperative interaction may be of importance if PrP associates with *Stat3*, as it may regulate expression of other as yet unidentified factors that influence prion propagation. If an association between PrP and *Stat3* is found, it is likely to involve Q41.

This is the first instance where Q41 has been linked to prion propagation. When both N-terminal mutations Q41A and K23A.K24A.R25A were expressed on the same construct as K23A.K24A.R25A.Q41, there was no further reduction in prion propagation compared to Q41A and K23A.K24A.R25A expressed independently, but an averaging of their respective propagation phenotypes (Figure R18). The results presented here highlight the importance of these two segments with regards propagation of the prion protein. They further imply that mutations at these two sites, K23.K24.R25 and Q41, may impact the same propagation pathway, as no additive effect is observed upon expression of the changes on the same construct (Figure R18). Finally, they show that these mutations are influenced by a rate-limiting or energy-barrier phenomenon, as observed from the dose-dependent improvement on RML propagation (Figure R18).

3.3.12 Q41 has a stronger control over prion propagation than K23.K24.R25

Region 23-25 and residue Q41 were found to reduce propagation capacity when substituted for alanine as K23A.K24A.R25A and Q41A (Figure R17). It was shown that expressing K23A.K24A.R25A and Q41A on the same construct did not strengthen the inhibition exerted by K23A.K24A.R25A and Q41A independently (Figure R18). These two changes were isolated instances of alanine mutations in region 23-88 of moPrP negatively affecting prion propagation (Figures R14 and R16).

The data presented here suggests that N-terminal fragments 26-40 and 42-88 can be modified without having a negative impact on propagation, but changes made to region 23-25 and residue 41 limit the capacity for prion protein propagation, by at least two- and five-fold, respectively (Figure R18).

Site-directed mutagenesis	Inhibition of prion propagation		moPrP domain
	KD cells		
K23A			CC1
K24A			
R25A			
K23A.K24A.R25A			
P26A.K27A			
P28A			
W31A.N32A.T33A			
S36A.R37A.Y38A			
Q41A			
K23A.K24A.R25A.Q41A			
S43A			OPR
N47A.R48A.W49A			
Q52A			
T55A.W56A			
Q58A			
H60A			
W64A			
Q66A			
H68A			
S71A.W72A			
Q74A			
H76A			
S79A.W80A			
Q82A			
H84A			
W88A			

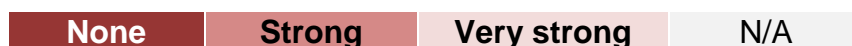


TABLE R3: LIST OF MOPRP ALANINE MUTATIONS IN REGION 23-88 OF THE PROTEIN.

All moPrP mutations expressed in KD cells propagated RML as well as the full-length protein, and displayed no limitations on propagation. Exceptions to this general trend in region 23-88 include K23A.K24A.R25A, Q41A, and K23A.K24A.R25A.Q41A, which are indicated as having a strong lack of propagation when challenged with RML prions (lighter bar: strong inhibition of propagation).

3.4 Charge cluster 2 replacements reduce prion propagation

3.4.1 Experimental strategy

The N-terminal deletion in moPrP Δ 23-88 abrogated prion propagation (Figure R11). Minimal mutations were made within the 23-88 segment, which lies in the 23-111 flexible region of the protein (Figure R23), to determine which residues play a role in limiting propagation (Section 3.3). The mutagenesis approach used in this study was extended to the entire unstructured region of the protein (23-111).

Alanine mutations were made from residue 90-111 in moPrP, to include: Q90A, T94A.H95A.N96A, Q97A.W98A, N99A.K100A, S102A.K103A, K105A.T106.N107A, L108A.K109A and H110A.V111A. This domain of the protein has a high concentration of charged residues and is known as the second charge cluster (CC2).

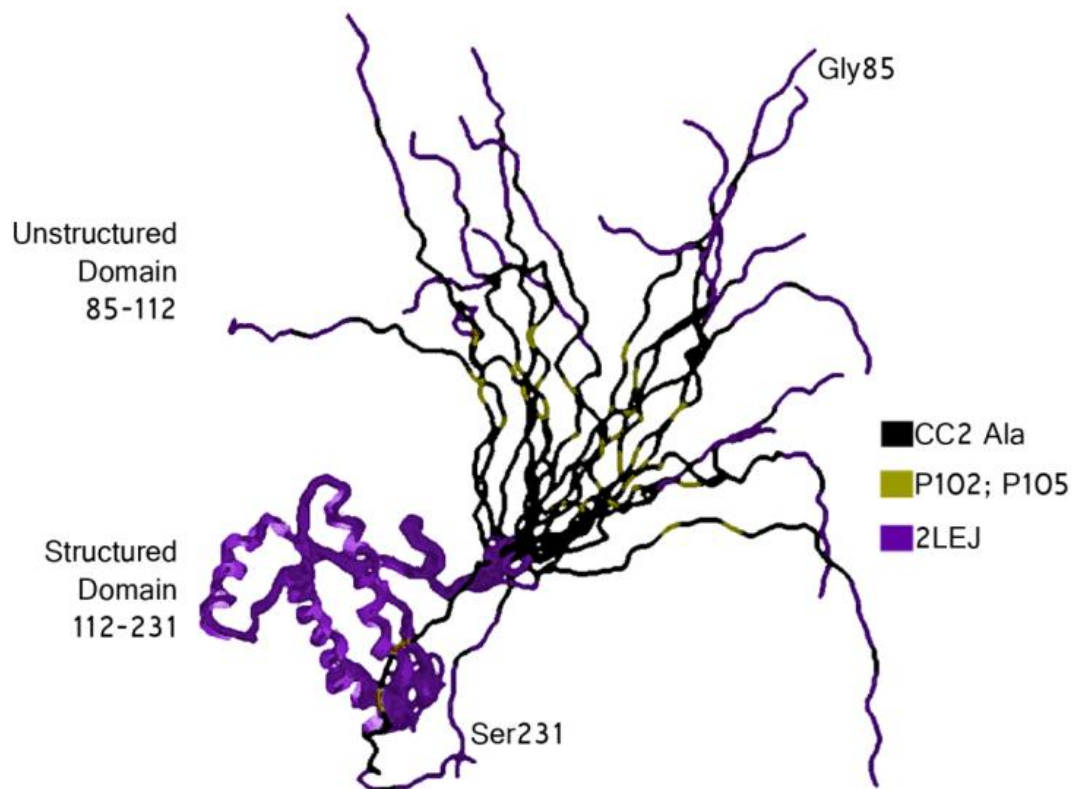


FIGURE R23: PDB ENTRY 2LEJ HUMAN PRP HIGHLIGHTS THE FLEXIBILITY OF N-TERMINAL REGIONS

The human prion protein is shown with CC2 region 90-111 in black; GSS-linked mutations which are within the CC2 region at positions P102 and P105 (human numbering) are shown in yellow and the remainder of the protein depicted in purple. The image was rendered in RasMol software and highlights the flexibility of the N-terminus as it is able to adopt all conformations shown. Image lines were smoothed in Photoshop.

3.4.2 Charge cluster 2 mutations significantly influence prion propagation

KD cells reconstituted with the eight alanine replacements in moPrP (Q90A, T94A.H95A.N96A, Q97A.W98A, N99A.K100A, S102A.K103A, K105A.T106.N107A, L108A.K109A and H110A.V111A) were assayed for their ability to propagate RML prions alongside KD cells reconstituted with W88A and the moPrP^{WT} by SCA (Figure R24).

In stark contrast to W88A, mutation Q90A, and every alanine replacement C-terminal to this, exhibited very limited capacity to propagate prions at the three time points sampled (Figure R24). There was a sharp distinction between altering residues at position 88 and position 90 in moPrP and their effects on prion propagation (Figure R24). While KD cells reconstituted with moPrP W88A consistently exhibited spot numbers higher than eight hundred – full propagation, those reconstituted with any of the eight alanine replacements within CC2 gave spot numbers of less than one hundred – severely limited propagation (Figure R24). The highest spot count for a mutation within CC2 region was 90 spots for N99A.K100A at split 6 (Figure R24).

The degree by which propagation was reduced in KD cells reconstituted with CC2 alanine mutants Q97A.W98A, S102A.K103A and H110A.V111A was almost as severe as that observed for KD cells reconstituted with Δ 23-88 (Figure R10) and non-reconstituted KD cells (Figure 24).

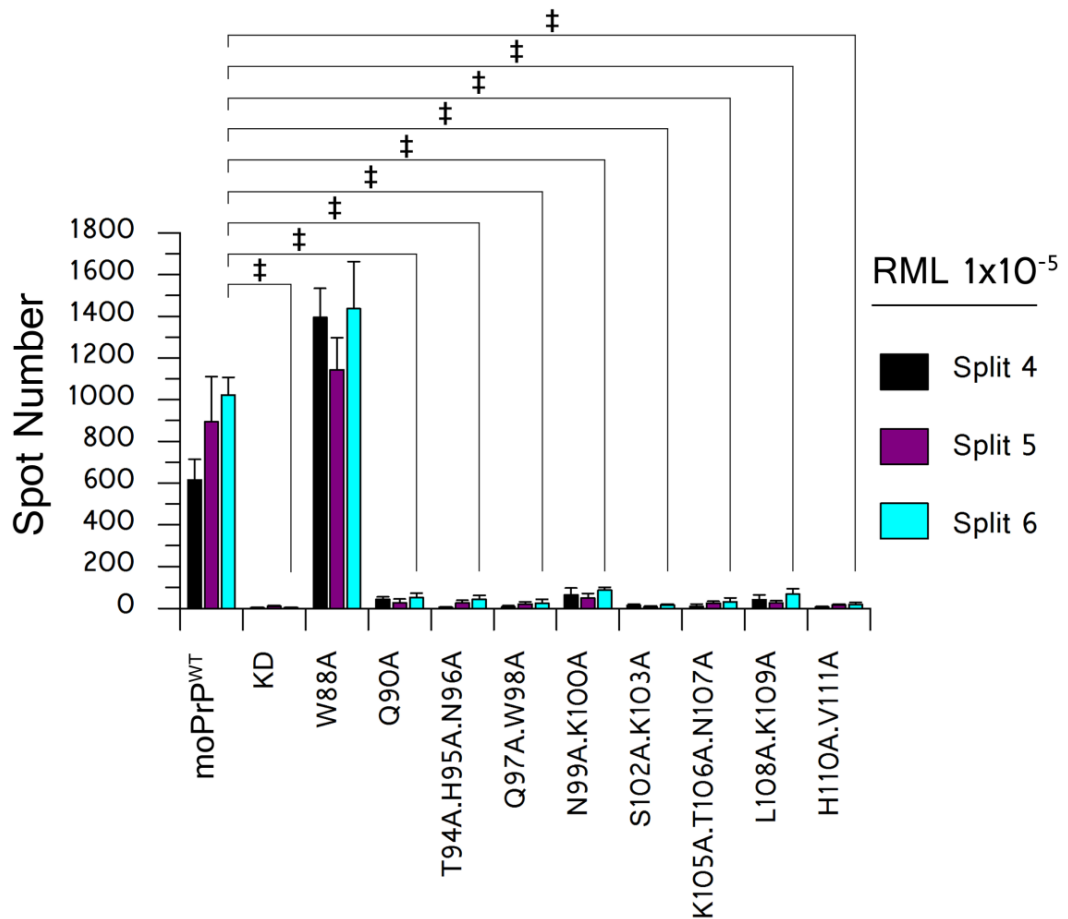


FIGURE R24: SCA OF KDMoPrP^{ALA} CELLS; MOPrP MUTATIONS IN REGION 90-111

KD cells reconstituted with either moPrP^{WT} or alanine mutants of the protein within region 88-111 were challenged with RML prions at a 1×10^{-5} dilution of infectious homogenate and their ability to propagate these prions assayed via SCA at three consecutive time points. All alanine substitutions made within region 90-111 exhibited markedly reduced propagation profiles, compared to moPrP^{WT} and single amino acid change W88A. Significance is indicated by ‡ for $P \leq 0.0001$. Significance only shown for split 6 for clarity; calculated in a one-way ANOVA with a Bonferroni correction for multiple comparisons.

Compared to mutations made in more N-terminal domains, CC2 mutations have a stronger effect on limiting prion propagation than alanine substitutions at CC1 residues K23.K24.R25 or Q41 (Section 3.3). To test whether propagation of CC2 alanine mutants can be improved with an increase in infectious inoculum, as observed for K23.K24.R25 and Q41 mutations (Figure R17), the dose of RML was increased ten-fold (Figure R25). Remarkably, and unlike the more N-terminal mutations K23.K24.R25 and Q41, increasing the concentration of infectious inocula had very little effect on recovering the limited propagation of KD cells expressing CC2 alanine mutations (Figure R25). All CC2 replacements tested gave spot numbers lower than one hundred, with the exception of mutation N99A.K100A which reported just over two hundred spots at split 6 (Figure R25). N99A.K100A represents the only mutation made in region CC2 that gave spot numbers in the two hundreds at RML dilutions of 1×10^{-4} (Figure R25). This is a two-fold increase in spot number, following a ten-fold increase in inocula – similar to the propagation profile observed for mutation Q41A (Figure R17). All mutations made in CC2 other than N99A.K100A resulted in spot numbers fewer than one hundred at RML dilutions of 1×10^{-4} and 1×10^{-5} (Figures R24 and R25). Thus, all mutations within CC2 had a stronger influence on prion propagation than CC1 mutations K23A.K24A.R25A or Q41A, as tested by SCA in this study (Figures R17, R24, and R25).

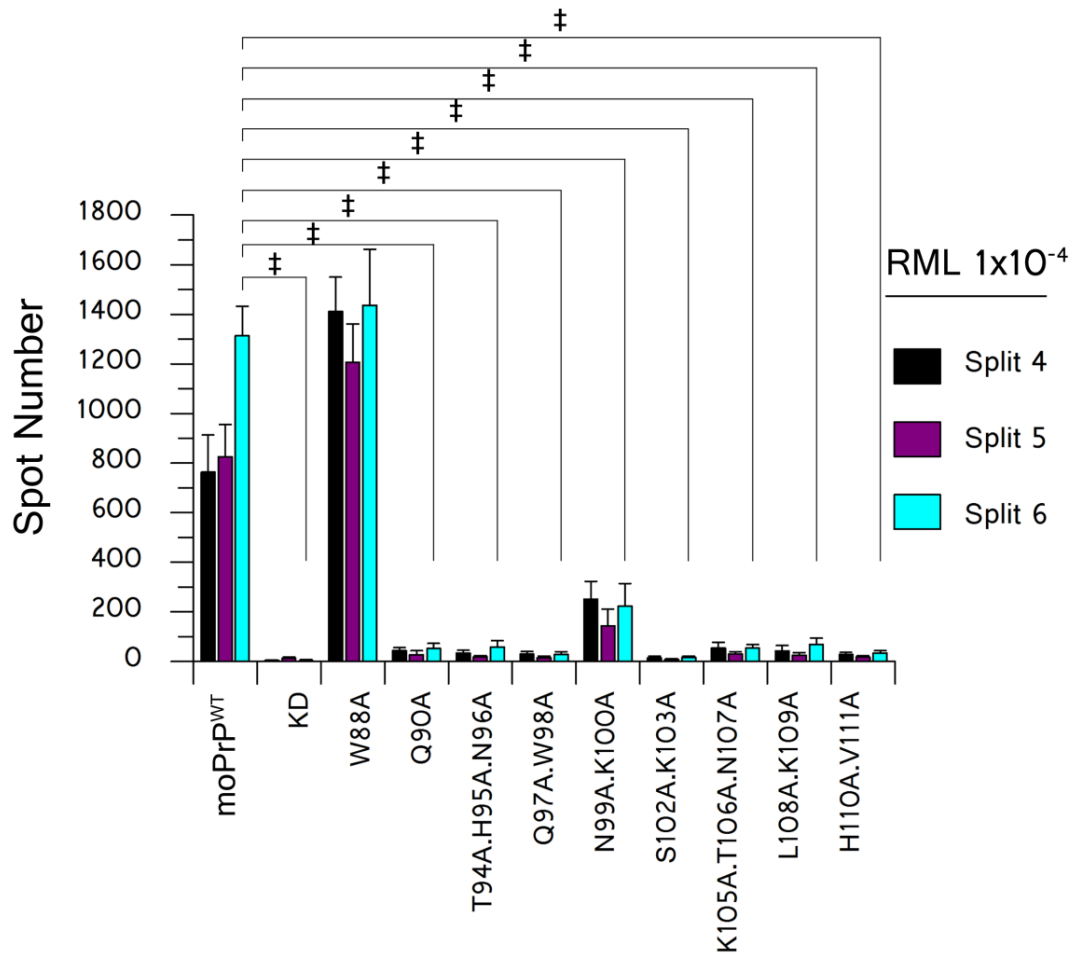


FIGURE R25: SCA OF KDMoPrP^{ALA} CELLS; MOPrP MUTATIONS IN REGION 90-111, INCREASED RML

KD cells reconstituted with either moPrP^{WT} or alanine-mutant variants of the protein within region 88-111 of moPrP were challenged with RML prions at a 1×10^{-4} dilution of infectious homogenate and their ability to propagate these prions assayed via SCA at three consecutive time points. This is a ten-fold higher dose of inocula compared to that used in Figure R20. All replacements C-terminal to and including Q90A, exhibited a significant reduction in their ability to propagate RML when compared to moPrP^{WT} and W88A. Of the 90-111 region alanine mutations, N99A.K100A exhibited the highest propagation capacity. Significance is indicated by ‡ for $P \leq 0.0001$. Significance only shown for split 6 for clarity; calculated in a one-way ANOVA with a Bonferroni correction for multiple comparisons.

3.4.3 Do CC2 mutations support prion propagation?

Mutating CC2 residues to alanine resulted in cells that had severely compromised propagation (Figure R24). Additionally, the propagation phenotype was only improved slightly, by a ten-fold increase in inoculum; at the most it was doubled (Figure R25). All replacements within region 90-111 inhibited prion propagation as tested under standard SCA conditions (Figure R24). Although spot numbers for the CC2 mutants tested were below one hundred, they were marginally above the negative control KD cells (un-reconstituted). This would indicate that the spots observed are not residual inocula, but generated *de novo*, and the slight increase by split 6 is indicative of a propagative trend; however, such a significant reduction in propagation is within the range of severely limited propagation and complete abrogation of propagation (Figure R12). This finding could mean that: (i) a very small proportion of cells within these mixed populations can propagate unhindered; or (ii) the cells are capable of propagation, but on a much slower time-scale such that cell division out-competes prion replication. Thus, since spot numbers fall below one hundred they must be defined as mutations that abrogate prion propagation based on the template used for SCA output guidelines in this study (Figures R12).

Furthermore, cell lines that propagate RML efficiently consistently give spot numbers above eight hundred by split 6 (Figure R12; Figure R25). By this criterion none of the alanine mutations within CC2 support full prion propagation. This includes single (Q90A), double (Q97A.W98A, N99A.K100A, S102A.K103A, L108A.K109A and H110A.V111A) and triple

substitutions (T94A.H95A.N96A and K105A.T106.N107A). This indicates that within the flexible tail of the protein (residues 23-111), there are three segments which limit propagation in increasing order of their position in sequence, such that CC2 mutations (region 90-111) restrict propagation to a greater extent than Q41, which in turn has a lower capacity to propagate prions than CC1 mutation K23A.K24A.R25A.

3.4.4 Cells expressing CC2 mutations in moPrP are viable

Deletion of region 105-125 in the mouse prion protein has been associated with neurotoxicity and neonatal lethality when expressed *in vivo*²⁵⁹. In cultured cells, this deletion confers hypersensitivity to the drug G418 and induced spontaneous ion channel activity¹⁷². Here, much more conservative changes were made to the protein, up to a maximum of three amino acid replacements. None of the moPrP alanine mutations in region 90-111 resulted in toxicity when expressed in KD cells. Furthermore, none of the cells expressing these CC2 alanine mutations displayed any obvious morphological differences from their parental PK1 and KD cells (Figure R26).

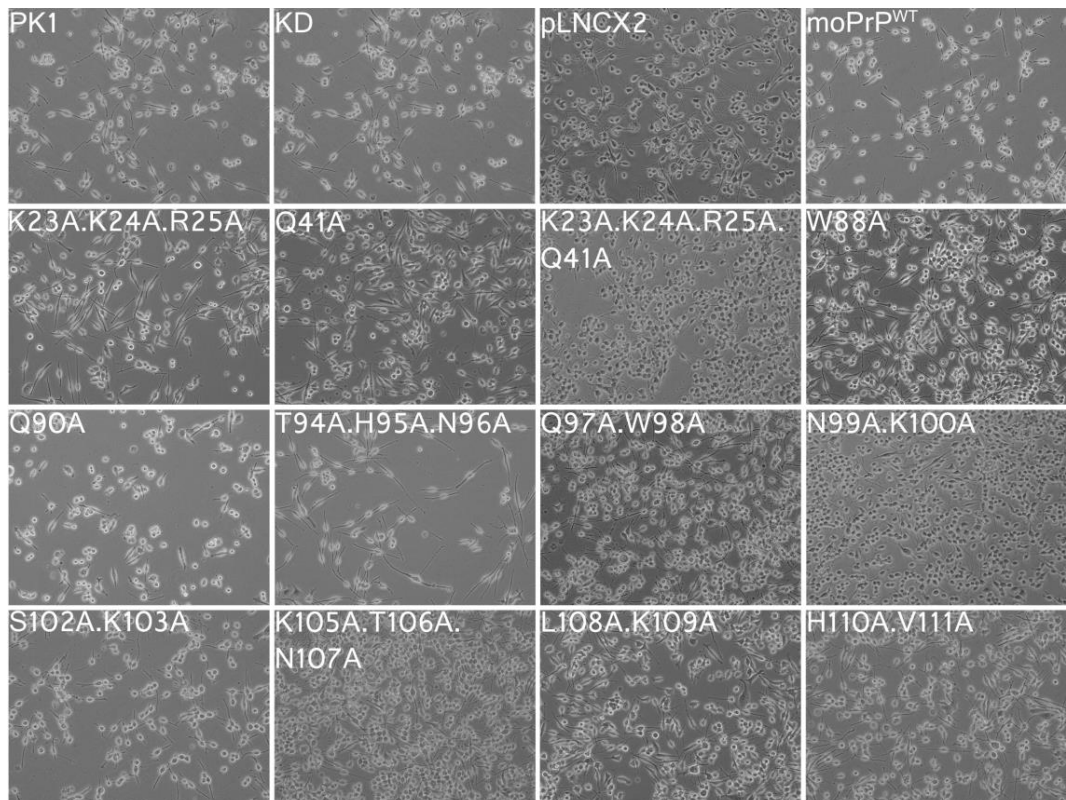


FIGURE R26: KDMoPrP^{ALA} CELLS; MUTATIONS IN REGION 90-111, PHASE CONTRAST

IMAGES

Phase contrast images of control cells in the top panel: PK1 cells that express endogenous moPrP; KD cells are PK1 cells in which moPrP expression has been silenced. pLNCX2 represents KD cells transduced with the empty vector. All other cells shown are KD cells reconstituted with moPrP and mutants thereof, using the pLNCX2 vector. K23A.K24A.R25A, Q41A and their combined mutant K23A.K24A.R25A.Q41A, represent mutations in region 23-88 that reduce propagation. W88A is shown as an example of a mutant that propagates RML prions efficiently and has a similar morphology both to control cells and the CC2 region replacements that limit propagation, shown in the bottom two panels. Magnification at x20.

3.4.5 Lack of propagation in moPrP mutations within the CC2 region is not due to lack of protein expression or cell-surface localisation

Just as protein expression was verified for moPrP mutants K23A.K24A.R25A and Q41A, KD cells reconstituted with moPrP bearing alanine mutants within the CC2 region were analysed for prion protein expression by immunoblotting (Figure R27). All reconstituted lines expressed moPrP above KD levels (Figure R27). Furthermore, similar levels of protein expression as that seen in CC2 mutations were seen in mutation W88A; this level of expression was sufficient for RML propagation (Figures R19 and R27).

Next we examined cell surface expression by immunofluorescence. All cells expressing moPrP with substitutions in region 90-111 expressed moPrP at levels above that of KD cells and at levels comparable to PK1 cells and KD cells reconstituted with moPrP^{WT} (Figure R28). The level of protein expression between mutant lines was similar, both by immunoblotting and immunofluorescence analysis (Figures R27 and R28). Slight variances in expression level such are not unusual, due the heterogeneous nature of bulk cultures (Figures R27 and R28).

Although KD cells reconstituted with mutations W88A and Q97A.W98A displayed lower levels of expression than PK1 and CC2 alanine mutations, they were still above KD levels (Figure R27). As for mutation N99A.K100A, which reported higher spot numbers in SCA that are indicative of better propagation, KD cells reconstituted with this construct did not have significantly higher expression levels than cells expressing moPrP^{WT} or

other alanine mutations of moPrP within CC2 (Figure R27). Despite this difference, N99A.K100A is not a bona fide propagator, as it exhibits severe limitations on propagation (Figures R12, R24 and R25), indicating the whole stretch of residues within CC2 is important for efficient prion propagation and that residues either side of 99-100 have a stronger inhibition on propagation within CC2 than residues 99-100. Together, these experiments show that residues within the N-terminal domain of the mouse prion protein – specifically amino acids within region 90-111 – have a strong impact on prion propagation. The results presented argue that substitutions made in the CC2 region 90-111 limit propagation to a greater extent than those observed for more N-terminal residues K23A.K24A.R25A and Q41A (Section 3.3). Interestingly however, a larger modification N-terminal to position 90, namely Δ 23-88, exhibited the same level of restriction on propagation as CC2 alanine-mutants (Figures R11 and R24). This deletion mutation consistently gave spot numbers below one hundred – a result comparable to KD cells and KD cells transduced with the empty vector (negative controls) and shown here, to KD cells reconstituted with moPrP bearing CC2 alanine mutations (Figure R24).

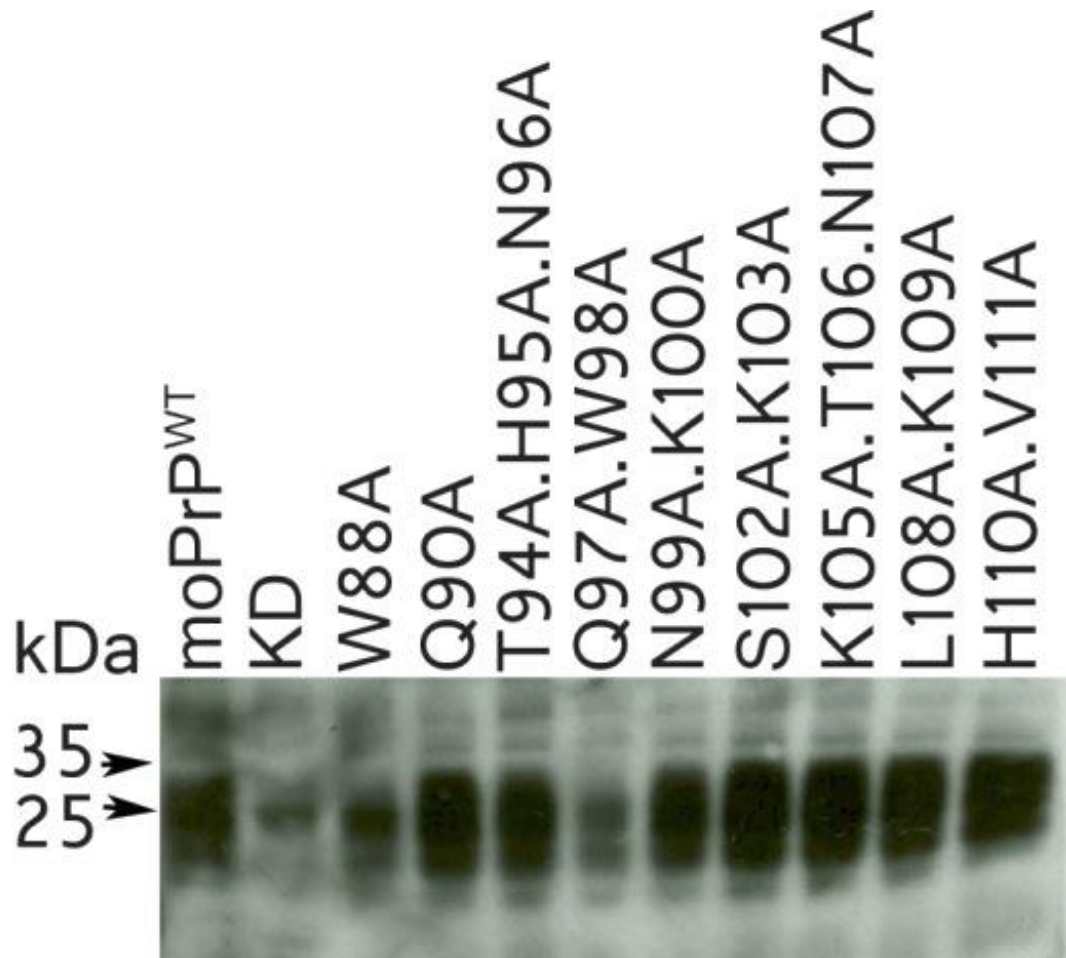
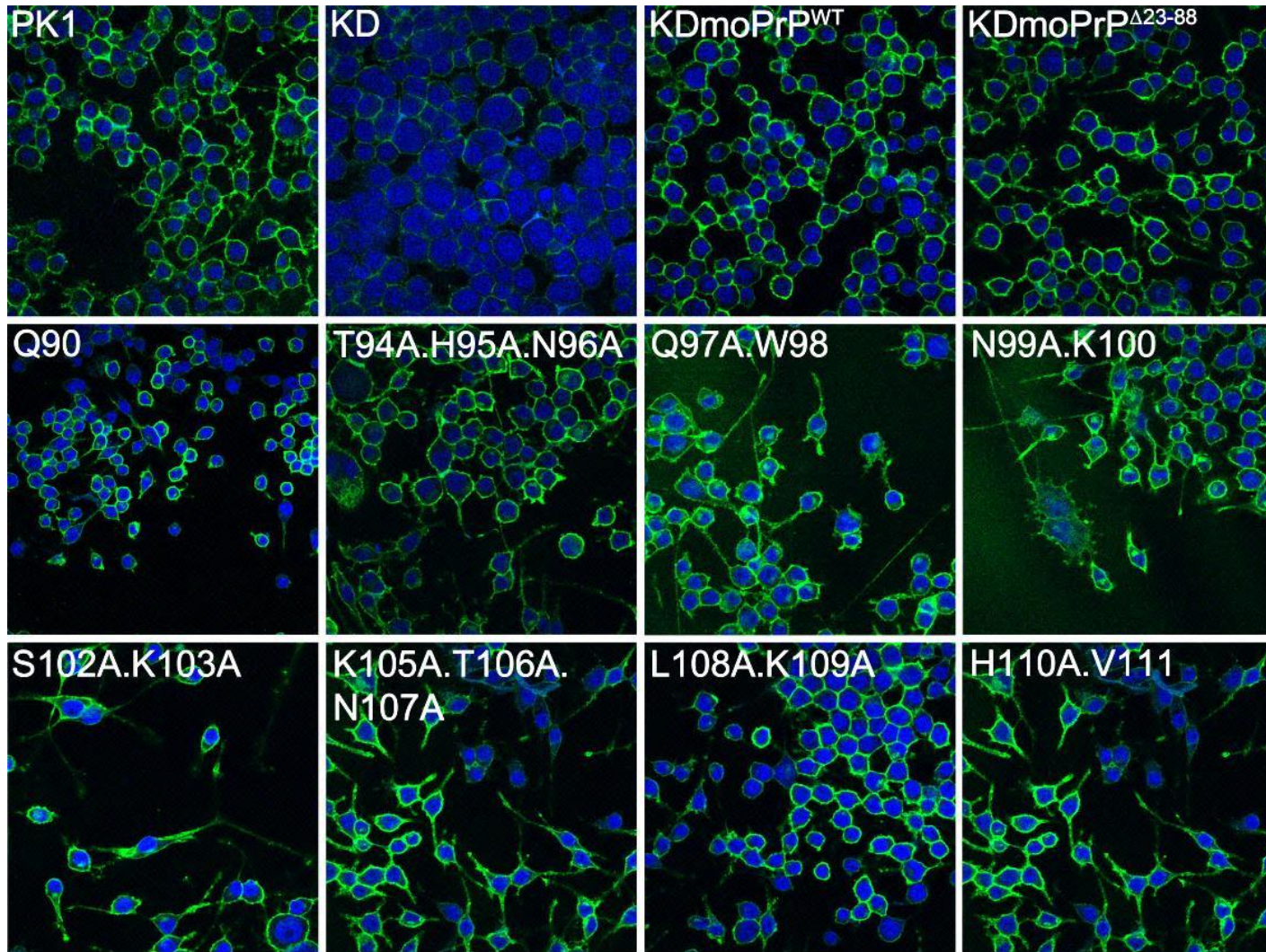


FIGURE R27: WESTERN BLOT OF KDMoPrP^{ALA} CELLS WITH MUTATIONS IN CC2

Immunoblot of PK1, KD and KD cells reconstituted with moPrP bearing alanine mutations within region 88-111. 35µg of protein was loaded per well of a 16% Tris-Glycine gel which was run for 90min at 200V; a biotinylated form of antibody ICSM35 (ICSM35b) was used to detect moPrP; goat anti-mouse Streptavidin conjugated to HRP was used as the secondary antibody, followed by ECL development. 3 min exposure.



**FIGURE R28: IMMUNOFLUORESCENCE IMAGES OF KDmoPrP^{ALA} CELLS WITH
MUTATIONS IN CC2**

Immunofluorescence analysis of KD cells reconstituted with CC2 alanine mutants of moPrP. The top panel represents control cell lines: PK1 cells that express endogenous moPrP; KD cells in which expression of the endogenous protein is silenced; KD cells reconstituted with full-length moPrP and with moPrP deletion mutation Δ 23-88. The second and third panels show KD cells reconstituted with moPrP bearing minimal alanine mutations within the CC2 region. moPrP^{Ala} is detected in these cell lines at the cell surface, following the same localisation pattern as KDmoPrP^{WT} on non-permeabilised cells. Blue: DAPI nuclear stain; green: moPrP. Magnification at x40.

3.4.6 Minimal mutations in prion protein CC2 significantly reduce prion propagation

SCA analysis of N-terminal alanine mutants of the prion protein revealed a distinct segment that when altered, markedly reduced prion propagation capacity. This included point, double and triple mutations made within region 90-111 of moPrP. Charge cluster (CC2) region 90-111 on PrP^C along with a smaller more N-terminal charge cluster (CC1) have been shown to interact with PrP^{Sc133}. The data presented here shows that CC2 mutations strongly inhibit propagation – more so than CC1 or Q41 mutations (Section 3.3).

SCA data showed that KD cells expressing mutation W88A gave spot numbers in the thousands (Figure R24), comparable to propagation profiles of KD cells reconstituted with the wild-type protein; this is in stark contrast to cells expressing mutation Q90A, where spot numbers remained below one hundred for all splits (Figure R24). This suggests that depending on position in the sequence, PrP can tolerate small modifications without greatly diminishing the protein's ability to convert PrP to a ProteinaseK-resistant form, following infection by RML prions. Every alanine replacement made C-terminal to residue W88 exhibited a profoundly reduced ability to propagate prions, compared to those tested N-terminal to this site (Figures R14, R16 and R24).

The data shows that modifications within region 90-111 as small as single replacements (Q90A) and up to three replacements within the native sequence with alanine (K105A.T106A.N107A) severely diminish the ability

of cells expressing the modified protein (moPrP with minimal replacements in CC2) to efficiently propagate prions (Figure R24).

Since all eight mutations made within CC2 segment 90-111 resulted in greatly reduced propagation at two concentrations of infectious inocula (Figures R24 and R25), we propose that this charge cluster represents an important region regarding native and aberrant PrP function. Whether the changes made led to a loss or gain of function phenotype, or whether it is linked to the binding of accessory proteins remains to be investigated.

The second charge cluster (CC2) divides the OPRs from the conserved hydrophobic region of the protein (Figure R23). CC2 is purported to have a myriad of interaction partners: A β ^{58, 105, 107, 139}, metal ions^{37, 59}, as well as undergoing self-association²⁶⁰. The interaction of CC2 with multiple partners may be attributed to the concentration of positive charge at this site. Additionally, the ease of interaction at CC2 could stem from the lack of steric restriction due to its glycine-rich, flexible N-terminal domain²⁶¹. It is possible that the alanine mutations made within region 90-111 of moPrP disrupt interactions of this domain with native interactors or aberrant associations that the native CC2 sequence would engage in following RML infection; this could explain the severely reduced propagation observed for all mutations in this region (Figure R24).

Earlier work on analysis of PrP function where deletion mutagenesis was employed to infer amino acid contributions produced conflicting results: transgenic mice overexpressing moPrP with deletions Δ 32-80 or Δ 32-93, developed disease, propagated prions and accumulated ProteinaseK-

resistant prion protein, following inoculation with prions⁴⁸. However, in the case of deletion mutation Δ 32-93 longer incubation times were reported, but propagation and disease ensued, suggesting that segment 32-93 was not required for propagation⁴⁸. When the deleted segment was widened to encompass residue 106 however (Δ 32-106), no prion propagation was observed¹²⁸.

The toxicity elicited by PrP deletion mutants has been studied extensively *in vivo* and points to the removal of the flexible region, especially deletions in CC2 and HC domains, as the principal contributors to the elicited neurotoxicity^{115, 173}. It is important to note that since a majority of the studies carried out in this region resulted in toxicity, previous efforts to study the individual contributions of amino acids within this segment was not always possible. Since then, many laboratories including ours have attempted to further characterise individual segments of the protein essential for the efficient propagation of prions, and found increasing evidence for a role of the N-terminus of PrP in prion propagation^{116, 134}. Here, a range of viable cell lines expressing moPrP^{Ala} have been established, with which specific functions of CC2 can be investigated; the focus in this study being primarily prion propagation following RML infection.

N-SS CC1 OPR **CC2** PTM β 1 α 1 β 2 α 2 α 3 SS-C

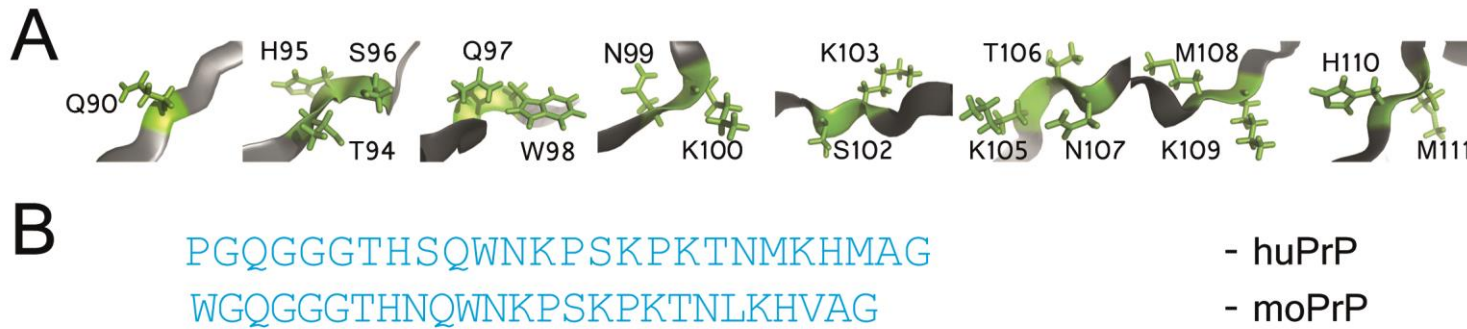


FIGURE R29: HUMAN AND MOUSE PRION PROTEIN SEQUENCE; REGION CC2

Panel A depicts the position and residues on prion protein structure PDB entry 2LEJ (huPrP) at which CC2 mutations to alanine were made in this study; these are outlined in green with side-chains shown as sticks on a grey protein backbone. As 2LEJ represents the human protein, the sequence composition varies from moPrP, which is the PrP isoform used in this study. Sequence differences between huPrP and moPrP are depicted in panel B, with the CC2 region (90-111 moPrP) in blue lettering. Sequence variation at CC2 occurs at positions 96 (S/N), 109 (M/L) and 111 (M/V).

3.4.7 CC2 is a solvent-exposed region of the prion protein with multiple interactors

CC2 is an important domain in the flexible region of the prion protein for a number of reasons: (i) point mutations within this region (P102 and P105; human numbering) are known to be associated with Gerstmann-Sträussler-Scheinker (GSS) forms of prion diseases. (ii) it is a highly immunogenic segment in the protein exemplified by the number of antibodies to which this region is epitope-mapped. This includes anti-prion antibody ICSM35 used for immunoblotting in this study (Table R4). (iii) CC2 is cited in the literature as interacting with a range of proteins or peptides: A β ¹⁰⁵, LRP1^{102, 249}, vitronectin²⁶², 14-3-3²⁶³, self-association²⁶⁴ as well as participating in metal ion binding³⁷. (iv) CC2 is also believed to regulate prion protein conversion through residues 100-104¹³⁴. (v) Novitskaya *et al.*, have shown using an immunoconformational assay, that segment 95-105 is a solvent exposed region⁸², which explains antibody access to this epitope^{137, 151} and reports of multiple protein interactions^{102, 105, 249, 262}; this also correlates well with ProteinaseK-sensitivity of this region in PrP^{C201}. The flexibility of CC2 combined with the concentration of charge at this site makes it an effective interaction surface. This study supports the involvement of CC2 in prion propagation, as point, double and triple mutations to alanine in this region negatively and significantly lowered prion protein propagation (Figure R24).

KD cells reconstituted with moPrP^{WT} propagated RML efficiently at a 1×10^{-5} dilution of homogenate (Figure R24), but in KD cells reconstituted with moPrP bearing CC2 alanine mutations, propagation was significantly reduced in comparison (Figure R24). All eight mutations made in this region

(Q90A, T94A.H95A.N96A, Q97A.W98A, N99A.K100A, S102A.K103A, K105A.T106.N107A, L108A.K109A and H110A.V111A) demonstrated a ten-fold lower response to RML propagation compared to the wild-type protein (Figure R24).

Additionally, a ten-fold increase in the dose of infectious inocula did not improve the limited capacity of mutations within region 90-111 to propagate prions, with the exception of N99A.K100A (Figure R25). This mutation showed a two-fold increase in propagation when more inoculum was made available (Figure R24 and R25). Cells expressing CC2 alanine mutations displayed similar morphology (Figure R28) and protein expression levels compared to PK1 wild-type cells and KD cells reconstituted with the wild-type protein (Figures R27 and R28). This suggests that the loss of propagation in these cells is due to the mutations in moPrP harboured within CC2 and not due to lack of protein expression. These data provide strong evidence for a modulatory role of the second charge cluster of PrP in prion propagation. A myriad of possible PrP-interactions may have been compromised when moPrP was expressed with alanine mutations in CC2 region 90-111. Such disruption in native interactions could have contributed to the loss of propagation phenotype observed for these mutations when expressed in KD cells (Figures R24 and R25).

Immunogen	Antibody	Epitope	Reference
Bovine peptide, ovarian peptide, recombinant human PrP	AB5058	78-97	Sanchez <i>et al.</i> ²⁶⁵
	12B2	89-93	Yull <i>et al.</i> ²⁶⁶
	6D11	93-109	Pankiewicz <i>et al.</i> ¹³⁶
	P4	93-99	Harmeyer <i>et al.</i> ²⁶⁷
	12B2	93-97	Jeffrey <i>et al.</i> ²⁶⁸
	POM3	95-100	Polymenidou <i>et al.</i> ¹⁵¹
	8G8	97-102	Féraudet <i>et al.</i> ²⁶⁹
	9A2	102-104	Yull <i>et al.</i> ²⁶⁶
	PrP-AA	106-110	Wei <i>et al.</i> ¹³⁵
	3F4	109-112	Zomosa-Signoret <i>et al.</i> ²⁷⁰
anti β -PrP (recombinant human PrP)	ICSM 35	93-105	Khalili-Shirazi <i>et al.</i> ¹³⁷
	ICSM 37	96-105	
	ICSM 42	96-105	
	ICSM 54	96-105	
	ICSM 61	96-105	
	ICSM 62	96-105	

TABLE R4: ANTIBODIES AVAILABLE AGAINST PRP REGION CC2

A vast array of antibodies available against the CC2 region of the protein are summarised here. The top half of the table shows antibodies generated from a range of immunogens, while the bottom half shows antibodies generated within the MRC Prion Unit using recombinant human PrP (with a high β -sheet content). ICSM35 used in this study, was generated using recombinant human PrP (high β -sheet content) as the immunogen.

Since the effects of mutating region CC2 affected propagation so dramatically, the data suggests that the entire region is required for efficient propagation, and not just a segment within it. Additionally, if the requirement for CC2 in propagation was only partial, we would expect propagation to improve at least gradually if not drastically as seen for W88A versus Q90A, with mutations made further from a hypothetical 'minimal site'. The only indication that differences in propagation existed within the CC2 region, was observed for N99A.K100A at a higher dose of inocula (Figure R24 and R25), indicating that these two residues are more tolerant of changes to the native sequence than amino acids either side of it. Despite the improvement in propagation seen for KD cells reconstituted with the N99A.K100A mutation in moPrP when infected with more inoculum (Figure R25), the ability of these cells to propagate RML was severely compromised compared to cells expressing the wild type protein (Figure R25).

It could be hypothesised that a key step in the prion propagation pathway is modulated by segment 90-111 and that the drop in propagation observed for CC2 mutants in this study, is due to a single or combined effect of disruption in the prion propagation pathway. Such an event may be endocytosis of the cellular protein, which has previously been linked to charge clusters in the N-terminal region of the prion, either through GAG binding¹¹³, LRP1^{102, 108, 271}, or other interactions. Conversion of PrP^C to PrP^{Sc} has been shown to occur at the plasma membrane both in cell culture¹⁰⁰ and *in vivo*²⁷². PrP^{Sc} reportedly forms string-like structures at the cell surface where it is retained for prolonged periods before eventual internalisation by unknown mechanisms²⁵¹. Following conversion, PrP^{Sc}

must be internalised if propagation is to be maintained. This is established through accumulation of PrP^{Sc} in early and recycling endosomes for sustained infection²⁷³. The accumulation of PrP^{Sc} is believed to affect recycling of the cellular protein, a feature which may be perturbed in CC2 alanine mutants of moPrP³⁸. It could be argued that if cell surface conversion occurs, the need for endocytosis is negated for propagation. However, for the PrP^{Sc} to spread to neighbouring cells, internalisation and recycling of both PrP^C and PrP^{Sc} are required²⁷³. CC1 alanine mutations in moPrP may alter the clathrin-mediated pathways for PrP^C endocytosis, but not those mediated through copper association or GPI-dependent pathways²⁵⁴. This may explain why a reduction in propagation is observed for CC1 mutations, but also why it is not abrogated as other compensatory mechanisms may enable propagation with reduced efficiency (Section 3.3).

Laurén *et al.* used deletion mutagenesis to outline region 95-105 of moPrP as the site of A β oligomer binding¹⁰⁵. This finding has since been supported by biophysical characterisation of the binding epitope¹³². The significance of this binding has implications on how the two proteins regulate one another in terms of endocytosis²⁷⁴, neurotoxicity¹⁰⁸ and synaptic plasticity¹⁰⁵. PrP^C has been shown to bind the metabotropic glutamate receptor 5 (mGluR5)⁶¹.

The complex of A β oligomers with PrP^C activates mGluR5-mediated calcium influx leading to compromised neuronal function⁶¹. It is interesting to consider that both prion disease and Alzheimer's disease arise from protein misfolding events and yet A β oligomers associate with the cellular form of PrP. It is possible that the aberrant forms of these proteins activate similar toxicity-inducing pathways that culminate in neuronal cell death. Through

association of A β with PrP and vice versa, these proteins may regulate the amount of misfolded protein in the cytosol to protect the cell from, or exacerbate the effects of the amyloid cascade hypothesis¹². In terms of PrP's interaction with A β oligomers, it is known that a smaller segment (95-105) within region 90-111 is involved in this association¹⁰⁵. Since CC2 residues 90-111 have also been shown to be implicated in the regulation of prion propagation in this study, it is possible that the native contacts in CC2 amino acids are unavailable for association in the PrP^{Sc} state, which may explain findings of A β interaction with PrP^C and none reported for its association with PrP^{Sc}. The range of mutations in PrP^C generated in this study can be used for future applications to further probe the PrP-A β interaction and subsequent cellular outcomes.

3.4.8 Minimal segment required for efficient prion propagation extends beyond a five-amino acid sequence (100-NKPSK-104)

Another group that undertook a mutagenic approach to identify regions required for prion conversion identified region 100-104 as the minimal segment responsible for the conversion of PrP^C to PrP^{Sc134}. They carried out their investigation exclusively in N2a and chronically Scrapie-infected N2a cells. The authors reported no loss in propagation when moPrP sequence 95-98 was replaced by equivalent residues in the chicken homolog. However, they focused their study on region 92-107 of the protein on the premise that anti-prion antibodies raised against this region of the protein show differential binding activities for PrP^C and PrP^{Sc134}.

Furthermore, they proposed that their interest in this region also stemmed from the fact that it is a heterogeneous and flexible region of the protein found in the N-terminal end after ProteinaseK digestion of PrP^{Sc275}. Moreover, they stated that their data supports previous reports on moPrP region 89-103 and 105-114 as not being the major interface for the initial binding and propagation of PrP^{Sc}, but rather playing a role in the conversion event¹³⁴.

The finding that CC2 residues 100-104 in particular govern prion conversion is extremely relevant in the context of this study; it is also both in agreement and conflict with the data presented here: firstly, our data is in support of the hypothesis that region 100-104 is crucial for efficient prion propagation, but it also shows a strong case for the involvement of CC2 as a region that extends beyond 100-104 at both termini (region 90-111) to regulate

propagation (Figures R24 and R25). The disparity that arises between our data set and that of Hara *et al.* may be down to technical differences. Hara *et al.* performed their investigation on a chimeric construct consisting of mouse PrP substituted for a chicken PrP sequence, tagged with a 3F4 epitope¹³⁴. Chicken residues replaced mouse PrP at sequence sections 95-104. Our study in contrast, is based exclusively on moPrP, with minimal alanine replacements made throughout the protein in a more non-targeted approach.

It is important to be mindful of the fact that Hara *et al.* tested the effects of their mutations in the presence of the endogenous protein whereas the SCA analysis performed in this study reports propagation of the expressed moPrP^{Ala} protein without the influences of the endogenous protein (Section 3.2). Data presented here shows that prion protein region CC2 can mediate propagation at the highest dose of inocula applied (RML 1×10^{-4}), as tested in eight CC2 mutations (Figures R24 and R25).

What this finding highlights is that single, double and triple alanine replacements within region 90-111 are able to limit the degree of propagation following infection. It further delineates position 90 as a strong regulator of propagation in the flexible region of the protein – stronger than previously identified more N-terminal regions CC1 and Q41 (Section 3.3). Additionally, mutational effects were recorded in the absence of tagged constructs and with maximal sequence identity to increase sensitivity for detection of propagation; in this system, detection is further improved through the use of PK1 cells which are highly sensitive to infection with RML prions⁹⁷.

3.4.9 Influences of the flexible amino-terminal region of the prion protein on propagation capacity

The minimal mutagenesis approach adopted in this study has identified region 90-111 within the flexible N-terminal tail of the protein as having strong influences on propagation. Eight constructs of moPrP were generated, each bearing mutations to alanine within the CC2 sequence. KD cells reconstituted with any of the eight alanine moPrP constructs generated, showed significant changes in propagation of RML prions (Figures R24 and R25).

In every instance of a CC2 alanine-mutation, prion propagation was severely compromised in cells expressing the mutated protein (Figure R24). Increasing the dose of infectious inocula did not restore the propagation of cells expressing the CC2 mutations in moPrP, to levels comparable with moPrP^{WT}-expressing cells (Figure R25). That single, double and triple replacements within the flexible tail of the protein can have such a strong limiting effect on overall protein propagation is remarkable.

The data further suggests that despite the C-terminal core being the essential component of the prion protein required for propagation^{88, 157, 160, 161, 206, 276}, the flexible N-terminal tail is a major player in the process that governs the efficiency with which propagation is achieved. The level of inhibition alanine mutations exerted on propagation capacity was stronger for mutations made more C-terminal to the signal sequence (residues 1-22); that is, CC2 mutations (region 90-111) exert stronger control over prion propagation than the more N-terminal residue Q41, which in turn has more

influence on propagation than CC1 amino acids K23.K24.R25 at the extreme N-terminus (Section 3.3).

The significance of prion protein region CC2 is widely covered in the literature in the context of A β -linked neurotoxicity/neuroprotection^{107, 139}, toxicity following PrP^{Sc} infection²⁵⁹ and in toxic PrP mutants¹¹⁵. Here, we show that minimal alanine substitutions (up to three amino acid replacements) in the 90-111 region of the protein do not give rise to toxic mutants and are well-expressed in KD cells (Figure R28). In terms of efficient prion propagation, CC2 is intolerant of changes, however minimal, to its native sequence: single replacement Q90A significantly reduced propagation compared to cells expressing the wild-type protein (Figure R24). Q90A defines the most N-terminal position in the flexible N-terminal tail of the protein that shows a ten-fold reduction in protein propagation, as W88A did not reduce propagation relative to moPrP^{WT}-expressing cells (Figures R24 and R25).

Site directed mutagenesis	Limitation on		moPrP domain
	KD cells	PK1 cells	
Q90A			CC2
T94A.H95A.N96A			
Q97A.W98A			
N99A.K100A			
S102A.K103A			
K105A.T106A.N107A			
L108A.K109A			
H110A.V111A			

None	Strong	Very	N/A
------	--------	------	-----

TABLE R5: LIST OF MUTATIONS MADE WITHIN CC2

List of mutations made within charge cluster 2 of the mouse prion protein. Native residues at these positions were changed to alanine and the modified protein expressed in KD cells to test the effect of the mutations on prion propagation. All cells expressing moPrP mutations within CC2 exhibited a very strong reduction in their ability to propagate RML prions in the scrapie cell assay. (N/A: not applicable).

3.4.10 Summary of mutations at moPrP region 90-111 (CC2)

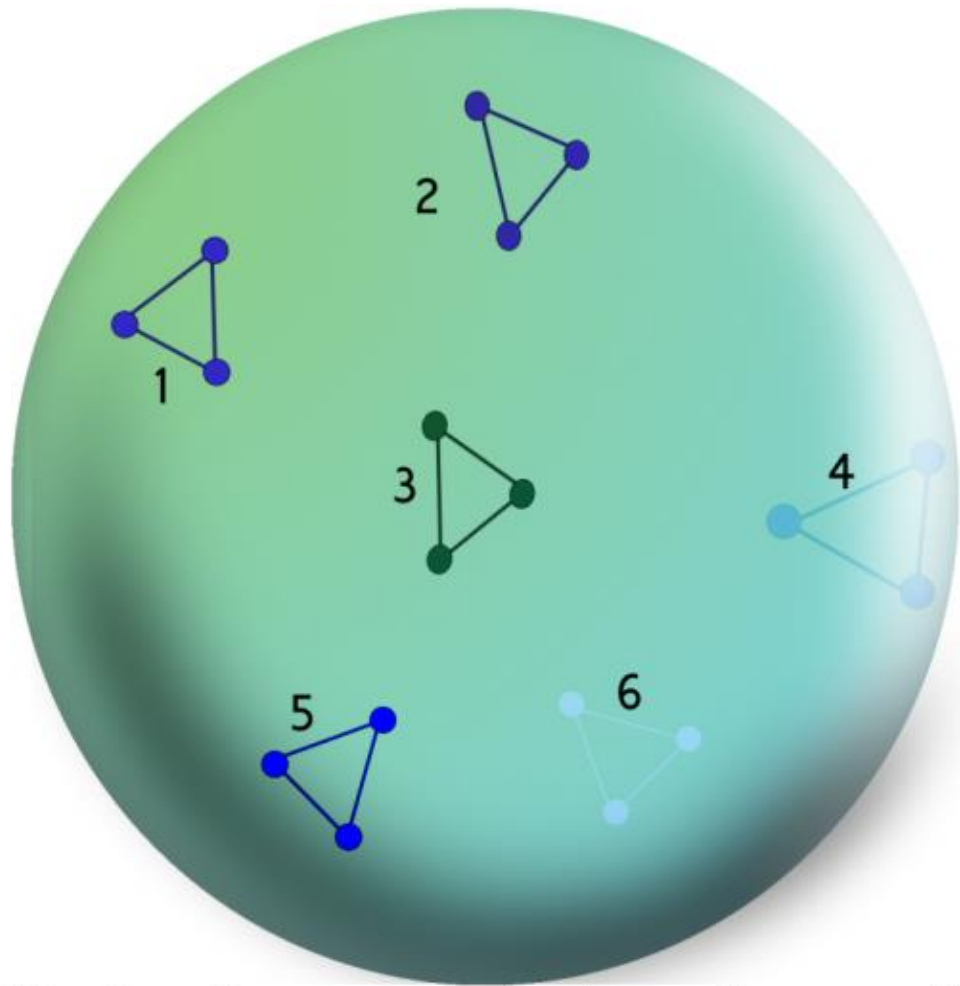
Single substitution Q90A, double replacements Q97A.W98A, N99A.K100A, S102A.K103A, L108A.K109A, H110.V111A and triple replacements T94A.H95A.N96A, K105A.T106A.N107A all markedly lowered the ability of KD cells expressing these mutations to propagate prions (Figure R21). This suggests that the entirety of CC2, region 90-111 inclusive, plays an important role in the efficiency with which prion propagation occurs. Notably, minimal perturbations in this segment of the protein, like Q90A, have a significant effect on the overall propagation pathway. This strengthens the evidence in favour of CC2 as having a strong controlling effect on propagation efficacy.

3.5 Targeted mutations in the structured region negatively impact prion propagation

3.5.1 Experimental strategy

The aim of this study was to identify regions within the prion protein that are important for the efficient propagation of prions. The prion protein has a long flexible N-terminal tail which constitutes roughly half the protein sequence. The other half of the protein is a C-terminal globular portion, for which structural information is available from X-ray crystallography and NMR data deposited in the protein data bank: <http://www.pdb.org/pdb/home/home.do>. Using the available structural information, targeted mutations were made within the structured region of moPrP at solvent-exposed residues. Triple alanine substitutions were made, with the intention of altering a small portion of spatially proximal surface residues. Each of these moPrP constructs was then sequence verified in pBluescriptSK+ vector, moved into pLNCX2, and stably expressed in KD cells as described in Chapter I.

They were then assayed for prion propagation by SCA. By targeting clusters of mutations at various sides of the protein surface, we investigated which ‘face’ or ‘faces’ of the protein were crucial for prion propagation (Figure R27). In addition to the alanine substitutions at the protein surface, a few other amino acid replacements were made within the buried hydrophobic core of moPrP to destabilise the protein and promote unfolding. The effects of such modifications on prion propagation were then analysed by SCA.



Globular protein domain

Surface residues targeted

FIGURE R30: TARGETED MUTAGENESIS OF THE STRUCTURED REGION OF MOPrP

Solvent-exposed residues within the structured region of PrP were targeted for alanine mutagenesis. The sphere represents the globular, structured domain of PrP (residues 121-230). Triangles labelled 1-6 represent six moPrP constructs, each with three alanine substitutions (filled circles) that are spatially proximal. Using this approach, we tried to generate sufficient substitution mutants to cover multiple faces of the protein.

Surface mutations on moPrP can be categorised as those targeting: (i) α -helices, (ii) loop regions and (iii) β -strands. Two destabilising mutations created in moPrP were M204A and double mutation C178A.C213A. The unfolding mutation M204Q.M205Q.V209Q.M212Q was designed to introduce charge residues within regions of the protein that are usually buried within the hydrophobic core, so as to disrupt native folding of the protein. All SCA experiments in this chapter were carried out using RML prions at a 1×10^{-5} dilution of 10% homogenate.

3.5.2 Substitution of native residues for alanine between the first β -sheet strand and the first α -helix of moPrP compromise prion propagation

The globular domain of PrP has three α -helices and two β -strands. Mutations made within and bordering β 1 and α 1 include G123A.L124A.G125A, just N-terminal to the first strand of the anti-parallel β -sheet; M128A.Y162A.Q216A which affects residues at both β -strands and a neighbouring residue in the third helix; L129A.S131A.Q159A which targets amino acids at the first β -strand and those in the vicinity of β 1 and β 2; S134A.R135A.M153A includes two amino acids at the loop region between the first β -strand and α -helix, as well as a nearby amino acid within α 1; H139A.G141A.D146A mutations bear changes in the loop region N-terminal to, and within, α 1; D142A.W144A.E145A and R147A.R150A.E151A are exclusively α 1 mutations within the moPrP sequence (Figure R32).

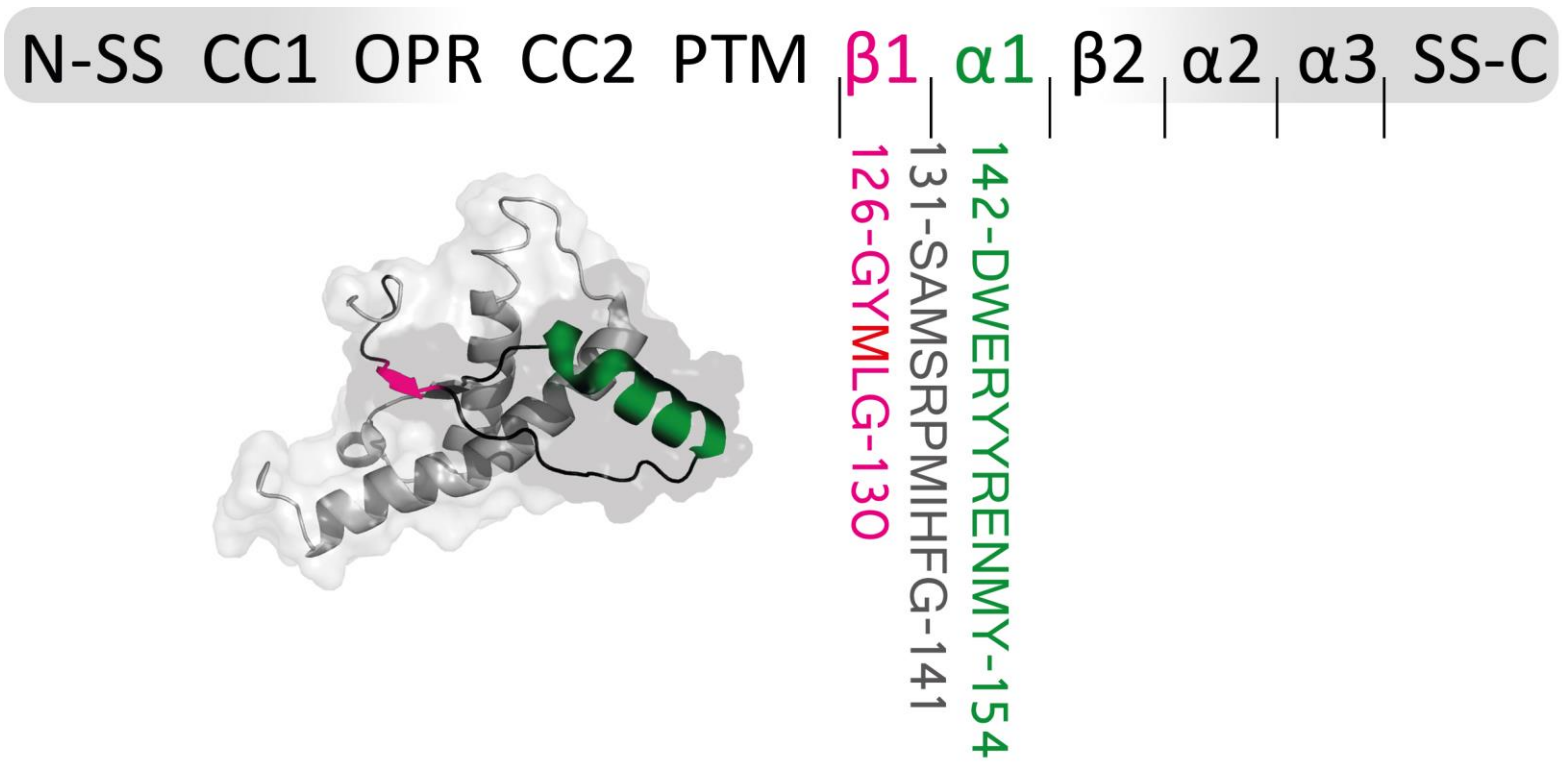


FIGURE R31: MOPrP STRUCTURED REGION; RESIDUES 123-151

Bar schematic of domains within moPrP. N-SS: N-terminal signal sequence; CC1: charge cluster 1; OPR: octapeptide repeat region; CC2: charge cluster 2; HC: conserved hydrophobic region; α 1: helix 1; β 1: strand 1; α 2: helix 2; α 3: helix 3; SS-C: C-terminal signal sequence. Residues 126-151 of moPrP are shown in single letter amino acid code; M/V polymorphisms known to influence susceptibility to prion disease are at position 128 (red). PDB entry 2L39 of moPrP.

These mutations were generated as described in Chapter I and stably expressed in KD cells. Their propensity for propagating prions was analysed via SCA, using RML as the infectious inoculum (Section 3.2). None of the mutations tested fully propagated RML prions based on the SCA guide (Figure R12) when compared to cells expressing the wild-type protein; each mutation presented spot numbers below two hundred (Figure R33, R36 and R39).

SCA analysis of KD cells reconstituted with moPrP^{WT} consistently gave values approaching or above eight hundred spots at split 6 following RML infection. This is a good indication of efficient prion propagation (Figure R12). For the alanine mutants tested in region 123-159, the highest recorded average count was one hundred spots (Figure R33). This ten-fold reduction in the ability of KD cells reconstituted with these mutations to propagate prions highlights the importance of these solvent-exposed amino acids in prion propagation. Region 123-151 therefore represents a portion of the prion protein that when mutated, significantly reduces the ability of susceptible cells to propagate prions (Figure R33).

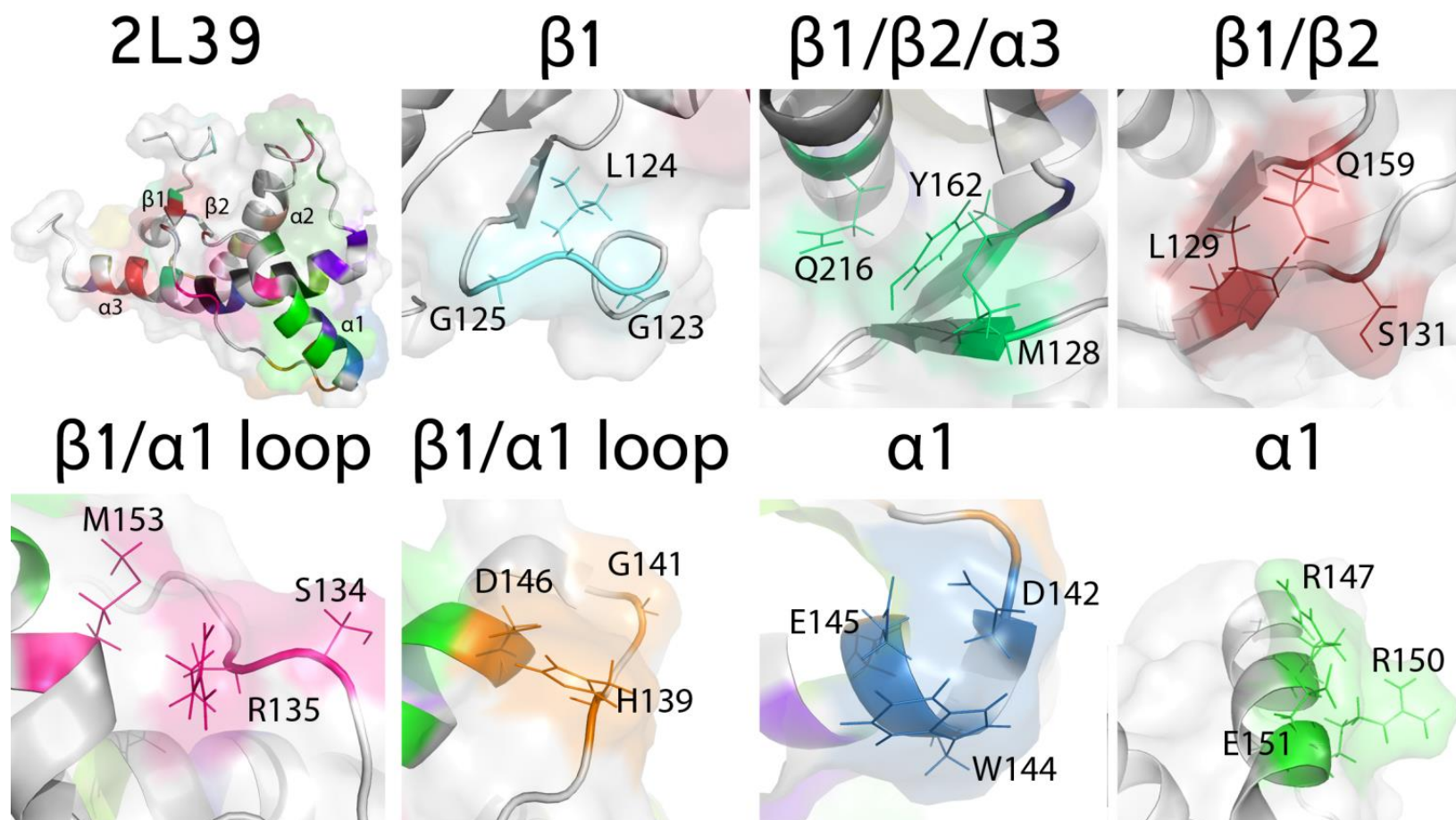


FIGURE R32: TARGETED SITES FOR MUTATIONS IN REGION 123-151 OF MOPrP

Mutations targeted to the surface of the globular domain on moPrP are depicted on PDB entry 2L39, shown in full in the top left corner, showing two β -strands and three α -helices with a surface outline. Areas of the protein that were not targeted for mutagenesis are shown in light grey; where residues have been mutated, areas are shown in any colour other than grey. Following this entry are various positions on the protein where targeted mutations to alanine were made. Secondary structures bearing moPrP mutations are indicated above each image. Mutation sites are shown with coloured backbone carbons and side chains (line display) on an otherwise grey backbone. All images were created in PyMol.

Low levels of expression of the cellular prion protein are known to abrogate prion propagation; indeed transgenic mice devoid of PrP are not susceptible to infection by prions⁴⁸. The moPrP surface mutations generated in this study expressed well in KD cells, thereby ruling out lack of protein expression as a factor for limited propagation (Figures R34, R37 and R41). One exception where the standard anti-PrP antibody ICSM18 could not be used for immunoblotting and immunofluorescence applications was for mutation R147A.R150A.E151A, since the antibody epitope is destroyed¹³⁷. In this instance, anti-PrP antibody ICSM35 was used to detect the protein (Figure R37), as its epitope lies within CC2 region 93-105¹³⁷.

From this data, a triple mutation of sequentially proximal residues G123A.L124A.G125A abrogated propagation (Figure R33). All the other mutations tested in this section also exhibited severe limitations on propagation (Figure R33). R147A.R150A.E151A also appears to abrogate propagation, but the effect on propagation of this mutation could not be verified in the current SCA setup, as the mutation destroys the binding site for ICSM18 which is used in the standard SCA setup and alternative anti-prion antibody ICSM35 could not be adapted for SCA as ELISPOT processing steps such as ProteinaseK digestion which cleaves PrP within the ICSM35 epitope site do not allow for sensitive detection (data not shown).

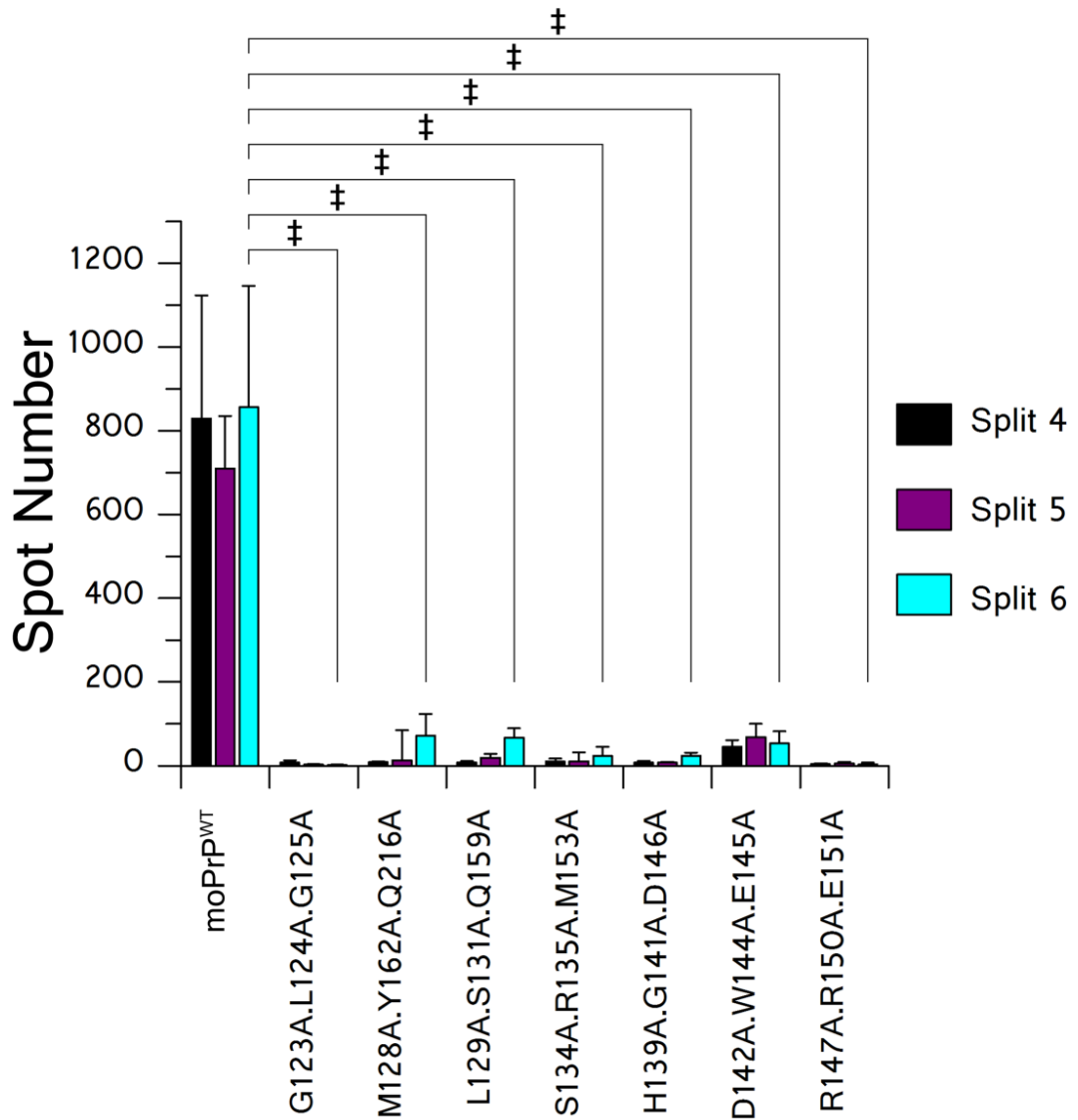


FIGURE R33: SCA OF KDMoPrP^{ALA} CELLS; MOPrP MUTATIONS IN REGION 123-151

KD cells reconstituted with either moPrP^{WT} or alanine mutant variants of the protein within region 123-159 of moPrP were challenged with RML prions at a 1×10^{-5} dilution of infectious homogenate and their ability to propagate these prions assayed via SCA for at least three consecutive passages. All replacements within this region exhibited a significant reduction in their ability to propagate RML when compared to moPrP^{WT}. Significance is indicated by ‡ for $P \leq 0.0001$. Significance only shown for split 6 for clarity; calculated in a one-way ANOVA with a Bonferroni correction for multiple comparisons.

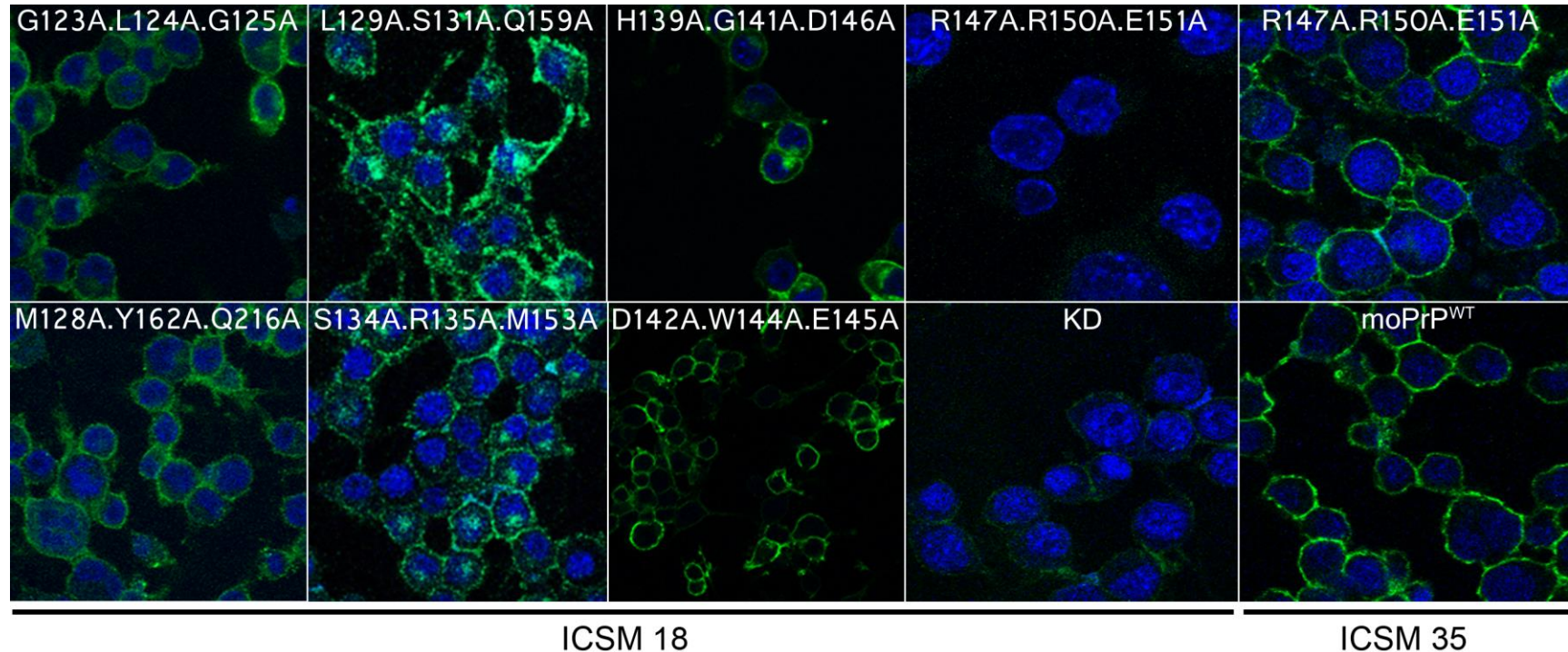


FIGURE R34: IMMUNOFLUORESCENT ANALYSIS OF KDMoPrP^{ALA} CELLS WITH MUTATIONS IN STRUCTURED REGION 123-151

Immunofluorescence analysis of KD cells reconstituted with structured region (123-151) mutants of moPrP. The top panel represents cells probed for moPrP using ICSM18 antibody. The lower panel shows moPrP^{WT} and KD cells stained with ICSM35. KD and moPrP^{WT} represent negative and positive control lines, respectively. moPrP mutant R147A.R150A.E151A was not detected by ICSM18, as the antibody epitope is in this region; it was however, recognised by another anti-moPrP antibody, ICSM35 whose epitope is more N-terminal (residues 93-105). All reconstituted KD lines expressed moPrP on the cell surface. DAPI nuclear stain; green: moPrP. Magnification at x40.

3.5.3 Alanine mutations made between the first and third α -helices of moPrP display strong inhibition of prion propagation

The second series of mutations on solvent-exposed regions of the prion protein included: Y148A.T198A.D201A where replacements were made in the first α -helix and the N-terminal cap of the third helix; R155A.K193A.E195A where R155 of α -helix 1 comes into close proximity with charge residues in the loop region between α -helices 2 and 3; R163A.Y168A.H176A with two loop region mutations between the first and second β -sheets, and one at α -helix 2; S169A.N170A.Y224A alters native residues in the loop region between β -sheet 2 and α -helix 2 as well as an α -helix 3 residue (Figures R31 and R32). F174A.V179A.I183A constitutes replacements exclusively in α -helix 2, V188A.T191A.T192A targets amino acids at the C-terminal cap of α -helix 3 and the following loop region; K203A.E206A.R207A, as well as E210A.Q211A.Y225A and K219A.E220A.Q222A, bear mutations at various positions along α -helix 3 (Figures R31 and R32). When assayed for their ability to propagate prions, these mutations appeared to be markedly limited in their propagative capacity (Figure R36). While KD cells reconstituted with the wild-type protein reported spot numbers in the thousands, KD cells reconstituted with these mutants yielded spot numbers of two hundred or fewer (Figure R36).

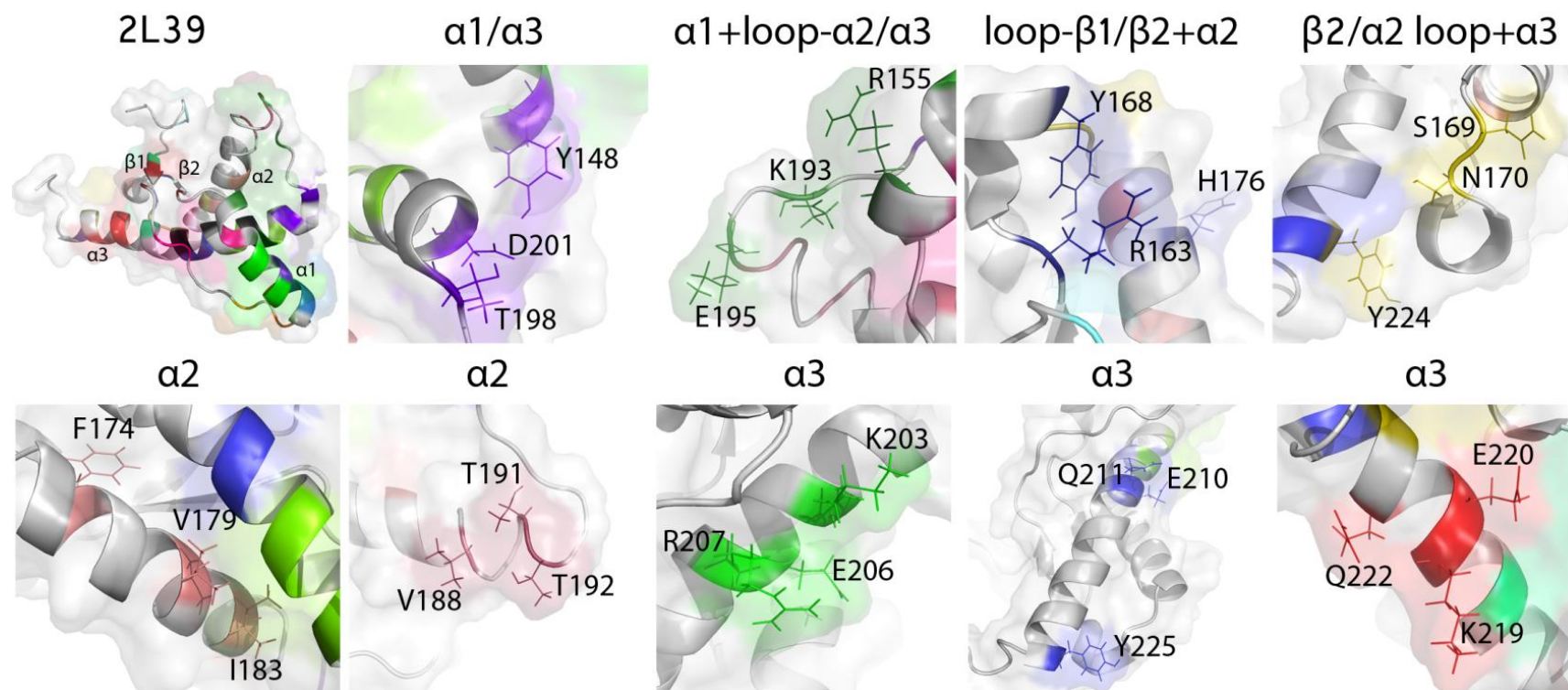


FIGURE R35: TARGETED SITES FOR MUTATIONS IN REGION 148-230 OF MOPrP

Mutations targeted to the surface of the globular domain on moPrP are depicted on PDB entry 2L39, shown in full in the top left corner, showing two β -strands and three α -helices with a surface outline. Areas of the protein that were not targeted for mutagenesis are shown in light grey; where residues have been mutated, areas are shown in any colour other than grey. Following this entry are various positions on the protein where targeted mutations to alanine were made. Secondary structures bearing moPrP mutations are indicated above each image. Mutation sites are shown with coloured backbone carbons and side chains (line display) on an otherwise grey backbone. All images were created in PyMol.

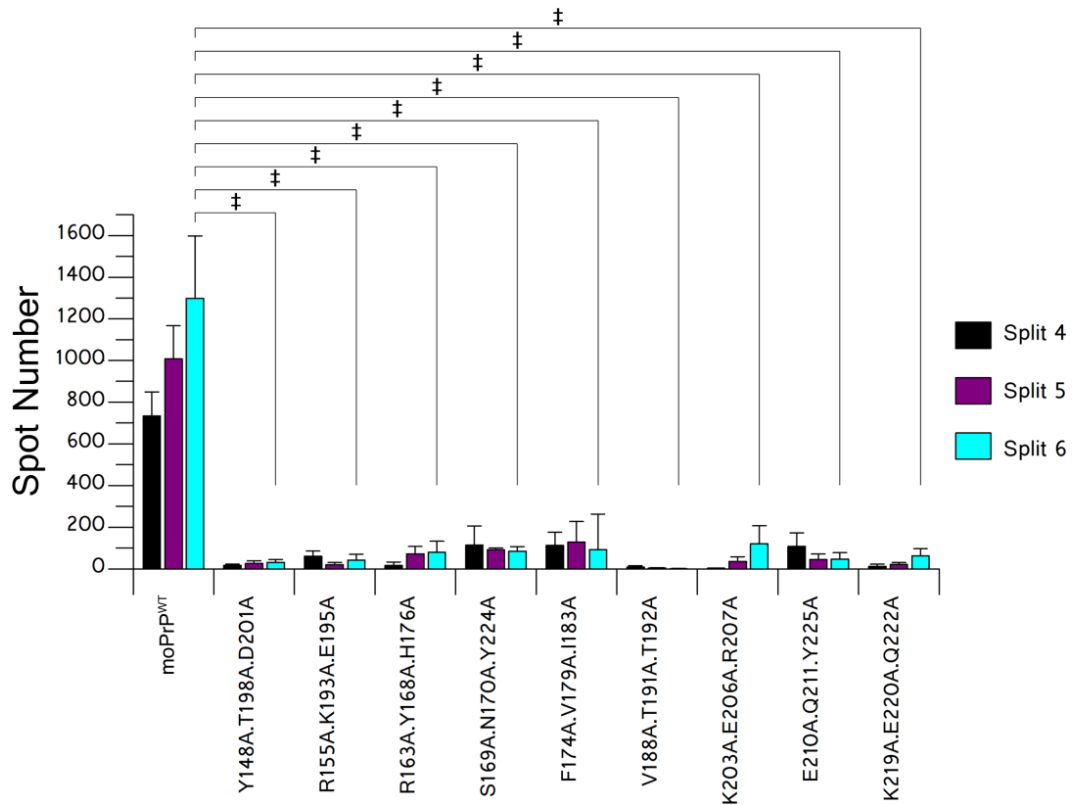


FIGURE R36: SCA OF KDMoPrP^{ALA} CELLS; MOPrP MUTATIONS IN REGION 148-230

KD cells reconstituted with either moPrP^{WT} or alanine mutant variants of the protein within region 148-230 of moPrP were challenged with RML prions at a 1×10^{-5} dilution of infectious homogenate and their ability to propagate these prions assayed via SCA at three consecutive time points. All KD cells expressing moPrP replacements within this region exhibited a significant reduction in their ability to propagate RML when compared to those expressing moPrP^{WT}. Significance is indicated by ‡ for $P \leq 0.0001$. Significance only shown for split 6 for clarity; calculated in a one-way ANOVA with a Bonferroni correction for multiple comparisons.

Mutations in region 148-225 of moPrP resulted in a reduced ability of cells expressing these constructs to propagate RML. KD cells expressing these mutations demonstrated a ten-fold reduction in their ability to propagate prions compared to moPrP^{WT}.

This is similar to the limitation on propagation exerted by alanine mutations within region 121-155 of moPrP at solvent-exposed regions (Figures R33 and R36). Neither set of surface mutations produced/yielded over 200 hundred spots at the final split, compared to the one-thousand spots obtained for KD cells expressing non-mutated moPrP^{WT} (Figures R33 and R36). Such values for propagation of RML prions are comparable to those reported for CC2 region 90-111 of the mouse prion protein (Section 3.4).

Spot numbers higher than background (KD cells; 50-spot threshold) were observed for some of the moPrP surface region mutations between splits 4-6. This includes values nearing on average one hundred spots for M128A.Y162A.Q216A, L129A.S131A.Q159A, D142A.W144A.E145A (Figure R33), R163A.Y168A.H176A, S169A.N170A.Y224A, F174A.V179A.I183A, K203A.E206A.R207A and E210A.Q211A.Y225A (Figure R36). This level of propagation in KDmoPrP^{Ala} cells with structured region mutations was ten times less than that of KD cells expressing the wild-type protein (Figures R33 and R36) and not due to a lack of cell-surface protein expression (Figure R34 and R37).

It is apparent from SCA analysis of moPrP surface region mutants, that propagation capacity is severely compromised by every change made within this 123-230 globular domain of the protein. However, some triple mutations showed a complete abrogation of propagation whereas others appeared to permit a low level of propagation (Figures R33 and R36).

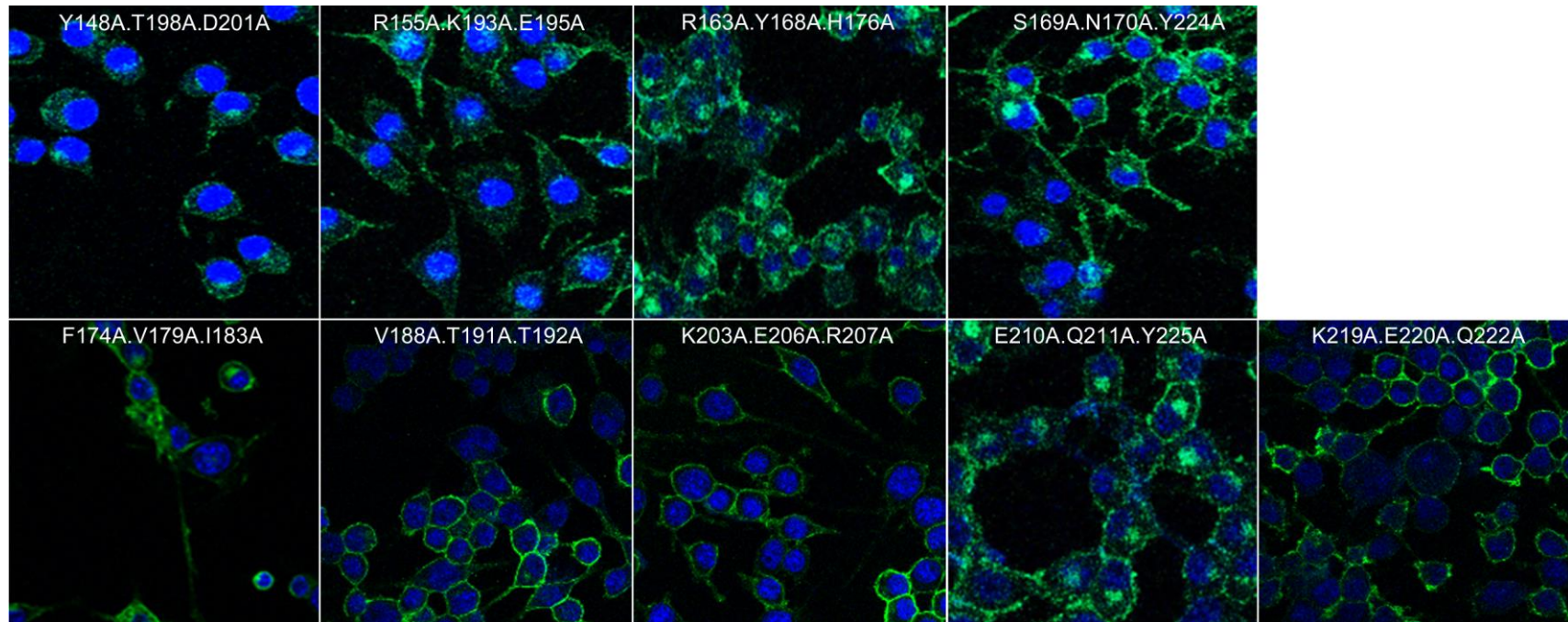


FIGURE R37: IMMUNOFLUORESCENT ANALYSIS OF KDMoPrP^{Ala} CELLS WITH MUTATIONS IN STRUCTURED REGION 148-230

Immunofluorescence images of KD cells reconstituted with structured region (148-230) mutants of moPrP. The cells were probed for moPrP expression using ICSM18 antibody. Expression detected in KD cells reconstituted with moPrP bearing mutations R163A.Y168A.H176A, S169A.N170A.Y224A and E210A.Q211A.Y225A was stronger than that for other mutations. Importantly, despite the difference in moPrP accumulation in these cells, all reconstituted KD cells expressed moPrP^{Ala}. DAPI nuclear stain; green: moPrP. Magnification at x40.

3.5.4 Mutations made within the core hydrophobic region of moPrP to destabilise the protein lower its capacity for propagating prions

Three mutants C178A.C213A, M204A and M204Q.M205Q.V209Q.M212Q were made at non-surface regions of the protein. They targeted hidden residues in the hydrophobic core of the protein and were designed to destabilise the protein. The third α -helix of the prion protein has a hydrophobic face formed predominantly of methionine and valine residues, with the former known to contribute to protein folding and stability^{156, 277-279}. In addition to substituting methionines, the effect of protein stability on prion propagation was also tested by replacement of cysteine residues that form the disulfide bridge between α -helices 2 and 3. RML prions were used to challenge cells expressing these mutations in the KDmoPrP^{Ala} cell system (Section 3.2). All destabilising mutations described here are located on α -helix 3 of moPrP, and in the case of disrupting the disulfide bond (C178.C213), also on α -helix 2 (Figure R38).

All mutations made to destabilise the protein or promote unfolding (M204A, C187A.C213A and M204Q.M205Q.V209Q.M212Q), showed a considerably reduced capacity for RML propagation (Figure R39). KD cells reconstituted with wild-type protein gave spot numbers of over one-thousand by split 6, in sharp contrast to spot numbers averaging one hundred at most, for destabilising mutations at the same split (Figure R39).

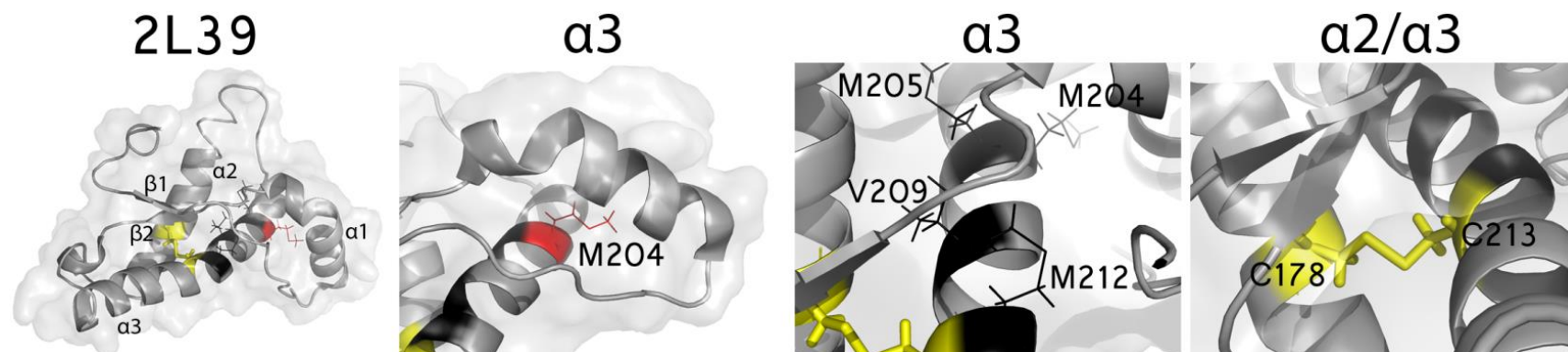


FIGURE R38: TARGETED SITES FOR MUTATIONS IN CORE HYDROPHOBIC RESIDUES OF moPrP

Mutations targeting core hydrophobic residues in moPrP are depicted on PDB entry 2L39, showing two β -strands and three α -helices with a surface outline (first image). The protein is coloured grey; positions at which destabilising mutations were created are coloured in red, black and yellow. Destabilising mutations are shown in the images zoomed at α -helix 3 in 2L39. Position 204 where the native methionine was mutated to alanine is shown in red with its side chain projecting from the protein backbone. Another mutation within α -helix 3 was created where core hydrophobic residues shown in black, were replaced with the amino acid glutamine; this quadruple mutation was predicted to cause the protein to unfold. The last image shows the disulfide bond between α -helices 2 and 3, which was destroyed by mutation C178A.C213A. Secondary structures bearing moPrP mutations are indicated above each image. Mutation sites are shown with coloured backbone carbons and side chains (line display) on an otherwise grey backbone. All images were created in PyMol.

It is interesting to note that moPrP-destabilising mutation M204A and unfolding mutation M204Q.M205Q.V209Q.M212Q exhibited spot numbers approaching three hundred at split 4 (for M204Q.M205Q.V209Q.M212Q this was true also for split 5), but then dropped to less than two hundred spots for the last split (Figure R39). If split 4 was to be considered solely, then propagation in these two moPrP mutants is not remarkably different from their wild-type counterpart. At split 6 however, due to high spot numbers achieved from true propagation in the moPrP^{WT}-expressing cells, the difference between spot numbers is significantly less in the mutant-expressing lines (Figure R39). Since results at split 6 are used to determine the propagation efficiency, destabilising and unfolding mutations in moPrP severely limit the propagation of prions (Figure R12). Lowering of spot numbers between passages, especially when spot count falls below two hundred for any split, is not indicative of full propagation. It could therefore be argued that the spots observed here may be due to protein aggregation as opposed to propagation. This is in fact, what is observed for KD cells reconstituted with moPrP bearing the mutation M204A at splits 5 and 6, but not for M204Q.M205Q.V209Q.M212Q at any split (Figure R39). This may be a case of the cells being susceptible to RML infection and initial propagation, but failed maintenance of prion propagation as described by Vorberg *et al*²⁸⁰. When comparing the RML-infected versus non-infected samples, spot numbers for KD cells reconstituted with moPrP^{WT} and M204Q.M205Q.V209Q.M212Q were significantly different at all three passages at which cells were sampled for ELISPOT processing (Figure 40).

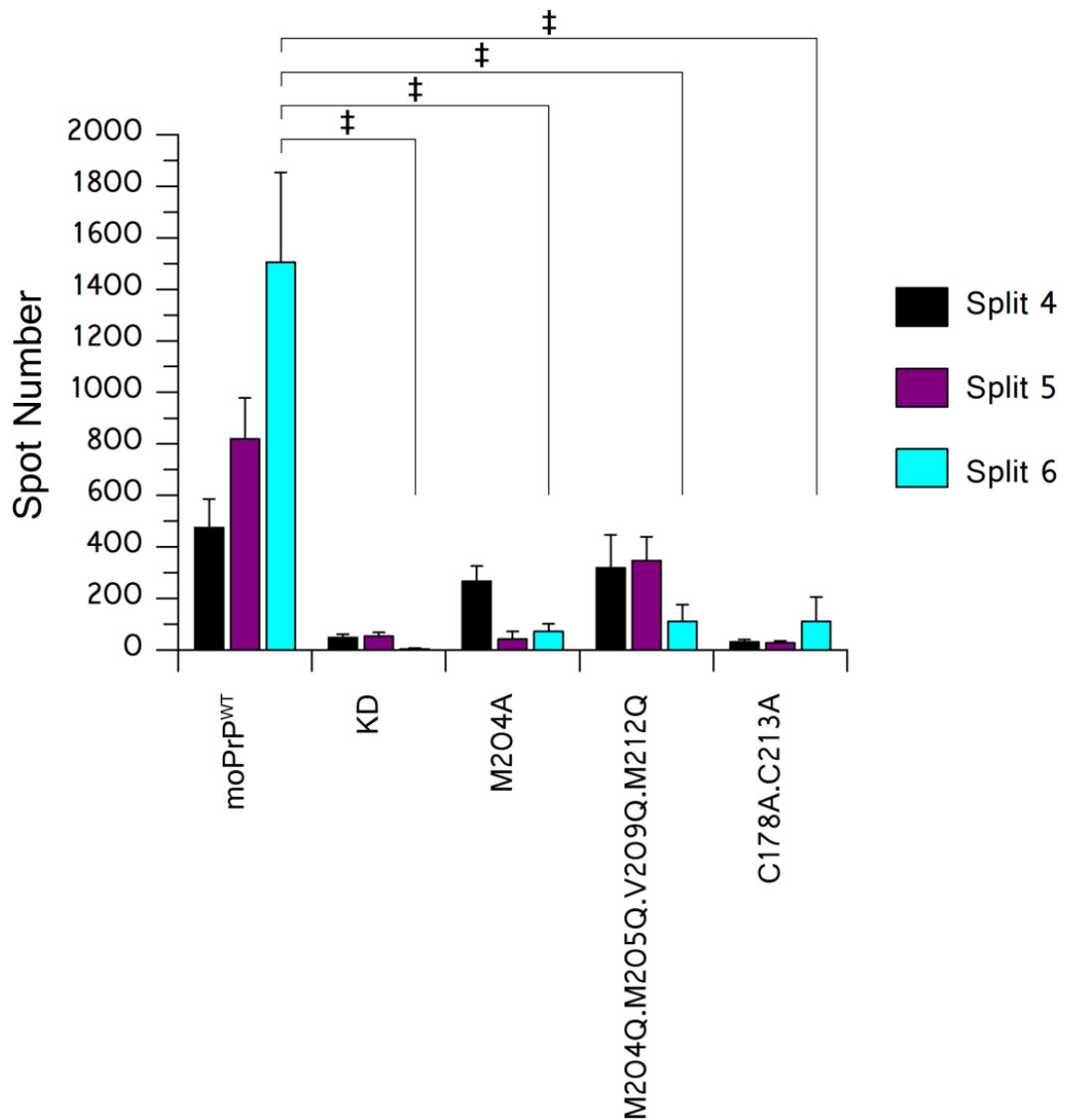


FIGURE R39: SCA OF KDMoPrP CELLS; MUTATIONS IN CORE HYDROPHOBIC REGIONS OF MoPrP

KD cells reconstituted with either moPrP^{WT}, alanine-substituted moPrP (M204A and C187A.C213A) or glutamine-substituted moPrP (M204Q.M205Q.V209Q.M212Q) were challenged with RML prions at a 1×10^{-5} dilution of infectious homogenate. Their ability to propagate these prions was assayed via SCA for at least three consecutive time points: split 4, 5 and 6. All replacements made exhibited a significant reduction in their ability to propagate RML when compared to moPrP^{WT}. Significance is indicated by **** for $P \leq 0.0001$. Significance only shown for split 6 for clarity; calculated in a one-way ANOVA with a Bonferroni correction for multiple comparisons.

All non-infected control plates were run in the same SCA as the RML-infected plates as is standard SCA procedure and processed for ELISPOT in the same way. None of the non-infected samples gave spot numbers above one hundred for any split (Figure R40). The number of spots obtained for non-infected samples in SCA is usually in the order of zero to fifty. This is the background 'noise' within the system and also represents the range of spot numbers recorded for KD cells, both in RML-infected and non-infected conditions (Figure R34).

The highest background value recorded from the samples presented here was 55 (averaged across six replicate wells). This is slightly higher than background values for non-infected KD cells reconstituted with the wild-type protein, but negligible (Figure R40). Nevertheless, spot numbers below two hundred represent severe inhibition of propagation and under four hundred, are reduced in their capacity to propagate prions based on the SCA guide used in this study (Figure R12). This indicated that cells expressing mutation M204A, a destabilising mutation, or the unfolding mutation M204Q.M205Q.V209Q.M212Q, are severely inhibited in their ability to propagate prions, relative to moPrP^{WT} (Figure R39). Many studies have indicated that increasing protein stability in the cellular prion protein makes it more resistant to prion infection and vice versa. Thus, it could be expected that cells expressing the destabilising and unfolding mutations introduced here (M204A M204Q.M205Q.V209Q.M212Q) would have propagation profiles higher than, or equalling that of moPrP^{WT}; this is not the case (Figure R40). SCA data for these mutations was further analysed to determine whether the nature of these mutations made the cells expressing

them more likely to form ProteinaseK-resistant material in the absence of RML-homogenate (Figure R40). Since the M204A-expressing cells showed spot numbers above two hundred at split 4, it suggests that this mutation allows for reduced propagation, but cannot maintain it for more than a few splits. There is also evidence of this for cells expressing the quadruple Gln mutation (Figure R39). Whether or not infectivity is retained in these cells following infection remains to be investigated.

For mutation C178A.C213A, spot numbers increased at the last split, from thirty to one hundred (Figure R39). Despite the trend of increasing spot number with subsequent passages, the spot count was below the eight hundred threshold to be considered efficient propagation, below the four hundred mark that represents reduced or inefficient propagation and fell within the range of fifty to two hundred, where propagation was taken to be severely inhibited (Figure R12).

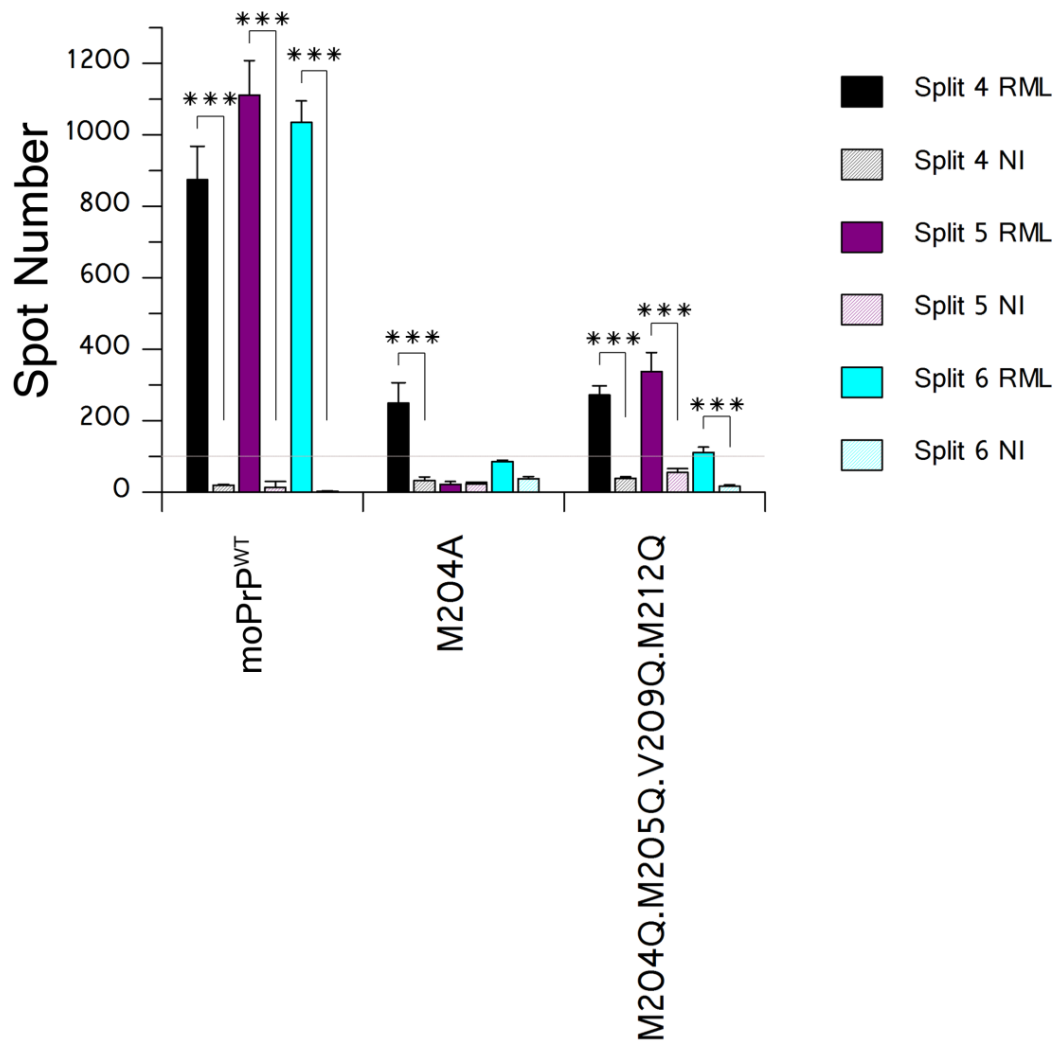


FIGURE R40: SCA ANALYSIS OF RML-INFECTED VERSUS NON-INFECTED KDMoPrP

CELLS WITH MUTATIONS MADE IN THE CORE HYDROPHOBIC RESIDUES OF THE PROTEIN

Comparison of SCA data collected from RML-infected samples versus non-infected samples. Shown above are representative data from three consecutive passages of cells that were either infected with RML or not infected with any prions (NI: non-infected). For KD cells reconstituted with moPrP^{WT}, or M204Q.M205Q.V209Q.M212Q, RML-infected samples gave significantly different values compared to their non-infected counterparts. For KD cells reconstituted with M204A however, the difference between infected and non-infected samples was only significant at split 4. A grey line at 100 spots demonstrates that none of the non-infected samples had values above this; still, the mutations reported higher background (non-infected samples) values than those collected for the wild-type protein. Significance is indicated by *** for $P \leq 0.001$. Significance is only shown for split 6 for clarity; calculated in a one-way ANOVA with a Bonferroni correction for multiple comparisons.

Overall, SCA analysis showed that introducing destabilising changes into the folded structure of the prion protein considerably lowered the ability of cells expressing these mutant forms of moPrP to propagate prions (Figure R39). Still, cells expressing mutation M204Q.M205Q.V209Q.M212Q were able to propagate prions for two splits – more than M204A. This indicates that propagation occurs in cells expressing the modified proteins, but cannot be maintained for multiple passages. Thus, alanine replacements made within core hydrophobic residues of the protein exert propagation-limiting effects on cells expressing them such that: (i) cells can propagate RML prions initially, but at a reduced rate compared to moPrP^{WT}; (ii) propagation reduced from split 4 to split 6; (iii) propagation cannot be maintained for six passages post-infection.

KD cells reconstituted with moPrP mutations M204A, C187A.C213A and M204Q.M205Q.V209Q.M212Q were seeded on coverslips and probed for prion protein expression using ICSM18. In all instances, protein expression was detected at the cell surface (Figures R34, R37 and R41). Thus, limitations on propagation for these mutants were not due to lack of expression. A complete analysis of mutations generated in the structured region of the prion protein could not be tested at an additional 1×10^{-4} dilution of homogenate due to time constraints. For comparison, some of the SCA data available at both doses of RML prions is shown (Figure R42). This corroborates findings within this chapter that show all changes made in this region severely reduced propagation.

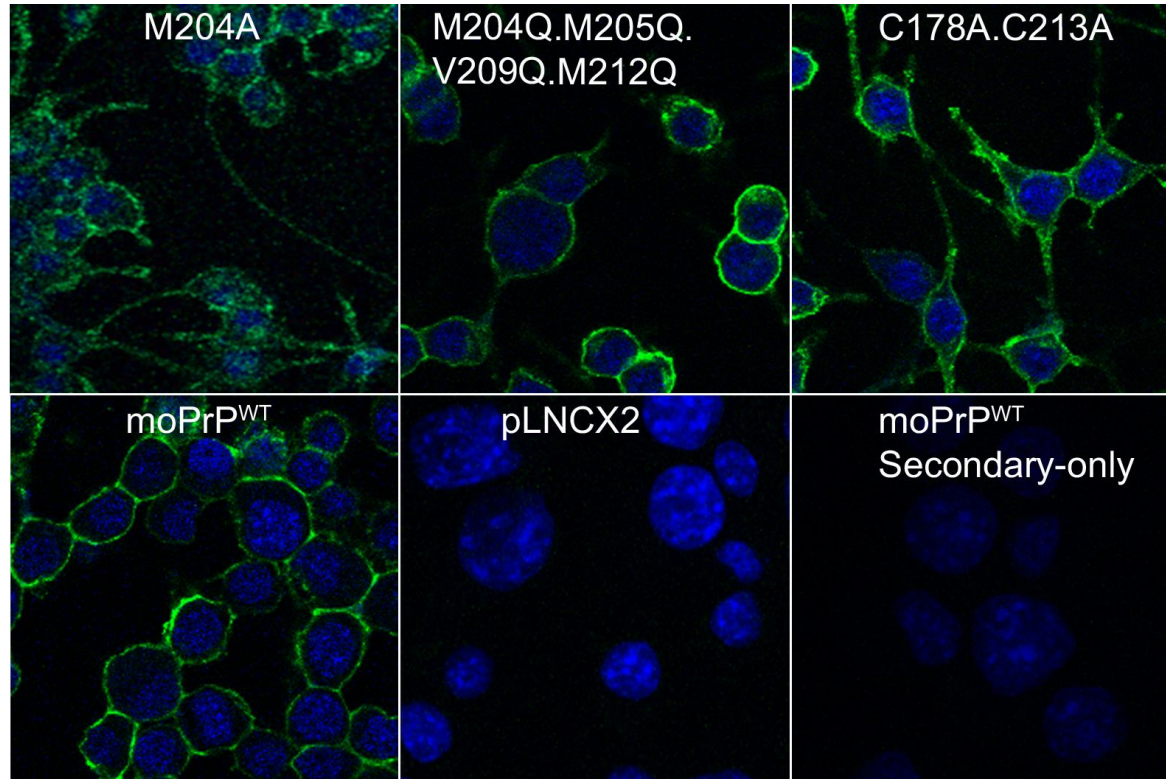


FIGURE R41: IMMUNOFLUORESCENCE IMAGES OF KDMoPrP CELLS WITH MUTATIONS IN CORE HYDROPHOBIC REGIONS OF THE PROTEIN

Immunofluorescence images of KD cells reconstituted with mutants of moPrP designed to destabilise the protein. Cells were probed for moPrP expression using ICSM18 antibody. All reconstituted KD cells expressed moPrP. The last three images represent control cell lines where moPrP^{WT} is a positive control showing expression of the wild-type protein, KdpLNCX2-only represents KD cells transduced with empty vector (negative control) and moPrP^{WT} Secondary only shows the background signal (noise) when the primary antibody (ICSM18) is omitted. DAPI nuclear stain; green: moPrP. Magnification at x40.

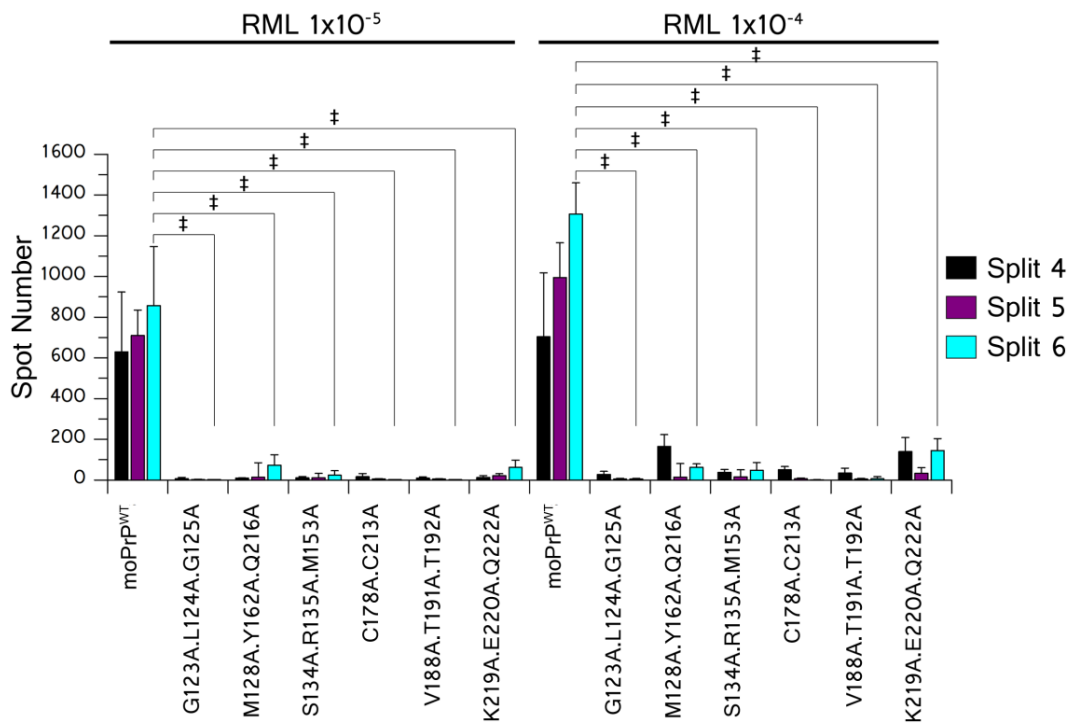


FIGURE R42: SCA ANALYSIS OF KDMoPrP^{ALA} CELLS WITH MUTATIONS IN THE STRUCTURED REGION TESTING TWO DOSES OF RML INOCULA

Comparison of SCA data collected from RML-infected samples at two doses of inocula versus non-infected samples. Shown above are representative data from three consecutive passages of cells. This demonstrates that samples tested at a ten-fold higher dose of infectious inocula displayed a very modest increase in response to RML as spot numbers remained below two hundred. Significance is indicated by ‡ for $P \leq 0.001$. Significance is only shown for split 6 for clarity; calculated in a one-way ANOVA with a Bonferroni correction for multiple comparisons.

Site directed mutagenesis	Limitation on propagation		moPrP domain
	KD cells	PK1 cells	
G123A.L124A.G125A			SR
M128A.Y162A.Q216A			
L129A.S131A.Q159A			
S134A.R135A.M153A			
H139A.G141A.D146A			
D142A.W144A.E145A			
R147A.R150A.E151A			
Y148A.T198A.D201A			
R155A.K193A.E195A			
R163A.Y168A.H176A			
S169A.N170A.Y224A			
F174A.V179A.I183A			
C178A.C213A			
V188A.T191A.T192A			
K203A.E206A.R207A			
M204A			
M204Q.M205Q.V209Q.M212Q			
E210A.Q211.Y225A			
K219A.E220A.Q222A			

None
Strong
Very
N/A

TABLE R6: LIST OF MUTATIONS MADE WITHIN THE STRUCTURED REGION OF MOPRP

List of mutations made within the structured region (SR) of the mouse prion protein. Native residues at these positions were changed to alanine or glutamine (Q) and the modified protein expressed in KD cells to test the effect of the mutations on prion propagation. All cells expressing moPrP mutations within the structured region exhibited a very strong reduction in their ability to propagate RML prions in the scrapie cell assay. (N/A: not applicable).

3.5.5 Integrity of the structured region 123-230 of the prion protein is necessary for efficient prion propagation

A series of moPrP mutations were generated in the structured 123-230 region of the mouse prion protein and expressed in cells susceptible to RML prions, to test the effect of these mutations on prion propagation. Mutations were designed based on two criteria: (i) targeting solvent-exposed regions of the protein to determine whether a particular face of the folded protein was integral to propagation and if so, which one; (ii) whether destabilising the protein by altering core hydrophobic residues facilitates or limits propagation.

It was found that mutations between the first β -sheet strand and the first α -helix of moPrP limited the ability of cells expressing these mutations to propagate RML. Propagation as measured by spot numbers in SCA showed at least a ten-fold reduction for moPrP bearing alanine mutations within this region compared to the wild-type protein (Figure R33). When similar analyses were performed for alanine mutations between the first and third α -helices of moPrP, it was found that most triple alanine replacements at solvent exposed sites within this region of the protein lowered the ability of cells expressing these constructs to propagate prions at least ten-fold with respect to moPrP^{WT} (Figure R36). Essentially, propagation was severely reduced in both instances, and by the same amount for both sets of mutations in the structured region of the protein.

Of note, mutations G123A.L124A.G125A, S134A.R135A.M153A and H139A.G141A.D146A, had the strongest inhibitory effect on propagation

within regions 121-153 of the protein (Figure R33). These represent changes made just N-terminal to β 1 and the loop region between β 1 and α 1 (Figure R32). From region 148 – 225 of moPrP, Y148A.T198A.D201A, R155A.K193A.E195A and V188A.T191A.T192A showed the strongest inhibition of propagation (Figure R36). These represent changes made to surface residues at α 1 and the loop region between α 2 and α 3 (Figure R35).

When alanine mutations were made within core hydrophobic regions of the protein, prion propagation was severely limited in cells expressing the modified protein (Figure R39). Interestingly, spot numbers of two hundred were readily achieved for both M204A and M204Q.M205Q.V209A.M212Q at split 4, but not for C178A.C213A (Figure R39). Additionally, spot numbers for M204A and M204Q.M205Q.V209A.M212Q fell at split 6, whereas for C178A.C213A, they increased at the last split. For single replacement M204A but not for M204Q.M205Q.V209A.M212Q, spot numbers observed for splits 5 and 6 were comparable to background levels where the cells expressing this mutation in moPrP had not been infected with RML prions (Figure R40). Thus, both C178A.C213A and the quadruple mutation M204Q.M205Q.V209A.M212Q, may be able to propagate prions at a low level but in the case of M204, the spots observed were not significantly different to background levels and thus, not indicative of true propagation (Figure R40). For M204A and M204Q.M205Q.V209A.M212Q, the higher spot numbers observed may be indicative of higher misfolding propensity in the protein as reported by Hirschberger *et al.*²⁷⁷ Both methods of altering prion protein stability used here – altering core hydrophobic residues and

disrupting the disulfide bond – are linked to conformational rearrangement of α -helix 1^{155, 277}. Data from the single mutation M204A and the quadruple change to Gln at M204.M205.V209.M212 suggest that although both changes reduce the ability of cells expressing these mutations to propagate RML prions relative to moPrP^{WT}, the larger change in the unfolding mutation is more amenable to propagation than a smaller destabilising mutation (Figure R39).

The reduction in propagation observed for all cells expressing moPrP^{Ala} here was not due to lack of prion protein expression, but due to the mutation introduced in the protein (Figures R33, R36, and R39). There have been a number of studies probing the replicative interface for PrP^C-PrP^{Sc} binding and conversion, each giving evidence for involvement of different regions of PrP: from α -helix 1^{88, 179, 205} and neighbouring residues²⁰⁵, to the loop region between α -helices 2 and 3¹⁵⁷, to specific methionine^{156, 159, 279} or tyrosine residues; all of which were determined by vastly different experimental approaches.

3.5.6 Effects of alanine mutations in α -helix 1 on prion propagation

Abalos *et al.* identified region 136-140 as residues involved in the specific binding interaction between PrP^C and PrP^{Sc}¹¹⁸; this followed earlier work by Moroncini *et al.*, who used motif-grafted antibodies to characterise two PrP^C-PrP^{Sc} interaction sites: one at N-terminal residues 89-112 and the other at 136-158, within the structured domain of the protein¹⁹⁹. The latter segment spans α -helix 1 and a few residues either side of the helix. Norstrom *et al.* used chronically Scrapie-infected cells to show that only charged residues within α -helix 1 region had a controlling effect on prion propagation⁸⁸. Other studies suggest that specific aspartate residues at positions 143 and 146 within this region govern this interaction¹⁷⁹, with regions N-terminal to α -helix 1 deemed unimportant for PrP^C-PrP^{Sc} interaction²⁰⁵. Our data supports the general argument that mutations made within and surrounding α -helix 1 have a distinct negative effect on prion propagation (Figures R33). Data presented here also suggests that propagation is mediated by residues other than charged moieties or α -helix 1 residues, as α 1 mutation D142A.W144A.E145A showed higher spot numbers for all three splits compared to loop region mutation G123A.L124A.G125A which is N-terminal to both α -helix 1 and β -sheet1, and not highly charged (Figure R33). It is important to note however, that in either instance, spot numbers were below the threshold considered to be efficient propagation (Figure R12). Thus although all mutations in this region severely inhibited propagation, not all can be labelled as 'abrogating' propagation as some were above fifty at split 6, the cut-off for background spots obtained with KD cells (Figure R12).

3.5.7 Loop regions determine prion propagation propensity

Structural comparisons of the prion protein in its cellular and disease-associated state showed that residues 132-167, which span β 1- α 1- β 2, relocate away from the α 2- α 3 core²⁰⁶ during prion protein conversion^{165, 281}. This may explain why changes to alanine within the β 1- α 1- β 2 region of the protein had a significant effect on prion propagation (Figures R33 and R36). Additionally, the β 2- α 2 loop has been shown to influence the outcome of prion propagation in terms of susceptibility to prion infection – transgenic mice expressing a triple amino acid substitution within the β 2- α 2 loop region Y168G.S170N.N173T were resistant to two strains of mouse prions¹⁶⁰.

A well-known fact in the prion field, with regards to disease transmission is that some species such as bank voles, elk and deer are considerably more susceptible to prions than others, such as rabbit⁷⁰. The higher tolerance in rabbit PrP is believed to be due to a more 'rigid-loop' structure in the rabbit sequence, with contributions from hydrogen-bonding interactions within the helix cap motif at this site¹⁵⁸. Mutations made in this study which encompass region β 2- α 2 include S169A.N170A.Y224A (underlined mutations S169A and N170A fall within β 2- α 2, but Y224A is in α -helix 3), which showed considerably lower propagation but did not completely abrogate prion propagation as spot numbers were above fifty (background threshold; Figure R36). However, other loop region mutations made in the structured region (G123A.L124A.G125A, S134A.R135A.M153A and H139A.G141A.D146A, R155A.K193A.E195A and V188A.T191A.T192A) exhibited some of the strongest inhibition, abrogating prion propagation and

reporting spot numbers under fifty when analysed via SCA (Figures R33 and R36). Helices $\alpha 2$ and $\alpha 3$ represent regions of the prion protein where a large number of pathogenic mutations are clustered⁵¹, and have been proposed to be major sites for initiating prion propagation¹⁵⁷.

Salamat *et al.*, investigated the effects of altering the sequence with the $\alpha 2$ - $\alpha 3$ loop region; peptide insertions in the loop region between α -helices 2 and 3 were found to have no effect on limiting prion propagation, leading the authors to conclude integrity of the $\alpha 2$ - $\alpha 3$ segment is not required for propagation²⁸². Findings from alanine mutagenesis presented here are contrary to this statement as minimal changes in areas within and surrounding α -helices 2 and 3, severely limited propagation (Figure R36). In particular, triple mutation at the C-terminal end of α -helix 2, V188A.T191A.T192A, displayed abrogation of propagation, akin to negative control KD cells (Figure R36). Our data therefore supports the finding that loop region mutations significantly affect the outcome of prion propagation. However, mutations within the $\alpha 2$ - $\alpha 3$ loop were found to have a stronger effect than those within the $\beta 2$ - $\alpha 2$ loop (Figure R33 and R36).

3.5.8 Protein stability as a determinant of prion propagation

The disease-associated PrP conformer PrP^{Sc} is characterised by its high β -sheet content and lower solubility with a high resistance to chemical denaturation^{44, 283, 284}. Smirnovas *et al.* showed that the prion protein undergoes major refolding during the conversion from soluble native PrP^C to insoluble PrP^{Sc79}. The refolding is hypothesised to originate from amino acid

region 80-90 (depending on prion strain) to the C-terminus⁷⁹. Higher stability in the prion protein is believed to be correlated with a lower misfolding propensity and lower susceptibility to prion infection²⁴². This follows the reasoning that if the protein exists in a more stable state, it is less likely to form non-native bonds that would encourage misfolding. Here, we generated mutations aimed at lowering native protein stability, either through modification of core hydrophobic residues or removal of the disulfide bond between α -helices 2 and 3. Following the reasoning for higher stability correlating with reduced misfolding propensity, it could be predicted that lowering stability would have the opposite effect and that higher propagation could be expected for PrP bearing destabilising mutations.

The SCA results obtained for prion propagation of moPrP bearing destabilising mutations showed that substituting methionine for alanine at position M204, or altering the charge at residues M204M205V209M212 by glutamine substitutions resulted in considerably reduced protein propagation (Figure R39). Interestingly for these mutations, there was a higher level of misfolding that led to detection of ProteinaseK-resistant material in the absence of prion infection (Figure R40). Upon RML prion infection however, low levels of propagation were observed for cell lines expressing both M204A and M204A.M205A.V209A.M212A, but significantly less than cells expressing the wild-type protein (Figure R39). Younan and colleagues undertook protein unfolding experiments and identified surface residues M205, V209, and M212 as key sites that were perturbed in the protein upon inducing oxidative stress²⁷⁹. The authors suggest a general

misfolding pathway for the protein, where methionine oxidation, which could be brought about by cellular oxidative stress, represents an early event in prion disease²⁷⁹. This finding is supported by Elmallah *et al.*, using huPrP 121-230 to show formation of monomeric molten-globule entities which are reportedly similar in their properties to misfolding intermediates observed for PrP⁵⁷.

If methionine oxidation facilitates misfolding to a PrP conformer closer to PrP^{Sc}, this may support the SCA findings reported here that cells expressing moPrP bearing the substitutions M204A.M205A.V209A.M212A are inefficient at propagating prions. It is possible that substitution of the exposed methionine residues to alanine protects the protein from the effects of oxidative stress on methionine, which could contribute to PrP^{Sc} formation and accumulation, defined as prion propagation.

In an alternative approach to lower the stability of moPrP, KD cells were reconstituted with the moPrP construct bearing mutations C178A.C213A which destroys the disulfide bridge between $\alpha 2$ and $\alpha 3$; this resulted in very limited propagation (Figure R39). Cells expressing this mutation did not show accumulation of ProteinaseK-resistant material in the absence of RML homogenate as analysed by SCA, unlike M204A and M204A.M205A.V209A.M212A-expressing cells (Figure R40). This suggests that although lowering protein stability makes it more likely to misfold, this does correlate with efficient prion propagation as the destabilising mutations exhibited reduced propagation relative to moPrP^{WT} (Figure R39).

3.5.9 The miniprion and its implication in PrP domains required for efficient prion propagation

A mouse prion protein construct with two large deletions, Δ 23-88 and Δ 141-176, assumes a protease-resistant conformation when expressed in cells that are chronically infected with Scrapie prions. This construct was termed 'miniprion' or PrP106 (consisting of 106 residues)²⁰⁴. Limitations of this construct, as addressed by the authors, lay in the incorporation of a His₍₆₎-tag which was predicted to aid the formation of protease-resistant fragments²⁰⁴. This is still considered to be the minimal segment of the prion protein capable of sustaining prion propagation^{76, 204}; indeed recent research on elucidating prion protein regions required for infection, conversion propagation and toxicity continue to employ deletion mutagenesis techniques²⁸⁵. We propose that modifications made to the cellular protein in this study are extremely slight, so as to reduce the amount of perturbations introduced. With this minimal approach, we were able to report significant differences in the response of these proteins to infectious prions (Figures R33, R36 and R39). Deletion Δ 23-88 in the miniprion corresponds to a large portion of the flexible N-terminus, retention of CC2, and domains C-terminal to it up to the second deletion Δ 141-176, which represents removal of α 1- β 2 and β 2- α 2 loop region, whilst retaining most of α 2 and α 3 in its entirety. It could be argued based on this model that residues that comprise α 1- β 2 are not required for prion propagation, nor are the loop regions between α 1 and β 2, and between β 2 and α 2. Although the data presented here does not show that propagation is nullified upon mutagenesis of α 1- β 2 residues, it shows that mutations in these regions

severely compromise the ability of cells expressing the modified protein to propagate prions (Figures R33 and R36).

3.5.10 Summary

Overall, nineteen constructs were generated in the structured region of the mouse prion protein, largely at solvent-exposed regions, to identify surfaces of the protein that are required for efficient propagation. Of these, sixteen constructs comprised triple alanine mutations at solvent-exposed regions, all of which hindered prion propagation. This was regardless of native position or biochemical property of the modified residue within the globular structured domain of the protein (Figures R33, R36 and R39). Three mutations made to alter the stability of the protein also displayed reduced propagation (Figure R40). Since all the prion protein mutations were expressed in KD cells, there are negligible contributions towards propagation of the endogenous protein (Section 3.2). Propagation is not completely blocked by the presence of these mutations, but its efficiency is severely impacted (Figure R12). Thus, the data collected from SCA analysis suggests that the integrity of the structured domain of PrP, 121-230 in moPrP, is essential for efficient prion propagation.

3.6 Dominant-negative inhibition of prion propagation by mutations in CC2

3.6.1 Experimental strategy

For the unstructured region 23-111 of the prion protein, bulk cultures of KDmoPrP^{Ala} cells were established and assayed on at least three independent SCAs to investigate their propagative potential following infection with RML prions (Section 3.3 and Section 3.4). It was found that within this segment of the protein, three distinct regions, when mutated to alanine, severely limited prion propagation. These were CC1, residue Q41 and CC2 of moPrP. Here, repeat infections of KD cells with virally packaged moPrP^{Ala} constructs were carried out; single-cell clones (SSCs) of the transduced cells were generated and assayed for their ability to propagate prions by SCA.

SSCs were established for each moPrP mutant construct of interest and re-tested for their propagative potential in independent SCAs in order to verify earlier findings from bulk cultures (Section 3.3 and 3.4). A ten-fold increase in the standard RML concentration from 1×10^{-5} dilution of homogenate to 1×10^{-4} was seen to improve the propagation profile for some, but not all cells expressing moPrP^{Ala} in SCA experiments (Section 3.3 and 3.4). For prion infection of SCCs therefore, the higher dose of inocula was selected to ensure a saturated system, such that any increase in the cells' ability to propagate RML would be easily detected. KDmoPrP^{Ala} cells tested included those with CC1 mutation K23A.K24A.K25A, point mutation Q41A and six of the eight mutations within CC2.

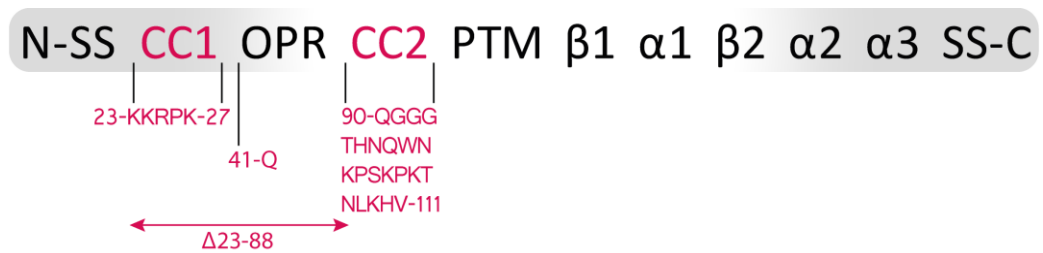


FIGURE R43: CC1, Q41 AND CC2 ARE IDENTIFIED AS MODULATORS OF PRION

PROPAGATION

Residues 23-111 of moPrP. Bar schematic of domains within moPrP. N-SS: N-terminal signal sequence; CC1: charge cluster 1; OPR: octapeptide repeat region; CC2: charge cluster 2; PTM: putative transmembrane region; α1: helix 1; β1: strand 1; α2: helix 2; α3: helix 3; SS-C: C-terminal signal sequence. Region 23-88 is defined by double-headed arrow; when deleted from the wild-type protein, results in abrogation of prion propagation. Sequence segments of moPrP shown in pink represent regions of the protein that when substituted for alanine, led to a significantly reduced ability in cells expressing these mutations to propagate RML prions.

3.6.2 Single-cells clones versus bulk cultures

To verify the stark differences observed for prion propagation when different regions of the N-terminus were mutated, new bulk cultures were established as biological replicates and from these, single-cell clones generated (Figure R44). KD cells stably transduced with pLNCX2 bearing the mutated moPrP ORF were plated at limiting dilutions and isolated cell clusters were picked from the plate and expanded separately to establish SCCs. The advantage of SCCs over bulk cultures is that all cells arise from one cell and should therefore be identical in characteristics such as growth and protein expression. Protein expression levels for the KD cells reconstituted with moPrP^{Ala} constructs and expanded as single-cell clones were found to be comparable to endogenous levels in PK1 cells by Western blotting and immunofluorescence (Figures R19 and R27; Figures R20 and R28).

Bulk Culture Single Cell Clone KDmoPrP^{Ala} (SCC)

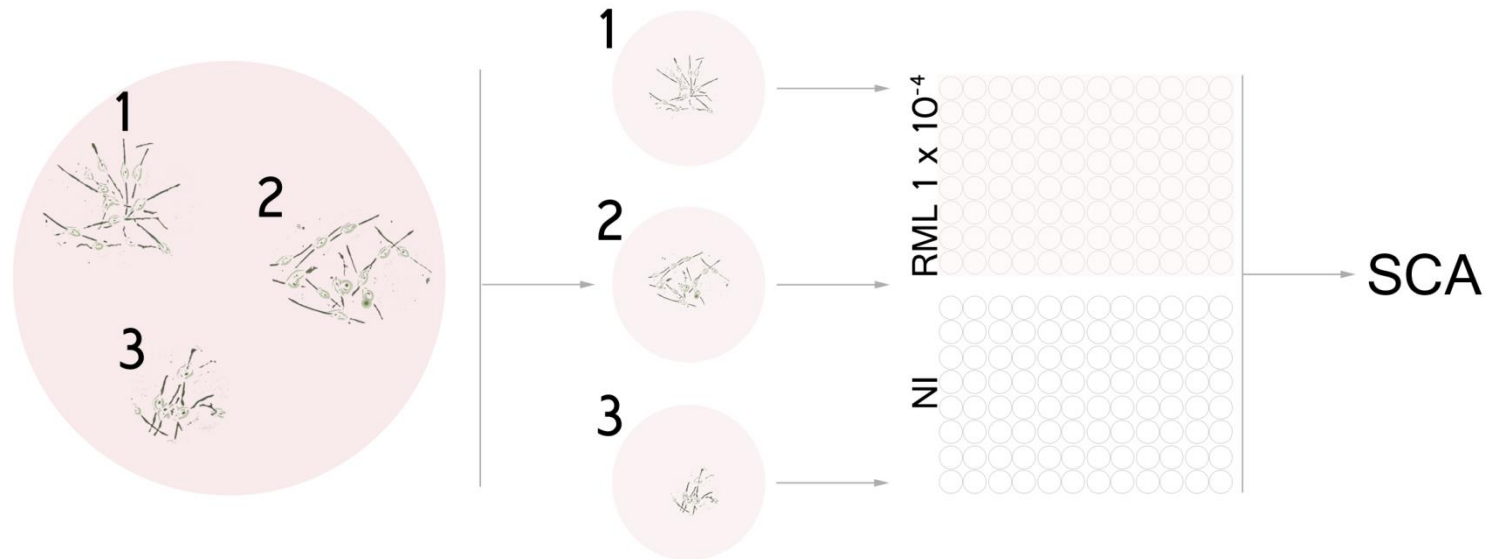


FIGURE R44: SINGLE CELL CLONING

KD cells were transduced with viral supernatant containing particles in which pLNCX2_moPrP was packaged and plated at limiting dilutions. Each moPrP ORF was sequence-verified for insertion of alanine mutations at targeted positions within CC1, at Q41 and within CC2, prior to cloning into pLNCX2 and transducing Phoenix cells to package the construct (Chapter I). This represents a bulk culture. Isolated cell clusters were isolated from the bulk culture plate and expanded separately to establish SCCs; eight SCCs were picked from each bulk culture; six of the eight SCCs that grew well under G418 selection were probed for moPrP expression; three of the six SCCs that had the greatest protein expression were taken forward to SCA to test their response to RML infection and propagation.

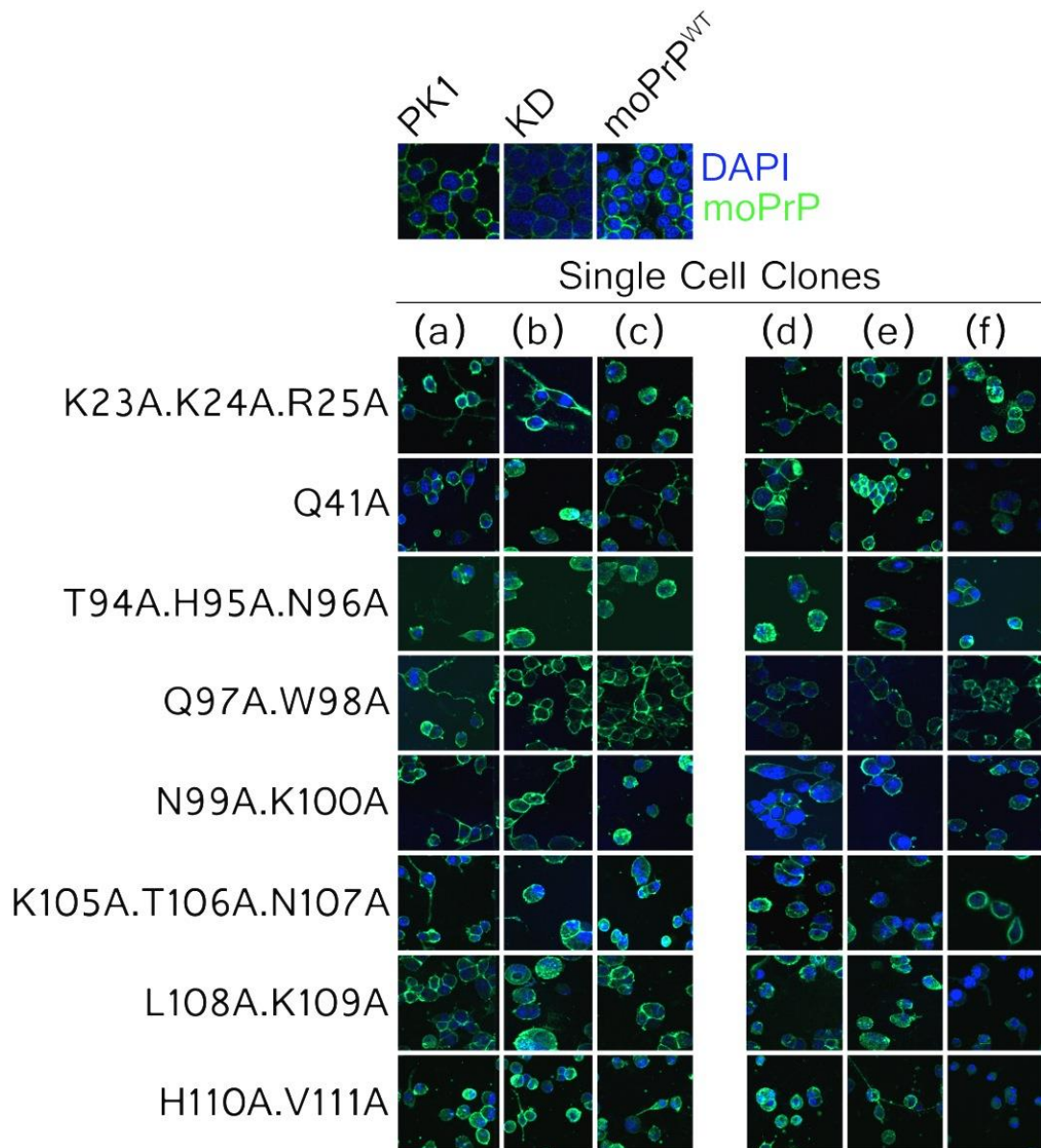


FIGURE R45: IMMUNOFLUORESCENCE IMAGES OF SINGLE CELL CLONES

Immunofluorescence was carried out on SCCs picked from bulk cultures plated at limiting dilutions. ICSM18 was used to detect moPrP in KD cells reconstituted with moPrP bearing various alanine mutations within the N-terminal region 23-111; DAPI was used as a nuclear stain. Each row represents SCCs of the indicated alanine replacement; letters (a-f) denote the individual SCC populations picked and expanded for each bulk culture. Clones (a-c) represent SCCs that displayed the highest protein expression and best growth profile; some clones (d-f) had higher expression levels but grew slowly compared to the parental PK1 or KDmoPrP^{WT} cells; these cells were excluded from the SCA on SCCs. Clones (a-c) were taken forward to SCA to test their ability to propagate RML prions. Top panel: PK1 cells show endogenous levels of moPrP. KD cells demonstrate the degree of silencing and moPrP^{WT} cells the level of moPrP expression achieved after reconstituting KD cells. Magnification at x40.

3.6.3 Clonal cell populations for alanine replacements in CC1, Q41 and CC2 of the mouse prion protein

Bulk cultures and SCCs of KD cells reconstituted with moPrP mutations K23A.K24A.R25A, Q41A, T94A.H95A.N96A, Q97A.W98A, N99A.K100A, K105A.T106.N107A, L108A.K109A and H110A.V111A were infected with RML at the highest dose of inocula for PK1 cells: 1×10^{-4} and analysed for their ability to propagate RML prions (Figure R46). Newly established bulk cultures displayed similar propagation profiles to those tested previously (Section 3.3 and 3.4), supporting the finding that CC1 mutation K23A.K24A.R25A in PrP lowers the ability of cells to propagate prions. Propagation was further limited when a mutation was made at position Q41. The most severe limitations on propagation however, were observed for mutations within the CC2 domain of the protein (Figure R46).

Interestingly, single-cell clones of K23A.K24A.R25A and Q41A that displayed strong protein expression (clone b; Figure R45) compared to their sister SCCs harbouring the same mutation, displayed no inhibition of RML propagation in SCA when infected with the homogenate at a dilution of 1×10^{-4} , reporting spot numbers comparable to cells expressing the wild-type protein (Figure R46). This is in contrast to the bulk cultures from which they were established. It may be that the clones isolated represented one extreme of clonal variation that exists in bulk cultures, simply because it was not representative of the average bulk culture, or of other clonal lines expressing the same mutation. KD cells reconstituted with moPrP bearing

CC2 alanine mutations showed a consistent profile of reduced RML propagation for every bulk culture and SCC tested (Figure R46).

All cell lines tested (both bulk cultures and SCCs) showed split-to-split increases in spot number indicative of propagation, with the exception of L108A.K109A and H110A.V111A where spot numbers reduced with progressive splits, or remained unchanged (Figure R46). For KD cells reconstituted with K23A.K24A.R25A, the bulk culture gave spot numbers approaching six hundred at split 6, compared to twelve hundred for KD cells reconstituted with moPrP^{WT} (Figure R46). Of the three SCCs tested for this mutation, two (clones a and c) displayed similar spot numbers ranging between three- to four hundred spots for split 6; the third SCC however (clone b), gave fifteen hundred for the same split (Figure R46). For Q41A, the bulk culture displayed the lowest spot number of approximately one hundred counts compared to three hundred (clone a), seven hundred (clone c) and sixteen hundred (clone b) for SCCs established from this culture. KD cells reconstituted with CC2 mutations showed similar spot numbers for bulk cultures and SCCs. Each KDmoPrP^{Ala} line expressing CC2 mutations gave spot numbers around two hundred or below for split 6 (Figure R46).

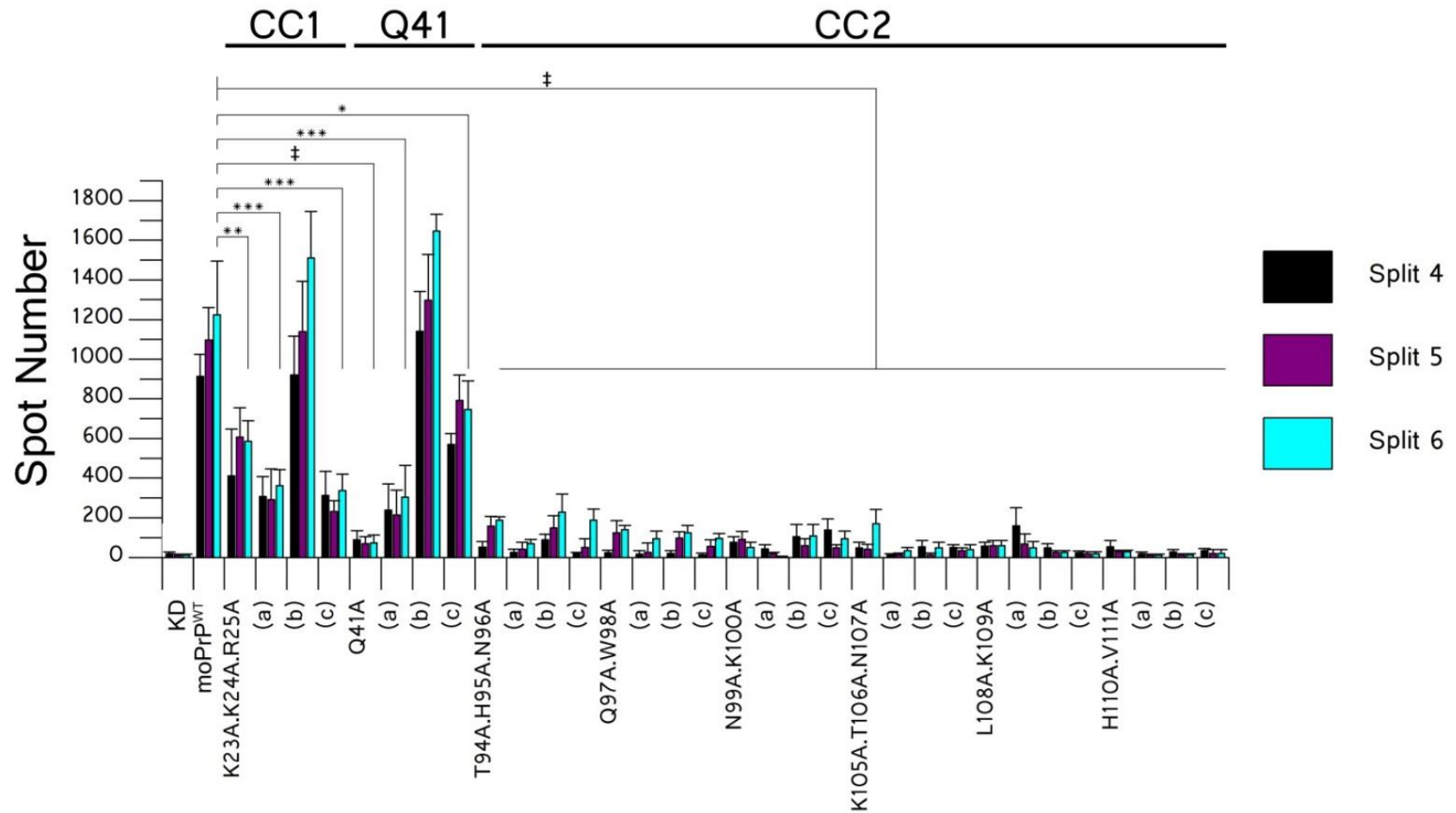


FIGURE R46: SCA ANALYSIS OF SINGLE CELL CLONES IN REGION 23-111

KD cell lines reconstituted with moPrP^{Ala} that exhibited 'inhibitory' phenotypes upon infection with RML (Section 3.3 and 3.4) were expressed as bulk cultures (mutation indicated in full) and SCCs (represented as clones a, b and c after each indicated mutation). Significance is indicated by ‡ for $P \leq 0.0001$, *** for $P \leq 0.0002$, * for $P \leq 0.005$; for clarity, this is only shown for split 6. Significance calculated in a one-way ANOVA with Bonferroni correction for multiple comparisons.

The alanine mutations on moPrP tested here show that when cells were selected for more uniform protein expression by single cell cloning, those bearing the CC1 mutation K23A.K24A.R25A and Q41A were able to reach levels of propagation that were similar to moPrP^{WT} such that no limitation on propagation was observed. However, cells expressing alanine mutations in CC2 maintained a severe reduction in propagation, despite testing SCCs that were selected for higher levels of moPrP protein expression (Figure R45). This is in line with the finding that CC2 mutations exert a stronger control over prion propagation than CC1 or Q41 mutations (Section 3.3 and 3.4). For K23A.K24A.R25A and Q41A, clones a, b, c were re-tested alongside clones d, e and f (Figure R38) at three dilutions of the RML homogenate (1×10^{-5} , 1×10^{-6} and 1×10^{-7}) to assess whether clone b for K23A.K24A.R25A and Q41A displayed high levels of propagation at all doses of RML, and whether similar propagation profiles would be observed for other as yet untested clones (d-e). It was found that clone b for both K23A.K24A.R25A- and Q41A-expressing cells, maintained higher spot numbers than their sister clones and bulk cultures at split 6 for every dose of RML tested (Figure R47). However, although K23A.K24A.R25A clone b gave spot numbers around one-thousand, Q41A clone b gave counts of around five hundred for RML infection at 1×10^{-5} dilution of homogenate (Figure R47). The range of SCCs tested demonstrates the variability in bulk cultures, but still supports the finding that K23A.K24A.R25A and Q41A reduce propagation.

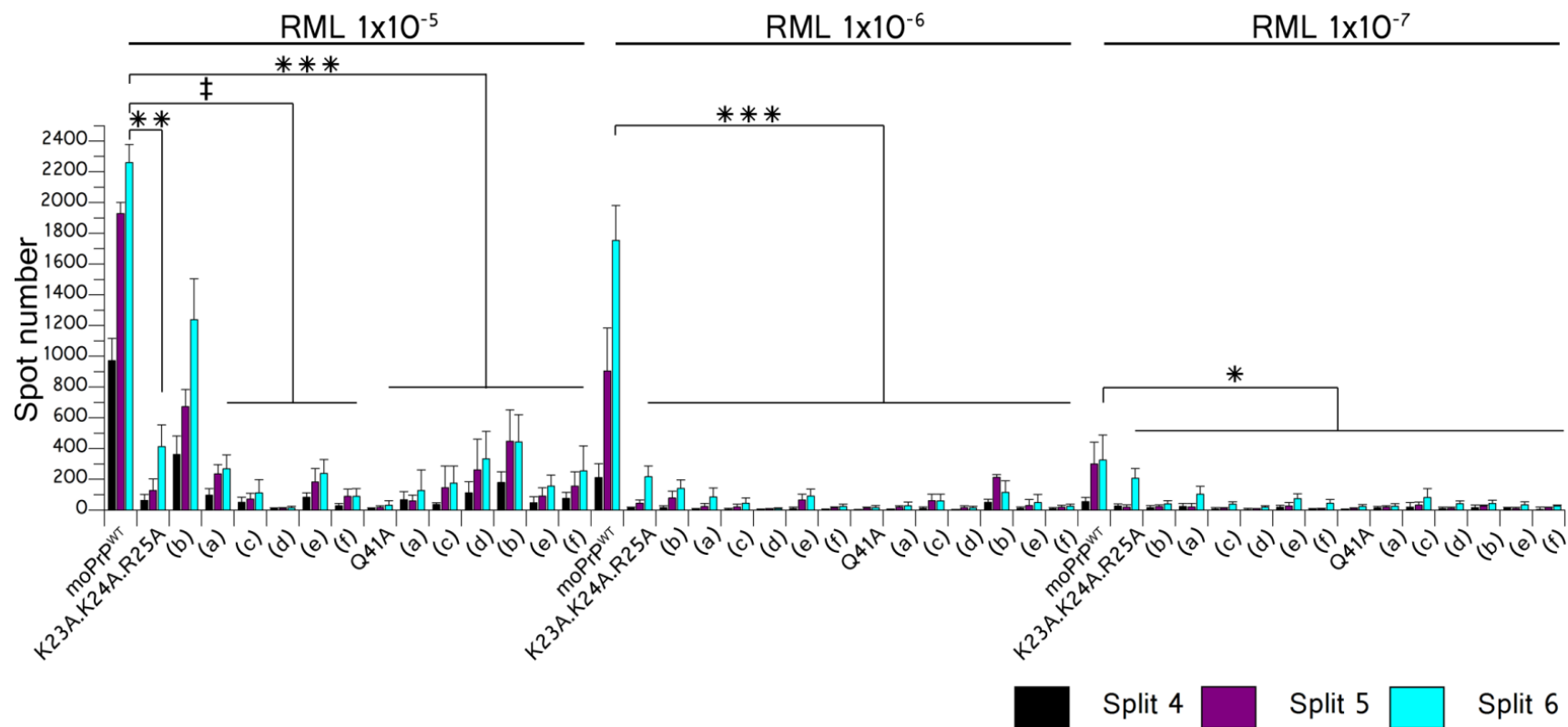


FIGURE R47: SCA ANALYSIS OF SINGLE CELL CLONES IN CC1 AND Q41 AT THREE DOSES OF INFECTIOUS INOCULA

SCA of bulk cultures and SCCs (a-f) of moPrP alanine mutations K23A.K24A.R25A and Q41A at three doses of RML infection. Significance is denoted by * for $P \leq 0.005$; ** for $P \leq 0.0025$; *** for $P \leq 0.0002$ and ‡ for $P \leq 0.0001$. Significance only shown for split 6 for clarity; calculated using a one-way ANOVA plus Bonferroni correction for multiple comparisons.

3.6.4 Experimental strategy II

From the results of SCA of clonal cell populations expressing moPrP CC1, Q41 and CC2 alanine mutations (Figure R46), it was evident that the flexible amino terminal region has a strong effect on prion propagation. The limitation on propagation exerted by these mutations could be for a number of reasons: (i) RML prions were not able to effectively infect KD cells reconstituted with these mutations; (ii) RML prions can infect KD cells reconstituted with N-terminal alanine mutations, but the reconstituted cells were subsequently unable to release their infectivity to surrounding cell populations, thereby limiting propagation; (iii) reconstituted KD cells were susceptible to infection by RML prions and can successfully release infectivity once infected, but the presence of alanine mutations at N-terminal regions inhibited formation of *de novo* prions; (iv) formation of *de novo* prions that allows successive propagation was achieved in the reconstituted KD system following RML infection, but the mutations exert a 'curing effect' on already formed prions, thereby reducing the total amount detected. A series of experiments were set up to address each of these possibilities (Figure R48).

Firstly, to test the hypothesis that the reconstituted KD cells were successfully infected by RML prions but unable to release their infectivity, KDmoPrP^{Ala} cells with CC1, Q41 and a number of CC2 alanine mutations were infected with RML under standard SCA conditions. The cells were grown for five splits and harvested at split 6. Lysates were then made by ribolysis of the infected samples. Lysates of individual KDmoPrP^{Ala} cells were subsequently used as infectious inocula for SCA analysis of PK1 cells. In this setup, PK1 cells acted as reporters of infectivity in the applied

lysates. If the KDmoPrP^{Ala} cells were successfully infected but hampered in their ability to release infectivity, collecting the cells at the last split of SCA would allow for maximal accumulation of prions, and ribolysis of the samples would release infectivity such that it is easily available to surrounding cell populations.

Secondly, KD cells reconstituted with moPrP bearing alanine mutations K23A.K24A.R25A, Q41A and a select number of CC2 alanine mutations were expressed on PK1 cells in which expression of the endogenous protein was not silenced. Since PK1 cells express moPrP^{WT} endogenously and propagate RML prions efficiently, expression of alanine-mutant moPrP in these cells allowed for direct analysis of the effects of moPrP^{Ala} on prion propagation of moPrP^{WT}. This allowed us to test whether expression of moPrP^{Ala} could exert limitations on the propagation of endogenous moPrP^{WT} – i.e. a dominant negative inhibition of propagation. Lastly, a few moPrP constructs with alanine mutations in CC2 were expressed on chronically RML-infected PK1 (iPK1) cells to determine if they would ‘cure’ prion infection; this was assayed by the number of ProteinaseK-resistant spots in the absence and presence of moPrP^{Ala} mutants.

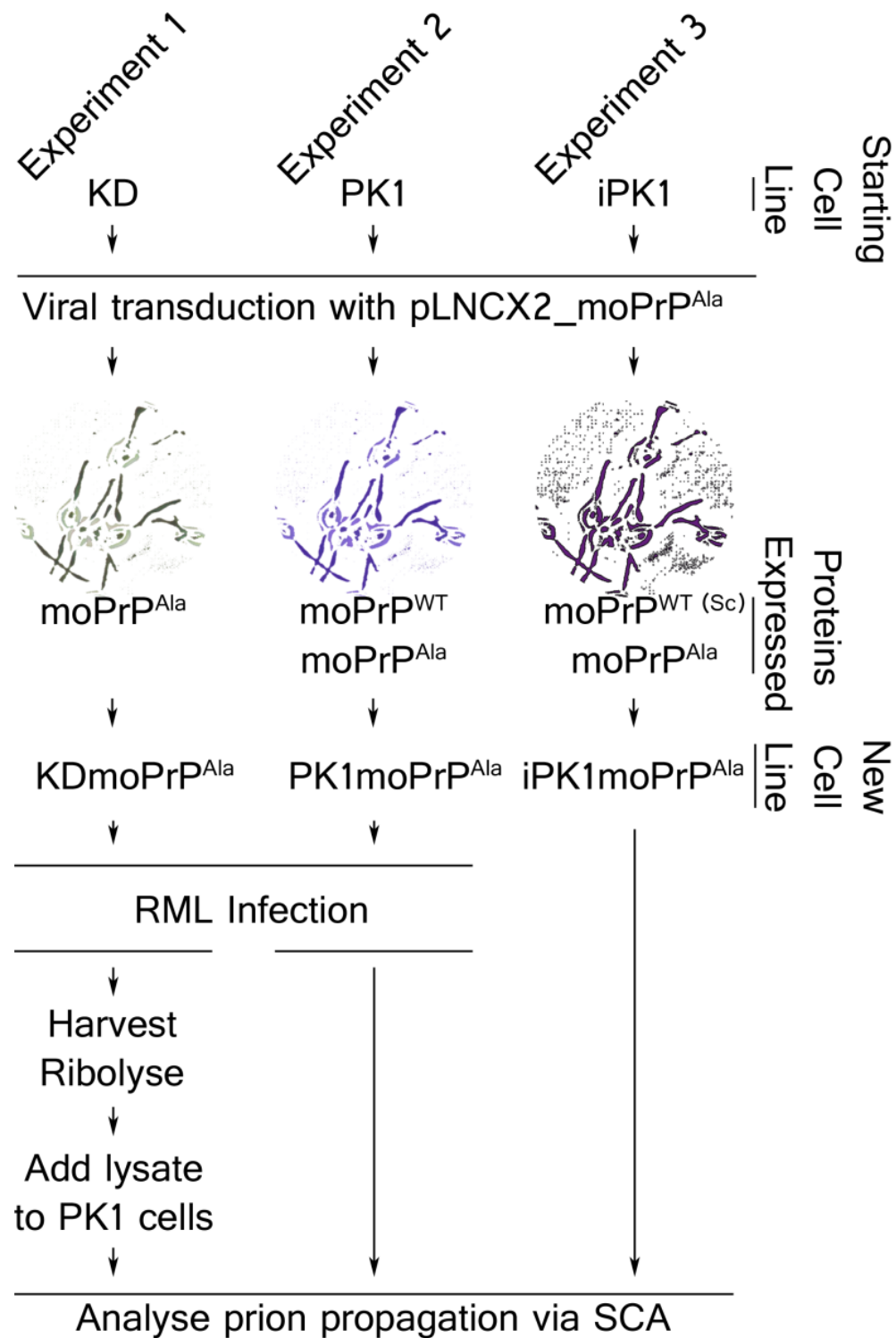


FIGURE R48: EXPRESSION OF moPrP^{ALA} IN KD, PK1 AND iPK1 CELLS

Schematic of experimental strategy; the ORF of moPrP bearing various alanine mutations was cloned into pLNCX2 and expressed in three different cell lines (1: KD cell in which suppression of the endogenous protein is silenced. Thus only the alanine-substituted protein is expressed; 2: PK1 cells in which both moPrP^{WT} and moPrP^{Ala} were expressed; 3: iPK1 cells where the disease-associated form (moPrP^{WT(Sc)}) and cellular moPrP^{Ala} proteins were expressed. The subsequent steps follow the layout of experiments described in experimental strategy II.

3.6.5 Lysates of RML-infected KD cells reconstituted with moPrP bearing alanine mutations in CC1, Q41 and CC2 retain infectivity and lead to prion propagation in PK1 cells

KDmoPrP^{Ala} cells expressing K23A.K24A.R25A and Q41A were infected with RML homogenate (1×10^{-5}) and passaged up to split 6, where they were harvested and ribolysed to make cell lysates at 1 million cells/ml in sterile 1xPBS.

To test whether the lysates retained infectivity post-RML infection, the ribolysed cells were applied to PK1 cells, and the PK1 cells tested for their ability to propagate RML in a modified SCA where the infectious inocula was not RML homogenate, but infected ribolysed KDmoPrP^{Ala} cells. PK1 cells were seeded in 96-well plates at 18,000 cells per well and the cell lysate added to the PK1 cells. 100 μ l of cell lysate was added to the seeded cells in 200 μ l of cell culture media. As per SCA protocol, PK1 cells were passaged for 6 splits, with spot numbers analysed at splits 4, 5 and 6.

Remarkably, the response of PK1 cells to the lysate applied mirrored the propagation profile of reconstituted KD cells when infected with RML homogenate. That is to say, the efficiency with which KD cells reconstituted with moPrP bearing various alanine mutations in the N-terminus propagated RML prions was reflected in the ability of cell lysates collected from these cells to infect PK1 cells (Figures R14, R16, R24 and R49).

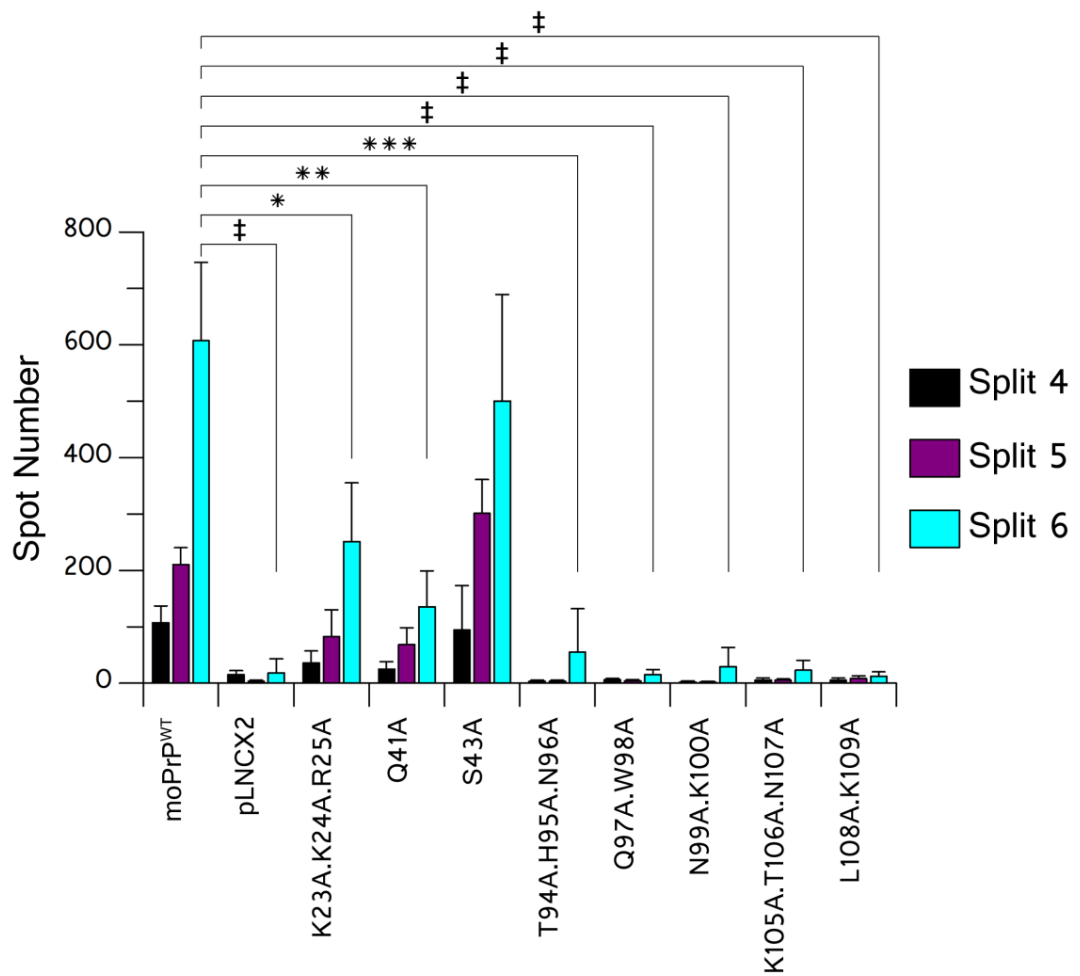


FIGURE R49: PK1 CELLS INFECTED WITH LYSATE FROM PRION-INFECTED KDMoPrP^{Ala}

CELLS

Response of PK1 cells to infection with lysates of RML-infected KD cells reconstituted with: the wild-type mouse prion protein (moPrP^{WT}), empty vector control (pLNCX2), or various moPrP constructs bearing point, double or triple alanine mutations (moPrP^{Ala}). Significance is denoted by * for $P \leq 0.005$; ** for $P \leq 0.0025$; *** for $P \leq 0.0002$ and ‡ for $P \leq 0.0001$. Significance only shown for split 6 for clarity; calculated using a one-way ANOVA plus Bonferroni correction for multiple comparisons.

KDmoPrP^{WT} cells and PK1 cells propagate RML efficiently, with spot numbers above eight hundred by split 6 when infected at a 1×10^{-5} dilution of homogenate (Figure R12). PK1 cells which were infected with cell lysate collected from RML-infected KDmoPrP^{WT} cells gave spot numbers of six hundred at split 6; this is the highest spot number obtained for PK1 cells with cell lysate infections (Figure R49).

Lysates collected from RML-infected KD cells reconstituted with S43A were also tested for their response on PK1 cells and used as a positive control in addition to KDmoPrP^{WT} as this mutation did not retard RML propagation (Figure R16). Infection of PK1 cells with KDmoPrP^{S43A} lysate gave five hundred spots at split 6 and was not significantly different from propagation of PK1 cells achieved with moPrP^{WT} lysate infection (Figure R49). For PK1 infections with lysates from KD cells expressing mutations K23A.K24A.R25A and Q41A, spot numbers below three hundred and two hundred, respectively, were obtained (Figure R49).

For infections with lysates from KD cells expressing moPrP alanine mutations in CC2 regions, spot numbers of less than one hundred were observed at all splits (Figure R49). In fact, for infections with lysates from KDmoPrP^{Q97A.W98A} and KDmoPrP^{L108A.K109A}, PK1 cells reported similar spot numbers to infections with lysate from KD cells expressing the empty pLNCX2 vector (Figure R49). Therefore, lysates collected from RML-infected KD cells reconstituted with moPrP bearing alanine mutations in CC2, at Q41 and at K23.K24.R25 were less infectious to PK1 cells than lysates from RML-infected KD cells reconstituted with the wild-type protein or that bearing mutation S43A (Figure R49). Additionally, lysates collected

from RML-infected KD cells expressing moPrP mutations K23A.K24A.R25A were more infectious to PK1 cells than those with the single mutation Q41A, which in turn was more infectious than any tested CC2 alanine mutation (Figure R49).

3.6.6 Expression of moPrP constructs bearing alanine mutations in PK1 cells

PK1 cells express the mouse prion protein endogenously. We used the available library of moPrP constructs bearing single, double, or triple alanine replacements to express these minimally mutated forms in PK1 cells such that expression of both moPrP^{WT} and moPrP^{Ala} proteins was achieved in the same cell line. These were established as described in Section 3.2 to test the hypothesis that alanine mutations in the flexible N-terminal region of the mouse prion protein can exert an inhibitory effect on the formation of prions not only on the protein bearing the minimal alanine mutations, but also on the wild-type protein.

PK1moPrP^{Ala} cells were infected with RML prions in a standard SCA (1×10^{-5} dilution of infectious inoculum) and analysed for their ability to propagate these prions (Figure R50). PK1 cells were transduced with virally packaged moPrP constructs bearing moPrP^{WT}, the N-terminal deletion mutant $\Delta 23-88$, CC1 mutation K23A.K24A.R25A, and CC2 mutations Q90A, T94A.H95A.N96A, Q97A.W98A, N99A.K100A, L108A.K109A and H110.V111A.

Neither deletion mutation $\Delta 23-88$, nor CC1 mutation K23A.K24A.R25A inhibited prion propagation when PK1 cells expressing these mutations were infected with RML prions, in contrast to all CC2 mutations tested which reduced propagation to at least half of that achieved for PK1moPrP^{WT} cells (Figure R50). PK1moPrP^{WT}, PK1moPrP ^{$\Delta 23-88$} and PK1moPrP^{K23A.K24A.R25A} all gave around eighteen hundred spots at split 6 (Figure R50).

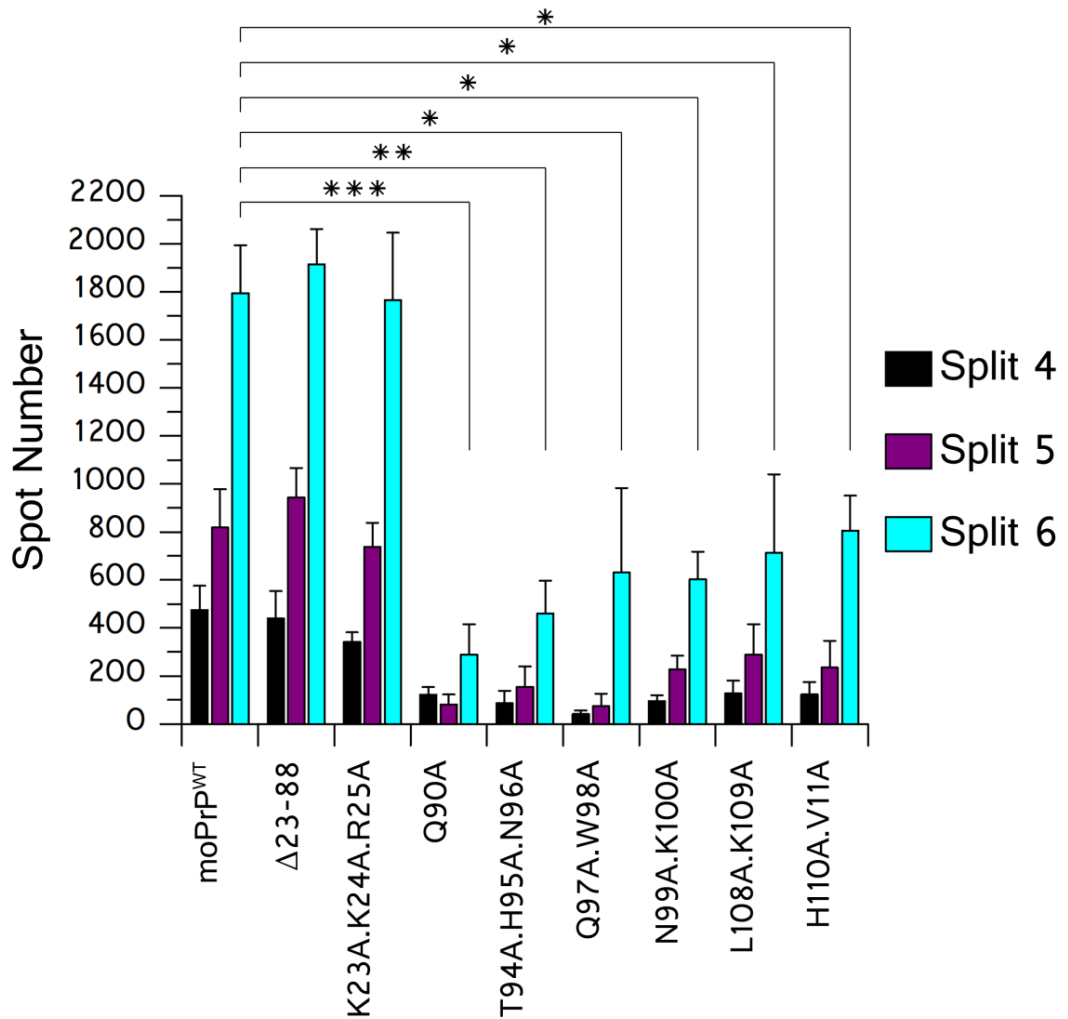


FIGURE R50: SCA OF PK1moPrP^{ALA} CELLS

PK1 cells were transduced with various moPrP constructs bearing alanine mutations cloned as point, double or triple replacements in the N-terminal regions 23-111 of the protein. PK1 cells expressing these alanine mutations on moPrP were assayed for their ability to propagate RML prions by SCA. Significance is denoted by * for $P \leq 0.005$; ** for $P \leq 0.0025$; *** for $P \leq 0.0002$. Significance only shown for split 6 for clarity; calculated using a one-way ANOVA plus Bonferroni correction for multiple comparisons.

Inhibition of propagation was equal for CC2 mutations Q97A.W98A, N99A.K100A, L108A.K109A, and H110.V111A with spot numbers of six- to eight hundred at split 6, compared to eighteen hundred for PK1 expressing moPrP^{WT}. PK1 cells expressing moPrP mutations Q90A and T94A.H95A.N96A reported lower spot numbers of three- and five hundred, respectively, at split 6 (Figure R50). Thus, a graded reduction in propagation, rather than poisoning of RML propagation was observed in PK1moPrP^{Ala} cells that express mutations in the CC2 region 90-111. This may be due to the association/dissociation of CC2 in the native form of the protein with a particular cellular factor or factors, an interaction that is competitively inhibited in the presence of alanine-mutant forms of moPrP, which has previously been shown to be a poor propagator (Section 3.4).

3.6.7 Expression of moPrP constructs bearing alanine mutations in chronically RML-infected PK1 (iPK1) cells

iPK1 cells are described as chronically infected cells as they produce ProteinaseK-resistant moPrP. They are typically used for cell curing assays to test the potency of various pharmacophores²⁸⁶. Here, they were transduced with virally packaged moPrP constructs bearing point, double or triple mutations in the flexible N-terminal region; this was to test whether expression of moPrP^{Ala} in these cells, would lead to a reduction in the amount of ProteinaseK-resistant material – a test for ‘curing’.

iPK1moPrP^{Ala} cells were established in the same way PK1moPrP^{Ala} and KDmoPrP^{Ala} cells were made (Chapter I). It was found that none of the moPrP constructs, regardless of the mutation expressed, cured iPK1 cells of prion infection as the levels of ProteinaseK-resistant material did not decrease after expression of moPrP^{Ala} in these cells (Figure R51).

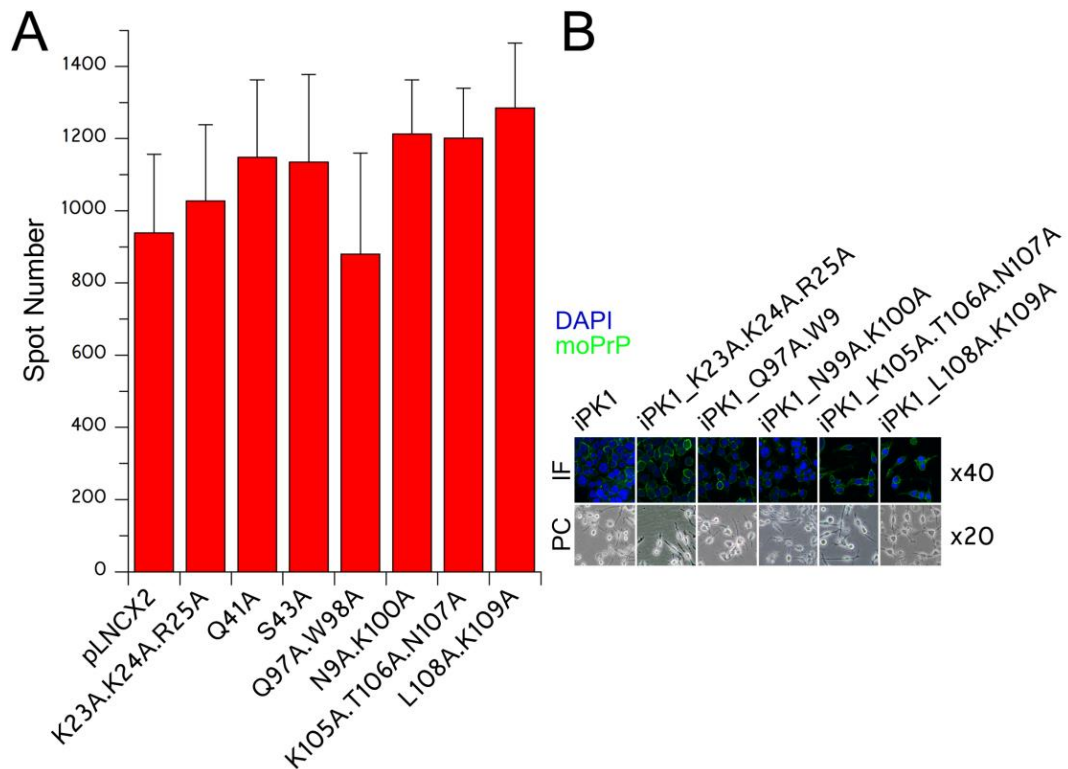


FIGURE R51: EXPRESSION OF moPrP^{ALA} DOES NOT RESCUE iPK1 CELLS FROM PRION

INFECTION

(A) iPK1 cells were transduced either with empty vector pLNCX2, or moPrP bearing various point, double or triple mutations within region 23-111 of the protein. Following antibiotic selection of transduced iPK1 cells, levels of ProteinaseK-resistant material were measured by ELISPOT. (B) Expression of moPrP in transduced iPK1 cells was tested alongside non-transduced cells to compare protein distribution; there were no apparent or statistically significant differences noted between samples expressing CC1 or CC2 alanine mutations and non-transduced iPK1 cells. IF: immunofluorescence; PC: phase contrast.

3.6.8 N-terminal mutations in moPrP at charge cluster regions protect cells from prion infection

Experiments were carried out to express moPrP^{Ala} with mutations targeted at charge clusters within the flexible N-terminal domain of the protein in KD, PK1 and iPK1 cells. They were then analysed for their ability to propagate RML prions by SCA.

KDmoPrP^{Ala} cells showed significantly limited propagation when alanine replacements K23A.K24A.R25A, Q41A, and various alanine mutations within CC2 region 90-111 were tested for RML prion propagation (Figures R46 and R47). To test whether this reduction in propagation was due to the inability of cells expressing the moPrP mutations to be infected by RML, or to release infectivity to surrounding populations of cells, RML-infected KDmoPrP^{Ala} cells were ribolysed and lysates subsequently added to PK1 cells (Figure R49). It was found that KDmoPrP^{Ala} cells were susceptible to RML infection to varying degrees and that the level of infection achieved depended on the region mutated, with alanine mutations at CC1, Q41 and CC2 lowering susceptibility to infection in increasing order (Figure R46). If the KDmoPrP^{Ala} cells were successfully infected by RML but unable to release their infectivity, ribolysing the cells would overcome this barrier. However, when RML-infected KDmoPrP^{Ala} cell lysates were tested for their infectivity on PK1 cells by SCA (Figure R49), only KDmoPrP^{WT} and KDmoPrP^{S43A} exhibited high levels of infectivity, suggesting that RML prions were successfully produced and accumulated in these cells following RML infection. This was followed by progressively lower infectivity for K23A.K24A.R25A, Q41A and alanine mutations in CC2, respectively

(Figure R49). The low level, but ever-present detection of ProteinaseK-resistant spots observed at split 6 for PK1 cells infected with cell lysates of KDmoPrP^{Ala} cells with CC1, Q41 and CC2 mutations (Figure R49) supports data on RML infection of KDmoPrP^{Ala} cells (Figure R46): CC1, Q41 and CC2 alanine mutations do not abrogate propagation, but considerably lowered the ability of cells expressing these mutations to propagate prions. This suggests that the presence of alanine mutations at these specific sites in the protein renders cells expressing them less susceptible to prion infection, rather than interfering with propagation/replication of prions, based on the low-level infectivity displayed by RML-infected KDmoPrP^{WT} cells as tested on PK1 cells (Figure R49). That is, when KDmoPrP^{Ala} cells were infected with RML, passaged for six splits at 1:8 to dilute out the initial inoculum and allow for propagation and accumulation of *de novo* prions, harvested and subsequently ribolysed, they displayed incredibly low infectivity within their respective cell lysates when applied to RML-susceptible PK1 cells compared to KDmoPrP^{WT} cells treated in the same way (Figure R49). This suggested a low titre of infectivity was present within the RML-infected KDmoPrP^{Ala} cells (Figure R46).

3.6.9 Dominant-negative inhibition of prion propagation by residues within CC2

Further analysis of alanine mutations within region 23-111 probed the question of whether they could exert a lowered propagation phenotype in the presence of the wild-type protein. To test this, constructs bearing moPrP^{Ala} were expressed in PK1 cells. The resultant cell line PK1moPrP^{Ala}, expressed both moPrP^{WT} and moPrP^{Ala} and was challenged with RML prions to assess its ability to propagate these prions. It was found that following RML infection of PK1moPrP^{Ala} cells, only alanine mutations in CC2, but not CC1, lowered the level of propagation observed (Figure R49). Furthermore, an N-terminal deletion which encompasses CC1, Q41 and OPR regions of the protein but not CC2 is known to abrogate RML prion propagation when expressed in KD cells (KDmoPrP^{Δ23-88}) – this mutation Δ23-88, had no inhibitory effect on prion propagation when expressed in PK1 cells, as PK1moPrP^{Δ23-88} cells propagated with the same efficacy as PK1moPrP^{WT} cells (Figure R42). This suggests that CC2, but not CC1 or Q41 alanine replacements exert dominant-negative inhibition of propagation by lowering the native ability of PK1 cells to propagate RML (Figure R42).

It also shows that small changes between one and three alanine replacements in CC2 have a stronger control over prion propagation than a large deletion (Δ23-88) N-terminal to CC2 region 90-111 (Figure R42). Together, this strengthens the case for CC2, with residue Q90 as the most N-terminal point within it, as a significant charge cluster within the flexible tail of the protein that modulates propagation. It further demonstrates that mild alterations within CC2 can inhibit *de novo* prion formation *in trans* by

limiting the ability of the PK1 cells expressing the wild-type prion protein to propagate RML prions. Since these mutations when expressed as KDmoPrP^{Ala} rendered the cells less infectious to other RML-susceptible cells (Figure R49) we could speculate the moPrP^{Ala} protein can lower infectivity of RML when applied to moPrP^{WT} as in PK1 cells (Figure R50) perhaps by sequestering some factor required for efficient propagation.

It is interesting to consider however, that Δ 23-88, like CC2 alanine mutations, abolished prion propagation in KD cells, but unlike CC2 alanine mutations did not exert an inhibitory effect in PK1 cells (Figure R50). This is an important finding as CC1 mutation K23A.K24A.R25A and point mutation Q41 were the only mutations identified within region 23-88 that when expressed in KD cells, reduced the ability of these cells to propagate prions relative to KD cells reconstituted with the wild-type protein. However, when both these changes were expressed on the same construct as K23A.K24A.R25.Q41A, the reduction in propagation was not as severe as Δ 23-88. We could infer then, that deletion of segment 23-88 may impinge on the positioning and ultimately the activity of the CC2 region; this would explain why prion propagation is similarly reduced for KD cells reconstituted with Δ 23-88 and CC2 alanine mutations.

The graded pattern of spot number reduction when moPrP^{Ala} is expressed in PK1 cells is characteristic of competitive inhibition where moPrP^{Ala} competes for the same moiety as moPrP^{WT}; a moiety that facilitates propagation. This may be in the form of a true binding interaction or a transient interaction either with PrP^{Sc}, or another cellular factor; this

association encourages the initiation of propagation, or its maintenance following successful initiation post-infection.

This would also account for the finding that CC2 alanine mutations, but not deletion $\Delta 23-88$ exhibit dominant negative inhibition of prion propagation, as small amino acid replacements, unlike deletion $\Delta 23-88$ are not likely to alter the positioning of CC2, but may affect its native activity within its cellular environment, i.e. interaction with a propagation facilitator.

In the context of region CC2 being critically involved in a cellular association that facilitates initiation of propagation, we would expect: (i) KDmoPrP^{Ala} cells with CC2 mutations to have significantly reduced propagation as it would never be established efficiently; (ii) the presence of moPrP^{Ala} CC2 alanine mutant forms in PK1 cells to deplete the available pool of the propagation-facilitating-factor, making its interaction with moPrP^{WT} less likely and thus, reduce the efficiency with which moPrP^{WT} can propagate RML prions. These are both results confirmed by SCA analysis.

3.6.10 Alanine replacements in CC2 inhibit *de novo* formation of prions, but cannot reverse the fate of existing prions

Since alanine mutations in CC2 were able to limit prion propagation in KDmoPrP^{Ala} cells (Figure R46) and inhibit prion propagation by the wild-type protein in PK1moPrP^{Ala} cells (Figure R50), we investigated whether they could cure chronically RML-infected cells of prion infection (Figure R51).

When CC2 alanine mutations were expressed on chronically infected cells as iPK1moPrP^{Ala}, none of them reduced the level of ProteinaseK-resistant spots relative to iPK1 or iPK1_pLNCX2 cells (Figure R51). Hence, they were not able to reverse the propagation phenotype by curing iPK1 cells of RML infection (Figure R51). In conclusion, charge cluster 2 region of the prion protein mediates the efficacy of prion propagation by regulating the susceptibility of cells to prion infection (Figures R46 and R49). There is a probable interaction of CC2 with a cellular factor that promotes initial propagation, but not maintenance of propagation. Additionally, CC2 mutations can regulate *in trans* the efficiency with which surrounding populations propagate prions (dominant-negative inhibition of prion propagation), probably by competing for binding to the facilitating factor, but cannot reverse the formation of prions once they have been established. This could be because promotion of initial propagation by binding to the facilitating factor is made redundant in chronically RML-infected cells.

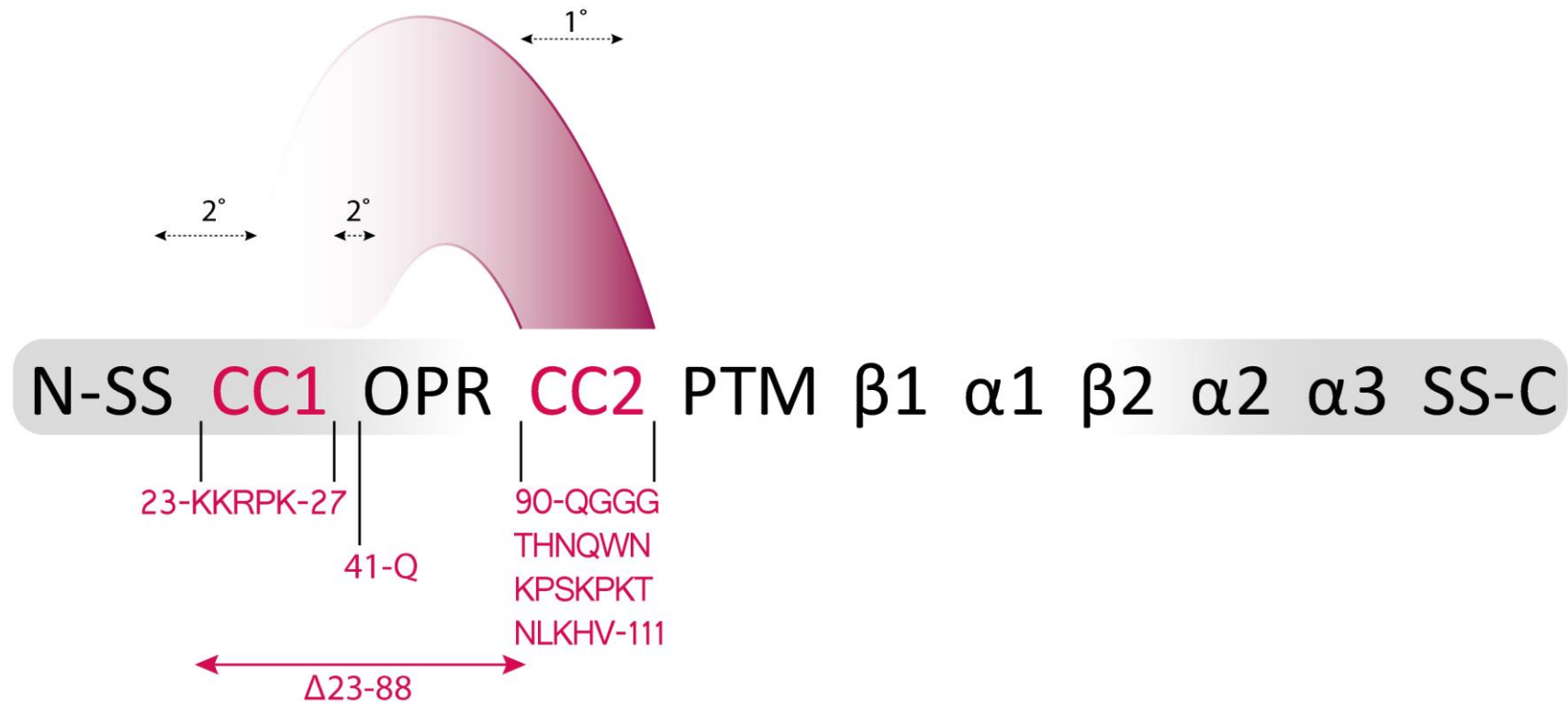


FIGURE R52: PROPOSED MECHANISM OF INHIBITION OF PRION PROPAGATION BY moPrP^{ALA} MUTATIONS IN CC1, Q41 AND CC2 REGIONS OF THE PROTEIN

Prion propagation is made more efficient by association of PrP^C to a propagation facilitator (pink) with its primary interaction (1°) domain in CC2, and accessory sites or secondary interactions (2°) at CC1 residues K23, K24, R25 and Q41. Bar schematic of moPrP, highlighting residues 23-111 within the protein. N-SS: N-terminal signal sequence; CC1: charge cluster 1; OPR: octapeptide repeat region; CC2: charge cluster 2; PTM: putative transmembrane region; α1: helix 1; β1: strand 1; α2: helix 2; α3: helix 3; SS-C: C-terminal signal sequence. Region 23-88 is defined by double-headed arrow. Sequence segments of moPrP shown in pink represent regions of the protein that when mutated (alanine replacement or deletion of 23-88), led to a reduced ability of cells expressing the mutated protein to propagate RML prions.

3.6.11 Features of charge cluster regions within PrP that may contribute to regulation of prion propagation.

A number of studies have focused on the roles of N-terminal PrP residues and their various contributions to prion infection, propagation and toxicity. This flexible region of the protein is believed to promote propagation through its inherent disorder¹³⁸; dissociation of fibrillar forms to generate more surfaces for conversion⁸⁷; regulation of α -cleavage in the cellular protein⁴⁹ and charge associations or repulsions that are involved in direct or indirect PrP^{Sc} binding^{101, 115, 117, 134}.

Region 23-31 at the extreme N-terminus of PrP^C has been shown to bind directly to PrP^{Sc116}, with Δ 23-31 reported to be defective in endocytosis¹¹⁶. The influence of this region on PrP^{Sc} formation is in line with the data presented here where KD cells reconstituted with moPrP bearing mutation K23A.K24A.R25A displayed a significant reduction in their ability to propagate RML prions (Figure R47).

There is very little evidence in the literature for the involvement of residue Q41 in prion propagation. Q41 comprises part of the YXXQ (YPGQ) consensus sequence motif for the recruitment and activation of Stat3²⁵⁵. Association of PrP with Stat3 has only been shown in terms of prion regulation of pluripotency in embryonic stem cells²⁵⁶. This however, is unlikely as mutations in surrounding residues such as Y38 in mutation S36A.R37A.Y38A or S43A did not exhibit any reduction in propagation (Figure R14 and R16). Although the mechanisms by which Q41A interferes with propagation in KD cells reconstituted with moPrP^{Q41A} are not known,

the effect observed here is clear (Figure R47). A study by Ushiki-Kaku *et al.* alluded to the involvement of Q41 as part of a novel epitope present in PrP^{Sc} but not PrP^C: QGSPGGN (moPrP 41–47)¹⁰¹. Their study involved peptide array analysis of sera from PrP-null mice injected with Scrapie homogenate and a screen for differential binding between infected and non-infected samples to uncover disparities in protein conformation and exposed residues in the cellular and aberrant protein forms. This data supports our finding that Q41 is a critical site that can mediate prion propagation, as KDmoPrP^{Q41A} cells propagate RML prions with markedly reduced efficiencies relative to KDmoPrP^{WT} cells (Figure R47).

Loss of prion propagation in deletion mutation Δ 23-88, but the subsequent inability of this mutation to inhibit formation of *de novo* prions in infected PK1 cells may be explained by phenomenon of intrinsically disordered regions^{29, 36}. The intrinsic flexibility of the N-terminal 23-111 domain of the protein may contribute to misfolding propensity, thereby encouraging prion propagation following infection. Removal of this region may then in turn, stabilise the native fold of PrP^C, making it less likely to misfold into PrP^{Sc} upon RML infection. Alternatively, the effects observed for Δ 23-88 may be a reflection on the displacement of CC2 residues made by this deletion, which have been shown to have a strong controlling effect on prion propagation (Figures R24, R25, R46, R49 and R50).

Qi *et al.* suggest that the flexible N-terminal region bears key histidine residues that when protonated under mildly acidic conditions contribute to fibril dissociation, a necessary event in prion propagation⁸⁷. They showed that fibrils formed from recombinant protein when placed in a mild acidic

environment such as that in late endosomal compartments, undergo dissociation both laterally and axially⁸⁷.

Oliviera-Martins *et al.* and Hara *et al.* highlighted the role of CC2 residues 100-104 in α -cleavage⁴⁹ and prion conversion¹³⁴ of the protein, respectively. In the first instance, lack of α -cleavage is stated as a shared characteristic of PrP^{Sc} and toxic PrP^C mutants; the authors infer that the α -cleavage tolerance of PrP with K109I.H110I mutations, which is also toxic in transgenic mice, points to the importance of region CC2 in regulating prion protein cleavage and may have consequential roles in disease pathogenesis⁴⁹. McDonald *et al.* present a revised report on the α -cleavage of PrP, suggesting that in the presence of copper, the protein is processed by ADAM family proteins between A119↓V120 and G227↓R228, in addition to the canonical K109↓H110 cleavage⁵⁰. Although this shifts α -cleavage outside the CC2 region, this region is still required for alternative ADAM-mediated cleavage, as copper coordination primarily occurs at histidine residues within OPR and CC2 segments of the protein¹²⁹.

Hara *et al.* used 3F4-epitope-tagged constructs to show the inability of moPrP mutants K100A, S102A, K103A and P104A to form ProteinaseK-resistant protein¹³⁴. This is consistent with our findings that CC2 mutations significantly lower prion propagation with spot numbers in the range of fifty to one hundred which falls in the range of severe limitation to, and abrogation of, prion propagation (Figure R47). Hara *et al.* also emphasise that CC2 alanine mutations within epitope 100-104 'eliminated the endogenous PrP^{Sc}' in chronically infected cells – this is in contrast to the

findings presented here, where CC2 alanine mutations do not have any effect on lowering ProteinaseK-resistant PrP in chronically infected cells (Figure R51) where RML-infection is already established, but exert dominant-negative inhibition on the *de novo* prion formation (Figure R50).

Site directed mutagenesis	Inhibition of prion			moPrP domain
	KD cells	PK1 cells	iPK1 cells	
K23A	Dark Red	Light Red	Dark Red	CC1
K24A	Dark Red	Light Red	Dark Red	
R25A	Dark Red	Light Red	Dark Red	
K23A.K24A.R25A	Light Red	Dark Red	Dark Red	
P26A.K27A	Dark Red	Light Red	Dark Red	
P28A	Dark Red	Light Red	Dark Red	
W31A.N32A.T33A	Dark Red	Light Red	Dark Red	
S36A.R37A.Y38A	Dark Red	Light Red	Dark Red	
Q41A	Light Red	Dark Red	Dark Red	
K23A.K24A.R25A.Q41A	Light Red	Dark Red	Dark Red	
S43A	Dark Red	Light Red	Dark Red	OPR
N47A.R48A.W49A	Dark Red	Light Red	Dark Red	
Q52A	Dark Red	Light Red	Dark Red	
T55A.W56A	Dark Red	Light Red	Dark Red	
Q58A	Dark Red	Light Red	Dark Red	
H60A	Dark Red	Light Red	Dark Red	
W64A	Dark Red	Light Red	Dark Red	
Q66A	Dark Red	Light Red	Dark Red	
H68A	Dark Red	Light Red	Dark Red	
S71A.W72A	Dark Red	Light Red	Dark Red	
Q74A	Dark Red	Light Red	Dark Red	
H76A	Dark Red	Light Red	Dark Red	
S79A.W80A	Dark Red	Light Red	Dark Red	
Q82A	Dark Red	Light Red	Dark Red	
H84A	Dark Red	Light Red	Dark Red	
W88A	Dark Red	Light Red	Dark Red	

TABLE R7: LIST OF MUTATIONS MADE WITHIN THE UNSTRUCTURED REGION OF THE MOUSE PRION PROTEIN.

N/A: not applicable. Colour intensity signifies the extent to which expression of the moPrP mutation limits propagation in the indicated cell line.

3.6.12 Mutational analysis of the flexible N-terminal tail of moPrP reveals three distinct regions that exert varying control over prion propagation

moPrP was expressed as the wild-type protein, or with point, double or triple mutations within region 23-111 in three cell lines: KD, PK1 and iPK1 cells. KD cells reconstituted with moPrP bearing alanine mutations K23A.K24A.R25A, Q41A, and mutations within CC2 region 90-111 demonstrated a significantly reduced ability to propagate prions, with the most pronounced reduction exerted by CC2 mutations. These results were verified by preparing SCCs (Figure R46).

Region 23-31 has been previously identified as a replicative surface for PrP^{Sc} formation¹¹⁶. Here, we propose that the minimal segment that contributes to prion propagation in this association is 23-25 (Figures R14, R15, R46 and R47). Q41 has been identified in this study as a novel point mutation that limits prion propagation. It is also the only residue in region 23-88 that has an effect on lowering propagation with incredible specificity, as it is a single amino acid change and mutation of neighbouring residues had no effect on prion propagation (Figures R14 and R16). CC2 region 100-104 has been identified as the key epitope for prion conversion¹³⁴. Here, we suggest that the entire region 90-111, and not 100-104 alone is significant in regulation of prion propagation (Figures R24 and 46). The reduced propagation presented in cells expressing these mutations was due to an acquired lower susceptibility to RML infection (Figure R49) – a characteristic that mutations within CC2 were able to exert in a dominant-negative manner (Figure R50). We hypothesise that CC2 acts as a region, which associates

with a cellular factor, whose accessory binding sites are at K23.K24.R25 and Q41. This association allows for the highly efficient propagation of prions (Figure R52).

3.7 Middle conserved region 112-135 of the prion protein may traverse the lipid bilayer

3.7.1 Experimental strategy

Residues 111-135 of the prion protein represent the most highly conserved domain within the protein, consisting almost exclusively hydrophobic residues⁵⁴. Indeed, when the native sequence is threaded into structure prediction programs, the nature of the residues within 111-135 leads to the same conclusion: that this section of the protein is predicted to have a transmembrane helix secondary structure (Figure R45). To test this hypothesis and the effect of altering the putative transmembrane helix structure of the protein on prion propagation, we designed point mutations to increase or decrease helix propensity, based on data by Li *et al*²⁸⁷ (Table R8).

Hegde *et al.* showed that depending on the orientation of PrP across the membrane, it may have toxic or protective functions^{63, 152}. Furthermore, when the full amino acid sequence of the mature protein is run in a program to predict fibril propensity, a large portion of residues that fall in the 'amyloidogenic' region are of the middle region of PrP (Figure R54)²⁸⁸.

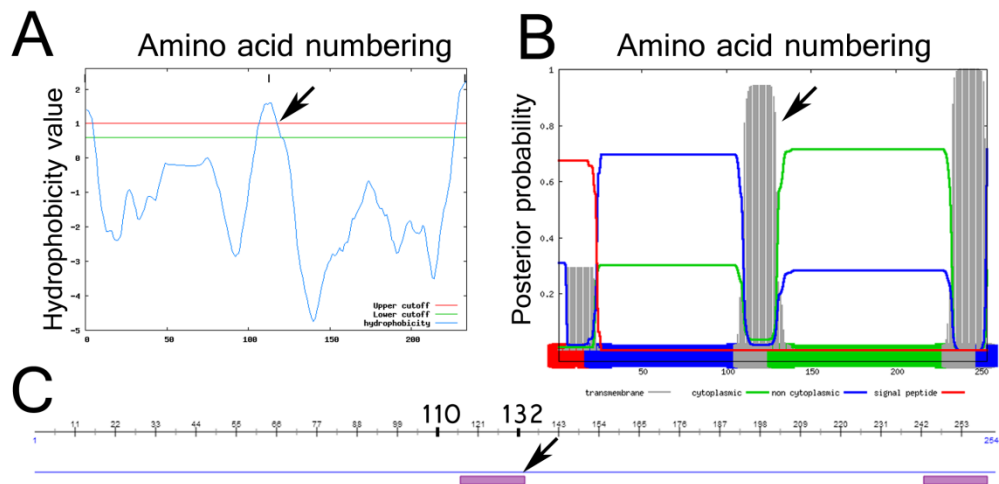


FIGURE R53: PREDICTION OF THE MIDDLE REGION OF MOPRP AS A MEMBRANE-TRAVERSING SEGMENT

Three prediction programs were used to predict the secondary structure of moPrP using the amino acid sequence of UniProtKB ID P04925. Each showed that the region encompassed within segment 111-135 of the protein is predicted to be a membrane traversing domain, indicated with a filled arrow in each instance.

(A) <http://mobyale.pasteur.fr/cgi-bin/portal.py?#forms::toppred>

(B) <http://www.ebi.ac.uk/Tools/pfa/phobius/>

(C) <https://www.predictprotein.org/>

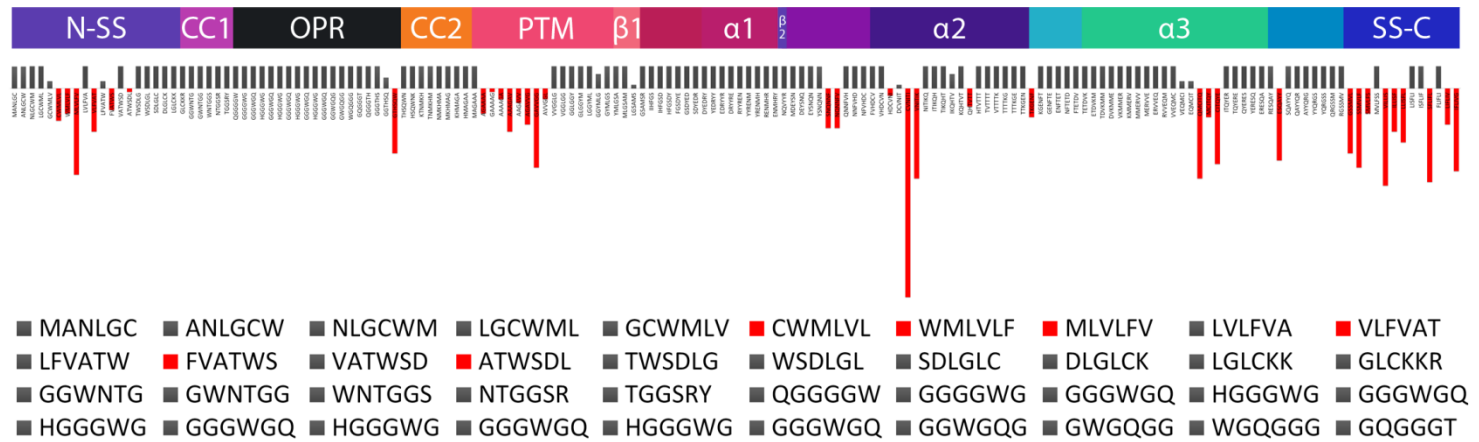



FIGURE R54: FIBRIL-FORMING SEGMENTS IN THE PRION PROTEIN

Thompson *et al.* designed a fibril-prediction program where the amino acid sequence of any protein is analysed six-amino acids at a time, across the length of the sequence. The energy of the six-amino acid sequence is calculated by mapping it to previously acquired data from their laboratory and if this energy is lower than the threshold value (shown here in red), the segment is predicted to be fibril-forming.



Residue	Mean residue ellipticity (deg cm ² dmol ⁻¹) at 222nm
Ile	25700
Leu	25100
Val	25000
Met	22700
Phe	21500
Ala	21100
Gln	19400
Tyr	18300
Thr	16600
Ser	16200
Asp	13800
Gly	12100
Pro	7400

TABLE R8: HELICAL PROPENSITY OF VARIOUS AMINO ACIDS

Li *et al.*²⁸⁷ carried out systematic studies of peptides by circular dichroism; shown here are results they obtained for association of peptides in SDS micelles, which allowed for a ranking order of helical propensity, with isoleucine (Ile) shown to be the strongest promoter of helicity and proline the weakest.

Using the rationale that mutations to isoleucine would increase helix propensity and those to proline decrease it (Table R8), a total of thirty-seven point mutations and two deletion mutations were designed in region 111-135 of the mouse prion protein via site-directed mutagenesis (Chapter I). The mutations were expressed in KD cells and the ability of cells expressing these mutations to propagate prions was tested by SCA (Section 3.2).

There were three main aims of generating mutations in this region and in particular, substituting native residues to amino acids other than alanine: (i) to test the effects of altering helix propensity on the propagative capacity of the altered protein; (ii) to probe the association of the PTM domain with

membranes; (iii) to test the possibility of a PrP homodimer through association of its PTM domain. From the SCA experiments carried out herein, only information on the helix stability and its effects on propagation can be deduced. Based on SCA data, we can also infer residues of interest within the PTM and whether PrP engages in homodimer interactions that contribute to the efficiency of prion propagation. We cannot however, answer questions on the membrane association of the protein through this domain; this work will be undertaken by other members of the department, using the available mutagenic library generated for moPrP (Table R1).

The changes made span the moPrP sequence from residue 111-135 (Figures R55-57). These changes are presented in three parts, analysing the effects of amino acid replacements on moPrP in region (i) 111-119, (ii) 121-127 and (iii) 127-135.

Residue ellipticity (deg cm ² dmol ⁻¹)						
Mutation	Overall change	Initial	Final	Helix propensity	moPrP domain	
V111M		2300	25000	22700	Decreased	PTM
A112L		-4000	21100	25100	Increased	
G113L		-13000	12100	25100	Increased	
A115G		9000	21100	12100	Decreased	
A116L		-4000	21100	25100	Increased	
A117L		-4000	21100	25100	Increased	
A117R			21100			
G118A		10000	12100	2100	Decreased	
G118L		-13000	12100	25100	Increased	
A119L		-4000	21100	25100	Increased	
A119P		13700	21100	7400	Decreased	

TABLE R9: MUTATIONS MADE WITHIN REGION 111-119 OF MOPRP

Mutations made within region 111-119 alter the helix propensity properties of the PTM by increasing or decreasing the helix stability of this region by varying degrees. The degree of change is indicated in the 'overall change' column where the difference between the initial and final values for the native and substituted residues is shown, based on the values provided in Table R8.

3.7.2 Scrapie cell assay analysis of mutations in residues 111-119 of moPrP

Point mutations made within moPrP PTM region 111-119 included six changes to leucines which are predicted to increase helix propensity, some that decrease helix propensity and a substitution to proline which is a helix/strand breaker (Table R9). Most of the KD cells reconstituted with mutations in this region displayed a propagation profile comparable to wild-type controls at split 4, the earliest time point where samples were analysed, but displayed lower spot numbers for splits 5 and 6 relative to wild-type controls (Figure R53).

This pattern of initially (split 4) high spot numbers followed by successive decreases in spot number compared to wild-type-expressing cells was observed for KD cells reconstituted with moPrP mutations V111M, A112L, G113L, A115G, G118A, G118L, A119L and A119P. For mutation A116L, spot numbers of six hundred were recorded for split 4; this number halved at split 5, but propagation was re-established with six hundred spots by split 6. Both mutations made at position A117, (A117L and A117R) displayed a consistent lack of propagation capacity across all splits (Figure R55). However, SCA analyses of moPrP in this study have been carried out using the last time point, split 6, as the cells should have had, if truly propagating, enough time to accumulate maximal levels of ProteinaseK-resistant PrP and the initial applied homogenate equally diluted, giving the best differential for detection of *de novo* prions (Section 3.2).

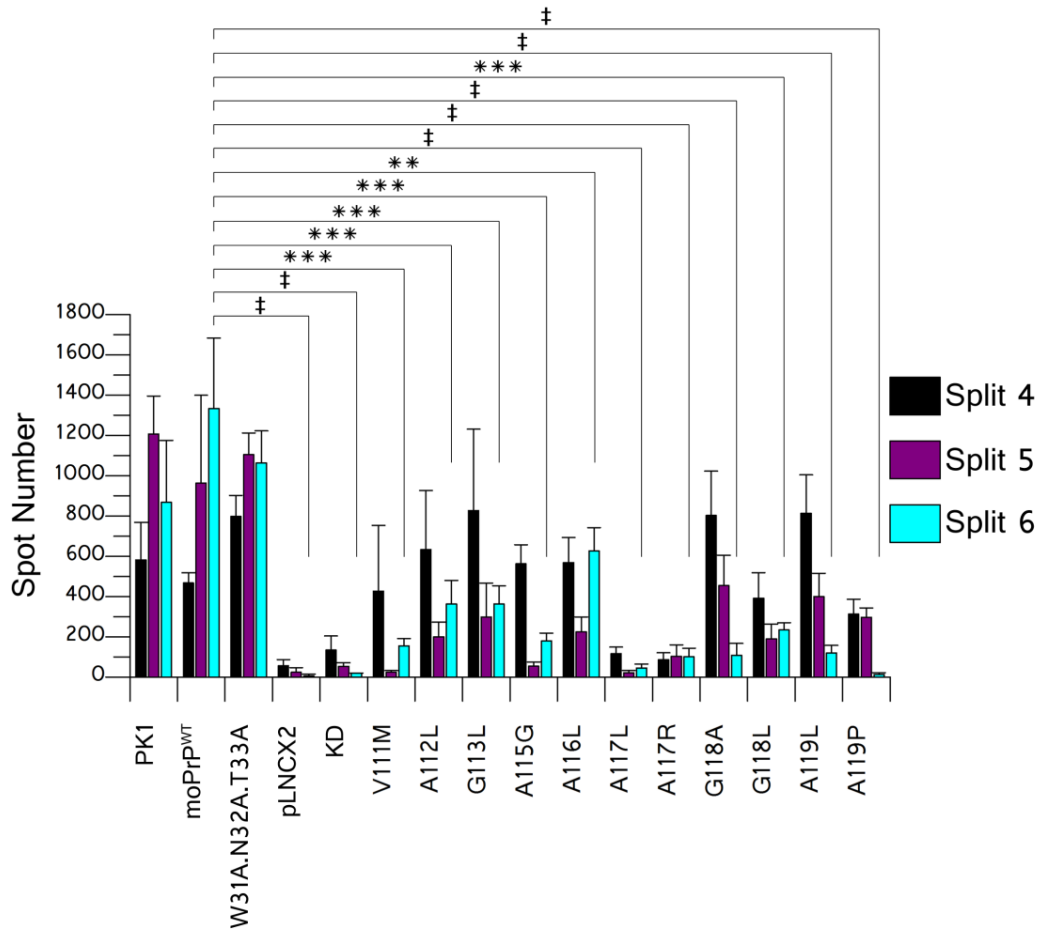


FIGURE R55: SCA ANALYSIS OF KDMoPrP^{ALA} CELLS WITH MUTATIONS IN REGION 111-119

SCA analysis of KD cells reconstituted with various mutations in moPrP. The first five cell lines represent three positive controls (PK1 cells, KD cells reconstituted with moPrP^{WT} and KD cells reconstituted with moPrP bearing a triple alanine mutation at the N-terminus); and two negative controls: KD cells reconstituted with empty vector pLNCX2 and un-reconstituted KD cells. The next 11 cell lines expressed moPrP bearing point mutations in sequence segment 111-119. Significance is denoted by * for $P \leq 0.005$; ** for $P \leq 0.0025$; *** for $P \leq 0.0002$ and ‡ for $P \leq 0.0001$. For clarity, significance is only shown for split 6, which is taken to be the time point with the best differential between detection of applied and *de novo* prions (Section 3.2); calculated using a one-way ANOVA plus Bonferroni correction for multiple comparisons.

Using these criteria, all mutations made in region 111-119 of moPrP displayed reduced propagation compared to wild-type controls at split 6 (Figure R55).

Spot numbers, although low for all cells expressing moPrP mutations, varied between cell lines such that: A119P< A117L< A117R< A119L< G118A< V111M< A115G< G118L< G113L≤ A112L< A116L. Thus, A116L affected spot number the least, with split 6 values of six hundred, and A119P lowered it the most with spot numbers below fifty and comparable to negative controls at the same split (Figure R55).

The next set of mutations analysed for their ability to propagate RML prions were in region 121-127 of the protein's PTM domain. All cells tested expressing single amino acid changes within this segment of the protein demonstrated a considerable and significant reduction in their ability to propagate prions (Figure R56). Like cells expressing mutations made in region 111-119 of the protein, those expressing mutations made in region 121-127 displayed higher spot counts for split 4 compared to split 6 for some replacements: V121A, L124A, L124I, G126L, G126V and Y127F (Figure R56). At split 6, the highest propagation was observed for KDmoPrP^{WT} cells, followed by KD cells reconstituted with W31A.N32A.T33A, a triple alanine-mutant positive control (Figure R14), and then PK1 cells (Figure R56). Of the PTM mutations, highest spot numbers at split 6 were recorded for G125A with six hundred spots;

Residue ellipticity (deg cm ² dmol ⁻¹)						moPrP domain
Mutation	Overall change	Initial	Final	Helix propensity		
V121A		3900	25000	21100	Decreased	PTM
G122A	-9000	12100	21100	Increased		
G122L	-13000	12100	25100	Increased		
G123A	-9000	12100	21100	Increased		
L124A	4000	25100	21100	Decreased		
L124I	-600	25100	25700	Increased		
L124V	100	25100	25000	Decreased		
G125A	-9000	12100	21100	Increased		
G126A	-9000	12100	21100	Increased		
G126L	-13000	12100	25100	Increased		
G126V	-12900	12100	25000	Increased		
Y127F	-3200	18300	21500	Increased		

TABLE R10: MUTATIONS MADE WITHIN REGION 121-127 OF MOPrP

Mutations made within region 121-127 alter the helix propensity properties of the PTM by increasing or decreasing the helix stability of this region by varying degrees. The degree of change is indicated in the 'overall change' column where the difference between the initial and final values for the native and substituted residues is shown, based on the values provided in Table R8.

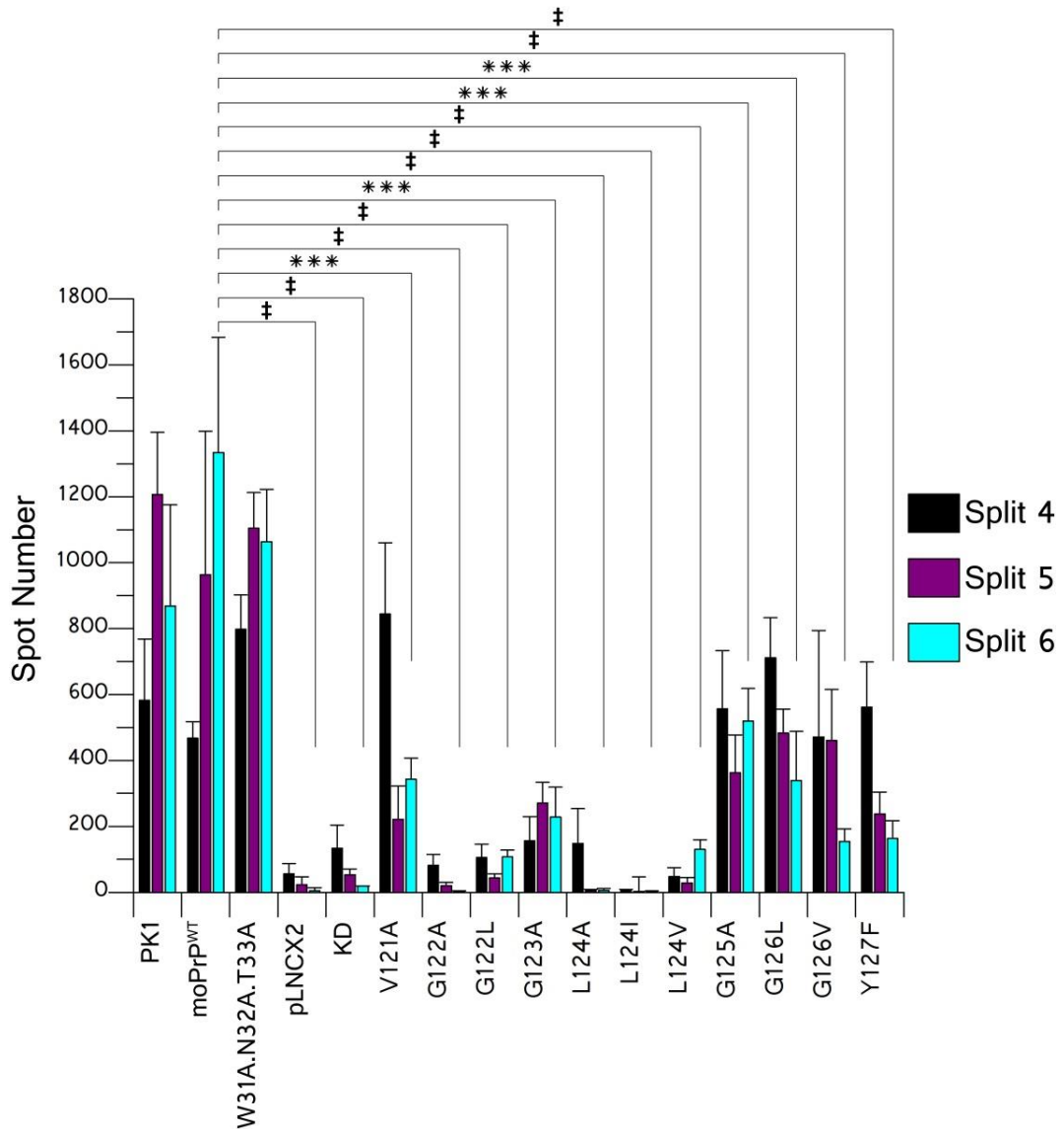


FIGURE R56: SCA ANALYSIS OF KDMoPrP^{ALA} CELLS WITH MUTATIONS IN REGION 121-127

SCA analysis of KD cells reconstituted with various mutations in moPrP. The first five cell lines represent three positive controls (PK1 cells, KD cells reconstituted with moPrP^{WT} and KD cells reconstituted with moPrP bearing a triple alanine mutation at the N-terminus); and two negative controls: KD cells reconstituted with empty vector pLNCX2 and un-reconstituted KD cells. The next 11 lines expressed moPrP bearing point mutations in sequence segment 121-127. Significance is denoted by * for $P \leq 0.005$; ** for $P \leq 0.0025$; *** for $P \leq 0.0002$ and ‡ for $P \leq 0.0001$. For clarity, significance is only shown for split 6, which is taken to be the time point with the best differential between detection of applied and *de novo* prions (Section 3.2); calculated using a one-way ANOVA plus Bonferroni correction for multiple comparisons.

three hundred for V121A and G126L; two hundred for G123A; one hundred for G122L, L124V, G126V and Y127F. Cells expressing G122A, L124A and L124I however, exhibited spot numbers comparable to negative controls (KD cells and KD cells transduced with the empty vector, pLNCX2).

Additional point mutations were made within 127-135, while one double replacement (A117R.Y127R) and two deletion mutations within the PTM domain were also tested (Table R11; Figure R57). Of the deletion mutations, the one with a smaller change, Δ 117-124 propagated RML prions better than the larger deletion construct Δ 112-129 (Figure R57).

Similar results as those observed for single amino acid changes in moPrP region 111-119 (Figure R55) and region 121-127 (Figure R56) were observed for changes made in region 127-135 of the protein (Figure R57), in that any changes made in this region reduced the ability of cells expressing these constructs to propagate prions. Other than positive control cells (PK1, moPrP^{WT} and W31A.N32A.T33A), the highest spot count at split 6 was observed for deletion mutation Δ 117-124 and point mutation G130L (approximately five hundred spots); this was followed by S131A, L129A, S132L, S134A, M128V, Y127R, R135E, Y127P Δ 112-129, A117R.Y127R and G130A (Figure R57).

Mutation	Residue ellipticity (deg cm ² dmol ⁻¹)		Initial	Final	Helix propensity	moPrP domain
	Overall change					
Y127P		-4400	18300	22700	Increased	PTM
Y127R		-6800	18300	25100	Increased	
M128L		-2400	22700	25100	Increased	
M128V		10600	22700	12100	Decreased	
L129A		0	25100	25100	Increased	
G130A		-13000	12100	25100	Increased	
G130L		10000	12100	2100	Decreased	
S131A		-8900	16200	25100	Increased	
A132L		-20600	2100	22700	Increased	
S134A		-4900	16200	21100	Increased	
R135E			.	.		
Δ112-129			.	.		
Δ117-124			.	.		

TABLE R11: MUTATIONS MADE WITHIN REGION 127-135 OF MOPrP

Mutations made within region 127-135 alter the helix propensity properties of the PTM by increasing or decreasing the helix stability of this region by varying degrees. The degree of change is indicated in the 'overall change' column where the difference between the initial and final values for the native and substituted residues is shown, based on the values provided in Table R8.

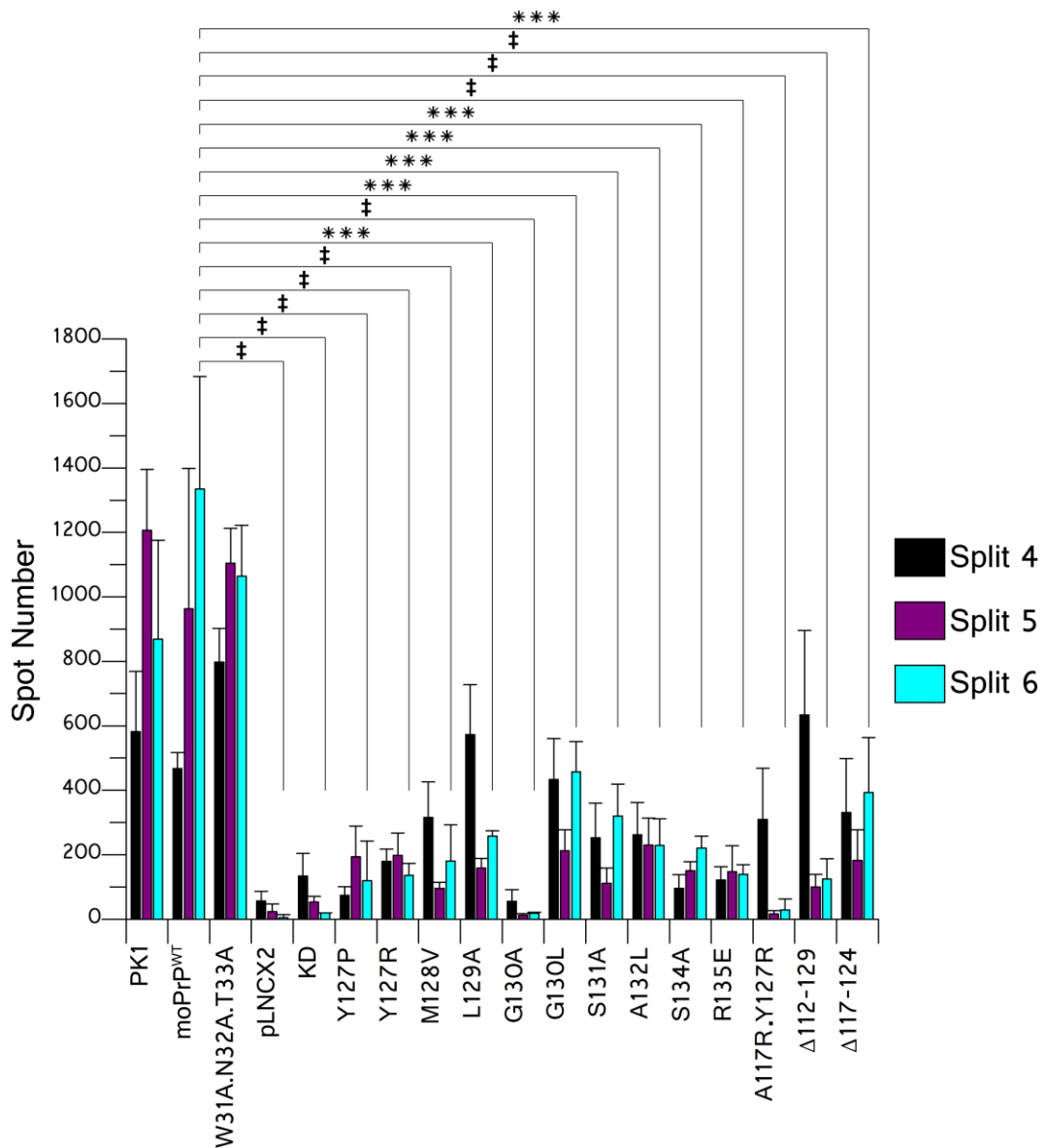


FIGURE R57: SCA ANALYSIS OF KDMoPrP^{ALA} CELLS WITH MUTATIONS IN REGION 127-135

SCA analysis of KD cells reconstituted with various mutations in the PTM region of moPrP. The first five cell lines represent three positive controls (PK1 cells, KD cells reconstituted with moPrP^{WT} and KD cells reconstituted with moPrP bearing a triple alanine mutation at the N-terminus); and two negative controls: KD cells reconstituted with empty vector pLNCX2 and un-reconstituted KD cells. The next 11 entries in the graph represent point mutations in moPrP within the segment 127-135. Significance is denoted by * for $P \leq 0.005$; ** for $P \leq 0.0025$; *** for $P \leq 0.0002$ and ‡ for $P \leq 0.0001$. For clarity, significance is only shown for split 6, which is taken to be the time point with the best differential between detection of applied and *de novo* prions (Section 3.2); calculated using a one-way ANOVA plus Bonferroni correction for multiple comparisons.

3.7.3 Does helix stability of the PTM region in moPrP correlate well with propagation efficiency?

Various mutations were made along the length of the PTM region in moPrP; KD cells were then reconstituted with these mutations and were found without exception, to reduce the propagative capacity of these cells relative to wild-type controls (Figures R55, R56 and R57).

An interesting phenomenon observed for some of the expressed mutations was a split-to-split drop in spot number which is the inverse trend of a true propagating line. This phenomenon is not well reported in the literature, with limited mentions 'acute infection' versus 'chronic infection' as described by Vorberg *et al* where levels of ProteinaseK-resistant fractions of PrP persist for a limited phase, or continue to persist long term respectively²⁸⁰. In any case, the overall analysis of the expressed mutations reveals that the levels of ProteinaseK-resistant PrP are significantly reduced in cells expressing PTM mutations at split 6. This does not correlate with the predicted effects on helical propensity, i.e. mutations that showed the most severe inhibition of propagation included A117L, A117R, A119P (Figure R53), G122A, L124A, L124I (Figure R54), G130A and Δ 112-129 (Figure R55) – which represent both changes to increase and decrease helical propensity, and in each case, is altered by varying amounts (Tables R9, R10 and R11).

3.7.4 Probing the PrP homodimer hypothesis

Most non-covalent protein-protein interactions that occur within the membrane are mediated mainly through transmembrane domains, with specific conserved motifs driving these interactions, the most over-represented of which is the GXXXG glycine zipper motif²⁸⁹. An interesting feature of the PrP PTM domain is that this motif exists as a series of three consecutive blocks in PrP, possibly forming a glycine zipper at residues 118-130 GAVVGGLGGYMLG in moPrP²⁹⁰.

If such interactions were to occur between PrP molecules, we could hypothesise that dimer formation is mediated through its PTM domain – a finding reported independently by Warwicker²⁹¹ and Rambold⁵⁶, and further pursued for its regulation of PrP trafficking to the cell surface²⁹².

Researchers alluded to the formation of prion protein dimers as early as 1995²⁹³. Warwicker carried out molecular modelling approaches to infer the significance of PrP dimers and their membrane interactions²⁹¹. A dimer model was proposed for PrP^{Sc} formation through β -hairpin stacking for oligomer extension. Furthermore, he suggested that the large-scale rearrangements involved in dimer binding, β -hairpin stacking and extensive cross-linking could be related to the measured lag between initial binding of PrP^C to PrP^{Sc} and the attainment of ProteinaseK-resistance²⁹¹, which is the readout for PrP^{Sc} formation by most conventional prion detection assays. Here, we attempted to investigate the possibility of PrP homodimer formations and designed mutations that would disrupt its formation.

A helix homodimer model of the human prion protein was generated by Laszlo Hosszu within the department, using PyMol software (Figure R58). The PTM region is shown within residues 111-135 aligned in parallel, using Molecular modelling programs BUDE (University of Bristol; program under development) and GrammX²⁹⁴ (Figure R58). This revealed residues A119, Y127 and G130 as being within 3Å distance of each other when analysed in BUDE (Figure R58, A) and V111, A115, G130, S134 and R135 observed within 3Å of one other when analysed in GrammX (Figure R58, B).

We could thus hypothesise that if homodimer associations occur in the cell and their maintenance is important for prion propagation, then introducing amino acid changes at positions where the side chains between the dimers are in close proximity would result in a reduction in spot number as measured by SCA. Using the moPrP mutation constructs available in the moPrP mutagenesis library (Table R1), SCA data for these PTM region mutations was revisited (Figures R55, R56 and R57) in the context of the homodimer hypothesis. Mutations tested in the PTM region included replacements that were made to increase or decrease helix propensity, introduce instability within the helix, and break the PTM helix (Figures R55, R56 and R57). Replacements that resulted in spot numbers below two hundred at split 6 are summarised below (Figure R58).

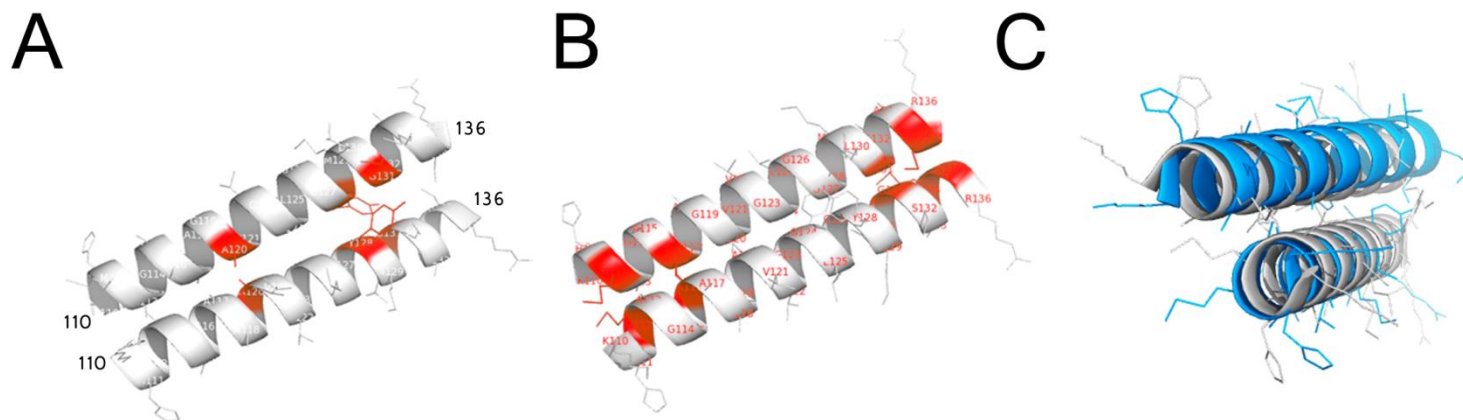


FIGURE R58: MOLECULAR MODELLING OF THE PTM REGION 110-136 IN THE HUMAN PRION PROTEIN

Molecular modelling of the PTM region 110-136 of the human prion protein (huPrP), with homodimers shown in: (A) BUDE; (B) GrammX; (C) overlay of models generated in BUDE (blue) and GrammX (grey). Residues highlighted in red in (A) and (B) are calculated to be within 3Å of one another and thus mutations made at these sites are predicted to interfere with possible dimer formation. (Note: since modelling was carried out on the human prion protein sequence, all residues indicated here represent the same in the mouse sequence +1, i.e. R135 in moPrP is equivalent to R136 in huPrP). Residues highlighted in red for (A) include A120, Y128 and G131; for (B), residues in red are V112, A116, G131, S134 and R135. This corresponds to residues A119, Y127 and G130A for (A) and V111, A115, G130, M133 and S134 for (B) in the mouse prion protein sequence.

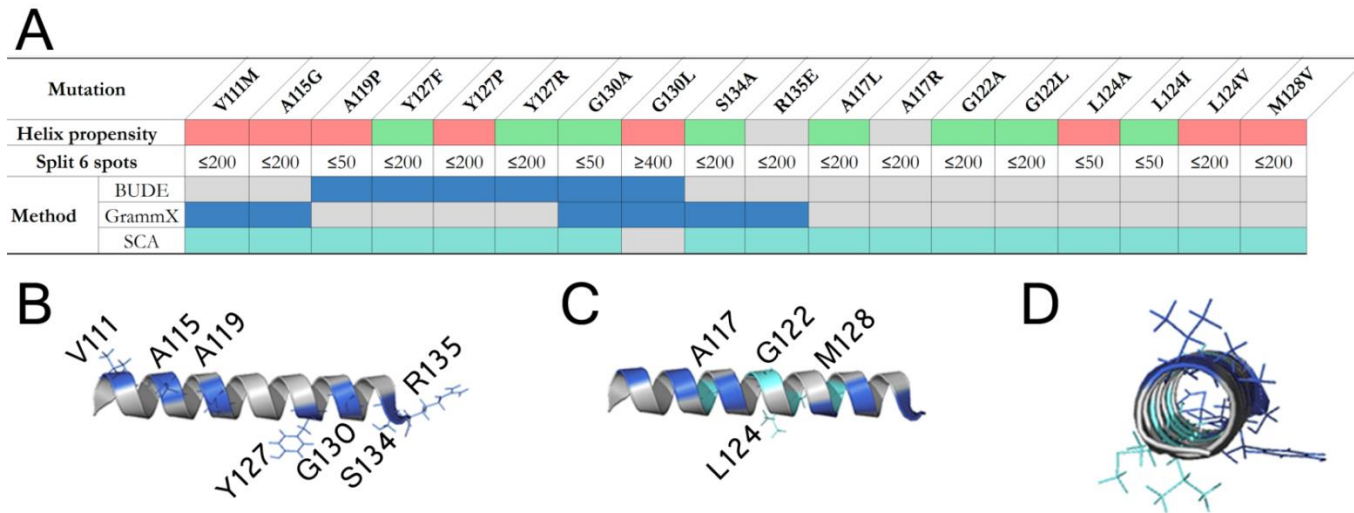


FIGURE R59: SUMMARY OF SITES WITHIN THE PTM DOMAIN PREDICTED TO DISRUPT DIMER FORMATION, MATCHED TO SCA DATA

Combined summary of BUDE, GrammX and SCA results. (A) Table showing the effects of the generated mutations on helix propensity of the PTM domain: red – decreased; green – increased. Split 6 spots refer to PK-resistant spots detected following RML infection of KD cells reconstituted with moPrP bearing the indicated mutations. Cells reporting spot numbers below 200 are considered to be severely restricted in their propagation capacity. Those with spot numbers below 50 are considered to no longer support prion propagation at split 6. BUDE and GrammX molecular docking programs were used to predict residues within 3Å of each other in a PrP homodimer model: highlighted in blue in (A-D). Mutations tested by SCA that reported split 6 spot numbers equalling or lower than 200 are indicated in cyan (A-D). (B) The amino acid sequence of moPrP PTM region was entered into PyMol (KHVAGAAAAGAVVGGGLGGYMLGSAVSR) and a helix built from this; shown in blue are the residues predicted to be within 3Å of each other. (C) Using the helix generated in (B), residues in cyan denote sites found to significantly reduce propagation when mutated, as tested by SCA, but not predicted by BUDE or GrammX as being spatially proximal (3Å) in the helix dimer model. (D) End-on view of the generated helix, highlighting two faces (blue and cyan) that when mutated, severely impact prion propagation.

Indeed, spot numbers for residues predicted to be within 3Å of one another (by BUDE and GrammX) were below the two hundred mark as analysed by SCA and thus labelled as mutations that result in severely limited propagation (Figure R12). G130L was the only exception with more than four hundred spots, but G130A was the only mutation predicted to affect dimer formation by both docking programs and confirmed as reducing propagation in SCA (Figure R59). SCA revealed additional sites within the PTM domain – not predicted to interfere with the homodimer interface – that when altered, resulted in severely limited propagation: A117L/R, G122A/L, L124A/I/V and M128V (Figure R59, C). When results of residues predicted to be in close proximity as observed in the peptide docking models of BUDE and GrammX were combined with SCA experimental data, there appeared to be two faces of the PTM domain that were important for prion propagation (Figure R59, D).

Amino acid replacements made in this study that would disrupt GXXXG motifs include replacements made at G118, G122, G126 and G130. Of these, mutations made at G122 and G130 demonstrated the most severe inhibition of prion propagation (Figures R56 and R57). These glycines lie on the same side of the PTM helix and along the side of the helix predicted to be involved in homodimer formation (Figure R59).

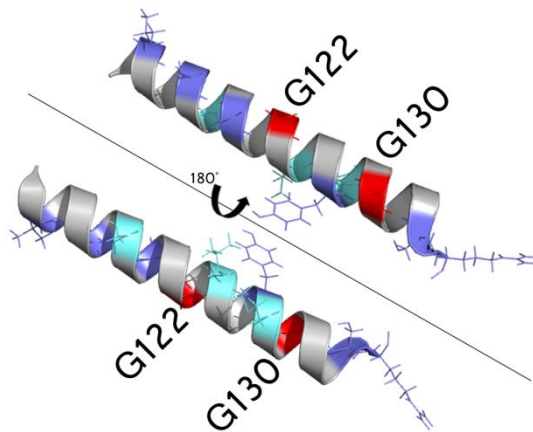


FIGURE R60: GLYCINE RESIDUES WITHIN THE PTM DOMAIN

Superimposition of G122 and G130 on PTM domain helix showing residues predicted to affect helix dimerisation, as determined by BUDE and GrammX (blue), and residues that when mutated severely impacted prion propagation as tested via SCA, but not predicted to affect dimer interface (cyan). The glycine residues of interest are better aligned to the side of the helix predicted to be involved in dimer interactions (BUDE and GrammX).

Neither alanine nor leucine replacements provide the same conformational flexibility offered by glycine, but the larger side chain of leucine makes it less amenable to helix-helix interactions in the membrane. However, when glycines at positions 122 and 130 were replaced by leucines the loss in propagation observed in cells expressing these moPrP constructs was less severe than equivalent alanine replacements (Figure R56 and R57). The reasons for this are not clear and further experiments would have to be carried out to fully characterise the interactions of the putative helix homodimer interface and reveal the underpinning role of the PTM glycines.

Harrison *et al.* showed in both cell and mouse bioassays that when glycine mutations in moPrP G118A/L/P, A119P, G122A/P, L124A and G130L/P are expressed, the ability of cells expressing these mutations to take up prions and propagate them is severely affected²⁹⁵. They further state that the glycines present within the PTM sequence constitute GXXXG motifs that could possibly function as canonical protein interaction sites²⁹⁶.

The analyses in this study revealed seven sites within the PTM domain predicted by BUDE and GrammX to be possible sites that would impact PrP-homodimer formation and, if such formation was pertinent to propagation, would also interfere with the propagation process: V111, A115, A119, Y127, G130, S134, R135. As confirmed by SCA, mutations at these sites did indeed significantly lower the capacity of cells expressing these mutations to propagate prions and revealed four additional residues: A117, G122, L124 and M128 that also reduced spot numbers, to below two hundred, when singly mutated (Figure R59). The results further show that any changes made to the PTM region of the protein poison prion

propagation, regardless of whether the change is made at a glycine residue or not. In fact, even non-glycine-to-glycine mutations, as in A115G, resulted in lowered propagation (Figure R55). Harrison *et al.* also reported that mutations G125A and G130A confer partial but not complete resistance to prion infection, as mice inoculated with lysate derived from moPrP-expressing cells with these mutations displayed no clinical signs of sickness, but immunohistochemistry on brain slices revealed presence of spongiform changes and PrP-reactive plaque deposition typical of prion disease pathology²⁹⁵.

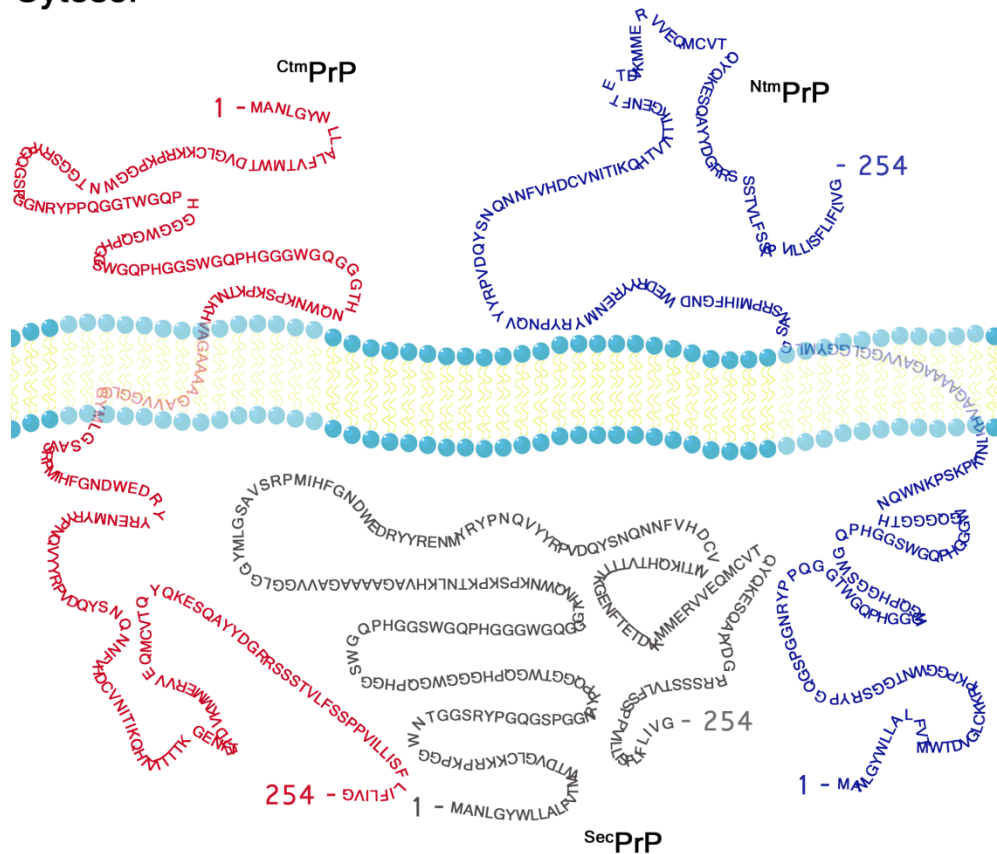
Choi *et al.* observed that anti-prion monoclonal antibody 1C5 recognises an epitope within the PTM region corresponding to the GXXXG motif in PrP^{Sc} but not PrP^{C290} and postulated that this region may play a crucial part in the initial conversion events leading up to prion propagation²⁹⁰. From the SCA data, we observed that all changes made to native glycine residues resulted in lowered prion propagation; this is in agreement with the data presented by Harrison *et al.*²⁹⁵ and give further evidence for the contributions of G122 and G130 to prion propagation.

3.7.5 PTM as a determinant of PrP-membrane association

The prion protein is a GPI-anchored glycoprotein tethered to the outer leaflet of the lipid bilayer. However, numerous reports have alluded to single-spanning transmembrane forms of the protein where it uses a middle highly hydrophobic sequence to associate with the ER membrane⁶³. The phenomenon of PrP existing both as secreted and transmembrane forms was first alluded to by Hay *et al.*²⁹⁷, further investigated in terms of prion protein biogenesis²⁹⁸⁻³⁰⁰ and fully characterised eight years later by Hegde *et al.*⁶³.

Three forms of PrP topology were identified at the ER: PrP^{Ctm}, where the C-terminal half of the protein is inside the ER lumen; PrP^{Ntm}, where the N-terminal half of the protein is in the ER lumen and PrP^{Sec} that represents the fully secreted protein, with no association to the ER membrane⁶³ (Figure R61). Note that these forms of PrP refer to the nascent polypeptide during protein biogenesis and its orientation across the ER membrane; it is not to be confused with the fully mature protein that is known to be GPI-anchored at the cell surface. The PTM domain has been shown to insert itself in the ER membrane in either an N-to-C or C-to-N terminus orientation using its hydrophobic sequence⁶³; the role of this sequence has been further investigated by introducing microdeletions and minimal mutations^{63, 152}. Amino acid substitutions in the signal sequence of the protein (residues 1-22) increased or decreased CtmPrP relative to NtmPrP and SecPrP, whereas mutations within the HC domain itself appeared to increase or decrease both CtmPrP and NtmPrP relative to SecPrP¹⁵².

Cytosol



ER Lumen

FIGURE R61: TRANSMEMBRANE FORMS OF THE PRION PROTEIN AT THE ER

A number of transmembrane forms have been reported for PrP where the protein is able to span the membrane through its putative transmembrane domain, region 111-135. Shown in red, black and blue are various forms of transmembrane PrP topologies, namely: (A) $C^{tm}PrP$; (B) $SecPrP$ and (C) $N^{tm}PrP$. Each topology shows the full peptide sequence of moPrP, inclusive of N- and C-terminal signal sequences.

The authors suggested that while the HC domain sequence determines the ratio of peptides that are membrane-associated (^{Ntm}PrP , ^{Ctm}PrP) or membrane-free at the ER (^{Sec}PrP), the signal sequence governs the proportion of transmembrane peptide that exists in the aberrant form (^{Ctm}PrP).

Here, no changes have been made to the signal sequence of moPrP, but amino acid replacements within the PTM were analysed for their prion propagation propensity (Figures R55, R56 and R57). Increased hydrophobicity of the PTM is thought to lead to increased pools of ^{Ctm}PrP and severe neurodegeneration³⁰¹. Disease-associated mutations P104L, G113V, A116V, G130V and A132V (mouse numbering) increase PTM hydrophobicity and may exert their neurotoxic effects through ^{Ctm}PrP expression. Positions G113, A116, G130 and A132 were mutated to leucine in this study.

Here, propagation was severely reduced but not abrogated in all instances with spot numbers recorded in the range of two- to four hundred (Figures R55 and R57). From SCA analyses, mutations made in the C-terminal region of the PTM domain had a more severe effect on reducing prion propagation compared to those made more N-terminally (Figure R57). Since the experiments carried out were primarily propagation-focused in terms of mutational effects, the reduced propagation profile was not fully characterised in terms of protein trafficking, making it difficult to establish direct comparisons to the formation and ratios of topological PrP assemblies.

Nonetheless, we can use data from Sauv  *et al.*³⁰² as a guide to predicting which amino acid changes would have the largest influences on association/disassociation with lipid membranes. They suggest interactions between region 111-114 at the micelle-water interface and burial of polar residues S131 and S134 within the micelle, with R135 engaged in electrostatic interactions with phosphate headgroups of the bilayer³⁰².

If the model predicted by Sauv  *et al.* holds true, mutations made at positions 111-114 have the potential to interfere with peptide interactions at the lipid surface, mutations at S131 and S134 may alter the positioning of these residues with respect to the bilayer and R135 mutations, which they postulate to be a driving force for initiating the PTM membrane insertion, would severely impact this association. Thus, if membrane association and indeed membrane insertion is critical for prion propagation, we would predict mutations at these sites to have a significant impact on RML propagation when tested via SCA (Figure R55, R56 and R57).

Mutations made between region 111-114 of moPrP PTM include V111M, A112L and G113L (Table R8). Of these, V111M appeared to have a stronger inhibitory effect on propagation compared to A112L and G113L for which propagation inhibition was comparable (Figure R59). In each case, spot numbers were comparable to moPrP^{WT} at split 4, indicative of uncompromised ability of cells expressing these mutations to be susceptible to, and replicate prions. However, propagation was not maintained as a considerable drop in spot number was observed at splits 5 and 6 (Figure R55). Mutations S134A and R135A severely inhibited propagation, giving spot numbers equal to or below two hundred (Figure R57). Analysis of

deletion mutations $\Delta 112-129$ and $\Delta 117-124$ revealed that $\Delta 117-124$ was able to propagate prions better than $\Delta 112-129$ (Figure R57) and this may highlight the importance of region 111-117 in prion propagation as mutations made here show low spot numbers (Figure R55).

This data, if applied to the model of Sauv   *et al.*, suggests that association of the PTM with lipid membranes facilitates the propagation process. In the context of PTM-lipid bilayer interactions therefore, the data presented here suggests that residues S134A and R135A have a more significant role to play in prion propagation than residues more N-terminal to this sequence (111-114) that are reported to associate with the outer layer of the lipid bilayer. This suggests then, that the stabilising interactions accomplished via R135 strongly influence prion propagation, and though association of residues 111-114 with the lipid membrane are perturbed by mutations at this site, they do not abrogate propagation (Figures R55 and R57).

All KD cells reconstituted with moPrP constructs bearing mutations in the PTM domain were viable and could be used successfully for SCA analysis (Figure R60). For some mutations however, it was not possible to prepare stable cultures of KD cells, in particular cells reconstituted with moPrP bearing mutations A115L; V120A, as there were no survivors following G418 selection. It is possible that the protein expressed in these instances was toxic to the cells as expression of these constructs could not be established in four independent attempts (Figure R62).

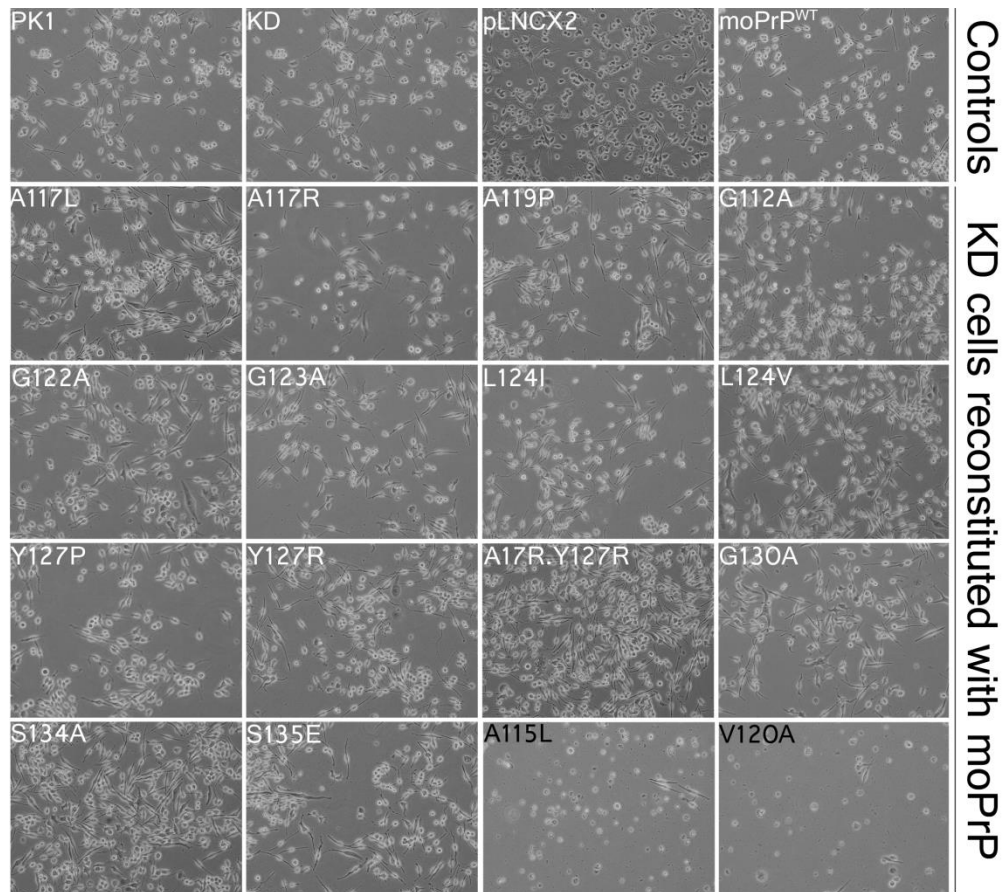


FIGURE R62: PHASE CONTRAST IMAGES OF KD CELLS RECONSTITUTED WITH MOPrP MUTATIONS IN THE PTM REGION OF THE PROTEIN. MAGNIFICATION AT X20.

The data presented here argues that a better model of PrP dimer association, both in association and without the influence of lipid bilayers could be established based on the propagation profile of the mutations analysed; additionally, the possibility of a dimer system existing *ex vivo* and not occurring in the native system should also be considered, as most reported instances of PrP dimers use inducible systems to identify the dimer interface^{56, 260, 293, 303, 304}. Indeed, protein prediction and molecular modelling programs base interactions on available structural data and cannot always emulate the complexity of protein interactions within a crowded cellular

environment, but are able to provide clues to assist further understanding of protein interactions.

In summary, analysis of moPrP mutations within the PTM domain of the protein revealed that: (i) prion propagation was reduced for some mutations (A112L, G113L, A116L, G125A, G130L and Δ 117-124), severely compromised for others (V111M, A115G, A117L/R, G122A/L, L124V, Y127F, Y127P, Y127R, M128V, S134A and S135E) and completely abrogated for a few (A119P, G130A, L124A and L124I); (ii) the severity of reduction in propagation capacity observed for the expressed mutations did not correlate with changes in helical stability, but were clustered on two faces of the helix – one of which was predicted to be at the homodimer interface; (iii) although the data presented is in agreement with that of other researchers in terms of the significance of glycine residues within the PTM²⁹⁵, and corroborates some of the interactions identified for the association of the PTM with lipid micelles³⁰², it shows that loss of propagation capacity is elicited by changes at multiple sites within the PTM and is not exclusive to glycine residues.

Chapter 4

Results summary, conclusions and future directions

4.1 Structural integrity is required for prion propagation and three sites in the N-terminal region mediate the efficacy of propagation

Following prion infection, propagation of the infectious PrP^{Sc} species occurs through recruitment of PrP^{C48}. This study and others have shown that in a cellular context, N-terminal deletion Δ 23-88 results in severely compromised propagation. However, expression of moPrP ^{Δ 23-88} in transgenic mice still culminated in disease, but with longer incubation times. In this study, expression of Δ 23-88 in the presence of the wild-type protein did not hinder prion propagation. Thus N-terminal deletions do not protect against prion infection^{128, 305}, but may mediate other aspects of PrP function (Section 3.6).

In contrast to the much debated role for the N-terminal residues, there has always been strong evidence that the C-terminal region of the prion protein forms the amyloid core in PrP^{Sc} and is largely responsible for PrP propagation, with the minimal segment that supports prion propagation – the miniprion – shown to be conversion and propagation supportive, despite bearing large deletions in the flexible N-terminal domain Δ 23-88 and part of the structured domain Δ 141-176⁷⁶.

To obtain a clearer picture of the significance of N-terminal residues on prion propagation, and to elucidate the role of surface amino acids in the C-terminal region of the prion protein, both within and outside the miniprion domain, we carried out an alanine mutagenesis screen of the mouse prion protein.

A library of alanine mutations in moPrP was generated, bearing between one and three amino acid replacements at a time. The mutations were expressed in a sub-clone of N2a (PK1) cells in which PrP expression had been silenced and their contributions to prion propagation assessed by challenging them with RML prions in the Scrapie Cell Assay (SCA). This approach provided better power compared to deletion mutagenesis, as the overall structure of the protein was (in theory) less compromised. Also, we did not express mutant PrP proteins in the presence of wild-type protein, which allowed us to assess the effect of individual mutations without interference from the endogenous protein.

Single, double and triple alanine substitutions made along the length of the moPrP ORF revealed differences in their ability to propagate RML prions depending on their position in the primary sequence of the protein. Generally, it was found that mutations within the C-terminus of the protein had a greater inhibitory effect on RML prion propagation than substitutions made in the flexible N-terminus. Exceptions of note were the charge cluster regions in the flexible N-terminus and residue Q41: when alanine replacements were made at these sites, cells expressing these mutants displayed markedly reduced prion propagation. The results highlight the importance of structural integrity in the C-terminal domain of the protein for successful prion propagation and uncover key sites within the N-terminus that regulate prion propagation.

Thus, while changes in the solvent-exposed structured region of the prion protein abrogated propagation, discrete domains within the unstructured region also regulated the efficiency of propagation. To summarise, it was

found that: (i) charge cluster regions within the flexible N-terminal region of the protein, CC1 – specifically residues K23.K24.R25 – and CC2, govern the efficiency of prion propagation alongside residue Q41, while mutations within OPR regions had no effect on propagation capacity; (ii) CC1 mutation K23A.K24A.R25A and Q41A likely hinder propagation through similar pathways as expression of K23A.K24A.R25A and Q41A on the same construct did not have an additive effect in reducing prion propagation; (iii) within the flexible region of the protein only CC2, but not CC1, Q41A, or Δ 23-88 mutations, were able to exert a dominant negative effect on prion propagation; (iv) Alanine replacements in N-terminal regions such as K23A.K24A.R25A nor those tested in CC2 were able to cure chronically RML-infected cells. (iv) in region 123-230 moPrP, no particular ‘face’ when mutated to alanine, showed preference for propagation over another – all mutations tested severely limited prion propagation, suggesting that structural integrity in this region is key to propagative efficiency; this was further exemplified by mutations within the hydrophobic core of the protein, which displayed equally poor propagation; (v) probing the interactions in the PTM domain of the protein showed that increasing or decreasing the helical propensity within this region did not correlate with changes in propagation. However, most of the point mutations made in this region that severely limited or abrogated propagation were on two faces of the PTM helix, and provided some evidence in favour of a dimerisation model.

Taken together, the mutagenic screen of the mouse prion protein showed that structural integrity is crucial to prion propagation and that propagation

efficiency is regulated by specific interactions at discrete residues within the flexible N-terminus (Figure C1).

Numerous studies have reported that the prion protein interacts with A β oligomers^{106, 107, 121, 132, 139} and that the primary A β oligomer binding site on PrP is located within CC2 (90-111)^{106, 121}, with CC1 (23-27) also thought to play an auxiliary role in binding^{106, 107}. It was shown here that CC1 mutation K23A.K24A.R25A, Q41 and all mutations made in the CC2 region significantly reduce the capacity of cells expressing these constructs to propagate prions, highlighting these regions of the protein as modulators of prion propagation. Chen *et al.* reported that deletion Δ 23-89 in human PrP displayed no binding to A β , whereas Δ 51-91 and Δ 111-125 showed binding characteristics similar to wild-type PrP. They also demonstrated a greater loss of A β binding in Δ 23-50 compared to CC1 deletion Δ 23-27¹⁰⁶. Superimposing the data obtained from our study with the A β binding sites on PrP, it could be postulated that if similar motifs are involved in aberrant PrP processing during prion infection and PrP-A β interactions, then the increased loss of A β binding observed in Δ 23-50 may have been due to the loss of Q41 contributions. Note that Q41 has never been quoted as a residue on PrP that contributes to A β oligomer bindings, despite the findings of Chen *et al.*¹⁰⁶ or reports by Kang *et al.*, who showed in an epitope mapping immunoassay that residues 23-40 represent one of three A β binding sites within the prion protein¹⁴⁰.

4.2 Conclusions and final remarks

The results presented here clearly highlight that the integrity of the structured 123-230 domain is critical for efficient propagation of RML prions and confirms previous findings that implicate this segment as the crucial entity in PrP^{Sc} formation. Importantly, this study identified residues 90-111 of the CC2 region as strong modulators of propagation efficacy, as minimal mutations in this region exerted severe limitations on prion propagation. Finally, these results show that in addition to CC2, Q41 and CC1 also regulate prion propagation, but to a lesser extent than CC2 or the structured domain of the protein. CC1 and Q41 most likely mediate events that promote but are not essential for successful maintenance of prion propagation, whereas CC2 may be more directly involved with PrP^{Sc} interactions such that initiation of propagation is compromised in cells expressing moPrP with CC2 alanine mutations.

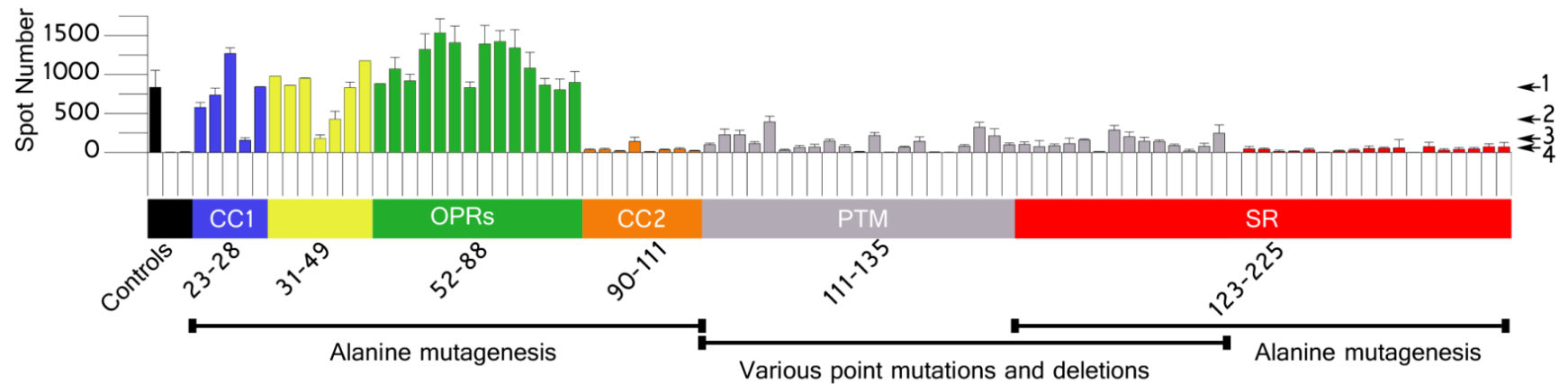


FIGURE C1: OVERALL SUMMARY OF CUMULATIVE SCA DATA ON KDMoPrP^{ALA} CELLS

Overall summary of cumulative SCA data showing spot numbers observed at split 6; this graph provides a prion propagation landscape for the length of the mouse prion protein as tested via mutagenic approaches used in this study. The first three black bars represent KDmoPrP^{WT}, KD and KDmoPrP^{Δ23-88} cell lines, respectively. All the other bars represent KD cells reconstituted with moPrP bearing various mutations (alanine replacement, other amino acid substitutions and deletions). Arrows on the right-hand side labelled 1-4 represent (1) 800 spots – full propagation; (2) 400 spots – reduced propagation; (3) 200 spots – severely limited propagation; (4) 50 spots – abrogation of prion propagation. CC1: charge cluster 1; OPRs: octapeptide repeats; CC2: charge cluster 2; PTM: putative transmembrane domain; SR: structured region. There is an overlap in residues tested between the PTM and SR. Bars are shown for mutagenesis in the PTM region where overlap exists, as this analysis covered more point mutations, whereas triple mutations were tested in the SR region that were not always sequential. It is important to note that within CC1, only triple mutation K23A.K24A.R25A, but not single mutations within this region, significantly lowered propagation.

4.3 Future directions

It is important to note that this study used one combination of cell line and prion strain, that is, PK1 cells and RML prions respectively. This is a powerful combination due to the sensitivity afforded by these cells to RML prions. However, to elucidate whether the findings of the study are cell- and strain- specific, or whether a general feature of prion propagation has been uncovered, the same screen must be carried out on a different cell type with a prion strain that is biochemically distinct from RML prions, such as 22L or Me7 prions. Furthermore, by lowering parameters such as the dose of infectious inocula applied and the number of cells seeded for the ELISPOT assay, the existing mutagenesis library could be assayed for mutations that confer increased prion propagation, either using SCA or SCEPA formats for analysis and investigate whether there are any correlations to the current study. Additionally, we believe the overlap in findings that identify residues 23-25, 41 and 90-111 as key mediators of propagation, and residues 23-37, 23-50 and 95-110 in as playing an important role in PrP-A β oligomer binding is striking^{106, 140}. The available library of moPrP alanine mutants could be used to better characterise this interaction and further pursue the cellular implication of this association. Over the years a number of PrP binding partners have been identified by a variety of methods such as yeast two-hybrid screening, co-immunoprecipitation, cross-linking and proteomics approaches. Despite this, the biological significance of such interactions in prion infection and propagation is not totally clear. Since the differences in propagation between KD cells reconstituted with moPrP^{WT} or moPrP^{Ala} with changes in

the CC2 domain were so stark, it is possible that different sets of interacting partners could be identified from them. It would be interesting to characterise such binding partners to identify key changes in protein complexes obtained from these cell lines, both pre- and post- prion infection (Figure C2). Rutishauser *et al.* have shown correct protein sorting, GPI-anchor attachment and cell surface expression for a Myc-tagged PrP construct¹⁹⁵. Using a similar strategy, we could express alanine mutants of interest on tagged moPrP, follow the prion propagation profiles of the tagged constructs and probe for any correlations with cellular interacting proteins – protein complex constituents could be identified using co-immunoprecipitation followed by mass spectrometry. Depending on the success of identifying differential binding partners for moPrP^{WT} and moPrP^{Ala}, experiments could be undertaken to determine if such factors contribute to efficient infection or propagation. Such characterisation of the protein and its interactors, both in the infected and non-infected states, may allow for elucidation of a cellular propagation pathway (Figure C2). This could potentially be taken forward to *in vivo* studies to identify critical components for PrP^{Sc} propagation. Should PrP interacting factors that affect *in vitro* prion propagation be identified, upon silencing or overexpression of such factors, the roles they play in prion propagation may be investigated in mouse models null for these factors.

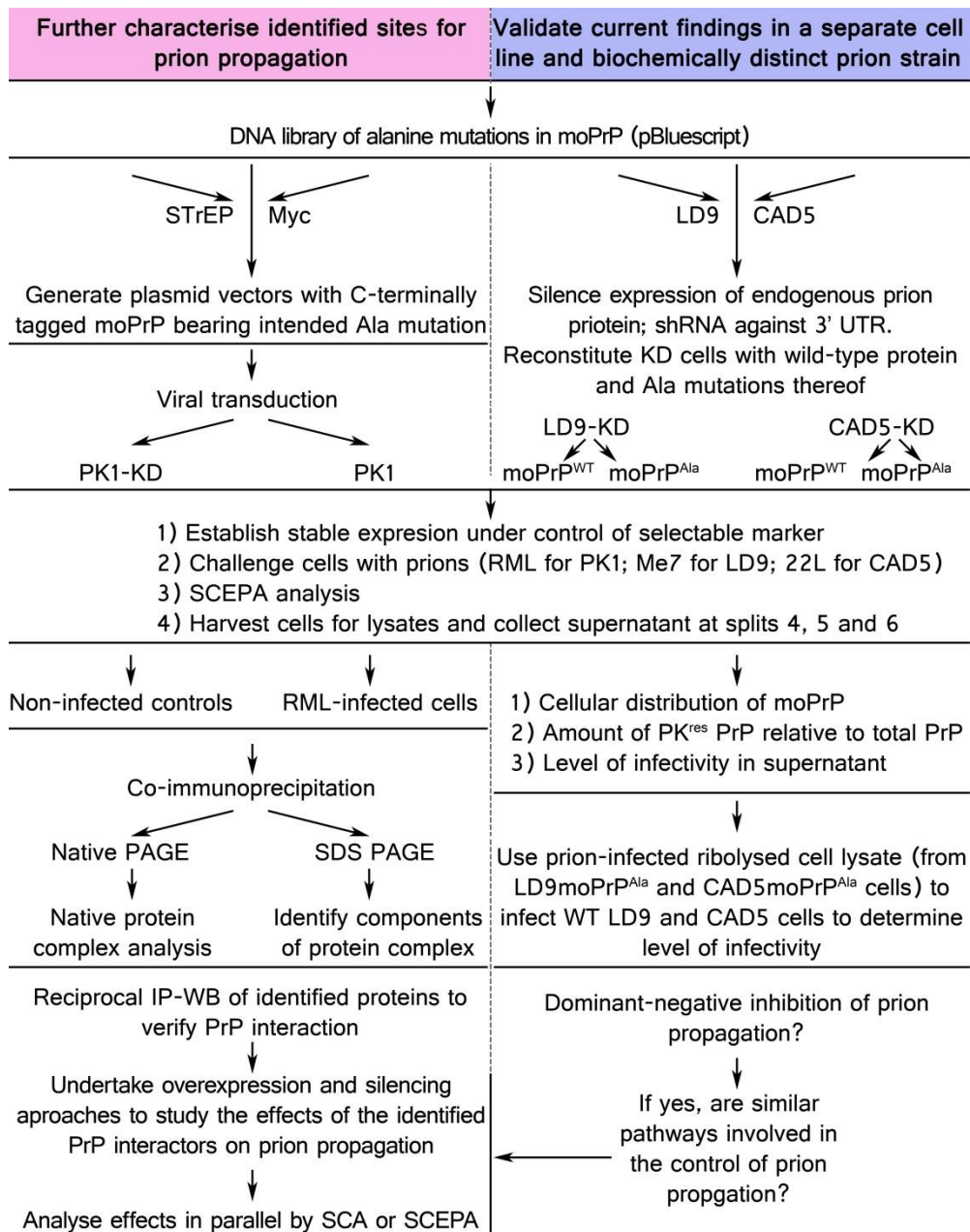


FIGURE C2: FUTURE DIRECTIONS

Proposed future work following the findings of the current study. moPrP (mouse prion protein), STrEP (streptavidin tag), Myc (polypeptide tag derived from c-Myc) UTR (untranslated region), KD (knockdown) PK^{res} (ProteinaseK-resistant). IP (immunoprecipitation), WB (western blot). SCEPA (Scrapie cell end-point assay), SCA (Scrapie cell assay). PAGE (polyacrylamide gel electrophoresis).

Chapter 5

References

Reference List

1. Voisine,C., Pedersen,J.S., & Morimoto,R.I. Chaperone networks: tipping the balance in protein folding diseases. *Neurobiol Dis* **40**, 12-20 (2010).
2. Loftfield,R.B. & Vanderjagt,D. The frequency of errors in protein biosynthesis. *Biochem J* **128**, 1353-1356 (1972).
3. Chiti,F., Stefani,M., Taddei,N., Ramponi,G., & Dobson,C.M. Rationalization of the effects of mutations on peptide and protein aggregation rates. *Nature* **424**, 805-808 (2003).
4. Hohn,T.J. & Grune,T. The proteasome and the degradation of oxidized proteins: Part III-Redox regulation of the proteasomal system. *Redox Biol* **2**, 388-394 (2014).
5. Eisenberg,D. & Jucker,M. The amyloid state of proteins in human diseases. *Cell* **148**, 1188-1203 (2012).
6. Prusiner,S.B. Biology and genetics of prions causing neurodegeneration. *Annu Rev Genet* **47**, 601-623 (2013).
7. Anfinsen,C.B. Principles that govern the folding of protein chains. *Science* **181**, 223-230 (1973).
8. McMorran,L.M., Brockwell,D.J., & Radford,S.E. Mechanistic studies of the biogenesis and folding of outer membrane proteins in vitro and in vivo: What have we learned to date? *Arch Biochem Biophys*(2014).
9. Feldman,D.E. & Frydman,J. Protein folding in vivo: the importance of molecular chaperones. *Curr Opin Struct Biol* **10**, 26-33 (2000).
10. Frydman,J., Nimmegern,E., Ohtsuka,K., & Hartl,F.U. Folding of nascent polypeptide chains in a high molecular mass assembly with molecular chaperones. *Nature* **370**, 111-117 (1994).
11. Saibil,H. Chaperone machines for protein folding, unfolding and disaggregation. *Nat Rev Mol Cell Biol* **14**, 630-642 (2013).
12. Hardy,J.A. & Higgins,G.A. Alzheimer's disease: the amyloid cascade hypothesis. *Science* **256**, 184-185 (1992).
13. Bolshette,N.B. *et al.* Protein folding and misfolding in the neurodegenerative disorders: A review. *Rev Neurol (Paris)*(2014).
14. Astbury,W.T., Dickinson,S., & Bailey,K. The X-ray interpretation of denaturation and the structure of the seed globulins. *Biochem J* **29**, 2351-2360 (1935).
15. Glenner,G.G. *et al.* Creation of "amyloid" fibrils from Bence Jones proteins in vitro. *Science* **174**, 712-714 (1971).

16. Cuanalo-Contreras,K., Mukherjee,A., & Soto,C. Role of Protein Misfolding and Proteostasis Deficiency in Protein Misfolding Diseases and Aging. *Int J Cell Biol* **2013**, 638083 (2013).
17. Onuchic,J.N., Luthey-Schulten,Z., & Wolynes,P.G. Theory of protein folding: the energy landscape perspective. *Annu Rev Phys Chem* **48**, 545-600 (1997).
18. Udgaonkar,J.B. Polypeptide chain collapse and protein folding. *Arch Biochem Biophys* **531**, 24-33 (2013).
19. Giachin,G., Biljan,I., Ilc,G., Plavec,J., & Legname,G. Probing early misfolding events in prion protein mutants by NMR spectroscopy. *Molecules* **18**, 9451-9476 (2013).
20. Goldschmidt,L., Teng,P.K., Riek,R., & Eisenberg,D. Identifying the amyloids, proteins capable of forming amyloid-like fibrils. *Proc Natl Acad Sci U S A* **107**, 3487-3492 (2010).
21. Williams,A.J. & Paulson,H.L. Polyglutamine neurodegeneration: protein misfolding revisited. *Trends Neurosci* **31**, 521-528 (2008).
22. McDonnell,A.V., Jiang,T., Keating,A.E., & Berger,B. Paircoil2: improved prediction of coiled coils from sequence. *Bioinformatics* **22**, 356-358 (2006).
23. Oliveberg,M. Waltz, an exciting new move in amyloid prediction. *Nat Methods* **7**, 187-188 (2010).
24. Fernandez-Escamilla,A.M., Rousseau,F., Schymkowitz,J., & Serrano,L. Prediction of sequence-dependent and mutational effects on the aggregation of peptides and proteins. *Nat Biotechnol* **22**, 1302-1306 (2004).
25. Trovato,A., Seno,F., & Tosatto,S.C. The PASTA server for protein aggregation prediction. *Protein Eng Des Sel* **20**, 521-523 (2007).
26. Calamai,M., Tartaglia,G.G., Vendruscolo,M., Chiti,F., & Dobson,C.M. Mutational analysis of the aggregation-prone and disaggregation-prone regions of acylphosphatase. *J Mol Biol* **387**, 965-974 (2009).
27. Toombs,J.A. *et al.* De novo design of synthetic prion domains. *Proc Natl Acad Sci U S A* **109**, 6519-6524 (2012).
28. Tsolis,A.C., Papandreou,N.C., Iconomidou,V.A., & Hamodrakas,S.J. A consensus method for the prediction of 'aggregation-prone' peptides in globular proteins. *PLoS One* **8**, e54175 (2013).
29. Forman-Kay,J.D. & Mittag,T. From sequence and forces to structure, function, and evolution of intrinsically disordered proteins. *Structure* **21**, 1492-1499 (2013).
30. Kosol,S., Contreras-Martos,S., Cedeno,C., & Tompa,P. Structural characterization of intrinsically disordered proteins by NMR spectroscopy. *Molecules* **18**, 10802-10828 (2013).

31. Beland,M. & Roucou,X. The prion protein unstructured N-terminal region is a broad-spectrum molecular sensor with diverse and contrasting potential functions. *J Neurochem* **120**, 853-868 (2012).
32. Cho,H.S. *et al.* Yeast heat shock transcription factor N-terminal activation domains are unstructured as probed by heteronuclear NMR spectroscopy. *Protein Sci* **5**, 262-269 (1996).
33. Garcia-Mayoral,M.F. *et al.* The solution structure of the N-terminal domain of human tubulin binding cofactor C reveals a platform for tubulin interaction. *PLoS One* **6**, e25912 (2011).
34. Sharma,A. *et al.* Evaluation of sequence features from intrinsically disordered regions for the estimation of protein function. *PLoS One* **9**, e89890 (2014).
35. Oldfield,C.J. & Dunker,A.K. Intrinsically Disordered Proteins and Intrinsically Disordered Protein Regions. *Annu Rev Biochem*(2014).
36. Dunker,A.K. *et al.* Intrinsically disordered protein. *J Mol Graph. Model.* **19**, 26-59 (2001).
37. Brown,D.R. Prions and manganese: A maddening beast. *Metallomics* **3**, 229-238 (2011).
38. Taylor,D.R., Watt,N.T., Perera,W.S., & Hooper,N.M. Assigning functions to distinct regions of the N-terminus of the prion protein that are involved in its copper-stimulated, clathrin-dependent endocytosis. *J Cell Sci* **118**, 5141-5153 (2005).
39. Dillin,A. & Cohen,E. Ageing and protein aggregation-mediated disorders: from invertebrates to mammals. *Philos. Trans R Soc Lond B Biol Sci* **366**, 94-98 (2011).
40. Sawaya,M.R. *et al.* Atomic structures of amyloid cross-beta spines reveal varied steric zippers. *Nature* **447**, 453-457 (2007).
41. Haass,C. & Selkoe,D.J. Soluble protein oligomers in neurodegeneration: lessons from the Alzheimer's amyloid beta-peptide. *Nat Rev Mol Cell Biol* **8**, 101-112 (2007).
42. Last,N.B. & Miranker,A.D. Common mechanism unites membrane poration by amyloid and antimicrobial peptides. *Proc Natl Acad Sci U S A* **110**, 6382-6387 (2013).
43. Bubeck,D. The making of a macromolecular machine: assembly of the membrane attack complex. *Biochemistry*(2014).
44. Prusiner,S.B. Novel proteinaceous infectious particles cause scrapie. *Science* **216**, 136-144 (1982).
45. Crick,F. Central dogma of molecular biology. *Nature* **227**, 561-563 (1970).

46. Morales,R., Abid,K., & Soto,C. The prion strain phenomenon: molecular basis and unprecedented features. *Biochim Biophys Acta* **1772**, 681-691 (2007).
47. Benetti,F., Geschwind,M.D., & Legname,G. De novo prions. *F1000. Biol Rep* **2**, (2010).
48. Weissmann,C. & Flechsig,E. PrP knock-out and PrP transgenic mice in prion research. *Br Med Bull* **66**, 43-60 (2003).
49. Oliveira-Martins,J.B. *et al.* Unexpected tolerance of alpha-cleavage of the prion protein to sequence variations. *PLoS One* **5**, e9107 (2010).
50. McDonald,A.J., Dibble,J.P., Evans,E.G., & Millhauser,G.L. A New Paradigm for Enzymatic Control of alpha-Cleavage and beta-Cleavage of the Prion Protein. *J Biol Chem* **289**, 803-813 (2014).
51. Lloyd,S., Mead,S., & Collinge,J. Genetics of prion disease. *Top Curr Chem* **305**, 1-22 (2011).
52. Sandberg,M.K., Al Doujaily,H., Sharps,B., Clarke,A.R., & Collinge,J. Prion propagation and toxicity in vivo occur in two distinct mechanistic phases. *Nature* **470**, 540-542 (2011).
53. Morrison,K.L. & Weiss,G.A. Combinatorial alanine-scanning. *Curr Opin Chem Biol* **5**, 302-307 (2001).
54. van Rheede,T., Smolenaars,M.M., Madsen,O., & de Jong,W.W. Molecular evolution of the mammalian prion protein. *Mol Biol Evol.* **20**, 111-121 (2003).
55. Fleisch,V.C. *et al.* Targeted mutation of the gene encoding prion protein in zebrafish reveals a conserved role in neuron excitability. *Neurobiol Dis* **55**, 11-25 (2013).
56. Rambold,A.S. *et al.* Stress-protective signalling of prion protein is corrupted by scrapie prions. *EMBO J* **27**, 1974-1984 (2008).
57. Elmallah,M.I., Borgmeyer,U., Betzel,C., & Redecke,L. Impact of methionine oxidation as an initial event on the pathway of human prion protein conversion. *Prion* **7**, 404-411 (2013).
58. Hooper,N.M., Taylor,D.R., & Watt,N.T. Mechanism of the metal-mediated endocytosis of the prion protein. *Biochem Soc Trans* **36**, 1272-1276 (2008).
59. Singh,N., Das,D., Singh,A., & Mohan,M.L. Prion protein and metal interaction: physiological and pathological implications. *Curr Issues Mol Biol* **12**, 99-107 (2010).
60. Resenberger,U.K. *et al.* The cellular prion protein mediates neurotoxic signalling of beta-sheet-rich conformers independent of prion replication. *EMBO J* **30**, 2057-2070 (2011).

61. Um,J.W. *et al.* Metabotropic glutamate receptor 5 is a coreceptor for Alzheimer abeta oligomer bound to cellular prion protein. *Neuron* **79**, 887-902 (2013).
62. Puig,B., Altmeyden,H., & Glatzel,M. The GPI-anchoring of PrP: Implications in sorting and pathogenesis. *Prion* **8**, (2014).
63. Hegde,R.S. *et al.* A transmembrane form of the prion protein in neurodegenerative disease. *Science* **279**, 827-834 (1998).
64. Wang,F. *et al.* Role of the highly conserved middle region of prion protein (PrP) in PrP-lipid interaction. *Biochemistry* **49**, 8169-8176 (2010).
65. Zahn,R. *et al.* NMR solution structure of the human prion protein. *Proc Natl Acad Sci U S A* **97**, 145-150 (2000).
66. Abskharon,R.N. *et al.* Probing the N-terminal beta-sheet conversion in the crystal structure of the human prion protein bound to a nanobody. *J Am Chem Soc* **136**, 937-944 (2014).
67. Biljan,I. *et al.* Toward the molecular basis of inherited prion diseases: NMR structure of the human prion protein with V210I mutation. *J Mol Biol* **412**, 660-673 (2011).
68. Serpa,J.J. *et al.* Using multiple structural proteomics approaches for the characterization of prion proteins. *J Proteomics* **81**, 31-42 (2013).
69. Collinge,J. & Clarke,A.R. A general model of prion strains and their pathogenicity. *Science* **318**, 930-936 (2007).
70. Fernandez-Borges,N. *et al.* Naturally prion resistant mammals: a utopia? *Prion* **6**, 425-429 (2012).
71. Supattapone,S. *et al.* Identification of two prion protein regions that modify scrapie incubation time. *J Virol* **75**, 1408-1413 (2001).
72. Roucou,X., Guo,Q., Zhang,Y., Goodyer,C.G., & LeBlanc,A.C. Cytosolic prion protein is not toxic and protects against Bax-mediated cell death in human primary neurons. *J Biol Chem* **278**, 40877-40881 (2003).
73. Naslavsky,N. *et al.* Sphingolipid depletion increases formation of the scrapie prion protein in neuroblastoma cells infected with prions. *J Biol Chem* **274**, 20763-20771 (1999).
74. Di Natale,G. *et al.* Membrane interactions and conformational preferences of human and avian prion N-terminal tandem repeats: the role of copper(II) ions, pH, and membrane mimicking environments. *J Phys Chem B* **114**, 13830-13838 (2010).
75. Tagliavini,F. *et al.* Synthetic peptides homologous to prion protein residues 106-147 form amyloid-like fibrils in vitro. *Proc Natl Acad Sci U S A* **90**, 9678-9682 (1993).

76. Bonetto,V. *et al.* Synthetic miniprion PrP106. *J Biol Chem* **277**, 31327-31334 (2002).
77. Chatterjee,B. *et al.* Amyloid core formed of full-length recombinant mouse prion protein involves sequence 127-143 but not sequence 107-126. *PLoS One* **8**, e67967 (2013).
78. Jain,S. & Udgaonkar,J.B. Evidence for stepwise formation of amyloid fibrils by the mouse prion protein. *J Mol Biol* **382**, 1228-1241 (2008).
79. Smirnovas,V. *et al.* Structural organization of brain-derived mammalian prions examined by hydrogen-deuterium exchange. *Nat Struct Mol Biol* **18**, 504-506 (2011).
80. Singh,J. & Udgaonkar,J.B. Dissection of conformational conversion events during prion amyloid fibril formation using hydrogen exchange and mass spectrometry. *J Mol Biol* **425**, 3510-3521 (2013).
81. Tycko,R. & Wickner,R.B. Molecular structures of amyloid and prion fibrils: consensus versus controversy. *Acc. Chem Res* **46**, 1487-1496 (2013).
82. Novitskaya,V. *et al.* Probing the conformation of the prion protein within a single amyloid fibril using a novel immunoconformational assay. *J Biol Chem* **281**, 15536-15545 (2006).
83. Milanesi,L. *et al.* Direct three-dimensional visualization of membrane disruption by amyloid fibrils. *Proc Natl Acad Sci U S A* **109**, 20455-20460 (2012).
84. Jarrett,J.T. & Lansbury,P.T., Jr. Seeding "one-dimensional crystallization" of amyloid: a pathogenic mechanism in Alzheimer's disease and scrapie? *Cell* **73**, 1055-1058 (1993).
85. Zurawel,A.A. *et al.* Prion nucleation site unmasked by transient interaction with phospholipid cofactor. *Biochemistry* **53**, 68-76 (2014).
86. Ganchev,D.N., Cobb,N.J., Surewicz,K., & Surewicz,W.K. Nanomechanical properties of human prion protein amyloid as probed by force spectroscopy. *Biophys J* **95**, 2909-2915 (2008).
87. Qi,X., Moore,R.A., & McGuire,M.A. Dissociation of recombinant prion protein fibrils into short protofilaments: implications for the endocytic pathway and involvement of the N-terminal domain. *Biochemistry* **51**, 4600-4608 (2012).
88. Norstrom,E.M. & Mastrianni,J.A. The charge structure of helix 1 in the prion protein regulates conversion to pathogenic PrPSc. *J Virol* **80**, 8521-8529 (2006).
89. Walsh,P., Simonetti,K., & Sharpe,S. Core structure of amyloid fibrils formed by residues 106-126 of the human prion protein. *Structure* **17**, 417-426 (2009).

90. Makin,O.S., Atkins,E., Sikorski,P., Johansson,J., & Serpell,L.C. Molecular basis for amyloid fibril formation and stability. *Proc Natl Acad Sci U S A* **102**, 315-320 (2005).
91. Head,M.W. Human prion diseases: molecular, cellular and population biology. *Neuropathology* **33**, 221-236 (2013).
92. Thompson,A.G. *et al.* The Medical Research Council prion disease rating scale: a new outcome measure for prion disease therapeutic trials developed and validated using systematic observational studies. *Brain* **136**, 1116-1127 (2013).
93. Flechsig,E. *et al.* Expression of truncated PrP targeted to Purkinje cells of PrP knockout mice causes Purkinje cell death and ataxia. *EMBO J* **22**, 3095-3101 (2003).
94. Mahal,S.P. *et al.* Prion strain discrimination in cell culture: the cell panel assay. *Proc Natl Acad Sci U S A* **104**, 20908-20913 (2007).
95. Mahal,S.P., Demczyk,C.A., Smith,E.W., Jr., Klohn,P.C., & Weissmann,C. Assaying prions in cell culture: the standard scrapie cell assay (SSCA) and the scrapie cell assay in end point format (SCEPA). *Methods Mol Biol* **459**, 49-68 (2008).
96. Eklund,C.M., Kennedy,R.C., & Hadlow,W.J. Pathogenesis of scrapie virus infection in the mouse. *J Infect Dis* **117**, 15-22 (1967).
97. Klohn,P.C., Stoltze,L., Flechsig,E., Enari,M., & Weissmann,C. A quantitative, highly sensitive cell-based infectivity assay for mouse scrapie prions. *Proc Natl Acad Sci U S A* **100**, 11666-11671 (2003).
98. Krauss,S. & Vorberg,I. Prions Ex Vivo: What Cell Culture Models Tell Us about Infectious Proteins. *Int J Cell Biol* **2013**, 704546 (2013).
99. Grassmann,A., Wolf,H., Hofmann,J., Graham,J., & Vorberg,I. Cellular aspects of prion replication in vitro. *Viruses* **5**, 374-405 (2013).
100. Goold,R. *et al.* Rapid cell-surface prion protein conversion revealed using a novel cell system. *Nat Commun* **2**, 281 (2011).
101. Ushiki-Kaku,Y. *et al.* Different antigenicities of the N-terminal region of cellular and scrapie prion proteins. *Microbiol Immunol* **57**, 792-796 (2013).
102. Parkyn,C.J. *et al.* LRP1 controls biosynthetic and endocytic trafficking of neuronal prion protein. *J Cell Sci* **121**, 773-783 (2008).
103. Pan,T. *et al.* Cell-surface prion protein interacts with glycosaminoglycans. *Biochem J* **368**, 81-90 (2002).
104. Osiecka,K.M. *et al.* Prion protein region 23-32 interacts with tubulin and inhibits microtubule assembly. *Proteins* **77**, 279-296 (2009).

105. Laurén,J., Gimbel,D.A., Nygaard,H.B., Gilbert,J.W., & Strittmatter,S.M. Cellular prion protein mediates impairment of synaptic plasticity by amyloid-beta oligomers. *Nature* **457**, 1128-1132 (2009).
106. Chen,S., Yadav,S.P., & Surewicz,W.K. Interaction between human prion protein and amyloid-beta (Abeta) oligomers: role of N-terminal residues. *J Biol Chem* **285**, 26377-26383 (2010).
107. Fluharty,B.R. *et al.* An N-terminal fragment of the prion protein binds to amyloid-beta oligomers and inhibits their neurotoxicity in vivo. *J Biol Chem* **288**, 7857-7866 (2013).
108. Rushworth,J.V., Griffiths,H.H., Watt,N.T., & Hooper,N.M. Prion protein-mediated toxicity of amyloid-beta oligomers requires lipid rafts and the transmembrane LRP1. *J Biol Chem* **288**, 8935-8951 (2013).
109. Shyng,S.L., Heuser,J.E., & Harris,D.A. A glycolipid-anchored prion protein is endocytosed via clathrin-coated pits. *J Cell Biol* **125**, 1239-1250 (1994).
110. Shyng,S.L., Moulder,K.L., Lesko,A., & Harris,D.A. The N-terminal domain of a glycolipid-anchored prion protein is essential for its endocytosis via clathrin-coated pits. *J Biol Chem* **270**, 14793-14800 (1995).
111. Mayor,S. & Riezman,H. Sorting GPI-anchored proteins. *Nat Rev Mol Cell Biol* **5**, 110-120 (2004).
112. Linden,R. *et al.* Physiology of the prion protein. *Physiol Rev* **88**, 673-728 (2008).
113. Warner,R.G., Hundt,C., Weiss,S., & Turnbull,J.E. Identification of the heparan sulfate binding sites in the cellular prion protein. *J Biol Chem* **277**, 18421-18430 (2002).
114. Turnbaugh,J.A., Westergard,L., Unterberger,U., Biasini,E., & Harris,D.A. The N-terminal, polybasic region is critical for prion protein neuroprotective activity. *PLoS One* **6**, e25675 (2011).
115. Solomon,I.H. *et al.* An N-terminal polybasic domain and cell surface localization are required for mutant prion protein toxicity. *J Biol Chem* **286**, 14724-14736 (2011).
116. Turnbaugh,J.A. *et al.* The N-terminal, polybasic region of PrP(C) dictates the efficiency of prion propagation by binding to PrP(Sc). *J Neurosci* **32**, 8817-8830 (2012).
117. Ostapchenko,V.G., Makarava,N., Savtchenko,R., & Baskakov,I.V. The polybasic N-terminal region of the prion protein controls the physical properties of both the cellular and fibrillar forms of PrP. *J Mol Biol* **383**, 1210-1224 (2008).
118. Abalos,G.C. *et al.* Identifying key components of the PrPC-PrPSc replicative interface. *J Biol Chem* **283**, 34021-34028 (2008).

119. Westergard,L., Turnbaugh,J.A., & Harris,D.A. A nine amino acid domain is essential for mutant prion protein toxicity. *J Neurosci* **31**, 14005-14017 (2011).
120. Boland,M.P. *et al.* Anionic phospholipid interactions of the prion protein N terminus are minimally perturbing and not driven solely by the octapeptide repeat domain. *J Biol Chem* **285**, 32282-32292 (2010).
121. Guillot-Sestier,M.V. *et al.* alpha-Secretase-derived fragment of cellular prion, N1, protects against monomeric and oligomeric amyloid beta (Abeta)-associated cell death. *J Biol Chem* **287**, 5021-5032 (2012).
122. Parkin,E.T. *et al.* Cellular prion protein regulates beta-secretase cleavage of the Alzheimer's amyloid precursor protein. *Proc Natl Acad Sci U S A* **104**, 11062-11067 (2007).
123. Vieira,T.C. *et al.* Heparin binding by murine recombinant prion protein leads to transient aggregation and formation of RNA-resistant species. *J Am Chem Soc* **133**, 334-344 (2011).
124. Hijazi,N., Kariv-Inbal,Z., Gasset,M., & Gabizon,R. PrPSc incorporation to cells requires endogenous glycosaminoglycan expression. *J Biol Chem* **280**, 17057-17061 (2005).
125. Kalastavadi,T. & True,H.L. Prion protein insertional mutations increase aggregation propensity but not fiber stability. *BMC Biochem* **9**, 7 (2008).
126. Yu,S. *et al.* Aggregation of prion protein with insertion mutations is proportional to the number of inserts. *Biochem J* **403**, 343-351 (2007).
127. Leliveld,S.R., Stitz,L., & Korth,C. Expansion of the octarepeat domain alters the misfolding pathway but not the folding pathway of the prion protein. *Biochemistry* **47**, 6267-6278 (2008).
128. Flechsig,E. *et al.* Prion protein devoid of the octapeptide repeat region restores susceptibility to scrapie in PrP knockout mice. *Neuron* **27**, 399-408 (2000).
129. Davies,P., McHugh,P.C., Hammond,V.J., Marken,F., & Brown,D.R. Contribution of individual histidines to prion protein copper binding. *Biochemistry* **50**, 10781-10791 (2011).
130. Stevens,D.J. *et al.* Early onset prion disease from octarepeat expansion correlates with copper binding properties. *PLoS Pathog* **5**, e1000390 (2009).
131. Thakur,A.K., Srivastava,A.K., Srinivas,V., Chary,K.V., & Rao,C.M. Copper alters aggregation behavior of prion protein and induces novel interactions between its N- and C-terminal regions. *J Biol Chem* **286**, 38533-38545 (2011).
132. Freir,D.B. *et al.* Interaction between prion protein and toxic amyloid beta assemblies can be therapeutically targeted at multiple sites. *Nat Commun* **2**, 336 (2011).

133. Solforosi,L. *et al.* Toward molecular dissection of PrPC-PrPSc interactions. *J Biol Chem* **282**, 7465-7471 (2007).
134. Hara,H. *et al.* Mouse prion protein (PrP) segment 100 to 104 regulates conversion of PrP(C) to PrP(Sc) in prion-infected neuroblastoma cells. *J Virol* **86**, 5626-5636 (2012).
135. Wei,X. *et al.* Human anti-prion antibodies block prion peptide fibril formation and neurotoxicity. *J Biol Chem* **287**, 12858-12866 (2012).
136. Pankiewicz,J. *et al.* Clearance and prevention of prion infection in cell culture by anti-PrP antibodies. *Eur J Neurosci* **23**, 2635-2647 (2006).
137. Khalili-Shirazi,A. *et al.* Beta-PrP form of human prion protein stimulates production of monoclonal antibodies to epitope 91-110 that recognise native PrPSc. *Biochim Biophys Acta* **1774**, 1438-1450 (2007).
138. Malinowska,L., Kroschwald,S., & Alberti,S. Protein disorder, prion propensities, and self-organizing macromolecular collectives. *Biochim Biophys Acta* **1834**, 918-931 (2013).
139. Younan,N.D., Sarell,C.J., Davies,P., Brown,D.R., & Viles,J.H. The cellular prion protein traps Alzheimer's Abeta in an oligomeric form and disassembles amyloid fibers. *FASEB J* **27**, 1847-1858 (2013).
140. Kang,M., Kim,S.Y., An,S.S., & Ju,Y.R. Characterizing affinity epitopes between prion protein and beta-amyloid using an epitope mapping immunoassay. *Exp Mol Med* **45**, e34 (2013).
141. Deng,Y. *et al.* Amyloid-beta protein (Abeta) Glu11 is the major beta-secretase site of beta-site amyloid-beta precursor protein-cleaving enzyme 1(BACE1), and shifting the cleavage site to Abeta Asp1 contributes to Alzheimer pathogenesis. *Eur J Neurosci* **37**, 1962-1969 (2013).
142. Larson,M. *et al.* The complex PrP(c)-Fyn couples human oligomeric Abeta with pathological tau changes in Alzheimer's disease. *J Neurosci* **32**, 16857-71a (2012).
143. Chen,R.J., Chang,W.W., Lin,Y.C., Cheng,P.L., & Chen,Y.R. Alzheimer's amyloid-beta oligomers rescue cellular prion protein induced tau reduction via the Fyn pathway. *ACS Chem Neurosci* **4**, 1287-1296 (2013).
144. Hutter,G., Heppner,F.L., & Aguzzi,A. No superoxide dismutase activity of cellular prion protein in vivo. *Biol Chem* **384**, 1279-1285 (2003).
145. Jones,S. *et al.* Recombinant prion protein does not possess SOD-1 activity. *Biochem J* **392**, 309-312 (2005).
146. Millhauser,G.L. Copper and the prion protein: methods, structures, function, and disease. *Annu Rev Phys Chem* **58**, 299-320 (2007).
147. Cui,H.L. *et al.* Prion infection impairs cholesterol metabolism in neuronal cells. *J Biol Chem* **289**, 789-802 (2014).

148. Sanghera,N. & Pinheiro,T.J. Binding of prion protein to lipid membranes and implications for prion conversion. *J Mol Biol* **315**, 1241-1256 (2002).
149. Lin,S.J. *et al.* Liberation of GPI-anchored prion from phospholipids accelerates amyloidogenic conversion. *Int J Mol Sci* **14**, 17943-17957 (2013).
150. Tompa,P., Tusnady,G.E., Cserzo,M., & Simon,I. Prion protein: evolution caught en route. *Proc Natl Acad Sci U S A* **98**, 4431-4436 (2001).
151. Polymenidou,M. *et al.* The POM monoclonals: a comprehensive set of antibodies to non-overlapping prion protein epitopes. *PLoS One* **3**, e3872 (2008).
152. Rane,N.S., Chakrabarti,O., Feigenbaum,L., & Hegde,R.S. Signal sequence insufficiency contributes to neurodegeneration caused by transmembrane prion protein. *J Cell Biol* **188**, 515-526 (2010).
153. Emerman,A.B., Zhang,Z.R., Chakrabarti,O., & Hegde,R.S. Compartment-restricted biotinylation reveals novel features of prion protein metabolism in vivo. *Mol Biol Cell* **21**, 4325-4337 (2010).
154. Wang,X., Wang,F., Arterburn,L., Wollmann,R., & Ma,J. The interaction between cytoplasmic prion protein and the hydrophobic lipid core of membrane correlates with neurotoxicity. *J Biol Chem* **281**, 13559-13565 (2006).
155. Ning,L., Guo,J., Jin,N., Liu,H., & Yao,X. The role of Cys179-Cys214 disulfide bond in the stability and folding of prion protein: insights from molecular dynamics simulations. *J Mol Model.* **20**, 2106 (2014).
156. Lisa,S. *et al.* The structural intolerance of the PrP alpha-fold for polar substitution of the helix-3 methionines. *Cell Mol Life Sci* **67**, 2825-2838 (2010).
157. Chen,J. & Thirumalai,D. Helices 2 and 3 are the initiation sites in the PrP(C) -> PrP(SC) transition. *Biochemistry* **52**, 310-319 (2013).
158. Sweeting,B., Brown,E., Khan,M.Q., Chakrabartty,A., & Pai,E.F. N-terminal helix-cap in alpha-helix 2 modulates beta-state misfolding in rabbit and hamster prion proteins. *PLoS One* **8**, e63047 (2013).
159. Sanchez-Garcia,J., Arbelaez,D., Jensen,K., Rincon-Limas,D.E., & Fernandez-Funez,P. Polar substitutions in helix 3 of the prion protein produce transmembrane isoforms that disturb vesicle trafficking. *Hum Mol Genet* **22**, 4253-4266 (2013).
160. Kurt,T.D. *et al.* Prion Transmission Prevented by Modifying the beta2-alpha2 Loop Structure of Host PrPC. *J Neurosci* **34**, 1022-1027 (2014).
161. Avbelj,M., Hafner-Bratkovic,I., & Jerala,R. Introduction of glutamines into the B2-H2 loop promotes prion protein conversion. *Biochem Biophys Res Commun* **413**, 521-526 (2011).
162. Ball,H.L., King,D.S., Cohen,F.E., Prusiner,S.B., & Baldwin,M.A. Engineering the prion protein using chemical synthesis. *J Pept Res* **58**, 357-374 (2001).

163. Yamaguchi,K., Matsumoto,T., & Kuwata,K. Critical region for amyloid fibril formation of mouse prion protein: unusual amyloidogenic properties of the helix 2 peptide. *Biochemistry* **47**, 13242-13251 (2008).
164. Kyle,L.M., John,T.R., Schatzl,H.M., & Lewis,R.V. Introducing a rigid loop structure from deer into mouse prion protein increases its propensity for misfolding in vitro. *PLoS One* **8**, e66715 (2013).
165. Serpa,J.J. *et al.* Using isotopically-coded hydrogen peroxide as a surface modification reagent for the structural characterization of prion protein aggregates. *J Proteomics*(2013).
166. Aurora,R. & Rose,G.D. Helix capping. *Protein Sci* **7**, 21-38 (1998).
167. Iovino,M., Falconi,M., Petruzzelli,R., & Desideri,A. Role of the helix capping in the stability of the mouse prion (180-213) segment: investigation through molecular dynamics simulations. *J Biomol Struct Dyn* **19**, 237-246 (2001).
168. Apostol,M.I., Perry,K., & Surewicz,W.K. Crystal structure of a human prion protein fragment reveals a motif for oligomer formation. *J Am Chem Soc* **135**, 10202-10205 (2013).
169. Piccardo,P. *et al.* Prion proteins with different conformations accumulate in Gerstmann-Straussler-Scheinker disease caused by A117V and F198S mutations. *Am J Pathol* **158**, 2201-2207 (2001).
170. Liberski,P.P. Gerstmann-Straussler-Scheinker disease. *Adv Exp Med Biol* **724**, 128-137 (2012).
171. Tremblay,P. *et al.* Mutant PrP^{Sc} conformers induced by a synthetic peptide and several prion strains. *J Virol* **78**, 2088-2099 (2004).
172. Solomon,I.H., Biasini,E., & Harris,D.A. Ion channels induced by the prion protein: mediators of neurotoxicity. *Prion* **6**, 40-45 (2012).
173. Solomon,I.H., Schepker,J.A., & Harris,D.A. Prion neurotoxicity: insights from prion protein mutants. *Curr Issues Mol Biol* **12**, 51-61 (2010).
174. Forloni,G. *et al.* Influence of mutations associated with familial prion-related encephalopathies on biological activity of prion protein peptides. *Ann Neurol* **45**, 489-494 (1999).
175. van der Kamp,M.W. & Daggett,V. The consequences of pathogenic mutations to the human prion protein. *Protein Eng Des Sel* **22**, 461-468 (2009).
176. Schiff,E. *et al.* Coexpression of wild-type and mutant prion proteins alters their cellular localization and partitioning into detergent-resistant membranes. *Traffic* **9**, 1101-1115 (2008).
177. Gonzalez Nelson,A.C. *et al.* Increasing prion propensity by hydrophobic insertion. *PLoS One* **9**, e89286 (2014).

178. Yu,Y., Wang,H.Y., Bai,M., & Perrett,S. Flexibility of the Ure2 prion domain is important for amyloid fibril formation. *Biochem J* **434**, 143-151 (2011).
179. Speare,J.O., Rush,T.S., Bloom,M.E., & Caughey,B. The role of helix 1 aspartates and salt bridges in the stability and conversion of prion protein. *Journal of Biological Chemistry* **278**, 12522-12529 (2003).
180. Pastore,M. *et al.* Creutzfeldt-Jakob disease (CJD) with a mutation at codon 148 of prion protein gene: relationship with sporadic CJD. *Am J Pathol* **167**, 1729-1738 (2005).
181. Krebs,B. *et al.* Creutzfeldt-Jakob disease associated with an R148H mutation of the prion protein gene. *Neurogenetics* **6**, 97-100 (2005).
182. Rangel,A., Race,B., Klingeborn,M., Striebel,J., & Chesebro,B. Unusual cerebral vascular prion protein amyloid distribution in scrapie-infected transgenic mice expressing anchorless prion protein. *Acta Neuropathol Commun* **1**, 25 (2013).
183. Skora,L. & Zweckstetter,M. Determination of amyloid core structure using chemical shifts. *Protein Sci* **21**, 1948-1953 (2012).
184. Ma,Q. *et al.* The contrasting effect of macromolecular crowding on amyloid fibril formation. *PLoS One* **7**, e36288 (2012).
185. Xiao,X. *et al.* Glycoform-selective prion formation in sporadic and familial forms of prion disease. *PLoS One* **8**, e58786 (2013).
186. Hosszu,L.L. *et al.* The H187R mutation of the human prion protein induces conversion of recombinant prion protein to the PrP(Sc)-like form. *Biochemistry* **49**, 8729-8738 (2010).
187. Zhong,L. Exposure of hydrophobic core in human prion protein pathogenic mutant H187R. *J Biomol Struct Dyn* **28**, 355-361 (2010).
188. Peoc'h,K. *et al.* Identification of three novel mutations (E196K, V203I, E211Q) in the prion protein gene (PRNP) in inherited prion diseases with Creutzfeldt-Jakob disease phenotype. *Hum Mutat* **15**, 482 (2000).
189. Peoc'h,K. *et al.* Substitutions at residue 211 in the prion protein drive a switch between CJD and GSS syndrome, a new mechanism governing inherited neurodegenerative disorders. *Hum Mol Genet* **21**, 5417-5428 (2012).
190. Guo,J., Ren,H., Ning,L., Liu,H., & Yao,X. Exploring structural and thermodynamic stabilities of human prion protein pathogenic mutants D202N, E211Q and Q217R. *J Struct Biol* **178**, 225-232 (2012).
191. De Simone,A., Dodson,G.G., Verma,C.S., Zagari,A., & Fraternali,F. Prion and water: tight and dynamical hydration sites have a key role in structural stability. *Proc Natl Acad Sci U S A* **102**, 7535-7540 (2005).
192. Guizzunti,G. & Zurzolo,C. The fate of PrP GPI-anchor signal peptide is modulated by P238S pathogenic mutation. *Traffic* **15**, 78-93 (2014).

193. Gu,Y., Singh,A., Bose,S., & Singh,N. Pathogenic mutations in the glycosylphosphatidylinositol signal peptide of PrP modulate its topology in neuroblastoma cells. *Mol Cell Neurosci* **37**, 647-656 (2008).
194. Lund,C., Olsen,C.M., Tveit,H., & Tranulis,M.A. Characterization of the prion protein 3F4 epitope and its use as a molecular tag. *J Neurosci Methods* **165**, 183-190 (2007).
195. Rutishauser,D. *et al.* The comprehensive native interactome of a fully functional tagged prion protein. *PLoS One* **4**, e4446 (2009).
196. Gaspersic,J. *et al.* Tetracycline-tagged prion protein allows discrimination between the native and converted forms. *FEBS J* **277**, 2038-2050 (2010).
197. Taguchi,Y., Hohsfield,L.A., Hollister,J.R., & Baron,G.S. Effects of FLAsH/tetracycline (TC) Tag on PrP proteolysis and PrPres formation by TC-scanning. *Chembiochem* **14**, 1597-610, 1510 (2013).
198. Jung,D., Min,K., Jung,J., Jang,W., & Kwon,Y. Chemical biology-based approaches on fluorescent labeling of proteins in live cells. *Mol Biosyst.* **9**, 862-872 (2013).
199. Moroncini,G. *et al.* Motif-grafted antibodies containing the replicative interface of cellular PrP are specific for PrPSc. *Proc Natl Acad Sci U S A* **101**, 10404-10409 (2004).
200. Georgieva,D. *et al.* Synthetic human prion protein octapeptide repeat binds to the proteinase K active site. *Biochem Biophys Res Commun* **325**, 1406-1411 (2004).
201. Howells,L.C., Anderson,S., Coldham,N.G., & Sauer,M.J. Transmissible spongiform encephalopathy strain-associated diversity of N-terminal proteinase K cleavage sites of PrP(Sc) from scrapie-infected and bovine spongiform encephalopathy-infected mice. *Biomarkers* **13**, 393-412 (2008).
202. Sajnani,G. *et al.* PK-sensitive PrP is infectious and shares basic structural features with PK-resistant PrP. *PLoS Pathog* **8**, e1002547 (2012).
203. Telling,G.C. *et al.* N-terminally tagged prion protein supports prion propagation in transgenic mice. *Protein Sci* **6**, 825-833 (1997).
204. Supattapone,S. *et al.* Affinity-tagged miniprion derivatives spontaneously adopt protease-resistant conformations. *J Virol* **74**, 11928-11934 (2000).
205. Taguchi,Y., Mistica,A.M.A., Kitamoto,T., & Schatzl,H.M. Critical Significance of the Region between Helix 1 and 2 for Efficient Dominant-Negative Inhibition by Conversion-Incompetent Prion Protein. *Plos Pathogens* **9**, (2013).
206. Prigent,S. & Rezaei,H. PrP assemblies: spotting the responsible regions in prion propagation. *Prion* **5**, 69-75 (2011).

207. Barmada,S., Piccardo,P., Yamaguchi,K., Ghetti,B., & Harris,D.A. GFP-tagged prion protein is correctly localized and functionally active in the brains of transgenic mice. *Neurobiol Dis* **16**, 527-537 (2004).
208. Bian,J. *et al.* GFP-tagged PrP supports compromised prion replication in transgenic mice. *Biochem Biophys Res Commun* **340**, 894-900 (2006).
209. Lee,K.S. *et al.* Internalization of mammalian fluorescent cellular prion protein and N-terminal deletion mutants in living cells. *J Neurochem* **79**, 79-87 (2001).
210. Magalhaes,A.C. *et al.* Endocytic intermediates involved with the intracellular trafficking of a fluorescent cellular prion protein. *J Biol Chem* **277**, 33311-33318 (2002).
211. De Keukeleire,B., Donadio,S., Micoud,J., Lechardeur,D., & Benharouga,M. Human cellular prion protein hPrPC is sorted to the apical membrane of epithelial cells. *Biochem Biophys Res Commun* **354**, 949-954 (2007).
212. Haigh,C.L. & Brown,D.R. Investigation of PrPC metabolism and function in live cells : methods for studying individual cells and cell populations. *Methods Mol Biol* **459**, 21-34 (2008).
213. Medrano,A.Z., Barmada,S.J., Biasini,E., & Harris,D.A. GFP-tagged mutant prion protein forms intra-axonal aggregates in transgenic mice. *Neurobiol Dis* **31**, 20-32 (2008).
214. Sakata,H., Horiuchi,M., Takahashi,I., & Kinjo,M. Conformational analysis of soluble oligomers of GFP tagged prion protein by fluorescence fluctuation spectroscopy. *Curr Pharm Biotechnol* **11**, 87-95 (2010).
215. Negro,A., De,F., V, Skaper,S.D., James,P., & Sorgato,M.C. The complete mature bovine prion protein highly expressed in Escherichia coli: biochemical and structural studies. *FEBS Lett* **412**, 359-364 (1997).
216. Sakudo,A. *et al.* Absence of superoxide dismutase activity in a soluble cellular isoform of prion protein produced by baculovirus expression system. *Biochem Biophys Res Commun* **307**, 678-683 (2003).
217. Petrakis,S. & Sklaviadis,T. Identification of proteins with high affinity for refolded and native PrPC. *Proteomics* **6**, 6476-6484 (2006).
218. Kunze,S. *et al.* Atomic force microscopy to characterize the molecular size of prion protein. *J Microsc* **230**, 224-232 (2008).
219. Taguchi,Y. *et al.* Specific biarsenical labeling of cell surface proteins allows fluorescent- and biotin-tagging of amyloid precursor protein and prion proteins. *Mol Biol Cell* **20**, 233-244 (2009).
220. Coleman,B.M. *et al.* Conformational detection of prion protein with biarsenical labeling and FIAsh fluorescence. *Biochem Biophys Res Commun* **380**, 564-568 (2009).

221. Yehiely,F. *et al.* Identification of candidate proteins binding to prion protein. *Neurobiol Dis* **3**, 339-355 (1997).
222. Korth,C., Kaneko,K., & Prusiner,S.B. Expression of unglycosylated mutated prion protein facilitates PrP(Sc) formation in neuroblastoma cells infected with different prion strains. *J Gen Virol* **81**, 2555-2563 (2000).
223. Milhavet,O., Mange,A., Casanova,D., & Lehmann,S. Effect of Congo red on wild-type and mutated prion proteins in cultured cells. *J Neurochem* **74**, 222-230 (2000).
224. Vorberg,I. *et al.* A novel epitope for the specific detection of exogenous prion proteins in transgenic mice and transfected murine cell lines. *Virology* **255**, 26-31 (1999).
225. Goold,R. *et al.* Alternative fates of newly formed PrPSc upon prion conversion on the plasma membrane. *J Cell Sci* **126**, 3552-3562 (2013).
226. Chang,L.K. *et al.* The importance of steric zipper on the aggregation of the MVGGVV peptide derived from the amyloid beta peptide. *J Biomol Struct Dyn* **28**, 39-50 (2010).
227. Barmada,S.J. & Harris,D.A. Visualization of prion infection in transgenic mice expressing green fluorescent protein-tagged prion protein. *J Neurosci* **25**, 5824-5832 (2005).
228. Dan,H., Balachandran,A., & Lin,M. A pair of ligation-independent Escherichia coli expression vectors for rapid addition of a polyhistidine affinity tag to the N- or C-termini of recombinant proteins. *J Biomol Tech* **20**, 241-248 (2009).
229. Garrec,J., Tavernelli,I., & Rothlisberger,U. Two misfolding routes for the prion protein around pH 4.5. *PLoS Comput. Biol* **9**, e1003057 (2013).
230. Singh,N., Singh,A., Das,D., & Mohan,M.L. Redox control of prion and disease pathogenesis. *Antioxid. Redox Signal* **12**, 1271-1294 (2010).
231. Supattapone,S. *et al.* Prion protein of 106 residues creates an artificial transmission barrier for prion replication in transgenic mice. *Cell* **96**, 869-878 (1999).
232. Walsh,P. *et al.* The mechanism of membrane disruption by cytotoxic amyloid oligomers formed by PrP(106-126) is dependent on bilayer composition. *J Biol Chem*(2014).
233. Vilches,S. *et al.* Neurotoxicity of prion peptides mimicking the central domain of the cellular prion protein. *PLoS One* **8**, e70881 (2013).
234. Salmona,M. *et al.* A neurotoxic and gliotrophic fragment of the prion protein increases plasma membrane microviscosity. *Neurobiol Dis* **4**, 47-57 (1997).
235. Kourie,J.I. *et al.* Copper modulation of ion channels of PrP[106-126] mutant prion peptide fragments. *J Membr. Biol* **193**, 35-45 (2003).

236. Yamaguchi, Y. *et al.* Biological and biochemical characterization of mice expressing prion protein devoid of the octapeptide repeat region after infection with prions. *PLoS One* **7**, e43540 (2012).
237. Dutta, A., Chen, S., & Surewicz, W.K. The effect of beta2-alpha2 loop mutation on amyloidogenic properties of the prion protein. *FEBS Lett* **587**, 2918-2923 (2013).
238. Legname, G. Early structural features in mammalian prion conformation conversion. *Prion* **6**, 37-39 (2012).
239. Kurt, T.D., Jiang, L., Bett, C., Eisenberg, D., & Sigurdson, C.J. A Proposed Mechanism for the Promotion of Prion Conversion Involving a Strictly Conserved Tyrosine Residue in the beta2-alpha2 loop of PrPC. *J Biol Chem* (2014).
240. Yamaguchi, K., Kamatari, Y.O., Fukuoka, M., Miyaji, R., & Kuwata, K. Nearly reversible conformational change of amyloid fibrils as revealed by pH-jump experiments. *Biochemistry* **52**, 6797-6806 (2013).
241. Stewart, R.S. & Harris, D.A. A transmembrane form of the prion protein is localized in the Golgi apparatus of neurons. *J Biol Chem* **280**, 15855-15864 (2005).
242. Kong, Q. *et al.* Thermodynamic stabilization of the folded domain of prion protein inhibits prion infection in vivo. *Cell Rep* **4**, 248-254 (2013).
243. Sedivy, J.M., Capone, J.P., RajBhandary, U.L., & Sharp, P.A. An inducible mammalian amber suppressor: propagation of a poliovirus mutant. *Cell* **50**, 379-389 (1987).
244. Swift, S., Lorens, J., Achacoso, P., & Nolan, G.P. Rapid production of retroviruses for efficient gene delivery to mammalian cells using 293T cell-based systems. *Curr Protoc Immunol* **Chapter 10**, Unit (2001).
245. Kinoshita, S., Chen, B.K., Kaneshima, H., & Nolan, G.P. Host control of HIV-1 parasitism in T cells by the nuclear factor of activated T cells. *Cell* **95**, 595-604 (1998).
246. Swanstrom, R. & Wills, J.W. Synthesis, Assembly, and Processing of Viral Proteins. (1997).
247. Oelschlegel, A.M., Fallahi, M., Ortiz-Umpierre, S., & Weissmann, C. The extended cell panel assay characterizes the relationship of prion strains RML, 79A, and 139A and reveals conversion of 139A to 79A-like prions in cell culture. *J Virol* **86**, 5297-5303 (2012).
248. Johnson, C.N. & Levy, L.S. Matrix attachment regions as targets for retroviral integration. *Virol J* **2**, 68 (2005).
249. Taylor, D.R. & Hooper, N.M. The low-density lipoprotein receptor-related protein 1 (LRP1) mediates the endocytosis of the cellular prion protein. *Biochem J* **402**, 17-23 (2007).

250. Hachiya,N.S., Watanabe,K., Yamada,M., Sakasegawa,Y., & Kaneko,K. Anterograde and retrograde intracellular trafficking of fluorescent cellular prion protein. *Biochem Biophys Res Commun* **315**, 802-807 (2004).
251. Rouvinski,A. *et al.* Live imaging of prions reveals nascent PrP^{Sc} in cell-surface, raft-associated amyloid strings and webs. *J Cell Biol* **204**, 423-441 (2014).
252. Sunyach,C. *et al.* The mechanism of internalization of glycosylphosphatidylinositol-anchored prion protein. *EMBO J* **22**, 3591-3601 (2003).
253. Watt,N.T., Griffiths,H.H., & Hooper,N.M. Neuronal zinc regulation and the prion protein. *Prion* **7**, 203-208 (2013).
254. Priola,S.A. & McNally,K.L. The role of the prion protein membrane anchor in prion infection. *Prion* **3**, 134-138 (2009).
255. Shao,H. *et al.* Structural requirements for signal transducer and activator of transcription 3 binding to phosphotyrosine ligands containing the YXXQ motif. *J Biol Chem* **279**, 18967-18973 (2004).
256. Miranda,A., Pericuesta,E., Ramirez,M.A., & Gutierrez-Adan,A. Prion protein expression regulates embryonic stem cell pluripotency and differentiation. *PLoS One* **6**, e18422 (2011).
257. Kraushaar,D.C. & Zhao,K. The epigenomics of embryonic stem cell differentiation. *Int J Biol Sci* **9**, 1134-1144 (2013).
258. Stuart,H.T. *et al.* NANOG Amplifies STAT3 Activation and They Synergistically Induce the Naive Pluripotent Program. *Curr Biol* **24**, 340-346 (2014).
259. Li,A. *et al.* Neonatal lethality in transgenic mice expressing prion protein with a deletion of residues 105-125. *EMBO J* **26**, 548-558 (2007).
260. Kaimann,T. *et al.* Molecular model of an alpha-helical prion protein dimer and its monomeric subunits as derived from chemical cross-linking and molecular modeling calculations. *J Mol Biol* **376**, 582-596 (2008).
261. Viles,J.H. *et al.* Local structural plasticity of the prion protein. Analysis of NMR relaxation dynamics. *Biochemistry* **40**, 2743-2753 (2001).
262. Hajj,G.N. *et al.* Cellular prion protein interaction with vitronectin supports axonal growth and is compensated by integrins. *J Cell Sci* **120**, 1915-1926 (2007).
263. Han,J. *et al.* Interaction between 14-3-3 β and PrP influences the dimerization of 14-3-3 and fibrillization of PrP¹⁰⁶⁻¹²⁶. *Int J Biochem Cell Biol* **47C**, 20-28 (2014).

264. Miller,M.B., Geoghegan,J.C., & Supattapone,S. Dissociation of infectivity from seeding ability in prions with alternate docking mechanism. *PLoS Pathog* **7**, e1002128 (2011).
265. Sanchez,A. *et al.* Toluidine blue-O staining of prion protein deposits. *Histochem Cell Biol* **116**, 519-524 (2001).
266. Yull,H.M. *et al.* Detection of type 1 prion protein in variant Creutzfeldt-Jakob disease. *Am J Pathol* **168**, 151-157 (2006).
267. Harmeyer,S., Pfaff,E., & Groschup,M.H. Synthetic peptide vaccines yield monoclonal antibodies to cellular and pathological prion proteins of ruminants. *J Gen Virol* **79 (Pt 4)**, 937-945 (1998).
268. Jeffrey,M. *et al.* Immunohistochemical features of PrP(d) accumulation in natural and experimental goat transmissible spongiform encephalopathies. *J Comp Pathol* **134**, 171-181 (2006).
269. Feraudet,C. *et al.* Screening of 145 anti-PrP monoclonal antibodies for their capacity to inhibit PrPSc replication in infected cells. *J Biol Chem* **280**, 11247-11258 (2005).
270. Zomosa-Signoret,V. *et al.* Sialylated and O-glycosidically linked glycans in prion protein deposits in a case of Gerstmann-Straussler-Scheinker disease. *Neuropathology* **31**, 162-169 (2011).
271. Jen,A. *et al.* Neuronal low-density lipoprotein receptor-related protein 1 binds and endocytoses prion fibrils via receptor cluster 4. *J Cell Sci* **123**, 246-255 (2010).
272. Godsave,S.F., Wille,H., Pierson,J., Prusiner,S.B., & Peters,P.J. Plasma membrane invaginations containing clusters of full-length PrPSc are an early form of prion-associated neuropathology in vivo. *Neurobiol Aging* **34**, 1621-1631 (2013).
273. Yamasaki,T., Baron,G.S., Suzuki,A., Hasebe,R., & Horiuchi,M. Characterization of intracellular dynamics of inoculated PrP-res and newly generated PrP(Sc) during early stage prion infection in Neuro2a cells. *Virology* **450-451**, 324-335 (2014).
274. Caetano,F.A. *et al.* Amyloid-beta oligomers increase the localization of prion protein at the cell surface. *J Neurochem* **117**, 538-553 (2011).
275. Peretz,D. *et al.* A conformational transition at the N terminus of the prion protein features in formation of the scrapie isoform. *J Mol Biol* **273**, 614-622 (1997).
276. Sigurdson,C.J. *et al.* Spongiform Encephalopathy in Transgenic Mice Expressing a Point Mutation in the beta 2-alpha 2 Loop of the Prion Protein. *Journal of Neuroscience* **31**, 13840-13847 (2011).

277. Hirschberger,T. *et al.* Structural instability of the prion protein upon M205S/R mutations revealed by molecular dynamics simulations. *Biophys J* **90**, 3908-3918 (2006).
278. Wolschner,C. *et al.* Design of anti- and pro-aggregation variants to assess the effects of methionine oxidation in human prion protein. *Proc Natl Acad Sci U S A* **106**, 7756-7761 (2009).
279. Younan,N.D., Nadal,R.C., Davies,P., Brown,D.R., & Viles,J.H. Methionine oxidation perturbs the structural core of the prion protein and suggests a generic misfolding pathway. *J Biol Chem* **287**, 28263-28275 (2012).
280. Vorberg,I., Raines,A., & Priola,S.A. Acute formation of protease-resistant prion protein does not always lead to persistent scrapie infection in vitro. *J Biol Chem* **279**, 29218-29225 (2004).
281. Gong,B. *et al.* Probing structural differences between PrP(C) and PrP(Sc) by surface nitration and acetylation: evidence of conformational change in the C-terminus. *Biochemistry* **50**, 4963-4972 (2011).
282. Salamat,K. *et al.* Integrity of helix 2-helix 3 domain of the PrP protein is not mandatory for prion replication. *J Biol Chem* **287**, 18953-18964 (2012).
283. Wille,H., Zhang,G.F., Baldwin,M.A., Cohen,F.E., & Prusiner,S.B. Separation of scrapie prion infectivity from PrP amyloid polymers. *J Mol Biol* **259**, 608-621 (1996).
284. Caughey,B.W. *et al.* Secondary structure analysis of the scrapie-associated protein PrP 27-30 in water by infrared spectroscopy. *Biochemistry* **30**, 7672-7680 (1991).
285. Sonati,T. *et al.* The toxicity of antiprion antibodies is mediated by the flexible tail of the prion protein. *Nature* **501**, 102-106 (2013).
286. Nicoll,A.J. *et al.* Pharmacological chaperone for the structured domain of human prion protein. *Proc Natl Acad Sci U S A* **107**, 17610-17615 (2010).
287. Li,S.C. & Deber,C.M. A measure of helical propensity for amino acids in membrane environments. *Nat Struct Biol* **1**, 368-373 (1994).
288. Thompson,M.J. *et al.* The 3D profile method for identifying fibril-forming segments of proteins. *Proc Natl Acad Sci U S A* **103**, 4074-4078 (2006).
289. Kim,S. *et al.* Transmembrane glycine zippers: physiological and pathological roles in membrane proteins. *Proc Natl Acad Sci U S A* **102**, 14278-14283 (2005).
290. Choi,J.K. *et al.* Generation of monoclonal antibody recognized by the GXXXG motif (glycine zipper) of prion protein. *Hybridoma (Larchmt.)* **25**, 271-277 (2006).
291. Warwicker,J. Modeling a prion protein dimer: predictions for fibril formation. *Biochem Biophys Res Commun* **278**, 646-652 (2000).

292. Beland,M., Motard,J., Barbarin,A., & Roucou,X. PrP(C) homodimerization stimulates the production of PrP^C cleaved fragments PrP^{N1} and PrP^{C1}. *J Neurosci* **32**, 13255-13263 (2012).
293. Priola,S.A., Caughey,B., Wehrly,K., & Chesebro,B. A 60-kDa prion protein (PrP) with properties of both the normal and scrapie-associated forms of PrP. *J Biol Chem* **270**, 3299-3305 (1995).
294. Tovchigrechko,A. & Vakser,I.A. GRAMM-X public web server for protein-protein docking. *Nucleic Acids Res* **34**, W310-W314 (2006).
295. Harrison,C.F. *et al.* Conservation of a glycine-rich region in the prion protein is required for uptake of prion infectivity. *J Biol Chem* **285**, 20213-20223 (2010).
296. Cymer,F., Veerappan,A., & Schneider,D. Transmembrane helix-helix interactions are modulated by the sequence context and by lipid bilayer properties. *Biochim Biophys Acta* **1818**, 963-973 (2012).
297. Hay,B., Prusiner,S.B., & Lingappa,V.R. Evidence for a secretory form of the cellular prion protein. *Biochemistry* **26**, 8110-8115 (1987).
298. Yost,C.S., Lopez,C.D., Prusiner,S.B., Myers,R.M., & Lingappa,V.R. Non-hydrophobic extracytoplasmic determinant of stop transfer in the prion protein. *Nature* **343**, 669-672 (1990).
299. Lopez,C.D., Yost,C.S., Prusiner,S.B., Myers,R.M., & Lingappa,V.R. Unusual topogenic sequence directs prion protein biogenesis. *Science* **248**, 226-229 (1990).
300. De Fea,K.A. *et al.* Determinants of carboxyl-terminal domain translocation during prion protein biogenesis. *J Biol Chem* **269**, 16810-16820 (1994).
301. Stewart,R.S., Piccardo,P., Ghetti,B., & Harris,D.A. Neurodegenerative illness in transgenic mice expressing a transmembrane form of the prion protein. *J Neurosci* **25**, 3469-3477 (2005).
302. Sauve,S., Buijs,D., Gingras,G., & Aubin,Y. Interactions between the conserved hydrophobic region of the prion protein and dodecylphosphocholine micelles. *J Biol Chem* **287**, 1915-1922 (2012).
303. Riley,M.L. *et al.* High-level expression and characterization of a glycosylated covalently linked dimer of the prion protein. *Protein Eng* **15**, 529-536 (2002).
304. Yang,X. *et al.* Using protein misfolding cyclic amplification generates a highly neurotoxic PrP dimer causing neurodegeneration. *J Mol Neurosci* **51**, 655-662 (2013).
305. Fischer,M. *et al.* Prion protein (PrP) with amino-proximal deletions restoring susceptibility of PrP knockout mice to scrapie. *EMBO J* **15**, 1255-1264 (1996).

Chapter 6 |

Appendix |

6.1 MOUSE PRION PROTEIN OPEN READING FRAME AS CLONED IN PBLUESCRIPTSK+ PLASMID VECTOR

10	20	30	40	50
GTCATCATGG	CGAACCTTGG	CTACTGGCTG	CTGGCCCTCT	TTGTGACTAT
GTGGACTGAT	GTCGGCCTCT	GCAAAAAGCG	GCCAAAGCCT	GGAGGGTGGA
ACACCGGTGG	AAGCCGGTAT	CCCGGGCAGG	GAAGCCCTGG	AGGCAACCGT
TACCCACCTC	AGGGTGGCAC	CTGGGGGCAG	CCCCACGGTG	GTGGCTGGGG
ACAACCCCAT	GGGGGCAGCT	GGGGACAACC	TCATGGTGGT	AGTTGGGGTC
AGCCCATGG	CGGTGGATGG	GGCCAAGGAG	GGGGTACCCA	TAATCAGTGG
AACAAGCCCA	GCAAACCAAA	AACCAACCTC	AAGCATGTGG	CAGGGGCTGC
GGCAGCTGGG	GCAGTAGTGG	GGGGCCTTGG	TGGCTACATG	CTGGGGAGCG
CCATGAGCAG	GCCCATGATC	CATTTTGGCA	CGACTGGGA	GGACCGCTAC
TACCGTGAAA	ACATGTACCG	CTACCCTAAC	CAAGTGTACT	ACAGGCCAGT
GGATCAGTAC	AGCAACCAGA	ACAACCTCGT	GCACGACTGC	GTCAATATCA
CCATCAAGCA	GCACACGGTC	ACCACCACCA	CCAAGGGGGA	GAACTTCACC
GAGACCGATG	TGAAGATGAT	GGAGCGCGTG	GTGGAGCAGA	TGTGCGTCAC
CCAGTACCAG	AAGGAGTCCC	AGGCCTATTA	CGACGGGAGA	AGATCCAGCA
GCACCGTGCT	TTTCTCCTCC	CCTCCTGTCA	TCCTCCTCAT	CTCCTTCTC
ATCTTCTGA	TCGTGGGATG	AGGCTCGAG		

FIGURE A1

The nucleotide sequence of the mouse prion protein open reading frame from template DNA in pBluescriptSK+ shown in a 5' to 3' direction. This sequence was inserted into the native pBluescriptSK+ sequence at the *Sma*I site of the plasmid's multiple cloning site region. The ATG coding the Methionine start site is indicated in green and the TGA stop site is shown in red. Shown in bold typeface are the 5' and 3' restriction site (*Sal*I and *Hind*III respectively) which were incorporated in the untranslated regions of the protein when cloning it into pBluescript.

6.2 PRIMERS DESIGNED FOR THE SITE-DIRECTED MUTAGENESIS OF MOPRP

Site directed mutagenesis		Primer Sequence 5' to 3'
1 K23A	F	CTGATGTCGGCCTCTGCGCCAAGCGGCCAAAGCCTGGAGGG
	R	CCCTCCAGGCTTTGGCCGCTTGCGCAGAGGCCGACATCAG
2 K24A	F	GATGTCGGCCTCTGCAAAGCCCGGCCAAAGCCTGGAGGG
	R	CCCTCCAGGCTTTGGCCGGGCTTTGCAGAGGCCGACATC
3 R25A	F	GTCGGCCTCTGCAAAAAGGCCCAAGCCTGGAGGGTGG
	R	CCACCTCCAGGCTTTGGGGCTTTTTCAGAGGCCGAC
4 K23A.K24A.R25A	F	CTGATGTCGGCCTCTGCGCCGCCGCCCAAGCCTGGAGGGTGG
	R	CCACCTCCAGGCTTTGGGGCGGCGGCAGAGGCCGACATCAG
5 P26A K27A	F	GGCCTCTGCAAAAAGCGGGCCGCCCTGGAGGGTGAACACCGG
	R	CCGGTGTTCACCTCCAGGGCGGCCCGCTTTTTCAGAGGCC
6 P28A	F	CTGCAAAAAGCGGCCAAAGCCGGAGGGTGAACACCGG
	R	CCGGTGTTCACCTCCGGCCTTTGGCCGCTTTTTCAG
7 W31A.N32A.T33A	F	CGGCCAAAGCCTGGAGGGCGCCGCCGGTGAAGCCGGTATCCCGG
	R	CCCGGATACCGGCTTCCACCGCGGCGGCCCTCCAGGCTTTGGCCG
8 S36A.R37A.Y38A	F	GGAGGGTGAACACCGGTGGAGCCGCCGCCCGGGCAGGGAAGCCCTGG
	R	CCAGGGTTCCCTGCCCGGGGGCGCGGCTCCACCGGTTCACCTCC
9 Q41A	F	GGAAGCCGGTATCCCGGGCCGGAAGCCCTGGAGGCAAC
	R	GTTGCCTCCAGGGCTTCCGGCCCGGGATACCGGCTTCC
10 S43A	F	CGGTATCCCGGGCAGGGAGCCCTGGAGGCAACCGTTAC
	R	GTAACGGTTGCCTCCAGGGGCTCCCTGCCCGGGATACCG

FIGURE A2 1

moPrP region 23-43. Forward and reverse primers (F and R) shown for mutations designed for use with Stratagene QuikChange® site-directed mutagenesis kit (Stratagene, Cat.No.200523).

Site directed mutagenesis		Primer Sequence 5' to 3'	
11	N47A.R48A.W49A	F	CAGGGAAGCCCTGGAGGCGCGCCGCCACCTCAGGGTGGCACCTGG
		R	CCAGGTGCCACCCTGAGGTGGGGCGGCGGCCTCCAGGGCTTCCCTG
12	Q52A	F	GGCAACCGTTACCCACCTGCCGGTGGCACCTGGGGGCGAG
		R	CTGCCCCAGGTGCCACCGGCAGGTGGGTAACGGTTGCC
13	T55A.W56A	F	CGTTACCCACCTCAGGGTGGCGCCGCGGCAGCCCCACGGTGGTGGCTGG
		R	CCAGCCACCACCGTGGGGCTGCCGCGGCGCCACCCCTGAGGTGGGTAACG
14	Q58A	F	CAGGGTGGCACCTGGGGGGCCCCCACGGTGGTGGCTGG
		R	CCAGCCACCACCGTGGGGGGCCCCCAGGTGCCACCCTG
15	H60A	F	CCTGGGGGAGCCCGCCGGTGGTGGCTGGGG
		R	CCCCAGCCACCACCGGCGGGCTGCCCCAGG
16	W64A	F	CAGCCCCACGGTGGTGGCGCCGACAACCCCATGGGGGC
		R	GCCCCATGGGGTTGTCCGGCGCCACCACCGTGGGGCTG
17	Q66A	F	CACGGTGGTGGCTGGGGAGCCCCCATGGGGCAGCTGG
		R	CCAGCTGCCCCATGGGGGCTCCCCAGCCACCACCGTG
18	H68A	F	GGTGGCTGGGGACAACCCGCGGGGGCAGCTGGGGAC
		R	GTCCCCAGCTGCCCCGCGGGTTGTCCCCAGCCACC
19	S71A.W72A	F	GGACAACCCCATGGGGGCGCGCCGGACAACCTCATGGTGG
		R	CCACCATGAGGTTGTCCGGCGGCGCCCCATGGGGTTGTCC
20	Q74A	F	CATGGGGGAGCTGGGGAGCCCTCATGGTGGTAGTTGG
		R	CCAACTACCACCATGAGGGGCTCCCCAGCTGCCCCATG

FIGURE A2 2

moPrP region 47-74. Forward and reverse primers (F and R) shown for mutations designed for use with Stratagene QuikChange® site-directed mutagenesis kit (Stratagene, Cat.No.200523).

Site directed mutagenesis		Primer Sequence 5' to 3'	
21	H76A	F	GCTGGGGACAACCTGCCGGTGGTAGTTGGGGTCAG
		R	CTGACCCCAACTACCACGGCAGGTTGTCCCAGC
22	S79A.W80A	F	GGACAACCTCATGGTGGTGCCGCCGGTCAGCCCATGGCGG
		R	CCGCCATGGGGCTGACCGGCGGCACCACCATGAGGTTGTCC
23	Q82A	F	CATGGTGGTAGTTGGGGTGCCCCCATGGCGGTGGATGG
		R	CCATCCACCGCCATGGGGGGCACCCAACTACCACCATG
24	H84A	F	GTAGTTGGGGTCAGCCCGCGGGCGGTGGATGGGGC
		R	GCCCCATCCACCGCCGGCGGGCTGACCCAACTAC
25	W88A	F	CCCCATGGCGGTGGAGCCGGCCAAGGAGGGGGTAC
		R	GTACCCCTCCTTGGCCGGCTCCACCGCCATGGGG
26	Q90A	F	CATGGCGGTGGATGGGGCGCGGAGGGGGTACCCATAATCAG
		R	CTGATTATGGGTACCCCTCCGGCGCCCATCCACCGCCATG
27	T94A.H95A.N96A	F	GGGGCCAAGGAGGGGGTGCCGCCGCCAGTGAACAAGCCCAGC
		R	GCTGGGCTTGTTCCACTGGGCGGCGGCACCCCTCCTTGGCCCC
28	Q97A.W98A	F	GGAGGGGTACCATAATGCCGCCAACAAGCCCAGCAAACC
		R	GGTTTGCTGGGCTTGTTGGCGGCATTATGGGTACCCCTCC
29	N99A.K100A	F	GGTACCATAATCAGTGGGCCGCCCCAGCAAACCAAAAACC
		R	GGTTTTTGGTTTGCTGGGGGCGGCCACTGATTATGGGTACC
30	P101A	F	CATAATCAGTGAACAAGGCCAGCAAACCAAAAACCAACCTC
		R	GAGGTTGGTTTTTGGTTTGCTGGCCTTGTTCCACTGATTATG

FIGURE A2 3

moPrP region 76-101. Forward and reverse primers (F and R) shown for mutations designed for use with Stratagene QuikChange® site-directed mutagenesis kit (Stratagene, Cat.No.200523).

Site directed mutagenesis		Primer Sequence 5' to 3'	
31	P101L	F	CATAATCAGTGGAACAAGCTGAGCAAACCAAAAACCAACCTC
		R	GAGGTTGGTTTTGGTTTGCTCAGCTTGTTCCACTGATTATG
32	P104A	F	CAGTGGAACAAGCCCAGCAAAGCCAAAACCAACCTCAAGCATGTG
		R	CACATGCTTGAGGTTGGTTTTGGCTTTGCTGGGCTTGTTCCACTG
33	P104L	F	CAGTGGAACAAGCCCAGCAAAGTAAAACCAACCTCAAGCATGTG
		R	CACATGCTTGAGGTTGGTTTTAGTTTGCTGGGCTTGTTCCACTG
34	P104T	F	CAGTGGAACAAGCCCAGCAAACAAAAACCAACCTCAAGCATGTG
		R	CACATGCTTGAGGTTGGTTTTGTTTTGCTGGGCTTGTTCCACTG
35	S102A.K103A	F	CATAATCAGTGGAACAAGCCCGCCGCCCCAAAACCAACCTCAAG
		R	CTTGAGGTTGGTTTTGGGGCGGCGGGCTTGTTCCACTGATTATG
36	K105A.T106A.N107A	F	GGAACAAGCCCAGCAAACCAGCCGCGCCCTCAAGCATGTGGCAGGG
		R	CCCTGCCACATGCTTGAGGGCGGCGGCTGGTTTGCTGGGCTTGTTCC
37	L108A.K109A	F	CCCAGCAAACCAAAAACCAACGCGCCCATGTGGCAGGGGCTGCG
		R	CGCAGCCCCTGCCACATGGGCGGCGTTGGTTTTGGTTTGCTGGG
38	K109E	F	CCAAAACCAACCTCGAGCATGTGGCAGGGGC
		R	GCCCCTGCCACATGCTCGAGGTTGGTTTTGG
39	H110A.V111A	F	CCAAAACCAACCTCAAGGCCGCGCAGGGGCTGCGGCAGCTGGG
		R	CCCAGCTGCCGCGAGCCCTGCGGCGGCTTGAGGTTGGTTTTGG
40	V111M	F	CCAACCTCAAGCATATGGCAGGGGCTGCGGC
		R	GCCGCGCCCTGCCATATGCTTGAGGTTGG

FIGURE A2 4

moPrP region 101-111. Forward and reverse primers (F and R) shown for mutations designed for use with Stratagene QuikChange® site-directed mutagenesis kit (Stratagene, Cat.No.200523).

Site directed mutagenesis		Primer Sequence 5' to 3'	
41	A112L	F	CCAACCTCAAGCATGTGCTAGGGGCTGCGGCAGC
		R	GCTGCCGAGCCCCTAGCACATGCTTGAGGTTGG
42	G113L	F	CCAACCTCAAGCATGTGGCACTGGCTGCGGCAGCTGGGGCAG
		R	CTGCCCCAGCTGCCGAGCCAGTGCCACATGCTTGAGGTTGG
43	A115G	F	CAAGCATGTGGCAGGGGCTGGGGCAGCTGGGGCAGTAGTGG
		R	CCACTACTGCCCCAGCTGCCCCAGCCCCTGCCACATGCTTG
44	A115L	F	CAAGCATGTGGCAGGGGCTCTGGCAGCTGGGGCAGTAGTGG
		R	CCACTACTGCCCCAGTGCCAGAGCCCCTGCCACATGCTTG
45	A116L	F	GCATGTGGCAGGGGCTGCGCTAGCTGGGGCAGTAGTGGGG
		R	CCCCACTACTGCCCCAGCTAGCGCAGCCCCTGCCACATGC
46	A117L	F	GTGGCAGGGGCTGCGGCACCTTGGGGCAGTAGTGGGGGGC
		R	GCCCCCACTACTGCCCAAGTGCCGCAGCCCCTGCCAC
47	A117R	F	GTGGCAGGGGCTGCGGCACGTGGGGCAGTAGTGGGGGGC
		R	GCCCCCACTACTGCCCCACGTGCCGCAGCCCCTGCCAC
48	G118A	F	GCAGGGGCTGCGGCAGCTGCGGCAGTAGTGGGGGGCCTTG
		R	CAAGGCCCCCACTACTGCCGCAGCTGCCGCAGCCCCTGC
49	G118L	F	GCAGGGGCTGCGGCAGCTCTGGCAGTAGTGGGGGGCCTTG
		R	CAAGGCCCCCACTACTGCCAGAGCTGCCGCAGCCCCTGC
50	A119L	F	GCAGGGGCTGCGGCAGCTGGGCTAGTAGTGGGGGGCCTTGGTGGC
		R	GCCACCAAGGCCCCCACTACTAGCCAGCTGCCGCAGCCCCTGC

FIGURE A2 5

moPrP region 112-119. Forward and reverse primers (F and R) shown for mutations designed for use with Stratagene QuikChange® site-directed mutagenesis kit (Stratagene, Cat.No.200523).

Site directed mutagenesis		Primer Sequence 5' to 3'	
51	A119P	F	GCAGGGGCTGCGGCAGCTGGGCCAGTAGTGGGGGGCCTTGGTGCC
		R	GCCACCAAGGCCCCCACTACTGGCCCAGCTGCCGAGCCCCTGC
52	V120A	F	GGGCTGCGGCAGCTGGGGCAGCAGTGGGGGGCCTTGGTGCTAC
		R	GTAGCCACCAAGGCCCCCACTGCTGCCCAGCTGCCGAGCCC
53	V121A	F	GCTGCGGCAGCTGGGGCAGTAGCGGGGGCCTTGGTGCTACATG
		R	CATGTAGCCACCAAGGCCCCCGCTACTGCCCAGCTGCCGAGC
54	G122A	F	GCACTGGGGCAGTAGTGGCGGGCCTTGGTGCTACATGCTG
		R	CAGCATGTAGCCACCAAGGCCCGCCACTACTGCCCAGCTGC
55	G122L	F	GCACTGGGGCAGTAGTGGTGGCCTTGGTGCTACATGCTG
		R	CAGCATGTAGCCACCAAGGCCAGCACTACTGCCCAGCTGC
56	G123A	F	GCTGGGGCAGTAGTGGGGGGCCTTGGTGCTACATGCTG
		R	CAGCATGTAGCCACCAAGGGCCCACTACTGCCCAGC
57	L124A	F	GCTGGGGCAGTAGTGGGGGGCCTTGGTGCTACATGCTGGGGAGC
		R	GCTCCCCAGCATGTAGCCACCAGCGCCCCCACTACTGCCCCAGC
58	L124I	F	GCTGGGGCAGTAGTGGGGGGCATTGGTGCTACATGCTGGGGAGC
		R	GCTCCCCAGCATGTAGCCACCAATGCCCCCACTACTGCCCCAGC
59	L124V	F	GCTGGGGCAGTAGTGGGGGGCCTTGGTGCTACATGCTGGGGAGC
		R	GCTCCCCAGCATGTAGCCACCAACGCCCCCACTACTGCCCCAGC
60	G125A	F	GGCAGTAGTGGGGGGCCTTGGTGCTACATGCTGGGGAGC
		R	GCTCCCCAGCATGTAGCCAGCAAGGCCCCCACTACTGCC

FIGURE A2 6

moPrP region 119-125. Forward and reverse primers (F and R) shown for mutations designed for use with Stratagene QuikChange® site-directed mutagenesis kit (Stratagene, Cat.No.200523).

Site directed mutagenesis		Primer Sequence 5' to 3'	
61	G126A	F	GTGGGGGGCCTTGGTGCCTACATGCTGGGGAGCGCC
		R	GGCGCTCCCAGCATGTAGCCACCAAGGCCCCCAC
62	G126L	F	GTAGTGGGGGGCCTTGGTCTCTACATGCTGGGGAGCGCC
		R	GGCGCTCCCAGCATGTAGAGACCAAGGCCCCCACTAC
63	G126V	F	GTAGTGGGGGGCCTTGGTGTCTACATGCTGGGGAGCGCC
		R	GGCGCTCCCAGCATGTAGACACCAAGGCCCCCACTAC
64	Y127F	F	GTGGGGGGCCTTGGTGGCTTCATGCTGGGGAGCGCCGTG
		R	CACGGCGCTCCCAGCATGAAGCCACCAAGGCCCCCAC
65	Y127P	F	GTGGGGGGCCTTGGTGGCCCATGCTGGGGAGCGCCGTG
		R	CACGGCGCTCCCAGCATGGGGCCACCAAGGCCCCCAC
66	Y127R	F	GTGGGGGGCCTTGGTGGCCCATGCTGGGGAGCGCCGTG
		R	CACGGCGCTCCCAGCATGCGGCCACCAAGGCCCCCAC
67	M128L	F	GTGGGGGGCCTTGGTGGCTACCTGCTGGGGAGCGCCGTGAGCAGG
		R	CCTGCTCAGGCGCTCCCAGCAGGTAGCCACCAAGGCCCCCAC
68	M128V	F	GTGGGGGGCCTTGGTGGCTACGTGCTGGGGAGCGCCGTGAGCAGG
		R	CCTGCTCAGGCGCTCCCAGCACGTAGCCACCAAGGCCCCCAC
69	L129A	F	GGCCTTGGTGGCTACATGGCGGGGAGCGCCGTGAGCAGG
		R	CCTGCTCAGGCGCTCCCCGCATGTAGCCACCAAGGCC
70	G130A	F	GGCCTTGGTGGCTACATGCTGGCGAGCGCCGTGAGCAGGCCATG
		R	CATGGGCCTGCTCAGGCGCTCGCCAGCATGTAGCCACCAAGGCC

FIGURE A2 7

moPrP region 126-130. Forward and reverse primers (F and R) shown for mutations designed for use with Stratagene QuikChange® site-directed mutagenesis kit (Stratagene, Cat.No.200523).

Site directed mutagenesis		Primer Sequence 5' to 3'	
71	G130L	F	GGCCTTGGTGGCTACATGCTGCTGAGCGCCGTGAGCAGGCCCATG
		R	CATGGGCCCTGCTCACGGCGCTCAGCAGCATGTAGCCACCAAGGCC
72	S131A	F	GGTGGCTACATGCTGGGGGCGCCGTGAGCAGGCCCATG
		R	CATGGGCCCTGCTCACGGCGGCCCCAGCATGTAGCCACC
73	A132L	F	GGTGGCTACATGCTGGGGAGCCTCGTGAGCAGGCCCATGATCC
		R	GGATCATGGGCCTGCTCACGAGGCTCCCCAGCATGTAGCCACC
74	S134A	F	CATGCTGGGGAGCGCCGTGGCCAGGCCCATGATCCATTTTGG
		R	CCAAAATGGATCATGGGCCTGGCCACGGCGCTCCCCAGCATG
75	R135A	F	CATGCTGGGGAGCGCCGTGAGCGCCCCATGATCCATTTTGGCAAC
		R	GTTGCCAAAATGGATCATGGGGGCGCTCACGGCGCTCCCCAGCATG
76	R135E	F	CTGGGGAGCGCCGTGAGCGAGCCCATGATCCATTTTGG
		R	CCAAAATGGATCATGGGCTCGCTCACGGCGCTCCCCAG
77	H139A	F	GCCGTGAGCAGGCCCATGATCGCCTTTGGCAACGACTGGGAGGACCGC
		R	GCGGTCTCCAGTCGTTGCCAAAGCGATCATGGGCCTGCTCACGGC
78	G141A	F	GTGAGCAGGCCCATGATCCATTTTGGCAACGACTGGGAGGACCGCTAC
		R	GTAGCGGTCCTCCAGTCGTTGGCAAAAATGGATCATGGGCCTGCTCAC
79	Δ112-129	F	CCCAGCAAACCAAAAACCAACCTCAAGCATGTGGGGAGCGCCGTGAGCAGGCCCATGATCCATTTTGGC
		R	GCCAAAATGGATCATGGGCCTGCTCACGGCGCTCCCCACATGCTTGAGGTTGGTTTTTGGTTTGCTGGG
80	Δ117-124	F	CCAACCTCAAGCATGTGGCAGGGGCTGCGGCAGGTGGCTACATGCTGGGGAGCGCCGTGAGC
		R	GCTCACGGCGCTCCCCAGCATGTAGCCACCTGCCGAGCCCCTGCCACATGCTTGAGGTTGG

FIGURE A2 8

moPrP region 130-141. Forward and reverse primers (F and R) shown for mutations designed for use with Stratagene QuikChange® site-directed mutagenesis kit (Stratagene, Cat.No.200523).

Site directed mutagenesis		Primer Sequence 5' to 3'	
81	G123A.L124A.G125A	F	GCAGCTGGGGCAGTAGTGGGGGCCGCCGGCTACATGCTGGGGAGCGCC
		R	GGCGCTCCCAGCATGTAGCCGGCGGGCCCCACTACTGCCCCAGCTGC
82	M128A*	F	GTGGGGGGCCTTGGTGGCTACGCCCTGGGGAGCGCCGTGAGC
		R	GCTCACGGCGCTCCCAGGGCGTAGCCACCAAGGCCCCAC
83	L129A.S131A*	F	GGCCTTGGTGGCTACATGGCCGGGGCCGCCGTGAGCAGGCCATG
		R	CATGGGCCCTGCTCACGGCGGCCCGGCCATGTAGCCACCAAGGCC
84	S134A.R135A*	F	CATGCTGGGGAGCGCCGTGGCCGCCCCCATGATCCATTTTGGC
		R	GCCAAAATGGATCATGGGGCGGCCACGGCGCTCCCAGCATG
85	H139A.G141A*	F	GCCGTGAGCAGGCCCATGATCGCCTTTGCCAACGACTGGGAGGACCGCTAC
		R	GTAGCGGTCTCCAGTCGTTGGCAAAGGCGATCATGGCCTGCTCACGGC
86	H139A.G141.D146A	F	GCCTTTGCCAACGACTGGGAGGCCCGCTACTACCGTGAAAAATG
		R	CATGTTTTACGGTAGTAGCGGGCCTCCAGTCGTTGGCAAAGGC
87	N142A.N144A.E145A	F	CCCATGATCCATTTTGGCGCCGACGCCCGCCGACCGCTACTACCGTGAAAAC
		R	GTTTTACGGTAGTAGCGGTTCGGCGGCGTCCGGCGCAAATGGATCATGGG
88	*D146A	F	CATTTTGGCAACGACTGGGAGGCCCGCTACTACCGTGAAAAATG
		R	CATGTTTTACGGTAGTAGCGGGCCTCCAGTCGTTGCCAAAATG
89	R147A.R150A.E151A	F	GGCAACGACTGGGAGGACGCTACTACGCCCAACATGTACCGTACCCTAAC
		R	GTTAGGGTAGCGGTACATGTTGGCGGCGTAGTAGGCGTCTCCAGTCGTTGCC
90	Y148A*	F	GGCACCGACTGGGAGGACCGCGCTACCGTGAAAACATGTACCGC
		R	GCGGTACATGTTTTACGGTAGGGCGGTCTCCAGTCGGTGCC

FIGURE A2 9

moPrP region 123-151. Forward and reverse primers (F and R) shown for mutations designed for use with Stratagene QuikChange® site-directed mutagenesis kit (Stratagene, Cat.No.200523). * indicates that this mutation was made to part of a larger mutational construct such as in the case of structured region mutations where the amino acids targeted are spatially, but not sequentially proximal.

Site directed mutagenesis		Primer Sequence 5' to 3'	
91	*M153A	F	CGCTACTACCGTGAAAACGCCTACCGCTACCCTAACCAAGTG
		R	CAC TTGGTTAGGGTAGCGGTAGGCGTTTTCACGGTAGTAGCG
92	R155A*	F	CTACCGTGAAAACATGTACGCCTACCCTAACCAAGTGTAC
		R	GTACACTTGGTTAGGGTAGGCGTACATGTTTTTCACGGTAG
93	*Q159A	F	CATGTACCCTACCCTAACGCCGTGTACTACAGGCCAGTGGATC
		R	GATCCACTGGCCTGTAGTACACGGCGTTAGGGTAGCGGTACATG
94	*Y162A*	F	C TAC CCT AAC CAA GTG TAC GCC AGG CCA GTG GAT CAG TAC
		R	GTA CTG ATC CAC TGG CCT GGC GTA CAC TTG GTT AGG GTA G
95	*Q216A	F	GAG CAG ATG TGC GTC ACC GCC TAC CAG AAG GAG TCC CAG
		R	CTG GGA CTC CTT CTG GTA GGC GGT GAC GCA CAT CTG CTC
96	R163A.Y168A*	F	CCTAACCAAGTGTACTACGCCCCAGTGGATCAGGCCAGCAACCAGAACAACCTTCGTG
		R	CACGAAGTTGTTCTGGTTGCTGGCCTGATCCACTGGGGCGTAGTACACTTGGTTAGG
97	S169A.N170A*	F	CAGGCCAGTGGATCAGTACGCCGCCAGAACAACCTTCGTGCAC
		R	GTGCACGAAGTTGTTCTGGGCGGCGTACTGATCCACTGGCCTG
98	F174A*	F	CAGTACAGCAACCAGAACAACGCCGTGCACGACTGCGTCAATATC
		R	GATATTGACGCAGTCGTGCACGGCGTTGTTCTGGTTGCTGTACTG
99	F174A.V179A	F	CAGTACAGCAACCAGAACAACGCCGTGCACGACTGCGCCAATATC
		R	GATATTGGCGCAGTCGTGCACGGCGTTGTTCTGGTTGCTGTACTG
100	*H176A	F	GCAACCAGAACAACCTTCGTGGCCGACTGCGTCAATATCACC
		R	GGTGATATTGACGCAGTCGGCCACGAAGTTGTTCTGGTTGC

FIGURE A2 10

moPrP region 153-216. Forward and reverse primers (F and R) shown for mutations designed for use with Stratagene QuikChange® site-directed mutagenesis kit (Stratagene, Cat.No.200523). * indicates that this mutation was made to part of a larger mutational construct such as in the case of structured region mutations where the amino acids targeted are spatially, but not sequentially proximal.

Site directed mutagenesis		Primer Sequence 5' to 3'
101 C178A*	F	CAGAACAAC TTCGTGCACGACGCCGTCAATATCACCATCAAGCAG
	R	CTGCTTGATGGTGATATTGACGGCGTCGTGCACGAAGTTGTTCTG
102 V179A	F	CAACTTCGTGCACGACTGCGCCAATATCACCATCAAGCAGCACACG
	R	CGTGTGCTGCTTGATGGTGATATTGGCGCAGTCGTGCACGAAGTTG
103 V179A.I183A*	F	CAACTTCGTGCACGACTGCGCCAATATCACCAGCAAGCAGCACACGGTCACC
	R	GGTGACCGTGTGCTGCTTGCGGTGATATTGGCGCAGTCGTGCACGAAGTTG
104 I183A	F	CACGACTGCGTCAATATCACCAGCAAGCAGCACACGGTCACC
	R	GGTGACCGTGTGCTGCTTGCGGTGATATTGACGCAGTCGTG
105 V188A.T191A.T192A	F	CACCATCAAGCAGCACACGGCCACCACCGCCCAAGGGGGAGAACTTCACC
	R	GGTGAAGTTCTCCCCCTTGCGCGCGGTGGTGGCCGTGTGCTGCTTGATGGTG
106 *K193A.E195A	F	CACACGGTCACCACCACCACCGCGGGGCCAACTTCACCGAGACCGATGTG
	R	CACATCGGTCTCGGTGAAGTTGGCCCCGGCGGTGGTGGTGGTACCCTGTG
107 *T198A.D201A	F	CCACCAAGGGGGAGAACTTCGCGGAGACCGCCGTGAAGATGATGGAGCGCGTG
	R	CACGCGCTCCATCATCTTCACGGCGGTCTCGGCGAAGTTCTCCCCCTTGGTGG
108 K203A.E206A.R207A	F	CTTCACCGAGACCGATGTGGCCATGATGGCCGCGGTGGTGGAGCAGATGTGCGTC
	R	GACGCACATCTGCTCCACCACGGCGGCCATCATGGCCACATCGGTCTCGGTGAAG
109 M204A	F	CACCGAGACCGATGTGAAGGCCATGGAGCGCGTGGTGGAG
	R	CTCCACCACGCGCTCCATGGCCTTCACATCGGTCTCGGTG
110 M204Q.M205Q*	F	CACCGAGACCGATGTGAAGCAGCAGGAGCGCGTGGTGGAGCAGATG
	R	CATCTGCTCCACCACGGCTCCTGCTGCTTCACATCGGTCTCGGTG

FIGURE A2 11

moPrP region 178-207. Forward and reverse primers (F and R) shown for mutations designed for use with Stratagene QuikChange® site-directed mutagenesis kit (Stratagene, Cat.No.200523). * indicates that this mutation was made to part of a larger mutational construct such as in the case of structured region mutations where the amino acids targeted are spatially, but not sequentially proximal.

Site directed mutagenesis		Primer Sequence 5' to 3'
111 *V209Q.M212Q	F	GTGAAGATGATGGAGCGCGTGCAGGAGCAGCAGTGCCTCACCCAGTACCAG
	R	CTGGTACTGGGTGACGCACTGCTGCTCCTGCACGCGCTCCATCATCTTCAC
112 M204Q.M205Q.V209Q.M212Q	F	GTGAAGCAGCAGGAGCGCGTGCAGGAGCAGCAGTGCCTCACCCAGTACCAG
	R	CTGGTACTGGGTGACGCACTGCTGCTCCTGCACGCGCTCCTGCTGCTTCAC
113 E210A.Q211A*	F	GATGATGGAGCGCGTGGTGGCCGCCATGTGCGTCACCCAGTACCAG
	R	CTGGTACTGGGTGACGCACATGGCGGCCACCACGCGCTCCATCATC
114 *C213A	F	GAGCGCGTGGTGGAGCAGATGGCCGTCACCCAGTACCAGAAGGAG
	R	CTCCTTCTGGTACTGGGTGACGGCCATCTGCTCCACCACGCGCTC
115 K219A.E220A.Q222A	F	GTGCGTCACCCAGTACCAGGCCGCTCCGCGCCTATTACGACGGGAGAAG
	R	CTTCTCCCGTCGTAATAGGCGCGGAGGCGGCTGGTACTGGGTGACGCAC
116 *Y224A	F	CAGAAGGAGTCCAGGCCGCTACGACGGGAGAAGATCC
	R	GGATCTTCTCCCGTCGTAGGCGGCTGGGACTCCTTCTG
117 *Y225A	F	GAAGGAGTCCAGGCCATATGCCGACGGGAGAAGATCCAGC
	R	GCTGGATCTTCTCCCGTCGGCATAGGCCTGGGACTCCTTC

FIGURE A2 12

moPrP region 178-207. Forward and reverse primers (F and R) shown for mutations designed for use with Stratagene QuikChange® site-directed mutagenesis kit (Stratagene, Cat.No.200523). * indicates that this mutation was made to part of a larger mutational construct such as in the case of structured region mutations where the amino acids targeted are spatially, but not sequentially proximal.

Sequencing Primers		Primer Sequence 5' to 3'
moPrPaa1_for	F	GGCGAACCTTGGCTACTG
moPrPaa164_for	F	GCCAGTGGATCAGTACAG
moPrPaa164_rev	R	CTGTACTGATCCACTGGC

FIGURE A2 13

Primers designed to anneal to moPrP ORF at amino acid 1 (forward) and amino acid 164 (forward and reverse primers); used for sequencing reactions to verify mutated sequence

6.3 MOUSE PRION PROTEIN OPEN READING FRAME IN PBLUESCRIPTSK+ AND PLNCX2

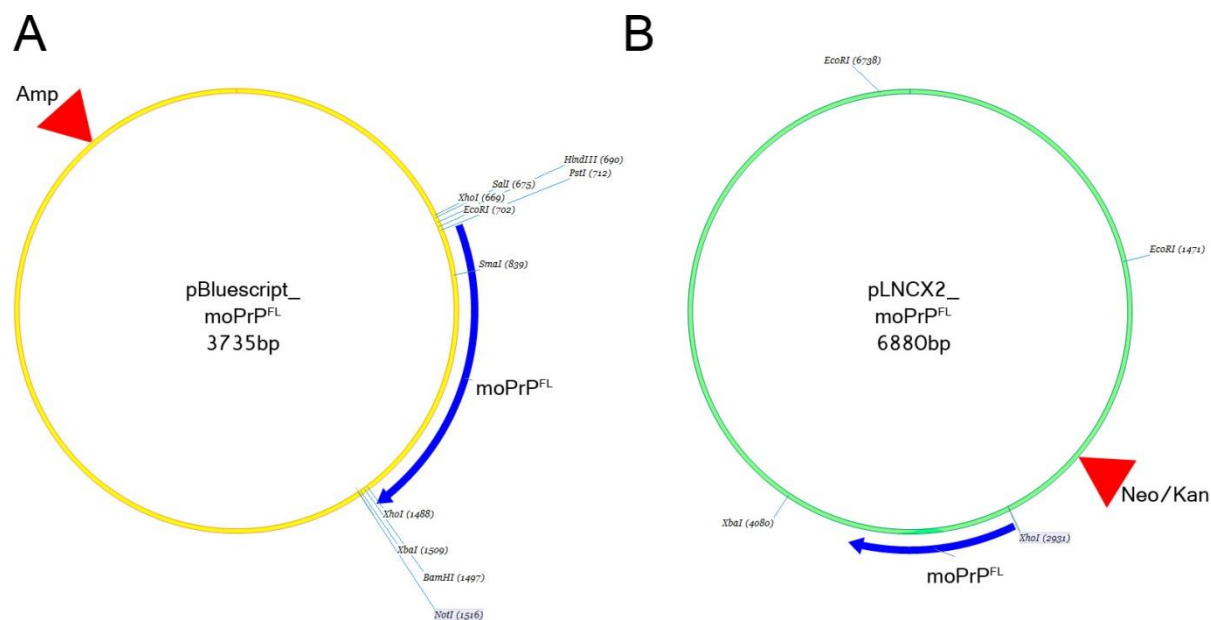


FIGURE A3

Schematics showing moPrP in both pBluescriptSK+ and pLNCX2 vectors; (A) moPrP ORF (in blue) as shown in Figure A1 was cloned into the pBluescriptSK+ vector at a *SmaI* site within the multiple cloning site. This construct was used to generate all alanine replacements via site directed mutagenesis. (B) Following *HindIII/XhoI* digestion of (A), moPrP^{Ala} was cloned into *HindIII/SalI* linearised pLNCX2. Shown in red are the resistance genes expressed by the vectors, and restriction sites

6.4 MOUSE PRION PROTEIN OPEN READING FRAME (PROTEIN SEQUENCE)

10	20	30	40	50	60	
<u>MANLGYWLLA</u>	<u>LFVTMWTDVG</u>	<u>LCKKRPKPGG</u>	WNTGGSRYP	QGSPGGNRY	PQGGTWGQP	- 60
GGGWGQPHG	SWGQPHGGS	GQPHGGGWG	GGGTHNQWN	PSKPKTNLKH	VAGAAAAGAV	- 12
VGGLGGYML	SAMSRPMIHF	GNDWEDRYY	ENMYRYPNQ	YYRPVDQYS	QNNFVHDCV	- 18
ITIKQHTVTT	TTKGENFTET	DVKMMERVVE	QMCVTQYQK	SQAYYDGRR	<u>SSTVLFSSPP</u>	- 24
<u>VILLISFLIF</u>	<u>LIVG</u>					

FIGURE A4

Single letter code protein sequence of moPrP. Signal sequences at both N- and C-terminus of the protein are underlined

6.5 ELISPOT REVELATION: PLATE READER VISUALISATION

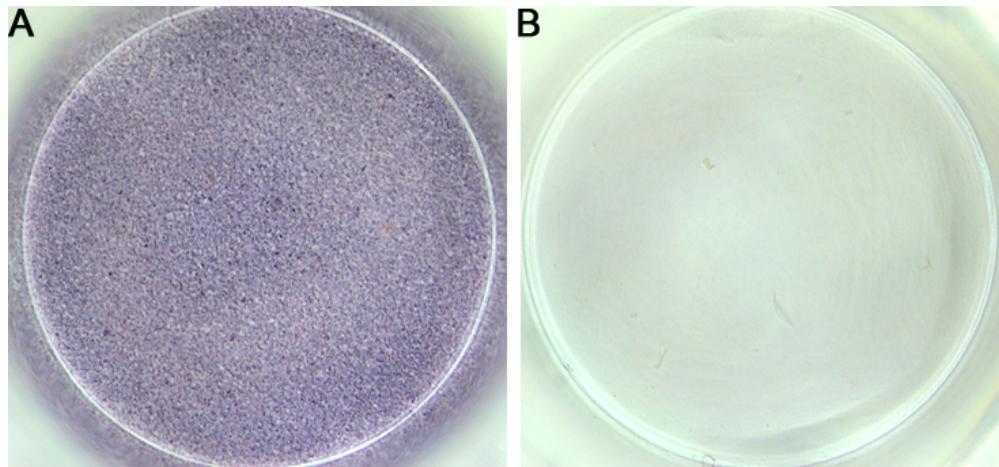


FIGURE A5

PVDF membrane on a 96-well plate on to which 25,000 PK1 cells were plated. (A) Positive control showing that ProteinaseK-resistant material is detected when RML homogenate is used to infect PK1 cells and (B) negative control showing that KD cells do not propagate RML prions as no PK-resistant is detected by SCA and ELISPOT analysis.